ICPMAT

1-4 December 2025

Chiang Mai, Thailand

19th International Conference on the Physical Properties and Application of Advanced Materials (ICPMAT2025)

Chiang Mai Marriott Hotel, Thailand

Abstract Book and Proceedings

Organized by

CHIANG MAI UNIVERSITY

FACULTY OF SCIENCE
CHIANG MAI UNIVERSITY

INDUSTRIAL CHEMISTRY
SCIENCE CHIANG MAI UNIVERSITY

MR CENTER
Faculty of Science Chiang Mai University

Welcome Address

Associate Professor Dr. Piyapong Niamsup

Dean of the Faculty of Science
Chiang Mai University

Distinguished speakers, honored guests, esteemed colleagues, and friends,
On behalf of the Faculty of Science, it is my great privilege and sincere pleasure to welcome all of you to beautiful Chiang Mai, Thailand, for the 19th International Conference on the Physical Properties and Application of Advanced Materials, or ICPMAT2025. We are delighted to host this premier annual forum from 1st to 4th December 2025, right here at the Marriott Hotel.

The objective of this conference is, and always has been, clear: to provide a vibrant platform for sharing cutting-edge research findings and innovative advancements in the critical field of Physical Properties and Application of Advanced Materials. ICPMAT has a proud history, established in 2006 through the collaborative efforts of the University of Toyama, Shanghai University, and the Japan Institute of Metals. It has expanded its community to include many leading international institutions, including Chiang Mai University. ICPMAT consistently focuses on the most vital areas of materials science and physics, encompassing raw, structural, and functional materials, as well as advanced characterization techniques and computational materials science. Our core mission is to explore these topics, foster community cohesion, encourage insightful discussions, and promote new collaborations.

We are truly proud to host speakers and experts from leading domestic and international institutions this year. We believe this event will foster meaningful cooperation between researchers, helping us collectively advance knowledge, strengthen our global community, and elevate our international standing.
As the Dean of the Faculty of Science, I would like to take a moment to express my sincere gratitude to our host—the Materials Science Research Center and the Department of Industrial Chemistry—for their outstanding and dedicated efforts in organizing this spectacular event. I also extend my deepest appreciation to the many companies and organizations whose generous support has made ICPMAT2025 possible.

Finally, I wish all participants a highly productive and enriching experience. May your time here lead to new insights and exciting collaborations. And, of course, I hope you thoroughly enjoy the unique hospitality and beauty of Chiang Mai.

Thank you for being part of ICPMAT2025.

Conference Report

Assistant Professor Dr. Chaiyasit Banjongprasert

Head of the Materials Science Research Center
Faculty of Science, Chiang Mai University

The 19th International Conference on the Physical Properties and Application of Advanced Materials (ICPMAT2025) successfully assembles in the vibrant city of Chiang Mai, Thailand, from December 1 to 4, 2025. Co-organized by the Materials Science Research Center and the Department of Industrial Chemistry, Faculty of Science, Chiang Mai University, the conference is an honor to host and an immediate success, drawing participants from Thailand and the wider global research community in total 13 countries including Thailand (165 participants), Japan (32 participants), South Korea (22 participants), China (15 participants), Poland (7 participants), Vietnam (6 participants), Czech Republic (5 participants), India (2 participants), Germany (1 participant), UAE (1 participant), Portugal (1 participant), United States (2 participants) and United Kingdom (1 participant). The total participants are 260.

The core objective of ICPMAT remains clear: to provide a vibrant, high-level platform for sharing cutting-edge research findings and innovative advancements in the critical field of advanced materials focusing on many areas encompassing raw, structural, and functional materials, as well as advanced characterization techniques and computational materials science. The mission is to foster community cohesion, encourage insightful discussions, and promote new collaborations.

The main scientific program, held across December 2nd and 3rd, offers an intensive schedule featuring distinguished global experts and rising researchers. The key sessions and presentations include three high-impact plenary lectures delivered by leading international experts. Twelve invited talks are presented by invited researchers, highlighting advances across the materials field. Technical seminars are organized across three distinct technical topics, allowing for focused discussions and knowledge exchange. 59 peer-reviewed oral presentations diverse research projects. 56 poster presentations provide ample opportunity for one-on-one networking and detailed discussion of emerging work.

A significant addition to the 2025 program is the special session titled, “Consortium for Nurturing High-Performance Postdoctoral and Postgraduate Researchers in Materials Science and Technology to Drive Thailand to BCG Economy.” This session is generously supported by the Program Management Unit for Human Resources & Institutional Development, Research and Innovation (PMUB), Thailand, featured 13 dedicated oral presentations and 7 poster presentations, underscoring the commitment to developing national research talent aligned with the Bio-Circular-Green (BCG) economic model.

The ICPMAT2025 Organizing Committee gratefully acknowledges the essential financial and logistical support provided by our corporate and institutional sponsors: 1 Platinum, 4 Gold, 1 Silver, 9 Bronze partners, and 2 supporters. Their contributions were instrumental in ensuring the high standard and smooth accomplishment of this international event.

In line with our mission to circulate knowledge, selected presentations from the conference will be published in the official conference proceedings and featured in affiliated academic journals, including the Chiang Mai Journal of Science.

The conference formally concludes on December 4th with an opportunity for participants to engage in relaxing excursions, allowing them to explore the rich local culture, heritage, and natural beauty of Chiang Mai. This social element provides a valuable counterpoint to the intensive scientific schedule and facilitates informal networking.

We extend our deepest gratitude to the dedicated members of the International Advisory Board, the Organizing Committee, the supporting staff, and all volunteers whose tireless efforts ensured the success of ICPMAT2025. We sincerely hope the experience was engaging, inspiring, and valuable for the professional work ahead for all participants. Let us continue to explore the invisible together.

Opening Remarks

Associate Professor Dr. Winita Punyodom

Vice President
Chiang Mai University

Distinguished Guests, Esteemed Plenary Speakers, Invited Researchers, Industry Partners, Ladies and Gentlemen,
On behalf of Chiang Mai University and the co-organizing committee, it is my distinct honor and pleasure to warmly welcome all of you to the 19th International Conference on the Physical Properties and Application of Advanced Materials—ICPMAT2025. We are exceptionally proud to host this gathering, which brings together leading researchers, industry experts, and brilliant students from across the country and around the world here in the beautiful city of Chiang Mai.

For nearly two decades, ICPMAT has served as a vital platform for sharing discoveries. Today, as we commence the 19th edition, we must recognize that the disciplines of Materials Science and Physics play a more key role than ever before. They are not only theoretical interest, but they are also the fundamental drivers in solving real-world community problems across several critical domains.
Every challenge we face—from achieving sustainable energy independence, to building resilient infrastructure and environment, to performing efficient environmental remediation, and ensuring seamless communication and information access—is ultimately a materials problem waiting for the solution from all of us. Our collective task is to provide the fundamental scientific understanding and the technological stuff that enables these new solutions.

At Chiang Mai University, our research activities are strategically structured around interdisciplinary pillars designed to meet the growing demands of Thailand's development model, including the BCG (Bio-Circular-Green) Economy, and global scientific challenges. Our robust research, spanning from fundamental nanoscience and applied polymer engineering to advanced materials and physics and material characterization, ensures that we are not just contributing to the global body of knowledge, but are actively providing real solutions and high-performance talent to drive the nation forward. We look forward to strengthening the partnerships here at ICPMAT2025, specifically to deliver solutions aligned with the sustainable development goals that are driving global innovation.

This conference is more than a schedule of presentations; it is a critical chance to share knowledge, challenge conventional thinking, learn from each other's expertise, and, most importantly, build new and lasting international partnerships.
We sincerely hope you will enjoy the high-quality technical seminars, the insightful presentations, and the vibrant discussions planned over the next four days.

Thank you for joining ICPMAT2025. I wish you all a successful and incredibly productive conference.
Welcome to ICPMAT2025!

Chair, Co-chair and International Advisory Board

Chair

Asst. Prof. Dr. Chaiyasit BANJONGPRASERT
Chiang Mai University (Thailand)
Asst. Prof. Dr. Worapong THIEMSORN
Chiang Mai University (Thailand)

Co-chair

Prof. Hideki ONO, University of Toyama (Japan)
Prof. Huynh Trung HAI, Hanoi University of Science and Technology (HUST) (Vietnam)

International Advisory Board

Prof. Hideki Ono - University of Toyama (Japan)
Prof. Tetsuo AIDA – University of Toyama (Japan)
Asst. Prof. Dr. Chaiyasit BANJONGPRASET – Chiang Mai University (Thailand)
Prof. Jana BIDULSKA – Technical University of Kosice (Slovakia)
Dr. Robert BIDULSKY – Bodva Industry and Innovation Cluster (Slovakia)
Prof. Tomasz BRYLEWSKI – AGH University of Science and Technology (Poland)
Prof. Zbigniew BRYTAN – Silesian University of Technology (Poland)
Prof. Shixun CAO – Shanghai University (China)
Prof. Torranin CHAIRUANGSRI – Chiang Mai University (Thailand)
Prof. Renchao CHE – Fudan University – Zhejiang Laboratory (China)
Prof. Jun-Yi GE – Shanghai University (China)
Prof. Marco Actis GRANDE – Politecnico di Torino (Italy)
Assoc. Prof. Takashi HASHIZUME – University of Toyama (Japan)
Prof. Randi HOLMESTAD – Norwegian Un. of Science and Techn. (Norway)
Prof. Wayne D. HUTCHINSON – University of New South Wales (Australia)
Prof. Takuya ISHIMOTO – University of Toyama (Japan)
Dr. Nguyen Hong HAI – Hanoi University of Science and Technology (Vietnam)
Prof. Lubos KASCAK – Technical University of Kosice (Slovakia)
Prof. Dang Quoc KHANH – Hanoi Un. of Science and Technology (Vietnam)
Prof. Pham Mai KHANH – Hanoi Un. of Science and Technology (Vietnam)
Prof. Tibor KVACKAJ – Bodva Industry and Innovation Cluster (Slovakia)
Prof. Malgorzata LEWANDOWSKA – Warsaw University of Techn. (Poland)
Prof. Zhe LI – Harbin Institute of Technology (China)
Prof. Diego MANFREDI – Politecnico di Torino (Italy)
Prof. Knut MARTHINSEN – Norwegian Un. of Science and Techn. (Norway)
Dr. Calin D. MARIOARA – SINTEF (Norway)
Prof. Kenji MATSUDA– University of Toyama (Japan)
Dr. Sarka MIKMEKOVA – Institute of Scientific Instrument of Czech Academy of Sciences (Czech Republic)
Prof. Mitsuhiro MURAYAMA – Virginia Tech (USA)
Prof. Katsuhiko NISHIMURA – University of Toyama (Japan)
Assoc. Prof. Dr. Kedsarin PIMRAKSA – Chiang Mai University (Thailand)
Prof. Wei REN – Shanghai University (China)
Prof. Seiji SAIKAWA – University of Toyama (Japan)
Prof. Atsushi SAIKI – University of Toyama (Japan)
Prof. Toshiya SHIBAYANAGI – University of Toyama (Japan)
Prof. Gary J. SHIFLET – University of Virginia (USA)
Prof. Emil SPISAK – Technical University of Kosice (Slovakia)
Prof. Miroslaw STYGAR – AGH University of Science and Technology (Poland)
Prof. Yutaka TAKAGUCHI – University of Toyama (Japan)
Prof. Le VAN LICH – Hanoi University of Science and Technology (Vietnam)
Prof. Zou YONG – Shandong University (China)
Prof. Guanghui MIN – Shandong University (China)
Prof. Jincang ZHANG – Shanghai University and Zhejiang Laboratory (China)
Dr. Ilona MÜLLEROVÁ - Czech Academy of Sciences (Czech Republic)
Dr. Enzo LIOTTI - University of Oxford (UK)
Prof. Soo Yeol LEE - Chungnam National University (South Korea)
Asst. Prof. Dr. Avala LAVAKUMAR, Department of Metallurgical and Materials Engineering, Indian Institute of Technology Ropar (India)
Dr. Takeshi SAITO, Hydro Aluminium
Asst. Prof. Dr. Tomoyo MANAKA - University of Toyama (Japan)
Asst. Prof. Dr. Kengo KATO - University of Toyama (Japan)
Asst. Prof. Dr. Abrar AHMED - University of Toyama (Japan)
Prof. Injoon SON – Kyungpook National University (South Korea)
Prof. Ho Seong LEE – Kyungpook National University (South Korea)
Prof. Sung Hyuk PARK – Kyungpook National University (South Korea)
Prof. Yuho MIN – Kyungpook National University (South Korea)
Prof. Kwi-Il PARK – Kyungpook National University (South Korea)
Prof. Le Van LICH – Hanoi University of Science and Technology (Vietnam)
Dr. Ha Minh TAN – Hanoi University of Science and Technology (Vietnam)
Prof. Nguyen Hoang VIET – Hanoi University of Science and Technology (Vietnam)
Prof. Nguyen Duong NAM – Vietnam Maritime University (Vietnam)

Organizing Committee of The 19th International Conference on the Physical Properties and Application of Advanced Materials (ICPMAT2025)
1-4 December 2025, Chiang Mai Marriott Hotel, Chiang Mai, Thailand

Committee from the Faculty of Science, Chiang Mai University

Steering Committee

1. Assoc. Prof. Dr. Piyapong Niamsup
2. Assoc. Prof. Dr. Jaroon Jakmunee
3. Assoc. Prof. Dr. Chayakorn Pumas
4. Asst. Prof. Dr. Chaiyasit Banjongprasert
5. Assoc. Prof. Dr. Panchika Prangkio
6. Asst. Prof. Dr. Kritsana Jitmanee
7. Assoc. Prof. Dr. Supab Choopun
8. Asst. Prof. Dr. Worapong Thiemsorn
9. Distinguished Prof. Dr. Torranin Chairuangsri
10. Assoc. Prof. Dr. Kedsarin Pimraksa
11. Mrs. Tadsawan Thepsuwan
12. Ms. Siriporn Chomputan

Organizing Committee

1. Asst. Prof. Dr. Chaiyasit Banjongprasert
2. Asst. Prof. Dr. Worapong Thiemsorn
3. Asst. Prof. Dr. Datchanee Pattavarakorn
4. Assoc. Prof. Dr. Panchika Prangkio
5. Assoc. Prof. Dr. Puttinan Meepowpan
6. Assoc. Prof. Dr. Kedsarin Pimraksa
7. Assoc. Prof. Dr. Wiradej Thongsuwan
8. Ms. Siriporn Chomputan
9. Mrs. Tadsawan Thepsuwan

Academic Subcommittee

1. Asst. Prof. Dr. Chaiyasit Banjongprasert
2. Asst. Prof. Dr. Sankum Nusen
3. Assoc. Prof. Dr. Panchika Prangkio
4. Assoc. Prof. Dr. Sukon Phanichphant
5. Professor Dr. Somchai Thongtem
6. Professor Dr. Arnon Chaipanich
7. Assoc. Prof. Dr. Pisith Singjai
8. Assoc. Prof. Dr. Thapanee Sarakonsri
9. Assoc. Prof. Dr. Kedsarin Pimraksa
10. Assoc. Prof. Dr. Piyarat Nimmanpipug
11. Assoc. Prof. Dr. Nawee Kungwan
12. Assoc. Prof. Dr. Narin Lawan
13. Assoc. Prof. Dr. Patnarin Worajittiphon
14. Assoc. Prof. Dr. Burapat Inceesungvorn
15. Assoc. Prof. Dr. Sulawan Kaowphong
16. Assoc. Prof. Dr. Anucha Watcharapasorn
17. Assoc. Prof. Dr. Saranpong Yimklan
18. Asst. Prof. Dr. Natthawat Semakul
19. Dr. Robert Molloy
20. Dr. Suphitcha Moonngam
21. Dr. Jetsada Panyafu
22. Asst. Prof. Dr. Worapong Thiemsorn
23. Asst. Prof. Dr. Nattapol Laorodphan Maejo University
24. Mr. Seksan Sornjai

Ceremonial and Reception Subcommittee

1. Distinguished Prof. Dr. Torranin Chairuangsri
2. Assoc. Prof. Dr. Kedsarin Pimraksa
3. Asst. Prof. Dr. Datchanee Pattavarakorn
4. Assoc. Prof. Dr. Panchika Prangkio
5. Assoc. Prof. Dr. Parimanan Cherntongchai
6. Asst. Prof. Satit Phiyanalinmat
7. Asst. Prof. Dr. Hataichanok Pandit
8. Asst. Prof. Dr. Sukrit Sucharitakul
9. Asst. Prof. Dr. Natthawat Semakul
10. Dr. Thanapat Autthawong
11. Dr. Phatthamon Kongkhambut
12. Dr. Sunsanee Komboonchoo
13. Ms. Maneerat Thala
14. Ms. Chanikan Kamphrom
15. Ms. Thaksaporn Boonsuk
16. Ms. Waritsara Thanacharoen
17. Ms. Ketsarin Ariya
18. Ms. Sunatcha Seerat
19. Ms. Thanaporn Duangdet
20. Ms. Chadaporn Thasingkham

Local Committee
Faculty of Science, Chiang Mai University

21. Mrs. Nongkarn Chaiyawang
22. Ms. Yupawadee Kamaun
23. Mr. Phattharaphong Sangboon

Public Relations and Information Technology Subcommittee

1. Assoc. Prof. Dr. Wiradej Thongsuwan
2. Asst. Prof. Dr. Sankum Nusen
3. Asst. Prof. Dr. Rattiyakorn Rianyoi
4. Mr. Nattaporn boonlow
5. Mr. Autian Fusri
6. Ms. Sainatee Jaihom
7. Ms. Jutakan kantalue
8. Mr. Ekkaphon Khamsaen
9. Mr. Seksan Sonjai

Registration and Documentation Subcommittee

1. Asst. Prof. Dr. Datchanee Pattavarakorn
2. Dr. Thanapat Autthawong
3. Asst. Prof. Dr. Yothin Chimupala
4. Asst. Prof. Dr. Nongnuch Rueangjitt
5. Ms. Nattakan Chotchaitanakorn
6. Dr. Sathienphong Ngamsomrit
7. Mr. Korawith Pimta
8. Ms. Saitharn Limsakul
9. Ms. Manunchaya Jaideekard
10. Ms. Pich Maneewan
11. Ms. Pornthida Yanapat
12. Ms. Pornhathai Rungsan
13. Ms. Nadruedee Leenarach
14. Ms. Wannisa Intaprasert

Venue, Audio-Visual, and Hospitality Subcommittee

1. Asst. Prof. Dr. Worapong Thiemsorn
2. Asst. Prof. Dr. Adisak Siyasuk
3. Assoc. Prof. Dr. Puttinan Meepowpan
4. Assoc. Prof. Dr. Patnarin Worajittiphon
5. Dr. Worawut Srisukkham
6. Mr. Kamron Inmassity
7. Mr. Nattaporn boonlow
8. Mr. Jatupon Comvon
9. Mr. Chawana Ruanmoon
10. Mr. Wattikon Sroila
11. Mr. Ativich Denprawat
12. Ms. Patrapee Saraphan
13. Mr. Supawit Sinturat
14. Ms. Sitawee Rojpanawat
15. Mr. Seksan Sornjai

Finance Subcommittee

1. Assoc. Prof. Dr. Panchika Prangkio
2. Asst. Prof. Dr. Jantrawan Pumchusak
3. Asst. Prof. Dr. Yothin Chimupala
4. Dr. Thanapat Autthawong
5. Ms. Sirichan Wongkaew
6. Mrs. Jarunee Ngernphacho
7. Ms. Thanikan Yamano
8. Mrs. Tassawan Thepsuwan
9. Ms. Siriporn Chomputan
10. Mr. Pattarapong Sangkaboon

Coordination and Secretariat Subcommittee

1. Assoc. Prof. Dr. Kedsarin Pimraksa
2. Assoc. Prof. Dr. Panchika Prangkio
3. Asst. Prof. Dr. Worapong Thiemsorn
4. Asst. Prof. Dr. Chaiyasit Banjongprasert
5. Ms. Pornhathai Rungsan
6. Ms. Wannisa Intaprasert
7. Ms. Siriporn Chomputan
8. Ms. Jindaporn Chaisorn
9. Ms. Yupawadee Kamaun
10. Mr. Seksan Sornjai
11. Mr. Pattarapong Sangkaboon

Sponsorship Subcommittee

1. Asst. Prof. Dr. Chaiyasit Banjongprasert
2. Asst. Prof. Dr. Yothin Chimupala
3. Mr. Panithan Intharawicha
4. Mr. Chitsanupong Phromma
5. Mr. Theeraphat Daenmueang
6. Mrs. Vanicha Watjanakunanun
7. Ms. Arachaporn Srichan
8. Ms. Sirinpha Chueakamlu
9. Mrs. Nongkhran Chaiwong
10. Ms. Jindaporn Chaisorn

The 19th ICPMAT conference 2025 organizing committee acknowledges with gratitude the generous suppert of our sponsors:

Exhibitions

Chiang Mai Marriott Hotel, Chiang Mai, Thailand

3rd Floor

EXHIBITION BOOTHS

G0 Faculty of Science - Chiang Mai University
G1 Keyence (Thailand) Co., Ltd
G2 Bara Scientific Co., Ltd.
S3 Its (Thailand) Co., Ltd
B1 Kinetics Corporation Ltd.
B2 Lab Connection Co., Ltd.
B3 Mega Matt Co., Ltd.
B4 Histocenter (Thailand) Co., Ltd.
B5 Crest Nanosolution (Thailand) Co., Ltd.
B6 Coax Group Corporation Co. Ltd.
B7 PBP-CMU Electron Linac Laboratory
B8 Becthai Bangkok Equipment and Chemical Co., Ltd.
C1 Puditec Co., Ltd.

Programme at a Glance

1 December 2025

13.00-17.30	Registration and Poster setup (Foyer, 4th Floor)
17.30-19.00	Welcome reception (Grand Ballroom, 2nd Floor)

2 December 2025

Time/Room	SUTHEP HALL				
08.00-08.30	Registration (Foyer, 4th Floor)				
08.30-09.15	Opening Ceremony				
09.15-10.00	PL01 Removal of Fe and Si from Aluminum via Extraction and Phase Separation Using Sn bath, **Prof. Hideki ONO,** University of Toyama, Japan Chair: Distinguished Prof. Dr. Torranin Chairuangsri				
10.00-10.15	Morning Break				
Room	**PASSAGE**	**EXPEDITION**	**JOURNEY**	**YOYAGE**	**EXCURSION**
Parallel Sessions	Structural Materials (S1)	Materials Processing and Engineering (S3)	Materials Processing and Engineering (S3)	Other Topics Related to Materials and Nano-technology (S5)	Consortium* (S6)
Chairs	**Dr. Enzo LIOTTI**	**Dr. Dongting Wu** **Dr. Narin Jantaping**	**Assoc. Prof. Dr. Nam Nguyen Duong**	**Prof. Daniel C.W. Tsang**	**Assoc. Prof. Dr. Kedsarin Pimraksa** **Assoc. Prof. Dr. Thapanee Sarakonsri**
10.15-10.35	S1_IV01, S1_01, S1_02, S1_06, S1_09, **S2_03, T01**	S3_IV01, S3_IV02, S3_01, S3_02, S3_03, S3_05	S3_IV04, S3_011, S3_013, S3_014, S3_016, S3_017, T02	S5_IV01, S5_02, S5_03, S5_04, S5_06, S6_07, T03	IT01, IT02, IT03
12.00-13.00	Lunch				
13.00-13.45 SUTHEP HALL	PL02 The Effect of Grain Boundary Structure on Nucleation and Growth of Theta ($CuAl_2$) Precipitates in Al-5 wt% Cu **Prof. Gary J. SHIFLET**, University of Virginia, USA Chair: Dr. Anchalee Manonukul				
Parallel Sessions	Advanced Materials Characterization Techniques and Instrumentations (S2)	Materials Processing and Engineering (S3)	Materials Processing and Engineering (S3)	Other Topics Related to Materials and Nano-technology (S5)	Consortium* (S6)
Chairs	**Dr. Sarka MIKMEKOVA** **Prof. Pengchao Si**	**Dr. Shuwei Duan**	**Prof. Malgorzata LEWAND-OWSKA**	**Prof. Lishu Zhang**	**Asst. Prof. Dr. Chaiyasit Banjongprasert** **Dr. Suphitcha Moonngam**
14.00-15.25	S2_IV01, S2_IV02, S2_01, S2_04, S2_05	S3_IV03, S3_06, S3_07, S3_08, S3_09	S3_IV05, S3_018, S3_019, S3_020, S3_023	S5_IV02, S5_08, S5_09, S5_010, S5_011	S6_09, S6_010, S6_012, S6_011, S6_04, S6_01
15.25-15.40	Afternoon Break				
Parallel Sessions	Advanced Materials Characterization Techniques and Instrumentations (S2)	Materials Processing and Engineering (S3)	Materials Processing and Engineering (S3)	Other Topics Related to Materials and Nano-technology (S5)	Consortium* (S6)
Chairs	**Prof. Ilona MÜLLEROVÁ** **Asst. Prof. Avala LAVAKUMAR**	**Dr. Anchalee Manonukul**	**Prof. Injoon SON**	**Asst. Prof. Dr. Yothin Chimupala**	**Assoc. Prof. Dr. Panchika Prangkio,** **Asst. Prof. Dr. Runglawan Somsunan**
15.40-17.20	S2_IV03, S2_IV04, S2_06, S2_07, S2_09	S3_030, S3_033, S3_035	S3_IV06, S3_024, S3_025, S3_026	S5_012, S5_013, S5_014	S6_02, S6_08, S6_05, S6_03, S6_013, S6_07, S6_06
17.00-18.30	Poster Session (4th Floor)				
18.30-21.00	Banquet (SUTHEP HALL, 4th Floor)				

*Consortium for Nurturing High-Performance Postdoctoral and Postgraduate Researchers in Materials Science and Technology to Drive Thailand to BCG Economy Year 3(S6)

Programme at a Glance

3 December 2025

Time/Room	Room: **SUTHEP HALL** 4th Floor
08.30-09.00	Registratioin
09.00-10.00	PL03 In situ Electron Microscopy - Data Analytics, **Prof. Mitsuhiro MURAYAMA**, Virginia Tech, USA Chair: Asst. Prof. Dr. Chaiyasit Baanjongprasert
10.00-10.15	Morning Break
	Chair: Asst. Prof. Dr. Chaiyasit Baanjongprasert
10.15-10.35	S3_IV07 Research Project on Recycling of Aluminum in Toyama - Joining of Recycled Aluminum Alloy, **Prof. Toshiya SHIBAYANAGI**
10.35-10.55	S2_IV05 Investigating the solidification of 'dirty' recycled aluminium alloys with X-ray imaging and artificial intelligence, **Dr. Enzo LIOTTI**
10.55-11.15	S2_IV06 Filtered Secondary Electron Imaging: Energy- and Angle-Resolved Contrast in SEM, **Dr. Sarka MIKMEKOVA**
11.15-12.00	Closing Ceremony
12.00-13.30	Lunch

4 December 2025

Time	
08.30-09.00	Registratioin
09.00-16.00	Technical tour/Excursion

Programme: 2 December 2025
Parallel Sessions

Time/Room	Room: PASSAGE, 3rd Floor
Session:	**Structural Materials (S1)** **Chairs: Dr. Enzo LIOTTI**
10.15-10.35	S1_IV01 High-Entropy Oxide Spinels as Functional Coatings for SOFC Interconnects: Structure and Properties **Prof. Miroslaw STYGAR**
10.35-10.50	S1_01 Correlation Between Hardness, Tensile Properties and Microstructure in Cold-Rolled and Aged of Al-Mg-Si-Cu Alloy, **Ngoc Hai Vu**
10.50-11.05	S1_02 Precipitation behavior in natural aged of Al-Mg-Si alloy containing Silicon in excess at peak hardness **SY QUAN TRAN**
11.05-11.20	S1_06 Formation Mechanism and Microstructural Evolution of Mullite Engobe beneath Celadon Glazes from Rice Husk Ash for Stoneware Wall Tiles **Asst. Prof. Dr. Nophawan Dechboon**
11.20-11.35	S1_09 Electron Microscopy of Unusual Phases in Cast Ni-Al Bronze, **Distinguished Prof. Dr. Torranin Chairuangsri**
11.35-11.50	S2_03 The relationship between hardness and microstructure in Zn/Mg ratio-controlled Al–Zn–Mg alloys aged at 200 °C, **Wanlalak Sanphiboon**
11.50-12.05	Technical talk: Microscope Applications in Materials Research, **Wasapon Fuangsawat**, Keyence (Thailand) Co., Ltd.
12.05-13.00	Lunch
13.00-13.45 SUTHEP HALL	PL02: Prof. Gary J. SHIFLET
Session:	**Advanced Materials Characterization Techniques and Instrumentations** Chairs: **Dr. Sarka MIKMEKOVA, Prof. Pengchao Si**
14.00-14.20	S2_IV01 Time-of-Flight Spectroscopy for Exploring Electron Scattering in 2D Materials and Ultrathin Films, **Prof. Ilona MÜLLEROVÁ**
14.20-14.40	S2_IV02 Nature of different deformation modes of a new metastable body-centered cubic Ti35Hf25Zr25Nb5Ta5Al5 high entropy alloy, **Asst. Prof. Avala LAVAKUMAR**
14.40-14.55	S2_01 Particle pushing and engulfment phenomenon in Al-TiC nanocomposites: Bridging experiments, physical models, and Cellular Automata–Finite Differences method, **Dr. Ewa Olejnik**
14.55-15.10	S2_04 Machine learning aided nanoscale visualization of grain boundaries using electron diffraction mapping, **Asst. Prof. Dr. Shiro Ihara**
15.10-15.35	S2_05 Effect of thermomechanical treatment on Ω-phase precipitation in Al-Cu-Mg alloys, **Assoc. Prof. Seungwon Lee**
15.35-15.40	Afternoon Break
Session:	**Advanced Materials Characterization Techniques and Instrumentations** Chairs: **Prof. Ilona MÜLLEROVÁ and Asst. Prof. Avala LAVAKUMAR**
15.40-16.00	S2_IV03 Lithium Nitrate Tailored Low-Temperature Electrolyte with a high voltage window over 5.5V and operation at wide-temperature-range, **Prof. Pengchao Si**
16.00-16.20	S2_IV04 Motivational Concepts for the Nobel Prize 2025: Development of Metal-Organic Frameworks (MOFs) **Dr. Brij Mohan**
16.20-16.35	S2_06 Effect of additive manufacturing method on the corrosion resistance of sintered materials produced by metal 3D printers, **Kenta Makizaki**
16.35-16.50	S2_07 Structural, magnetic and mechanical characterisation of Fe-Co-Ni-Mn-Ti medium-entropy alloys prepared by mechanical alloying, spark plasma sintering and arc-melting, **Dr. hab. Lukasz Hawelek**
16.50-17.05	S2_09 Infrared FEL-Induced Alteration of Zeta Potential in Electro-chemically Grown Quantum Dots: Insights into Ion Modification **Asst. Prof. Dr. Sukrit Sucharitakul**
17.00-18.30	Poster Session

Programme: 2 December 2025
Parallel Sessions

Time/Room	Room: EXPEDITION, 3rd Floor
Session:	**Materials Processing and Engineering (S3)** Chairs: **Dr. Dongting Wu, Dr. Narin Jantaping**
10.15-10.35	S3_IV01 Friction Surfacing Deposition of High-Strength Aluminum Alloys: From Homogeneous Al-Cu-Li to Heterogeneous Al-Cu-Li/Al-Zn-Mg-Cu Structures **Dr. Shuwei Duan**
10.35-10.55	S3_IV02 Rethinking Metal Forming: Merging Old Wisdom with New Additive Technologies, **Dr. Anchalee Manonukul**
10.55-11.10	S3_01 Microstructural characterisation and hardness evaluation of bimetallic 316L/17-4PH stainless steel fabricated by filament-based material extrusion additive manufacturing **Natthaphat Parsompech**
11.10-11.25	S3_02 Manufacturing process and wear performance of metal matrix composites in the aspect of high temperature wettability **Łukasz Szymański**
11.25-11.40	S3_03 Effect of Infill Geometry and Density on the As-Printed Flexural Performance of 316L Specimens Fabricated by Material Extrusion Additive Manufacturing **Pharadee Suwannak**
11.40-11.55	S3_05 Enhanced Room-Temperature Formability of Mg-Zn-Zr Alloy through Texture Weakening by Reduction Rate Control **Seoung-yooun Yu**
11.50-13.00	Lunch
13.00-13.45 SUTHEP HALL	PL02: Prof. Gary J. SHIFLET
Session:	**Materials Processing and Engineering (S3)** Chairs: **Dr. Shuwei Duan**
14.00-14.20	S3_IV03 Microstructure and Properties of Nano-TiC Modified Mar-M247 Superalloy Processed by Wire Arc Additive Manufacturing, **Dr. Dongting Wu**
14.20-14.35	S3_06 The microstructure and corrosion behavior analysis of different aging Al-Zn-Mg-Cu alloys manufactured by additive friction stir deposition **Dr. Fuqiang Guo**
14.35-14.50	S3_07 Process Optimization in FCAW of High Manganese Steel: Evaluating Temperature and Layer Effects on Hardness and Heat-Affected Zone, **Dr. Narin Jantaping**
14.50-15.05	S3_08 Influence of extrusion ratio on dynamic recrystallization, microstructure, and tensile properties of Mg–5Bi–3Al alloy, **Gun Woong An**
15.05-15.20	S3_09 Effect of Ag addition on microstructure and properties of Al-Zn-Mg-Cu alloys, **Qinghua Zhang**
15.20-15.40	Afternoon Break
Session:	**Materials Processing and Engineering (S3)** Chairs: **Dr. Anchalee Manonukul**
15.40-16.00	S3_030 Effects of Process Parameters and Prior-Forming Process in Gaseous Ferritic Nitrocarburising of Low Carbon Steels **Dr. John Thomas Harry Pearce**
16.00-16.15	S3_033 A Self-Assembled Metal-Organic Framework Network-Reinforced Solid Electrolyte via In Situ Polymerization for Lithium Metal Batteries **JianWei Qiu**
16.15-16.30	S3_035 Improved High-Temperature Performance of Al–Ce–Ni Alloys via Mg Solid-Solution Strengthening **Abid Abdu Mohammed**
16.30-16.45	
17.00-18.30	Poster Session

Programme: 2 December 2025
Parallel Sessions

Time/Room	Room: JOURNEY, 3rd Floor
Session:	**Materials Processing and Engineering (S3)** Chairs: **Assoc. Prof. Dr. Nam Nguyen Duong**
10.15-10.35	S3_IV04 Joining ultrafine grained materials using FSW and LBW techniques **Prof. Malgorzata LEWANDOWSKA**
10.35-10.50	S3_011 Effect of Ag Addition on the Morphology of the β-Phase in Al-Mg-Si Alloys **Dr. ABRAR AHMED**
10.50-11.05	S3_013 Microstructure observation of Al-7%Si-0.3%Mg cast alloy, **Dr. Taiki Tsuchiya**
11.05-11.20	S3_014 Initial oxidation properties of nickel-based Al-Cr-Fe-Ni high entropy alloys under thermal shock conditions **Dr. Richard Gawel**
11.20-11.35	S3_016 Influence of Laser Texturing on the Surface Properties of Magnesium Alloy **Jirayu Hemwat**
11.35-11.50	S3_017 Effect of Processing Parameters on the Densification of Magnesium Alloy Fabricated by Laser Powder Bed Fusion **Khettawan Panchamat**
11.50-12.05	Technical talk: In-Situ correlative Raman spectroscopy and SEM analysis from Renishaw, **Dr. Tan See Hua,** Its (Thailand) Co., Ltd.
12.05-13.00	Lunch
13.00-13.45 SUTHEP HALL	PL02: Prof. Gary J. SHIFLET
Session:	**Materials Processing and Engineering (S3)** Chairs: **Prof. Malgorzata LEWANDOWSKA**
14.00-14.20	S3_IV05 Recent Research on Electroplating Technologies for Reducing Gold Consumption **Prof. Injoon SON**
14.20-14.35	S3_018 Microstructure, mechanical properties and wear resistance of in-situ cast TiC/A356 composites **Assoc. Prof Dr. Wojciech Maziarz**
14.35-14.50	S3_019 Effect of TiC volume fraction on the mechanical response and structure and microstructure evolution of Al-based composites **Prof. Robert Chulist**
14.50-15.05	S3_020 Effect of Mo Addition on Microstructural Evolution of Al–Si alloys Containing High Iron Impurity **Pongpat Phetchanasongkhram**
15.05-15.20	S3_023 Determination of Interaction Coefficient of La with Cr in Molten Iron and Analysis on Formation of La Compounds in High-Chromium Steel **Shinya Oba**
15.15-15.40	Afternoon Break
Session:	**Materials Processing and Engineering (S3)** Chairs: **Prof. Injoon SON**
15.40-16.00	S3_IV06 Effect of post weld heat treatment on the microstructure and hardness distribution of TIG welded Ti-6Al-4V/Ti-CP joints **Assoc. Prof. Dr. Nam Nguyen Duong**
16.00-16.15	S3_024 Effects of Elemental Diffusion and Intermetallic Phases on the Microstructure, Mechanical Properties of Ti/Ti-6Al-4V Dissimilar Welding **Kien Vu Trung**
16.15-16.30	S3_025 Hierarchical Si@T-Nb_2O_5 Core-Shell Confined within Conductive Carbon Nanofiber Scaffolds for High-Capacity Lithium-Ion Storage **Yongtao Zhao**
16.30-16.45	S3_026 Anion-Tailored Solvation Clusters in Methyl Acetate Electrolyte: Achieving Concurrent Low Temperature Operation and High Voltage Stability **Dr. Jiaxuan Feng**
17.00-18.30	Poster Session

Programme: 2 December 2025
Parallel Sessions

Time/Room	Room: VOYAGE, 3rd Floor
Session:	**Other Topics Related to Materials and Nanotechnology (S5)** Chairs: **Prof. Daniel C.W. Tsang**
10.15-10.35	S5_IV01 Influence of Altermagnetism on the Orbital Hall Effect in RuO_2, **Prof. Lishu Zhang**
10.35-10.50	S5_02 Preparation and properties of polymer hydrogel from boric acid-crosslinked PVA for urea slow-release fertilizer **Dr. Pattranuch Pongsuk**
10.50-11.05	S5_03 Improved Efficiency and Stability in $MAPbI_3$ Perovskite Solar Cells through Bulk Defect Passivation with Benzyl Trimethylammonium Tribromide **Prof. Adel Najar**
11.05-11.20	S5_04 Synthesis of Low Carbon Polymorph Belite Cement: A Comparison of Pure Oxides and Lignite Bottom Ash **Chadapohn Tashingkam**
11.20-11.35	S5_06 Application of Impurity Removal through Selective Extraction and Phase Separation to the recovery of Al from Cast Al alloy, **Dr. Kengo Kato**
11.35-11.50	S5_07 Investigation on Dehydroxylation Temperature of Clay Minerals Affecting Mechanical Properties of Limestone-Calcined Clay Cement, **Ketsarin Ariya**
11.50-12.05	Technical Talk: Material analysis techniques using XPS and EPMA (Material analysis techniques using XPS and EPMA), **Praween Chaiya**, Bara Scientific Co., Ltd.
12.05-13.00	Lunch
13.00-13.45 SUTHEP HALL	PL02: Prof. Gary J. SHIFLET
Session:	**Other Topics Related to Materials and Nanotechnology (S5)** Chairs: **Prof. Lishu Zhang**
14.00-14.20	S5_IV02 Porous Carbon for Sustainable Construction Materials, **Prof. Daniel C.W. Tsang**
14.20-14.35	S5_08 Influence of Short-Range Order and Precipitates on the Mechanical and Magnetic Properties of Multicomponent Alloys, **Dr. Anna Wojcik**
14.35-14.50	S5_09 Design of Porous Carbon/Organic Polymer Composites as Cathode Materials in Li–S Batteries **Kittiputh Kunniyom**
14.50-15.05	S5_010 Development of Anode from Zinc Powder with Polyvinyl Alcohol Binder for Solid-state Zinc-air Batteries **Jinnapat Khemtong**
15.05-15.20	S5_011 Removal of Impurities from Die-cast ADC12 Aluminum Alloy Via Molten Tin, **Satoshi Iwasawa**
15.20-15.40	Afternoon Break
Session:	**Other Topics Related to Materials and Nanotechnology (S5)** Chairs: **Asst. Prof. Dr. Yothin Chimupala**
15.40-15.55	S5_012 Enhanced Photocatalytic Activity of Zn-MOF and TiO2 Nanocomposite for Methyl Orange Removal **Pemika Chaichana**
15.55-16.10	S5_013 Magnesium removal from Al-Mg alloy through molten salt electrolysis using LiCl-KCl-MgCl2 at 723K **Hikaru Fujioka**
16.10-16.25	S5_014 Wear Behavior of Ti6Al4V Titanium Alloy Against Steel Balls Under Dry Sliding Conditions, **Asst. Prof. Dr. Nutthanun Moolsradoo**
17.00-18.30	Poster Session

ABSTRACT

Content

Content

Session 2: Advanced Materials

Session 3: Materials Processing

Content

Content

Content

Session 6: Consortium for Nurturing High-Performance Postdoctoral and Postgraduate Researchers in Materials Science and Technology to Drive Thailand to BCG Economy Year 3

Content

Poster presentation

Session 1: Structural Materials

Session 2: Advanced Materials

Content

Session 3: Materials Processing

Content

Content

FULL PAPER IN PROCEEDINGS

Removal of Fe and Si from Aluminum via Extraction and Phase Separation Using Sn bath

Hideki Ono[1,*], Kenjiro Maeda[2], Kengo Kato[1]
[1]Department of Materials Science and Engineering, Faculty of Sustainable Design, University of Toyama, Toyama, Japan
[2]Graduate School of Science and Engineering, University of Toyama, Toyama, Japan
Email: ono@sus.u-toyama.ac.jp
*Corresponding author

Abstract

The smelting process for aluminum ore requires significant amounts of electricity, whereas recycling aluminum scraps consumes less energy. Accordingly, aluminum recycling is a critical issue for achieving carbon neutrality. Recycled aluminum contains not only the alloying elements present in the original scrap, but also various impurities introduced during the recovery process. Consequently, it is currently recycled into cast alloys, which tolerate higher impurity levels. To increase aluminum recycling rates in the future, recycling aluminum scrap into wrought alloys is essential. However, major components of aluminum alloys (Si, Mn, Fe, Ni, Cu, Zn, etc.) are difficult to remove using current pyrometallurgical processes. Therefore, it is necessary to develop a new method for removing impurities in Al, which enables the recycling of aluminum scraps into wrought aluminum alloys. This study investigated a method for removing Fe and Si from aluminum using extraction and phase separation with a tin bath. At about 873K, while aluminum is soluble in molten tin, silicon and iron are not. By utilizing the difference in solubility of Al, Fe, and Si in molten tin, aluminum can be selectively extracted into the tin bath from the Al-Fe-Si alloy, and the precipitated Fe and Si can be separated by phase separation. This study conducted experiments to verify the effectiveness of a method for removing Fe and Si. Precipitates of Si and Al_3Fe were observed in the upper layer of the sample, and these compounds were not detected in the bulk of the Al-Sn alloy. The Fe, Si, and Al contents of the Al-Sn alloy were analyzed using ICP-AES, and the results showed the effectiveness of this method.

Keywords: Al recycling; Iron removal; Silicon removal; Extraction; Phase Separation

The Effect of Grain Boundary Structure on Nucleation and Growth of q ($CuAl_2$) Precipitates in Al-5 wt% Cu

Gary J. Shiflet[1,*]
[1]Materials Science and Engineering, University of Virginia, Charlottesville, VA USA
*Email: gjs@virginia.edu

Abstract

This presentation examines the nucleation and growth kinetics of grain boundary allotriomorphs incorporating both boundary, D_b, and volume, D_v, diffusion of Cu. Solute distributions are also included in the analysis with a focus on grain boundary misorientations and their width, d, uncoupled from boundary diffusion formulations, i.e., (D_b d). A more detailed understanding of microstructure evolution kinetics in aluminum alloys was the research goal, particularly extending the analysis to calculate precipitate free zone (PFZ) width as a function of temperature and time. Experimentally, q precipitate allotriomorph density and growth on grain boundaries were measured using transmission electron microscopy in Al-5 wt% Cu as a function of grain misorientation, temperature and time. The effect of grain boundary structure on q precipitate densities and precipitate lengthening indicated that grain misorientation was of primary importance in explaining the measurements with the grain boundary plane orientation playing a secondary role. O-lattice modeling allowed investigation of grain boundary orientation on nucleation site density. Analytically, growth kinetics were analyzed using a modified Brailsford and Aaronson treatment of the collector plate mechanism. The precipitate length was determined to vary in a reciprocal manner as a function of misorientation between the two grains. The Cu concentration profile both along the grain boundary and in the matrix near the grain boundary was analyzed using a finite difference solution to the Fisher model of grain boundary diffusion. From these data, with appropriate models for the precipitate growth and grain boundary diffusivity, clarification of the relationship between grain boundary misorientation, width, and diffusion will be discussed. Acknowledgements to Dr. M. A. Cantrell and the US Department of Energy, Office of Basic Science, for support.

Keywords: grain boundary precipitation; nucleation; growth; diffusion

In situ Electron Microscopy - Data Analytics

Mitsuhiro Murayama[1,2]
[1]Materials Science and Engineering, Virginia Tech, Blacksburg, VA 24060, USA.
[2]Institute for Materials Chemistry and Engineering, Kyushu University,
Kasuga, Fukuoka 816-8580, Japan.
Email: murayama@vt.edu

Abstract

The application of data analytics tools to experimental outcomes has become an irreversible trend in scientific research. Although early attempts were sometimes misleading, data-driven approaches are now well-established and can significantly enhance the competitiveness of funding proposals and the impact of journal publications.

In the context of electron microscopy, data analytics plays a critical role in three key areas. First, it enables fully objective, data-driven operation. While often discussed alongside autonomous data collection (i.e., unmanned operation), the original intent was to choose the best-suitable analytical methods and operational parameters without relying on highly trained specialists. Second, it facilitates unbiased data processing. Third, it supports the integration and interpretation of multi-dimensional datasets—combining electron microscopy with other experimental techniques—to derive scientifically valid conclusions or uncover unexpected phenomena, thereby reducing labor-intensive iterative processes [1].

Unbiased data processing is particularly crucial for extracting meaningful insights from *in situ* experiments, which often capture multiple, interrelated phenomena. In such cases, subjective interpretation by experienced specialists has traditionally been necessary. However, recent advancements in imaging technologies now allow for the digital recording of real-time object dynamics at sub-millisecond resolution. This progress makes it increasingly feasible to extract quantitative and scientifically robust information with minimal prior knowledge. Our ongoing efforts focus on developing quantitative and unbiased methods for *in situ* data processing and analysis, which will be outlined in this presentation.

The integration of multiple experimental techniques often introduces complexity rather than clarity, i.e., brings chaos than cosmos. For instance, discrepancies between functional (e.g., magnetic) or macroscopic physical (e.g., bulk tensile) measurements and microstructural characterization are not uncommon. Machine learning offers a promising solution to bridge these gaps across different parameters and scales. As a demonstration of this approach, we will present an exploratory research project aimed at fabricating a novel superconducting phase.

Keywords: Transmission Electron Microscopy; dynamic (in situ) observation; microstructure; data analytics

[1] for example, Towards data-driven next-generation transmission electron microscopy, *Nature Materials*, **20**, 274–279 (2021).

High-Entropy Oxide Spinels as Functional Coatings for SOFC Interconnects: Structure and Properties

Mirosław Stygar[1*], Margarita Nowakowska[1], Ewa Durda[1], Marek Zajusz[1]
[1]Department of Physical Chemistry and Modelling, Faculty of Materials Science and Ceramics, AGH University of Krakow, Krakow, Poland.
Email: stygar@agh.edu.pl
*Corresponding author

Abstract

This work presents the synthesis, structural analysis, and properties of high-entropy spinels within the Co-Cr-Fe-Mg-Mn-Ni-O system in terms of application as protective layers for interconnects for solid oxide fuel cell (SOFC) technology. Single-phase spinels, specifically $(Co,Cr,Fe,Mn,Ni)_3O_4$, $(Cr,Fe,Mg,Mn,Ni)_3O_4$, and $(Co,Cr,Fe,Mg,Mn)_3O_4$, were successfully synthesized by modified Pechini method. All materials exhibited similar thermomechanical properties, with thermal expansion coefficients ranging from 8.8 to 9.8·10 K^{-1}, suggesting compatibility with materials used in SOFC technology, particularly interconnects.

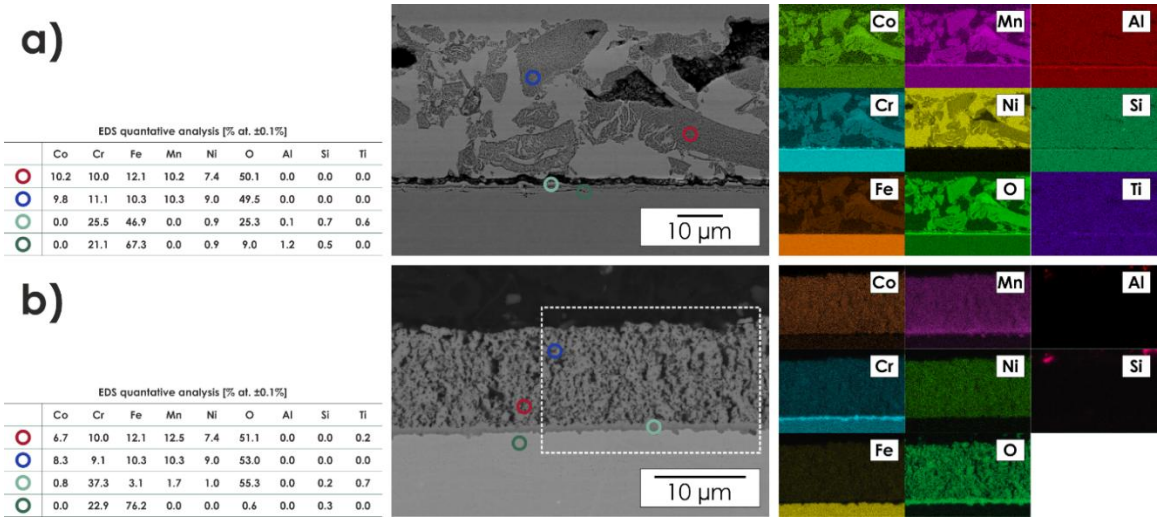

Fig. 1. SEM Cross-sections and EDS mapping results of Crofer 22APU-$(Co,Cr,Fe,Mn,Ni)_3O_4$ composite after oxidation at 800 °C for 100 h in the air: a) screen printing method; b) electrophoresis method.

Drawing parallels to conventional spinels and based on the electrical and thermomechanical characteristics of the studied high-entropy spinels, their use as protective-conductive coatings for SOFC interconnects is proposed. Taking into account the inherent traits of high-entropy systems, such as lattice distortion that may influence cation diffusion rates, these materials may offer notable advantages for SOFC applications, particularly for corrosion resistance and mitigating Cr-poisoning effects.

Preliminary tests on the application of these coatings on Crofer 22APU ferritic stainless steel, along with an initial performance evaluation of the ceramic/metallic composite system, were also conducted.

Time-of-Flight Spectroscopy for Exploring Electron Scattering in 2D Materials and Ultrathin Films

Ilona Müllerová[1*], Ivo Konvalina[1], Aleš Paták[1], Lukáš Průcha[1], Jakub Piňos[1], Michal Štulpa[1], Veronika Pizúrová[1], Tomáš Fořt[1], Eliška Materna Mikmeková[1]
[1]Department of Electron Microscopy, Institute of Scientific Instruments of the CAS, v. v. i., Brno, Czech Republic
Email: ilona.mullerova@isibrno.cz
*Corresponding author

Abstract

A deep understanding of electron scattering at very low energies is crucial for advancing electron spectroscopy and next-generation electronic materials, yet reliable inelastic mean free path data remain scarce. Here, we study scattering in 2D materials and ultrathin films under both transmission and reflection conditions.
Our approach combines a custom time-of-flight (ToF) spectrometer [1] with density functional theory (DFT) modeling, benchmarked against graphene [2]. The ToF device, integrated into an ultra-high vacuum low-energy electron microscope, enables simultaneous imaging and low-energy loss spectra acquisition.
For samples, commercial 2D materials were deposited on copper grids with lacey carbon supports. Nanometer-thin foils were fabricated by graphene CVD and subsequent magnetron sputtering. Experimental spectra are compared with DFT-derived energy-loss functions, providing new insight into electron scattering in low-dimensional systems.

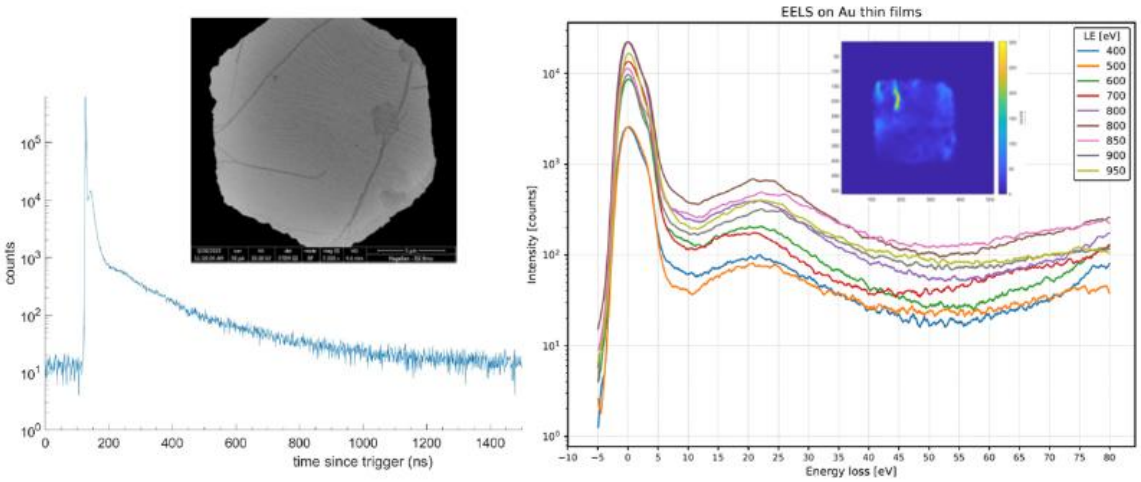

Acknowledgement:
The research was supported by the Technology Agency of the Czech Republic, grant number TN02000020 together with institutional support RVO:68081731. With support of Strategy AV21, program Breakthrough Technologies for the Future – Sensing, Digitisation, Artificial Intelligence and Quantum Technologies.

References:

1. I. Konvalina, et al., Nanomaterials 2021, 11, 2435
2. A. Paták, et al., Phys. Rev. B 2025, 111, 125113

Keywords: 2D material; ultrathin film; ToF spectroscopy; graphene

Nature of different deformation modes of a new metastable body-centered cubic Ti35Hf25Zr25Nb5Ta5Al5 high entropy alloy

Sushree P Mohapatra[1], Rajeshwar R. Eleti[2], Avala Lavakumar[1,*]
[1]Department of Metallurgical and Materials Engineering, Indian Institute of Technology Ropar, Punjab, India
[2]Department of Metallurgical and Materials Engineering, Indian Institute of Technology Roorkee, Uttarakhand, India.
Email: lava@gmail.com
*Corresponding author

Abstract

Titanium alloys are widely used in aerospace and biomedical sectors due to their high specific strength and corrosion resistance. Extending Ti alloy design strategies to high-entropy alloys (HEAs) has recently enabled the development of Ti-rich body-centered cubic (BCC) HEAs that exhibit remarkable strain-hardening and ductility through transformation-induced plasticity (TRIP) and twinning-induced plasticity (TWIP). Such deformation mechanisms provide a route to overcome the strength–ductility trade-off typical in metallic materials. In this work, we investigate a newly designed metastable non-equiatomic BCC-HEA, $Ti_{35}Hf_{25}Zr_{25}Nb_5Ta_5Al_5$, developed using the bond order (Bo)–mean d-orbital energy (Md) approach combined with molybdenum equivalence (Mo_{eq}) as an additional design parameter. The alloy was synthesized via vacuum arc melting, thermomechanically processed, and systematically characterized to probe its deformation behavior. Microstructural studies revealed the interplay of dislocation slip, martensitic β→α" transformation, and twinning during tensile loading, highlighting the complex synergy of multiple deformation modes. Our findings demonstrate that tailoring phase stability through Bo–Md and Mo_{eq} effectively enhances yield strength and strain-hardening without compromising ductility. The severe lattice distortion effect inherent to HEAs is further expected to interact with Mo_{eq}, enabling unique phase transformation pathways. This study establishes a pathway for designing metastable HEAs with balanced strength, ductility, and thermal stability, providing promising candidates for next-generation structural applications in automotive, construction, and high-temperature environments.

Keywords: High-entropy alloys (HEAs); Titanium alloys; Molybdenum equivalence, TRIP/TWIP Ti alloys.

Lithium Nitrate Tailored Low-Temperature Electrolyte with a high voltage window over 5.5V and operation at wide-temperature-range

Zhaojun Liu[1,2], Jiaxuan Feng[1], Rui Yang[1], Shen-ao Wang[1], Xiaochen Wu[1], Xiangyu Zhang[1], Sujuan Cheng[4], Ning Liu[3], Teng Long[1*], Pengchao Si[1*]
[1]Key Laboratory for Liquid-Solid Structural Evolution and Processing of Materials (Ministry of Education), School of Materials Science and Engineering, Shandong University, Jinan 250061, China
[2]Institute of Industrial Technology, School of Mechanical, Electrical and Information Engineering, Shandong University, Weihai 264209, China
[3]Wuhan Institute of Marine Electric Propulsion, Wuhan 430064, China
[4]Dongying Vocational Institute, Dongying 257000, China
*Corresponding Author. E-mail addresses: pcsi@sdu.edu.cn (P. Si), tenglong@sdu.edu.cn

Abstract

Achieving stable cycling of lithium-ion batteries with high active material loading across wide temperature ranges remains notably challenging. While carbonate-based electrolytes dominate commercial applications for their graphite compatibility, their strong solvent-ion interactions and elevated viscosity below -20°C significantly compromise low-temperature performance. Here, we address this limitation through a rationally designed electrolyte combining low-melting carboxylate ester solvents with fluoroethylene carbonate and lithium nitrate additives. This formulation enables weak solvation structures and stabilizes electrode interfaces, supporting full cells (NCM811//G) with 3.5 mAh/cm2 cathode loading under extreme conditions. The optimized system achieves 70% capacity retention at -40°C (0.1C rate) relative to room temperature performance, sustains 89% capacity after 350 cycles at 25°C (1C rate), and maintains functionality at 70°C. This work establishes a nitrate-enhanced electrolyte design paradigm for temperature-resilient batteries, demonstrating practical viability through multi-physics coordination strategies.

Keywords: Lithium nitrate; High active material; Wide-temperature; Lithium-ion battery

Motivational Concepts for the Nobel Prize 2025: Development of Metal–Organic Frameworks (MOFs)

Brij Mohan[1,2*]
[1]Centro de Química Estrutural, Instituto Superior Técnico, Universidade de Lisboa (ULisboa)-1049-001, Portugal
[2]Faculty of Science, Chiang Mai University, Chiang Mai, 50200 Thailand
Email: brij.mohan@tecnico.ulisboa.pt
*Corresponding author

Abstract

Metal–Organic Frameworks (MOFs) have transformed materials science with their remarkable structural flexibility, tunable porosity, and diverse functional properties. This lecture explores the scientific principles that establish MOFs as one of the most innovative classes of materials in modern chemistry—and strong contenders for Nobel Prize recognition in 2025. The narrative focuses on three inspiring concepts: "from useless to useful," "from wooden to crystal," and "MOFs that can cover a football ground." These ideas illustrate the evolution of MOFs from simple molecular structures to large crystalline architectures with unmatched precision and scalability. Driven by modular synthesis, coordination chemistry, and reticular design principles, MOFs have linked molecular chemistry to materials engineering, enabling groundbreaking advances in gas storage, catalysis, energy conversion, environmental cleanup, and biomedical applications. Tracing their development from basic frameworks to multifunctional, stimuli-responsive systems, the lecture highlights not only scientific innovation but also the human creativity, perseverance, and vision that transformed a once "useless" idea into a leading material frontier—embodying the core of Nobel-worthy discoveries.

Keywords: Metal–Organic Frameworks (MOFs); Design and Generations; Defects and Engineering; Advanced Applications

Investigating the solidification of 'dirty' recycled aluminium alloys with X-ray imaging and artificial intelligence

Enzo Liotti[1,*], Andrew Zisserman[2], Patrick Grant[1], Shikang Feng,[1,3], Andrew Lui[1], Alessandro De Nardi[1], Akash Aggarwall[1], Shun Yang[1], Mehmet Bozkurt[1], Carlos Arteta[1], Simon H. Hogg[4], Yuki Zhang[4], Mika Shearwook[5], Dominic Banks[5], Tim Nicholls[5], Sion Richards[5] and Matthew D Wilson[5]

[1]Department of Materials, University of Oxford, Parks Road, OX1 3PH, UK
[2]Department of Engineering, University of Oxford, Parks Road, OX1 3PH, UK
[3]School of Engineering and Informatics, University of Sussex, Brighton, BN1 9RH, UK
[4]Department of Materials, Loughborough University, Loughborough, LE11 3TU, UK
[5]Science and Technology Facilities Council, Rutherford Appleton Laboratory, Harwell Science and Innovation Campus, Didcot, OX11 0DE, UK

Email: enzo.liotti@materials.ox.ac.uk
*Corresponding author

Abstract

As aluminium production shifts toward higher fractions of scrap, the long-held notion of "clean metal" becomes untenable: recycled feeds typically carry elevated impurity levels, especially Fe and Si. Even small additions of these elements promote detrimental microstructural defects and Fe/Si-rich intermetallic compounds (IMCs). Conventional mitigation during primary alloy fabrication uses minor additions of "neutralising" elements (e.g., Mn, Cr, Co) to stabilise compact, cubic α-AlFeSi IMCs instead of the more deleterious, plate-like β-AlFeSi. However, most evidence underpinning these strategies derives from commercial alloys with relatively low Fe (~0.6 wt.%), and the mechanisms governing phase selection at higher Fe contents relevant to recycled feedstocks remain unclear. Progress has also been limited by a reliance on post-solidification characterisation, which obscures the dynamic interplay between solidification conditions, solute segregation and phase formation.

This study presents real-time observations of phase selection and morphological evolution of Fe-rich IMCs during solidification of recycled Al alloys with elevated Fe concentrations (up to 2.5 wt.%). We track nucleation and growth pathways of critical Fe-bearing phases and quantify how thermal history and local chemistry steer morphology from plate-like to more compact forms. The resulting insights clarify the conditions under which α- versus β-AlFeSi are favoured at higher Fe levels and relate these transitions to feeding behaviour and hot-tear susceptibility. The findings provide a mechanistic basis for alloy and process design that enables greater use of lower-grade scrap while controlling defect formation.

Keywords: Al recycling; In-situ X-ray imaging; Artificial intelligence.

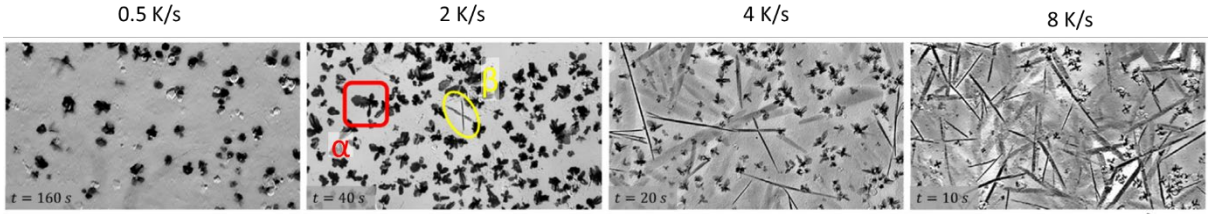

Figure 1: Effect of cooling rate on the solidification of a 365 +2.5 wt%Fe alloy.

Filtered Secondary Electron Imaging: Energy- and Angle-Resolved Contrast in SEM

Šárka Mikmeková[1*], Ivo Konvalina[1], Kenji Matsuda[2], and Ilona Müllerová[1]
[1]ISI Brno CAS, Electron Microscopy Department, Brno, Czech Republic
[2]University of Toyama, Faculty of Sustainable Design, Department of Materials Design and Engineering, Academic assembly, Toyama, Japan
Email: sarka@isibrno.cz
*Corresponding author

Abstract

Secondary electrons (SEs) constitute one of the most critical imaging signals in scanning electron microscopy (SEM). Recent advances in SEM technology have introduced highly sophisticated multi-detector systems capable of simultaneous signal acquisition and effective separation of electrons based on their energy and emission angle. Such filtration of SEs enables selective imaging, offering enhanced sensitivity to variations in surface topography, chemical composition, and electronic structure. In this study, we investigate the effects of energy- and angle-filtered SE imaging across a wide range of materials, including non-ferrous alloys. The results demonstrate that contrast variations in filtered SE micrographs provide complementary information on material properties, enabling a more comprehensive characterization of complex surfaces.

Keywords: SEM; secondary electrons; electron filtering

Friction Surfacing Deposition of High-Strength Aluminum Alloys: From Homogeneous Al-Cu-Li to Heterogeneous Al-Cu-Li/Al-Zn-Mg-Cu Structures

Shuwei Duan[1,*], Yimeng Ye[1], Fuqiang Guo[2], Yong Zou[2], Kenji Matsuda[3],
[1] College of Nuclear Equipment and Nuclear Engineering, Yantai University, Yantai 264005, P. R. China
[2] Key Laboratory for Liquid-Solid Structural Evolution and Processing of Materials (Ministry of Education), Shandong University, Jinan, 250061, P. R. China
[3] Department of Materials Design and Engineering, Faculty of Sustainable Design, University of Toyama, Toyama 930-8555, Japan
Email: shuwei01@163.com
*Corresponding author

Abstract

Friction surfacing deposition additive manufacturing (FSD-AM) offers a solid-state approach for fabricating high-performance aluminum alloy components with complex geometries. This study explores the microstructure and mechanical properties of both homogeneous Al–Cu–Li and heterogeneous Al–Cu–Li/Al–Zn–Mg–Cu composite structures. For the monolithic Al-Cu-Li alloy, FSD-AM produces fine, equiaxed grains with heterogeneous size distribution, contributing to excellent ductility. A key finding is the formation of distinct ultrafine-grained bands at the interfaces between successive Al-Cu-Li layers, characterized by a unique crystallographic orientation and high recrystallization fraction. Post-treatment strategies reveal that solution treatment followed by pre-rolling and aging significantly enhances strength through high-density T_1 phase precipitation. In the composite structure, sound interfacial bonding is achieved between dissimilar alloys without extensive elemental diffusion. The Al–Zn–Mg–Cu layers show superior strength and finer grains due to enhanced dynamic recrystallization, while the Al–Cu–Li layers offer better ductility. Interfacial regions display distinct recrystallization behaviors and strain localization, influenced by alloy-specific thermal-mechanical responses. This work provides critical insights into the interfacial design and property control of high-strength aluminum alloy heterostructures via solid-state additive manufacturing.

Keywords: Friction surfacing deposition; High strength aluminum alloy; Heterogeneous structures; Microstructure; Mechanical properties

Rethinking Metal Forming: Merging Old Wisdom with New Additive Technologies

Anchalee Manonukul[1*]
[1]National Metal and Materials Technology Center (MTEC), National Science and Technology Development Agency (NSTDA), 111 Thailand Science Park, Paholyothin Road, Klong 1, Klong Luang, Pathumthani 12120, Thailand
*Email: anchalm@mtec.or.th

Abstract

Metal forming has shaped the foundation of modern manufacturing for centuries, guided by principles of deformation, densification, and surface integrity. Today, as additive manufacturing redefines how we create metallic components, these long-standing concepts are being rediscovered and reinterpreted through new lenses. This talk explores how traditional metal forming wisdom—such as metal injection moulding (MIM) and shot peening —can be merged with emerging metal extrusion (MEX) additive technologies. By drawing parallels with processes like shot peening and sintering, the talk highlights how mechanical and microstructural control can be embedded into layer-by-layer fabrication. The result is a vision of manufacturing that unites tradition and innovation—reshaping not only how metals are formed, but how we think about forming itself.

Keywords: MEX; MIM; Shot Peening

Microstructure and Properties of Nano-TiC Modified Mar-M247 Superalloy Processed by Wire Arc Additive Manufacturing

Zhu Zihao[1,2], Wu Dongting[1,3*], Liu Yue[2], Yin Haidong[2], Zou Yong[4,*]
[1]Key Laboratory of Liquid-Solid Structural Evolution and Processing of Materials, Ministry of Education, Shandong University， Jinan, Shandong, 250061, China
[2]School of Materials Science and Engineering, Shandong University, Jinan, Shandong, 250061, China
[3]State Key Laboratory of Clean and Efficient Turbomachinery Power Equipment, Deyang, Sichuan, 618000, China
[4]Shandong Engineering & Technology Research Center for Modern Welding, Shandong University, Jinan, Shandong, 250061, China
Email: wudongting@sdu.edu.cn, yzou@sdu.edu.cn
*Corresponding author

Abstract

The issue of hot cracking in precipitation-strengthened nickel-based superalloys during Wire Arc Additive Manufacturing (WAAM) is addressed. A method is proposed for incorporating nano TiC particles into Mar-M247 superalloy cored wire, and Cold Metal Transfer (CMT) process parameters are optimized for layer deposition. It is found that the nano TiC particles act as heterogeneous nucleation sites, markedly refining the grain structure and disrupting the continuous growth of columnar crystals, thereby preventing the formation of crystalline cracks. The tensile strength of the resultant superalloy surpasses that of conventional Mar-M247 baseplates. After subsequent solution treatment and aging, a minor decrease in strength and a slight expansion in grain size are observed; however, ductility is substantially improved. A novel strategy is presented for enhancing the processability and overall properties of highly alloyed nickel-based superalloys in additive manufacturing.

Keywords: Wire Arc Additive Manufacturing; nickel-based superalloy; nano TiC; hot cracking; microstructure

Joining ultrafine grained materials using FSW and LBW techniques

Malgorzata Lewandowska[1*], Marta Lipinska[1], Florian Pixner[2], Andreas Hütter[2], Norbert Enzinger[2]
[1] Warsaw University of Technology, Faculty of Materials Science and Engineering, Warsaw, Poland
[2] Graz University of Technology, Institute of Materials Science, Joining and Forming, Graz, Austria
Email: malgorzata.lewandowska@pw.edu.pl
*Corresponding author

Abstract

Ultrafine-grained (UFG) materials are known to exhibit superior mechanical properties compared to their coarse-grained (CG) counterparts, owing to the high density of structural defects such as grain boundaries and dislocations. However, UFG materials suffer from reduced thermal stability, leading to rapid grain growth at elevated temperatures. This presents a challenge for high-temperature post-processing operations, such as welding.

In this work, two UFG materials are investigated: commercially pure aluminium and an Al-Mg-Si alloy. Two joining techniques are applied. The first is the solid-state method of friction stir welding (FSW), in which intense plastic deformation joins the materials at temperatures above room temperature but below their melting point. In FCC metals such as aluminium, dynamic recrystallization occurs during FSW, affecting both microstructure and weld properties. The second method is electron beam welding (EBW), a fusion process characterized by highly concentrated heat input, which minimizes the size of fusion and heat-affected zones.

The welds are comprehensively analyzed in terms of microstructure evolution using LM, SEM/EBSD, TEM, and STEM, and the results are correlated with mechanical properties such as microhardness and tensile strength. Comparisons are made between the two welding techniques, as well as with CG counterparts.

For FSW, the stir zone exhibited grain coarsening to ~4–5 µm compared to the ~1 µm grain size of the UFG base material. This resulted in reduced mechanical properties relative to the UFG base materials but still superior to annealed aluminium. EBW, by contrast, induced significant microstructural changes, including grain growth, grain shape modifications, an increase in high-angle grain boundaries, and dissolution of strengthening precipitates in the Al-Mg-Si alloy. These factors strongly influenced the mechanical performance of the welds. Post-welding heat treatment is also explored as a way to enhance the mechanical performance of the welds.

Keywords: ultrafine grained materials; friction stir welding; laser beam welding

Acknowledgments: Research was funded by Warsaw University of Technology within the Excellence Initiative: Research University (IDUB) programme.

Recent Research on Electroplating Technologies for Reducing Gold Consumption

Injoon Son[1,*]

[1] Department of Materials Science and Metallurgical Engineering, School of Materials Science and Engineering, Kyungpook National University, Korea
Email: ijson@knu.ac.kr
*Corresponding author

Abstract

Gold alloy electroplating is widely used in electrical connectors for electronic components. These connectors are typically produced by depositing a nickel barrier layer and a gold alloy top layer onto copper alloy substrates. The nickel layer suppresses copper diffusion, while the gold layer ensures low contact resistance and reliable solder bonding. Although Au–Co and Au–Ni alloy coatings are commonly employed due to their high hardness, they contain more than 99.5 wt% gold, making them effectively similar to pure gold coatings. Recent increases in gold prices have driven strong demand for selective gold plating and alternative alloy systems that can reduce overall gold consumption without compromising reliability. Also, thermal aging of conventional Au–Co and Au–Ni coatings led to significant Ni diffusion toward the gold surface, resulting in increased contact resistance and degraded solderability. This study aims to develop gold alloy electroplating processes that (i) reduce gold usage, (ii) maintain or improve electrical contact performance, and (iii) enhance solderability and long-term reliability. Recently, Au–Ag alloy plating was applied to increase alloy content and reduce gold consumption. Au–Sn alloy plating systems are also investigated as alternatives to conventional Au–Co and Au–Ni coatings.

Keywords: Au (Gold); Au-Sn; Intermetallic (IMC); Contact resistance; Ni diffusion

Effect of post weld heat treatment on the microstructure and hardness distribution of TIG welded Ti-6Al-4V/Ti-CP joints

Sai Manh Thang[1], Nguyen Anh Xuan[2], Vu Viet Quyen[2], Pham Mai Khanh[3,*], Nguyen Duong Nam[2,*]

[1] Military Science and Technology Institute, Hanoi, Vietnam

[2] School of Mechanical Engineering, Vietnam Maritime University, Hai Phong, Vietnam

[3]School of Materials, Hanoi University of Science and Technology, Hanoi, Vietnam

Email: khanh.phammai@hust.edu.vn, namnd.khcs@vimaru.edu.vn

*Corresponding author

Abstract

The present study examined the evolution of microstructure and hardness in dissimilar welded joints between Ti-6Al-4V (ASTM Grade 5) and commercially pure titanium (Ti-CP, ASTM Grade 2), with particular emphasis on the effects of post-weld heat treatment (PWHT). The joints were fabricated using the tungsten inert gas (TIG) welding process. PWHT was conducted through several regimes, including annealing, solution treatment at 890 °C followed by water quenching, and subsequent artificial aging at 400 °C for 4 h, 525 °C for 1, 4, and 7 h, and 650 °C for 4 h. Microstructural analysis and phase characterization revealed the formation of a distinct transition zone at the weld interface with an average thickness of 7–8 µm. To evaluate the mechanical response, Vickers microhardness traverses were measured across the weld cross-section, beginning from the Ti-CP side at the weld root and extending into the Ti-6Al-4V fusion zone. The resulting hardness profiles clearly reflected the influence of PWHT on the interfacial region between Ti-CP and Ti-6Al-4V. Quantitatively, the hardness differences between the peak values in the transition zone and the Ti-CP base metal were determined as 234, 243, 211, 365, 124, and 382 HV, respectively, under the investigated conditions. Corresponding hardness differences relative to the Ti-6Al-4V fusion zone were 182, 79, 30, 80, 80, and 113 HV. These findings highlight the pronounced heterogeneity of the welded joints and underscore the significant role of PWHT in tailoring the microstructural features and mechanical performance of Ti-6Al-4V/Ti-CP dissimilar weldments

Keywords: Ti6Al4V; Ti- CP GRADE 2; TIG welding; Microstructure; Hardness

Research Project on Recycling of Aluminum in Toyama
- Joining of Recycled Aluminum Alloy -

Toshiya Shibayanagi[1,*] , Kensuke Shimode[2], Kazufumi Nomura[3]
[1]Aluminum Research Center, University of Toyama, 180 Futagami-machi, Takaoka, Toyama, 933-8588, Japan
[2]Division of Materials and Manufacturing Science, Osaka University, 2-1 Yamada-oka, Suita, Osaka 565-0871, Japan
[3]Graduate Student, University of Toyama, 3190 Gofuku, Toyama, 930-8555, Japan
Email: toshiya@sus.u-toyama.ac.jp
*Corresponding author

Abstract

University of Toyama has been promoting a national project called “COINEXT” since 2024 focused on aluminum recycling with the support of the Japan Science and Technology Agency (JST). This project aims to establish a comprehensive system that begins with the collection of scrap materials and encompasses sorting, refining and impurity removal, alloy design, extrusion processing, surface treatment, welding and joining, dross treatment, and the development of a quality assurance system through data science. The project brings together academic experts from Tohoku, Osaka, Waseda, and Kansai Universities, in collaboration with local governments and stakeholders from the aluminum sector.

Unlike alloy design, recycling is a subtractive approach to materials science. Recycled aluminum, even after undergoing refining, may retain various alloying elements. While its composition may conform to standard specifications, unforeseen phenomena may arise in aging characteristics, extrusion performance, weldability and so on. In welding processes, recycled aluminum is significantly affected by residual impurities and internal strain accumulated during its preceding processing stages. Consequently, recycled materials may be susceptible to weld cracking or various joint failures under real-world operating conditions.

The objective of this research is to elucidate, through experimental methods, the welding behavior of recycled aluminum alloys. Friction stir spot welding is applied to extruded specimens of a simulated recycled aluminum alloy equivalent to 6063, and the resulting joint microstructure and mechanical characteristics are examined.

Friction stir spot welding was conducted at 7000 RPM by stacking a simulated recycled aluminum alloy sheet atop a standard 6063 aluminum alloy sheet. The recycled alloy demonstrated higher resistance to plastic flow compared to the standard material, which is attributed to decreased deformability resulting from impurity elements. These findings highlight that recycled materials can adversely affect formability and weldability, underscoring the need for effective impurity reduction during the refining process. In addition to this case study, we also plan to discuss the importance of evaluating weldability in relation to recycling technologies.

Keywords: recycling; aluminum alloys; friction stir spot welding, weldability

Influence of Altermagnetism on the Orbital Hall Effect in RuO_2

Lishu Zhang[1,2,3,*]
[1] School of Materials Science and Engineering, Shandong University, Jinan, 250061, China
[2] Department of Physics and Astronomy, University of Nebraska, Lincoln, NE 68588, USA
[3] Peter Grünberg Institute and Institute for Advanced Simulation, Forschungszentrum Jülich, 52425 Jülich, Germany
Email: lishu.zhang@sdu.edu.cn
*Corresponding author

Abstract

In recent years, RuO_2 has garnered significant attention as a key material for understanding the fundamental properties of exchange-split collinear antiferromagnets, now known as altermagnets. However, there have been conflicting reports regarding the presence of magnetism in RuO_2. Their study reveals that RuO_2 does not exhibit antiferromagnetic (AFM) order in the bulk crystal, contrary to previous reports suggesting AFM ordering with a Ru magnetic moment of ~0.05μB. And the previous work suggests that the magnetic spin Hall effect plays a significant role in the generation of spin currents in RuO_2. In this work, we employ first-principles calculations based on density functional theory (DFT) to explore the effect of magnetism on the orbital Hall effect in this nominally altermagnetic compound. By varying the Hubbard U correction to DFT, we find that electron-electron correlations strongly affect the magnetism in RuO_2, leading to a transition from a nonmagnetic to altermagnetic state with the increasing U value. We further compute the spin and orbital Hall conductivities of bulk RuO_2 across its nonmagnetic and magnetic phases. Our results demonstrate that the orbital Hall effect in RuO_2 is correlated in a non-trivial way with the emergence of altermagnetism in this compound. Our findings provide new insights into the magnetic and transport properties of RuO_2 and offer a new way to reveal the presence of altermagnetism in this material.

Keywords: Altermagnetism; Ruthenium Dioxide; Orbital Hall Effect

Porous Carbon for Sustainable Construction Materials

Muduo Li[1], Yuying Zhang[1], Daniel C. W. Tsang[1,2*]
[1]Department of Civil and Environmental Engineering, The Hong Kong University of Science and Technology, Hong Kong, China
[2]Research Center on Decarbonization Technology, The Hong Kong University of Science and Technology, Clear Water Bay, Hong Kong, China
Email: cedan@ust.hk
*Corresponding author

Abstract

Porous carbon holds transformative potential for sustainable construction by uniting structural performance, functional versatility, and climate resilience. As exemplified by architected biochar, its tunable microstructure enables enhanced strength, ductility, and self-sensing capabilities in cementitious systems. Moving beyond conventional filler roles, porous carbon can serve as an active design element, bridging material science and structural engineering. Unlocking this potential requires architecture-aware approaches that link internal topology to macroscopic behavior, to drive the next generation of low-carbon, high-resilient intelligent infrastructure.

Keywords: Architected biochar; Topology-fracture interaction; Resilient cementitious composites; Multifunctional infrastructure; Smart construction

In-Situ correlative Raman spectroscopy and SEM analysis from Renishaw

Dr. Tan See Hua
Renishaw Plc.

Raman spectroscopy is a non-contact and non-destructive optical technique which is superior at providing detailed information on the identity and chemical structure of materials. Each molecule has its own unique Raman spectrum, which provides insights into various chemical bonds and their characteristics.

On the other hand, scanning electron microscopy (SEM) deploys an electron beam to probe the sample instead of a visible light source, it provides much higher magnifications and can resolve structures down to a few nanometers. In addition to producing highly detailed images, conventionally, SEM can be combined with energy-dispersive X-ray spectroscopy (EDS) to reveal the elemental composition of the sample. However, SEM-EDS does not provide information about chemical bonds or structure within a sample.

In this presentation, we would like to showcase recent technological advancement from Renishaw on the integration of a Raman spectroscopy system with a scanning electron microscope (SEM) and present several applications demonstrating the advantages of correlative microscopy using these technologies. The molecular information provided by Raman spectroscopy complements the ultrastructural details from SEM imaging, providing comprehensive insights into the chemistry and structure of the samples.

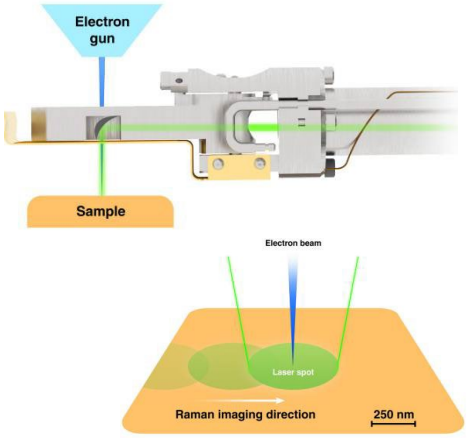

Gold Sponsor (Bara Scientific Co., Ltd.)

Advanced Surface and Interface Analysis Using the Fully Automated AXIS Supra^{+} System

Praween Chaiya
Bara Scientific Co., Ltd.

Surface and interface chemistry governs the functional behavior of many advanced materials, including thin films, semiconductors, catalysts, nanomaterials, and hybrid organic–inorganic systems. X-ray Photoelectron Spectroscopy (XPS) is a powerful technique for probing elemental composition, oxidation states, and electronic structure within the top few nanometers of a material. This abstract highlights the capabilities of the fully automated Kratos AXIS XPS platform, which integrates Ultraviolet Photoemission Spectroscopy (UPS), Hard X-ray Photoelectron Spectroscopy (HAXPES), and the Gas Cluster Ion Source (GCIS) to enable comprehensive surface and interface characterization with a spatial resolution at the level of 1 micron.

Kratos Analytical Ltd, a Shimadzu Group company, has over five decades of experience in XPS development. The fully automated system integrates high-sensitivity optics, automatic alignment, stable charge neutralization, and seamless multi-technique operation. These automated functions improve measurement consistency and user efficiency while ensuring long-term stability. In Thailand, XPS adoption continues to grow across academic and industrial sectors, supported by Bara Scientific as the official distributor.

Three essential aspects highlight the relevance of this fully automated system for modern materials research. First, its chemical state sensitivity enables accurate differentiation of oxidation states and bonding environments. Second, its surface specificity makes it ideal for thin films, perovskites, MXenes, and other 2D materials where properties differ significantly from the bulk. Third, electronic structure analysis using UPS, demonstrated through a perovskite thin-film case study, where the work function shift observed after GCIS cleaning confirms the influence of adventitious carbon and highlights the capability of GCIS to reveal the true surface electronic structure of the material with high accuracy.

The fully automated AXIS Supra^{+} platform integrates all essential surface-analysis capabilities into a single system, providing a powerful and reliable solution that supports advanced research in interface engineering, materials innovation, and next-generation electronic devices.

Correlation Between Hardness, Tensile Properties and Microstructure in Cold-Rolled and Aged of Al-Mg-Si-Cu Alloy

Vu Ngoc Hai[1*], Seungwon Lee[1], Taiki Tsuchiya[1], Tetsuya Katsumi[2], Kazuhiko Kita[2], Kenji Matsuda[1]
[1]University of Toyama, Toyama, Japan
[2]YKK Corporation, Toyama, Japan
Email: vungochaibk61@gmail.com
*Corresponding author

Abstract

This study investigates how pre-aging and deformation applied after solution heat treatment affects the precipitation behavior and mechanical properties obtained during artificial aging. A comprehensive approach, including microstructural analysis, hardness evaluation, and tensile testing, was used to evaluate the differences between the deformed and non-deformed conditions. Transmission electron microscopy (TEM), specifically scanning transmission electron microscopy (STEM) with high-angle annular dark-field (HAADF) imaging, was used to clarify the correlation between precipitation characteristics and mechanical properties in an Al-0.98%Mg-0.36%Si-1.0%Cu (wt.%) alloy. The results showed that deformation significantly enhanced age-hardening behavior, the non-deformed conditions showed lower hardness and did not reach peak aging after one week at 160℃. In contrast, the deformed conditions achieved peak hardness more rapidly and maintained a higher hardness during over-aging, due to accelerated precipitation formation promoted by dislocation. These findings highlight the role of thermomechanical processing on tailoring the microstructure and achieving a desirable balance of strength and ductility. This study offers a foundation for improving thermomechanical processing routes of age-hardenable alloys.

Keywords: deformation; artificial aging; aluminum; precipitation; STEM.

Precipitation behavior in natural aged of Al-Mg-Si alloy containing Silicon in excess at peak hardness

Tran Sy Quan[1], Seungwon Lee[2], Taiki Tsuchiya[2], Ahmed Abrar [2], Susumu Ikeno[2], Kenji Matsuda[2]
[1]Graduate school of science and Engineering for Education, University of Toyama, Toyama, 930-8555, Japan
[2]Graduate school of science and Engineering for Research, University of Toyama, Toyama, 930-8555, Japan
Email: quants.mse@gmail.com
*Corresponding author

Abstract

Al-Mg-Si alloys (6000 series) constitute an important heat-treatable alloy system. They are applied for various industries since they have unique mechanical properties such as good formability and good corrosion resistant. In practice, the processed components often require a delay ranging from several hours to several months for assembly or transportation before being subjected to artificial aging. During this waiting period, Natural aging (NA) inevitably occurs, and this phenomenon significantly alters the hardness response during the final aging process. In this study, three Al-Mg-Si alloys with different compositions: Al-1.6Mg_2Si, Al-1.6%Mg_2Si-ex. 0.4%Mg, and Al-1.6%Mg_2Si-ex. 0.4%Si (mass%) were investigated the hardness and microstructure. The sample was cast and homogenization at 575 ℃ for 10 hours. Then, it was cut into smaller pieces followed by heat treatment at 575 ℃ for 1 hour and immediately quenched in ice-water (0℃). The NA condition was performed for various time and the final aging at 200℃. The aged sample was used for Vickers Micro Hardness and the Transmission Electron Microscopy. The results show that the samples reach a peak aging at 200 min at 200 ℃ and value of peak hardness decrease in all stage during NA. The microstructure of Al-1.6%Mg_2Si-ex. 0.4%Si (mass%) for peak aging was observed by TEM consisting of β" phase, which is the main precipitates strength to contribute increasing hardness of Al alloys. The number density of precipitates was decreased with NA performed that indicated the negative effect of NA. This tendency in case of balance and ex. Mg alloys is quite similar. In this study, the influence of NA on the precipitation microstructure during final aging will be examined. The number density, precipitate length and precipitate types will be characterized to clarify the negative effects of NA in Al alloys, which is represented a critical issue for practical application.

Keywords: Natural Aging, precipitation, TEM, Al1.6Mg_2si ex 0.4Si

Formation Mechanism and Microstructural Evolution of Mullite Engobe beneath Celadon Glazes from Rice Husk Ash for Stoneware Wall Tiles

Nophawan Dechboon[1,*], Worawut Tarat[1], Tida Tungyai[1]
[1]Faculty of Art and Architecture, Rajamangala University of Technology Lanna, Chiang Mai, 50300, Thailand
Email: aofdechboon@gmail.com, aof_iccmu@hotmail.com, nophawan@rmutl.ac.th
*Corresponding author

Abstract

This study investigates the formation mechanism and microstructural evolution of mullite engobe beneath celadon glazes derived from rice husk ash, applied to stoneware wall tiles from the Wiang Bua kiln. The rice husk ash was employed as a sustainable silica-rich raw material to promote mullite formation during firing at 1200-1250 °C. Phase development was characterized by X-ray diffraction (XRD) and scanning electron microscopy (SEM/EDS), revealing the progressive crystallization of mullite needles and their interlocking network within the engobe layer. The interfacial reactions between engobe and celadon glazes were analyzed, showing the diffusion of CaO and alkali components that enhanced densification and bonding at the interface. Mechanical and thermal properties were evaluated, indicating that the optimized engobe-glazes system exhibited reduced porosity, higher adhesion strength, and improved resistance to thermal shock compared to conventional compositions. These findings demonstrate that rice husk ash can be utilized as a structural ceramic component by linking phase evolution and microstructural development with the enhanced performance of stoneware wall tiles.

Keywords: Mullite engobe; Celadon glazes; Rice husk ash; Phase evolution; Microstructural development

Electron Microscopy of Unusual Phases in Cast Ni-Al Bronze

Sankum Nusen[1,2], D. Morikawa[3], K. Tsuda[3], John T.H. Pearce[1,2] and Torranin Chairuangsri*[1,2]
[1]Department of Industrial Chemistry, Faculty of Science, Chiang Mai University, 50200 Thailand
[2]Centre of Excellence in Materials Science and Technology, Chiang Mai University, 50200 Thailand
[3]Institute of Multidisciplinary Research for Advanced Materials (IMRAM), Tohoku University,
Sendai 980-8577, Japan
E-mail address: tchairuangsri@gmail.com, torranin.c@cmu.ac.th
*Corresponding author

Abstract

Cast Ni-Al bronze (NAB) is utilised extensively for components exposed to marine environments due to its suitable combination of corrosion resistance and mechanical properties. The usual microstructural constituents in cast NAB consist of a Cu-rich solid solution (fcc α-Cu phase) with distributed intermetallic phases (Kappa phases, κ). Kappa phases with varying compositions are classified into (i) Fe_3Al with Ni, Mn and Cu substituting Fe in the Fe_3Al structure and (ii) NiAl with Fe, Mn and Cu substituting Ni in the NiAl structure, whereas Si can substitute Al in both Fe_3Al and NiAl structures. In the present study, electron microscopy has been used to characterize a cast Cu-9Al-4Fe-5Ni-1Mn produced in 3D sand printed mould. Backscattered electron imaging in scanning electron microscope revealed unusual phases with spheroidal morphology, distributed in the fcc α-Cu matrix and mainly associated with the segregation of P. Results from energy dispersive X-ray spectroscopy and selected area electron diffraction in transmission electron microscopy suggested that these unusual spheroidal phases consist mainly of Fe_3Al (κ_{II}), cubic Al_2FeNi and triclinic $Mn_3Fe_9P_4$, tentatively formed around carbide particles enriched in carbide-forming elements (Ti, V and Mo). The results reflect the potential influence on properties of carbide-forming elements (Ti, V and Mo) as impurities and P segregation, even at a relatively low content of 0.012 wt% P, since such compositional and microstructural variations can affect the corrosion resistance and mechanical properties of NAB cast components.

Keywords: Ni-Al Bronze; Electron Microscopy; Phosphorus Segregation; Al_2FeNi; $Mn_3Fe_9P_4$; Carbides

Particle pushing and engulfment phenomenon in Al-TiC nanocomposites: Bridging experiments, physical models, and Cellular Automata–Finite Differences method

Ewa Olejnik[1,2*], Paweł Kurtyka[2], Andriy Burbelko[1], Agnieszka Czajka[1], Sebastian Sobula[1], Katarzyna Biegun[2,3], Robert Chulist[4], Anna Wójcik[4], Wojciech Maziarz[5]

[1]Faculty of Foundry Engineering, AGH University of Krakow, Krakow, Poland

[2]Innerco Sp. z o.o., Krakow, Poland

[3]Faculty of Non-Ferrous Metals, AGH University of Krakow, Krakow, Poland

[4]Faculty of Metals Engineering and Industrial Computer Science, AGH University of Krakow, Krakow, Poland

[5]Institute of Metallurgy and Materials Science of the Polish Academy of Sciences, Krakow, Poland

Email: eolejnik@agh.edu.pl

*Corresponding author

Abstract

Uniform particle distribution remains one of the main challenges in the in-situ fabrication of lightweight and high-strength aluminium matrix composites (AMMCs). Interactions at the solid–liquid particle interface during solidification, governed by pushing–engulfment phenomena, strongly influence microstructure and properties, making their understanding essential for process optimization. In this study, Al 1000 alloy reinforced with titanium carbide (TiC) was synthesized in situ by introducing 5, 10, and 15 wt.% TiC reactive compacts during casting. The composites were then analysed to determine their microstructure, phase composition, and mechanical performance. Results showed that TiC particles were mainly distributed in interdendritic regions of the aluminium matrix. Increasing Ti+C content caused particle coarsening and agglomeration, which intensified heterogeneity. Nevertheless, all composites exhibited improved tensile and compressive strength with higher TiC content, though ductility decreased noticeably from 10 wt.% and most strongly at 15 wt.% due to fluctuations in particle distribution. To link processing conditions with particle behaviour, experimental data were compared with numerical predictions. Simulations using the Cellular Automata–Finite Differences (CAFD) method reproduced particle–solidification front interactions and revealed mechanisms of particle engulfment or rejection. This combined experimental–computational approach demonstrates an effective pathway for optimizing Al–TiC composites and defining processing parameters needed to achieve tailored microstructures and mechanical properties.

Keywords: MMCs; casting; in situ; TiC; CAFD

Acknowledgment

Financial support of the National Science Centre, Poland (project no. 2021/43/B/ST8/03271) is greatly acknowledged.

The relationship between hardness and microstructure in Zn/Mg ratio-controlled Al–Zn–Mg alloys aged at 200 °C

Wanlalak Sanphiboon[1*], Seungwon Lee[2], Taiki Tsuchiya[2], Abrar Ahmed[3], Susumu Ikeno[4], Satoshi Murakami[5], Karin Shibata[6], Hiroaki Matsui[6], Tomoo Yoshida[6], Kenji Matsuda[2,3]
[1]Graduate School of Science and Engineering for Education, University of Toyama, Toyama, Japan
[2]Graduate School of Science and Engineering for Research, University of Toyama, Toyama, Japan
[3]Advanced Aluminum International Research Center, University of Toyama, Toyama, Japan
[4]Professor Emeritus, University of Toyama, Toyama, Japan.
[5]University of Toyama, Toyama, Japan
[6]AISIN KEIKINZOKU Co., LTD, Nagonoe, Imizu, Toyama, Japan
Email: wanloliasanphiboon@gmail.com
*Corresponding author

Abstract

The Al–Zn–Mg alloy system includes high-strength age-hardenable Al alloys. They gain strength through the formation of metastable, semi-coherent, nano-sized precipitates during artificial aging (AA). Studying aging at high temperature helps simulate these real-world conditions, such as welding or heat exposure of components, so 200 °C was selected to speed up diffusion, leading to rapid precipitation and phase changes, making it important to study over-aging and stable phases. In this study, we designed alloys to optimize the balance between strength and high-temperature performance with a wide range of Zn/Mg ratios but a similar total amount of (Zn+Mg), which are Al-1.4Zn-5.8Mg as ZM16, Al-2.1Zn-5.2Mg as ZM25, Al-3.0Zn-4.0Mg as ZM34, Al-4.2Zn-3.3Mg as ZM43, Al-4.8Zn-1.9Mg as ZM52, and Al-6.0Zn-1.0Mg as ZM61. The alloys were cast, hot extruded, and heat-treated by aging the alloys at 200°C. The micro-Vickers hardness was measured. Based on the results, the peak-aging conditions were used to age Transmission Electron Microscopy (TEM) samples to observe the microstructure. The micro-Vickers hardness can be noticed that the alloy with high zinc seems to create higher hardness and age hardening ability than the alloy with high Mg; however, the balance between Zn and Mg also gives better results than the one with extremely high Zn or Mg, with an earlier peak aging time by increasing the amount of Zn. For the TEM observation, the number density also has increased with the increase in the amount of Zn. According to the Selective Area Electron Diffraction (SAED) patterns and bright field images, the types of precipitates were analyzed into three groups. T’/T phase group including ZM16 and ZM25, T'/T & η’/ η phase group including ZM34 and ZM43, and η’/ η phase group including ZM52 and ZM61. These show that the alloys with η’/ η phase or co-precipitation between T'/T & η’/ η phase have a better effect on the hardness.

Keywords: Al-Zn-Mg alloy; Heat treatment; TEM observation; Precipitation

Machine learning aided nanoscale visualization of grain boundaries using electron diffraction mapping

Shiro Ihara[1*] and Mitsuhiro Murayama[1,2]
[1]Institute for Materials Chemistry and Engineering, Kyushu University,
6-1 Kasugakoen, Kasuga, Fukuoka, Japan
[2]Virginia Tech, VA 24061, Blacksburg, USA.
Email: ihara-shiro@cm.kyushu-u.ac.jp
*Corresponding author

Abstract

Heat treatment of metals plays a crucial role in controlling grain size distribution, which significantly influences the physical and mechanical properties of the material. Visualization of grain boundaries (GBs) at the nanoscale would stimulate a deeper understanding of the fundamental mechanisms governing GB migration. In this study, we demonstrate the visualization procedure using electron diffraction mapping combined with machine learning. We focused on variations in the electron diffraction patterns of adjacent grains. we first obtained a series of diffraction maps from an austenitic steel using ASTAR (NanoMEGAS) as shown in the far left of Fig. 1. Using multivariate least squares, we quantified feature variations as coefficients changes, with representative diffraction patterns as the basis, as shown in the second left of Fig.1. The coefficient map was segmented into three groups using spectral clustering, where the similarity of the coefficient around each point on the specimen was used as a feature value, as shown in the third in Fig.1. This algorithm enabled to roughly detect the grains and GB. After the clustering, we also performed regression scheme to precisely detect the GB edge. By repeating these procedures for the three grains, the GB area was clearly extracted as shown in the far right of Fig.1. The developed scheme was further applied to visualize GB migration in an austenitic steel with high fidelity. Morphological changes before and after heating will also be discussed in the presentation.

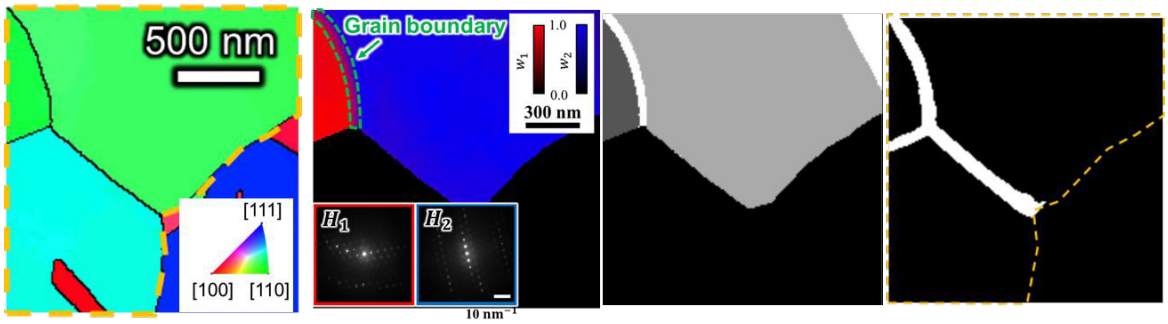

Fig.1 Summary of the procedure for grain boundary area extraction.

Keywords: Transmission electron microscopy; Machine learning; Electron diffraction, Heat treatment

Effect of thermomechanical treatment on Ω-phase precipitation in Al-Cu-Mg alloys

Seungwon Lee[1,*], Kenta Koshiishi[2], Taiki Tsuchiya[1], Kenji Matsuda[1], Susumu Ikeno[2]
[1] Academic Assembly, Faculty of Sustainable Design, University of Toyama, Toyama 930-8555, Japan
[2] Graduate School of Science and Engineering, University of Toyama, Toyama 930-8555, Japan
[2] Professor Emeritus, University of Toyama, Toyama 930-8555, Japan
Email: swlee@sus.u-toyama.ac.jp
*Corresponding author

Abstract

Al–Cu–Mg alloys are representative age-hardenable aluminum alloys widely used in aerospace and high-strength structural applications. The precipitation behavior varies with the Cu/Mg ratio, and when Cu/Mg ≈ 3, the formation of S′, θ′, and Ω phases has been reported. In this study, an Al–1.5Cu–0.5Mg alloy (Cu/Mg = 3) was investigated to clarify the effect of thermo-mechanical processing on Ω phase precipitation.

The alloy was solution-treated at 773 K for 3.6 ks, cold-rolled to reductions of 0, 10, 30, and 60%, and aged at 423, 473, and 523 K. Vickers microhardness testing was performed to evaluate age-hardening behavior, and the microstructure was analyzed using TEM and HAADF-STEM.

Increasing rolling reduction enhanced both the as-rolled and peak hardness while shortening the time to reach the peak. Higher aging temperatures resulted in lower peak hardness and further reductions in the peak time. TEM observations revealed θ′, S′, and a small amount of Ω phase. With increasing rolling reduction, the overall precipitate density rose and the fraction of Ω phase increased markedly, whereas the fractions of θ′ and S′ phases declined. The average precipitate length decreased sharply from 0% to 10% reduction and then remained nearly constant at higher reductions. As the aging temperature increased, total precipitate density decreased; in the 0% rolled material the phase fractions remained almost unchanged, while in the 60% rolled material the Ω fraction decreased slightly and the S′ fraction increased. HAADF-STEM analysis showed that the Ω phase consists of alternating Cu–Al layers with an Mg-rich outer layer, and structures containing a small number of Cu atomic columns exhibited characteristic interlayer spacing variations.

These results demonstrate that even modest deformation (around 10% reduction) strongly promotes Ω phase precipitation, producing a significant increase in number density and refinement of precipitates. Careful control of rolling reduction and aging conditions is therefore crucial for optimizing the microstructure, and process designs aimed at stable, high-density Ω precipitation are expected to be effective for future alloy development.

Keywords: Al–Cu–Mg alloy; Ω phase precipitation; Thermo-mechanical processing; Age-hardening behavior; TEM/HAADF-STEM characterization

Effect of additive manufacturing method on the corrosion resistance of sintered materials produced by metal 3D printers

Yuhei Matsuo[1], Kenta Makizaki[1], Masahiko Hatakeyama[2*], Yuto Asai[1], Akinobu Arakawa[1], Kenta Oda[1], Fuma Kobayashi[1], Shota Otaki[1], Satoshi Sunada[2], Masahiro Kaido[3], Manabu Noguchi[3], Ryotaro Yamamoto[3], Hiroaki Nakamoto[3,]
[1]Graduate School of Material Science and Engineering for Education, University of Toyama, 3190 Gofuku Toyama 930-8555, Japan
[2]Graduate School of Material Science and Engineering for Research, University of Toyama, 3190 Gofuku Toyama 930-8555, Japan
[3]EBARA corporation, 4-2-1 Honfujisawa, Fujisawa-shi, Kanagawa 251-8502, Japan
Email: hatake@sus.u-toyama.ac.jp
*Corresponding author

Abstract

The corrosion resistance of sintered materials produced by metal 3D printers was investigated. It is known that sintered materials possess different thermal histories depending on the manufacturing method and manufacturing location, which affects their corrosion resistance. In this study, the effects of manufacturing method and manufacturing position on the corrosion resistance of sintered materials were investigated using dynamic potential polarization measurements in a neutral chloride environment. Austenitic stainless steel SUS316L powder was used as the specimen, and Laser Beam Additive Manufacturing Material (LBAMM) and Electron Beam Additive Manufacturing Material (EBAMM) were prepared. LBAMM showed better pitting corrosion resistance compared to EBAMM, although its corrosion rate was higher. The upper part of EBAMM showed better pitting corrosion resistance and a lower corrosion rate than the lower part. The amount of precipitation of an intermetallic compound called the σ phase differed between the upper and lower parts of EBAMM. The σ phase precipitates by depriving Cr and Mo from its surroundings. Consequently, the surrounding Cr and Mo concentrations decrease, leading to a deterioration in corrosion resistance. In the upper part of EBAMM, the exposure time to high temperatures was shorter, resulting in less σ phase precipitation compared to the lower part of EBAMM. Therefore, it was confirmed that the upper part of EBAMM has excellent corrosion resistance since a strong film forms.

Keywords: metal 3D printer; Laser Beam Additive Manufacturing Material (LBAMM); Electron Beam Additive Manufacturing Material (EBAMM); corrosion resistance; σ phase

Structural, magnetic and mechanical characterisation of Fe-Co-Ni-Mn-Ti medium-entropy alloys prepared by mechanical alloying, spark plasma sintering and arc-melting

L. Hawelek[1], T. Warski[1], K. Pecak[1], A. Czech[1], W. Maziarz[2]
[1] Lukasiewicz Research Network – Institute of Non-Ferrous Metals, Gliwice, Poland
[2] Institute of Metallurgy and Materials Science of the Polish Academy of Sciences, Kraków, Poland

Abstract

High- and medium-entropy alloys constitute a novel class of materials that attract significant attention due to their exceptional combination of mechanical properties. Among them, alloys based on ferromagnetic elements represent a particularly important subgroup. In this work, Fe-Co-Ni-based medium-entropy alloys were synthesised using two different routes: (i) mechanical alloying followed by spark plasma sintering (SPS) and (ii) arc melting (AM). The influence of subsequent vacuum annealing on bulk samples was systematically examined. Structural and functional characterisation was carried out by wide-angle X-ray diffraction, X-ray microanalysis, differential scanning calorimetry, transmission electron microscopy, tensile testing, and magnetic measurements. Fully dense bulk samples were obtained after both SPS and AM processing. The resulting microstructure consisted of a dominant FCC phase accompanied by minor secondary precipitates. The evolution of the measured properties was analysed as a function of Ti content.

Infrared FEL-Induced Alteration of Zeta Potential in Electro-chemically Grown Quantum Dots: Insights into Ion Modification

Sukrit Sucharitakul[1,2,3,4], Siripatsorn Thanasanvorakun[1,2], Vasan Yarangsi[1,2], Suparoek Yarin[1,2], Kritsada Hongsith[1,2], Monchai Jitvisate[4], Hideaki Ohgaki[6], Surachet Phadungdhitidhada[1,2], Heishun Zen[6], Sakhorn Rim-jaem[1,3,4,7] , Supab Choopun[1,2*]

[1] Department of Physics and Materials Science, Faculty of Science, Chiang Mai University, Chiang Mai, 50200, Thailand

[2] Physics of Low-dimensional Systems for Opto-electronic Applications, Department of Physics and Materials Science, Faculty of Science, Chiang Mai University, 50200, Thailand

[3] Research Unit for Development and Utilization of Electron Linear Accelerator and Ultrafast Infrared/Terahertz Laser, Chiang Mai University, Chiang Mai, 50200, Thailand

[4] Thailand Center of Excellence in Physics, Ministry of Higher Education, Science, Research and Innovation, Bangkok 10400, Thailand, Bangkok, Thailand

[5] School of Physic, Institute of Science, Suranaree University of Technology, 111 University Avenue Muang Na-khon Ratchasima 30000, Thailand

[6] Institute of Advanced Energy, Kyoto University, Gokasho, Uji, Kyoto, 611-0011, Japan

[7] PBP-CMU Electron Linac Laboratory, Plasma and Beam Physics Research Facility, Department of Physics and Materials Science, Faculty of Science, Chiang Mai University, Chiang Mai, 50200, Thailand

*Correspondence: supab99@gmail.com

Abstract

This study explores the use of mid-infrared (MIR) free-electron laser (FEL) irradiation as a tool for tailoring the surface properties of electrochemically synthesized TiO_2–graphene quantum dots (QDs). The QDs, prepared in colloidal form via a cost-effective electrochemical method in a KCl–citric acid medium, were exposed to MIR wavelengths (5.76, 8.02, and 9.10 μm) at the Kyoto University FEL facility. Post-irradiation measurements revealed a pronounced inversion of zeta potential by 40–50 mV and approximately 10% reduction in hydrodynamic size, indicating double-layer contraction and ionic redistribution at the QD–solvent interface. Photoluminescence spectra showed enhanced emission for GQDs and TiO_2/GQD composites, while Tauc analysis revealed modest bandgap blue shifts (0.04–0.08 eV), both consistent with trap-state passivation and sharper band edges. TEM confirmed intact crystalline structures, verifying that FEL-induced modifications were confined to surface chemistry rather than bulk lattice damage. Taken together, these results demonstrate that MIR FEL irradiation provides a resonance-driven, non-contact method to reorganize ions, suppress defect states, and improve the optoelectronic quality of QDs. This approach offers a scalable post-synthetic pathway for enhancing electron transport layers in perovskite solar cells and highlights the broader potential of photonic infrastructure for advanced nanomaterial processing and interface engineering in optoelectronic and energy applications.

Keywords: Quantum Dots; Free Electron Laser; Irradiation; Electrochemical Process; Optoelectronics

Microstructural characterisation and hardness evaluation of bimetallic 316L/17-4PH stainless steel fabricated by filament-based material extrusion additive manufacturing

Natthaphat Parsompech*, Pattarapong Kaewkamyan, Pharadee Suwannak, Chanun Suwanpreecha, Anchalee Manonukul
National Metal and Materials Technology Center (MTEC), National Sciences and Technology Development Agency (NSTDA), 111 Thailand Science Park, Paholyothin Road, Klong 1, Klong Luang, Pathumthani 12120, Thailand
Email: natthaphat.par@ncr.nstda.or.th
*Corresponding author

Abstract

Filament-based material extrusion additive manufacturing (FB-MEX) offers a promising approach for fabricating bimetallic components, owing to its design flexibility, process simplicity and cost competitiveness. In this study, tensile-specimen-shaped bimetallic parts combining austenitic 316L stainless steel, known for its excellent ductility and corrosion resistance, with martensitic 17-4PH stainless steel, valued for its high strength and hardness, were fabricated using in-house developed filaments. The effects of different joining configurations — cross-sectional, layered longitudinal, upper–lower and inverse upper–lower on the physical, microstructural, and hardness properties of the bimetallic specimens were investigated. These were compared to their monotonic material counterparts. Only the cross-sectional configuration could be successfully sintered without any defects, whereas the other configurations were deformed. Key evaluations included defect analysis, densification, microstructure, interfacial bonding and hardness. This work highlights the potential and challenges of integrating dissimilar stainless steel into a single sintered structure via FB-MEX for multifunctional applications.

Keywords: Material extrusion additive manufacturing; Bi-metallic; 316L; 17-4PH

Manufacturing process and wear performance of metal matrix composites in the aspect of high temperature wettability

Ł. Szymański[1,2*], K. Peddeti[3], E. Olejnik[2,4], A. Bigos[5], N. Sobczak[5], J. Sobczak[2]
[1]FLSmidth Mining Technologies GmbH, 12 Schleebergstrasse St., 59320, Ennigerloh, Germany
[2]Faculty of Foundry Engineering, AGH University of Krakow, 23 Reymonta St., 30-059, Krakow, Poland
[3]FLSmidth Inc., 1110 American Parkway, Allentown, PA, 18109, USA
[4]Innerco sp. z o.o., 17 Wladyslawa Siwka St., 31-588, Krakow, Poland
[5]Institute of Metallurgy and Materials Science, Polish Academy of Sciences, 25 Reymonta St., 30-059, Krakow, Poland
Email: lukaszszymanski14@gmail.com
*Corresponding author

Abstract

Metal-matrix composites (MMCs) based on iron alloys reinforced with ceramic particles are characterized by good mechanical properties and high wear resistance. The technological processes of producing MMCs are conditioned by obtaining the relevant bonding (wetting) at the interface between matrix and reinforcing phase. In the first part of research, the high-temperature wettability tests (sessile drop method) were conducted for various types of ceramics oxide as well as reactive system (Ti+C_{gr} and W+C_{gr})/cast iron. At the next stage, composite castings reinforced by ZrO_2/Al_2O_3 (ceramic foams), TiC (reactive insert) and WC (reactive insert, laser cladding) were produced with the use of ex-situ or in-situ techniques. The samples taken from the composite castings were analyzed, considering their microstructure (LM, SEM), chemical composition (EDS), mechanical properties (Vickers hardness) and wear properties (Miller test, cavitation-erosion resistance). High-temperature wettability test indicated that all types of ceramics oxide are characterized by lack of wetting with ferrous alloys. In contrast, Ti+C_{gr} and W+C_{gr} systems showed with the same alloy wetting behavior and high reactivity. The reactive compacts that contained tungsten, titanium and carbon allowed us to produce in-situ WC and TiC which were well-bonded with metal matrix. Observations indicated that the ceramic foams were fully infiltrated by the liquid alloys. The process of reinforcing iron-based alloys with ceramic phases in the form of carbides and metal oxides resulted in increases in hardness at a minimum level of about 200HV1. The Miller test showed that the composite materials were characterized by better abrasion resistance than ferrous alloys. In contrast, each of the composite materials showed lower resistance to cavitation-slurry erosion when compared to iron alloys. An analysis of the results indicated that the composites that were produced using in-situ techniques had better resistance to erosion; this may have been related to their better bonding to the matrix.

Keywords: MMC; wear; carbides; casting; wettability

Effect of Infill Geometry and Density on the As-Printed Flexural Performance of 316L Specimens Fabricated by Material Extrusion Additive Manufacturing

Pharadee Suwannak*, Natthaphat Parsompech, Chanun Suwanpreecha and Anchalee Manonukul

National Metal and Materials Technology Center (MTEC), National Sciences and Technology Development Agency (NSTDA), 111 Thailand Science Park, Paholyothin Road, Klong 1, Klong Luang, Pathumthani 12120, Thailand

Email: pharadee.suw@ncr.nstda.or.th

*Corresponding author

Abstract

Manufacturing steps in material extrusion additive manufacturing of metals (MEX/M) process are printing, debinding, and sintering. Among these steps, the as-printed properties play a critical role, as they reflect the material's handling ability. This study investigates the effect of infill pattern and density on the as-printed flexural behaviour of specimens fabricated via MEX/M using an in-house-developed 316L filament. Flexural performance was evaluated by three-point bending (3PB) tests. Four infill geometries, which are line, triangle, hexagon, and gyroid, were examined at infill densities of 20%, 40%, 60%, and 80%. A line infill pattern with 100% density was used as the reference. The results indicate that increasing infill density markedly enhances flexural strength, while reducing deflection under equivalent loads. Specimens with 80% infill achieved the highest load-bearing capacity, whereas those with 20% infill exhibited the lowest mechanical performance. In addition, the influence of infill pattern was more pronounced at higher infill densities but diminished with decreasing density. These findings highlight the importance of infill design in optimising the balance between mechanical performance and material efficiency in 3D-printed metallic components.

Keywords: Material extrusion additive manufacturing; Infill geometry; Infill density; As-printed condition; Flexural property; austenitic stainless steel

Enhanced Room-Temperature Formability of Mg-Zn-Zr Alloy through Texture Weakening by Reduction Rate Control

Seoung-yooun Yu[1], Young Min Kim[2], Byeong-Chan Suh[2], Sung Hyuk Park[1,*]
[1]Kyungpook National University, Daegu 41566, Republic of Korea
[2]Korea Institute of Materials Science, Changwon 51508, Republic of Korea
Email: sh.park@knu.ac.kr

Abstract

Magnesium alloys are increasingly considered promising lightweight structural materials. However, their widespread applications are hindered by poor room-temperature formability, which arises from the strong basal texture developed during conventional rolling. Previous attempts to overcome this limitation have relied on adding rare earth elements or employing severe plastic deformation techniques such as equal-channel angular pressing (ECAP) and high-pressure torsion (HPT). While effective, these approaches are costly, compositionally restrictive, and impractical for large-scale production. This study proposes a cost-effective and industrially viable approach to improve the formability of magnesium alloys without rare earth additions, by controlling the rolling reduction rate in combination with conventional thermo-mechanical treatments. Rolling experiments were performed on Mg-Zn-Zr and Mg-Zn-Zr-Gd alloys under various reduction conditions. The evolution of crystallographic texture was systematically characterized using electron backscatter diffraction (EBSD) and X-ray diffraction (XRD), while formability was evaluated by the Erichsen cupping test at room temperature. The results show that controlling the rolling reduction rate significantly suppresses basal pole clustering in the Mg-Zn-Zr alloy, reducing the maximum basal pole intensity from ~6.1 to ~4.4 m.r.d. This texture weakening directly improved plastic anisotropy and led to a nearly 80% increase in the Erichsen index, achieving values comparable to those of the rare-earth-containing Mg-Zn-Zr-Gd alloy. These findings demonstrate that careful control of reduction rate during rolling, combined with conventional thermo-mechanical treatment, offers a practical route to improve the formability of rare-earth-free Mg alloys and enables their scalable use in lightweight structural applications.

Keywords: Magnesium alloys; Texture; Formability; Rolling process; Thermo-mechanical treatment

The microstructure and corrosion behavior analysis of different aging Al-Zn-Mg-Cu alloys manufactured by additive friction stir deposition

Fuqiang Guo[1], Yong Zou[1*]
[1] School of Materials Science and Engineering, Shandong University, Jinan, 250061, China
Email: yzou@sdu.edu.cn
*Corresponding author

Abstract

The microstructure and corrosion behavior of Al-Zn-Mg-Cu alloys prepared by additive friction stir deposition (AFSD) after different heat treatments were studied. The AFSD alloy consists of uniform dynamically recrystallized equiaxed grains (<5.5 um), devoid of defects and delamination. The stirring effect of the AFSD process can break up large phases in the BM and improve the corrosion resistance. AFSD alloys can precipitate small-sized η' phases under artificial ageing at 120°C for 8 hours. This process can enhance the mechanical properties (486 MPa, elongation 4.74%), and the alloy has many large-sized T and η phases which surrounded by PFZ, resulting in low corrosion resistance. The AFSD alloy after solution treatment and artificial aging have many fine η' phase with low film capacitance value, which increases pitting and intergranular corrosion (IGC) resistance. But the alloys underwent grain growth and grain boundary migration during the solid solution process, resulting in the absence of precipitate free zone (PFZ) and low plasticity.

Keywords: Al-Zn-Mg-Cu alloy; AFSD; Corrosion; Precipitates

Process Optimization in FCAW of High Manganese Steel: Evaluating Temperature and Layer Effects on Hardness and Heat-Affected Zone

Narin Jantaping[1,2], Kumron Kaewpad[1], Sittipong Jaipayuk[1,2], Sakoltit Wonghom[1,2], and Man Tuiprae[1,2*]

[1]Department of Industrial Engineering, Faculty of Engineering, Rajamangala University of Technology Lanna, 128 Huay Kaew Road, Muang, Chiang Mai, Thailand, 50300

[2]Innovation and Testing of Railway Transportation System Products Research Unit, Center of Excellence in professional and technology, Faculty of Engineering, Rajamangala University of Technology Lanna, 128 Huay Kaew Road, Muang, Chiang Mai, Thailand, 50300

[*]*Email: tman@rmutl.ac.th, Phone: +66 (0) 819607046*

*Corresponding author

Abstract

This study investigates the optimization of Flux-Cored Arc Welding (FCAW) parameters for joining high manganese steel, specifically for railway frog applications. The research examines how substrate temperature and the number of weld layers influence hardness distribution and heat-affected zone (HAZ) characteristics. Welding was performed using a 1.6 mm high manganese steel cored wire on a base material of the same classification, with process parameters maintained at 180 A, 27 V, and a travel speed of 30 cm/min. The experimental methodology evaluated various substrate temperature conditions and deposition sequences to determine their impact on microstructural evolution and mechanical properties. Primary evaluation criteria included HAZ width reduction and minimization of hardness variance between weld metal and HAZ to ensure structural integrity. Microstructural analysis indicated that substrate temperature significantly affects carbide precipitation and grain growth in the HAZ. Results demonstrate that welding at lower substrate temperatures with multiple deposition layers produced optimal outcomes, generating a refined microstructure that resulted in the narrowest HAZ and most uniform hardness distribution. This parameter combination effectively reduces HAZ softening while maintaining appropriate weld metal strength. The findings provide valuable insights for developing enhanced welding procedures for high manganese steel components in heavy-duty applications where impact toughness and wear resistance are crucial performance requirements.

Keywords: Flux-Cored Arc Welding (FCAW); high manganese steel; heat-affected zone (HAZ); hardness; welding parameters

Influence of extrusion ratio on dynamic recrystallization, microstructure, and tensile properties of Mg–5Bi–3Al alloy

Gun Woong An[1], Sang-Cheol Jin[2], Sung Hyuk Park[1,*]
[1]Kyungpook National University, Daegu 41566, Republic of Korea
[2]HD Korea Shipbulding & Offshore Engineering, Ulsan, 44032, Republic of Korea
Email: sh.park@knu.ac.kr

Abstract

The Mg–5Bi–3Al (BA53, wt.%) alloy is a newly developed magnesium alloy that enables high-temperature, high-speed extrusion with excellent strength. To broaden industrial application, further study of extrusion parameters is required. Among them, the extrusion ratio (ER) governs accumulated strain, influencing dynamic recrystallization (DRX), particle distribution, grain growth, and texture development, while also defining the final product size and shape. This study examines the effect of ER on recrystallization, microstructure, and mechanical properties of BA53 alloy under high-temperature, high-speed extrusion. For systematic analysis, BA53 billets were extruded at 400 °C with ERs of 10, 25, 50, and 76.5. The relationships between recrystallization kinetics, grain growth, microstructural features—including grain size, crystallographic texture, and second-phase particle distribution—and tensile properties such as yield strength and elongation were examined. As ER increased from 10 to 76.5, the maximum extrusion load rose from 168 to 254 tons, indicating higher deformation resistance. Undissolved Mg_3Bi_2 particles fragmented during extrusion, producing more fine particles at higher ERs. The greater strain energy promoted DRX in the initial stage, yielding a higher fraction of DRXed grains. Nevertheless, all materials showed fully DRXed microstructures, with ER 10 retaining finer grains and a weaker basal texture. Yield strength improved from 175 to 203 MPa as ER increased, while elongation declined from 13.8% to 7.9%, due to stronger texture and particle hardening. The results provide insights for optimizing extrusion parameters of Mg–Bi–Al alloys toward tailored properties.

Keywords: BA53 alloy; Extrusion ratio; Dynamic recrystallization; Microstructure; Mechanical properties

Effect of Ag addition on microstructure and properties of Al-Zn-Mg-Cu alloys

Qinghua Zhang[1], Fuqiang Guo[1], Yong Zou[2,*]
[1]Key Laboratory for Liquid-Solid Structural Evolution and Processing of Materials (Ministry of Education), School of Materials Science and Engineering, Shandong University, Jinan, 250061, China
[2]Shandong Engineering & Technology Research Center for Modern Welding, Shandong University, Jinan, 250061, China
Email: yzou@sdu.edu.cn (Yong Zou)
*Corresponding author

Abstract

This study investigated the influence of Ag microalloying on the microstructure and properties of Al-Zn-Mg-Cu alloys through corrosion properties testing, scanning electron microscope (SEM), transmission electron microscopy (TEM). The results indicate that Ag addition increases the hardness of the peak-aged Al-Zn-Mg-Cu alloy and delays its over-aging process. Furthermore, the addition of Ag reduces the intergranular corrosion (IGC) depth in the peak-aged alloy and improves its corrosion resistance. Ag promotes the formation of the GP zone and η′ phase, increases the density of precipitates, and reduces the width of the precipitate-free zones (PFZ).

Keywords: Al-Zn-Mg-Cu alloy; Ag addition; Precipitates

Effect of Ag Addition on the Morphology of the β-Phase in Al-Mg-Si Alloys

Abrar Ahmed[1,*], Taiki Tsuchiya[2], Seungwon Lee[2], Susumu Ikeno[2], Kenji Matsuda[2]
[1]Advanced Aluminum International Research Center, University of Toyama, Takaoka city, Toyama, Japan
[2]Graduate School of Science and Engineering for Research, University of Toyama, Toyama, Japan
Email: abrar@sus.u-toyama.ac.jp
*Corresponding author

Abstract

The β(Mg_2Si) phase is one of the most influential precipitates in 6xxx series aluminum alloys, as its morphology, interface, and growth behavior strongly determine the alloys' microstructural stability and mechanical performance. Understanding its anisotropic growth mechanisms and the role of alloying elements such as silver (Ag) is therefore importance for advancing the design of high-performance aluminum alloys. The aim of this study is to investigate the morphology and interfacial growth characteristics of the octagonal plate-shaped β-phase in Al-Mg-Si alloys and to clarify how Ag addition changes its evolution. A combination of advanced characterization techniques, including optical microscopy (OM), focused ion beam (FIB), transmission electron microscopy (TEM), scanning transmission electron microscopy (STEM), high-resolution TEM, and energy-dispersive X-ray spectroscopy (EDS), was employed to capture both the global morphology and atomic-scale interfacial features of the β-phase. In the Ag-free Al-Mg-Si alloy, three distinct interfacial facets were observed, namely, reflecting a highly anisotropic and complex faceted growth mode. However, the Ag-containing alloy exhibited only two facets, indicating that Ag modifies the growth. Further interfacial characterization by HR-TEM and EDS mapping revealed Ag segregation at the β-phase/Al matrix interface, which is believed to stabilize certain facets while restricting others, thereby refining the overall morphology of the precipitate. These observations demonstrate that the addition of Ag plays a critical role in altering the β-phase growth behavior, interfacial energy balance, and facet stability. The results provide novel insights into the atomic-scale mechanism by which Ag controls the morphology of β-phase precipitates, offering new guidelines for microstructural engineering in Al-Mg-Si-based alloys. This work contributes to the broader field of alloy design by highlighting the importance of interfacial segregation phenomena in tailoring the precipitation sequence and mechanical response of structural aluminum alloys.

Keywords: Aluminum; Precipitate; Microstructure; Interfacial

Microstructure observation of Al-7%Si-0.3%Mg cast alloy

Taiki Tsuchiya[1,*], Seungwon Lee[1], Abrar Ahmed[2], Susumu Ikeno[3], Kenji Matsuda[1]
[1]University of Toyama (Academic Assembly, Faculty of Sustainable Design, 3190 Gofuku, Toyama city, Toyama, Japan)
[2] University of Toyama (Advanced Aluminum International Research Center, 180 Futakami, Takaoka city, Toyama, Japan)
[3]University of Toyama (Professor of Emeritus, 3190 Gofuku, Toyama city, Toyama, Japan)
Email: tsuchiya@sus.u-toyama.ac.jp
*Corresponding author

Abstract

Al-Si alloys have been used as casting materials for automobile parts. Al-Si-Mg alloys enhance its strength due to precipitation of metastable phase. Moreover, it is effective for increasing both strength and corrosion resistance with Mg addition. However, precipitation sequence is not clear in T5 condition. The aim of this work is to estimate mechanical properties and to clarify precipitates by Micro Vickers hardness measurement and microstructure observation of Al-Si-Mg alloy in T5 condition. Alloy was fabricated by casting using iron mold having Y-shape cavity. Alloy was cooled in the mold and temperature was measured. When temperature drops to 773K, alloy was quenched into ice water. After casting, artificial aging was carried out at 323K~523K. Micro Vickers hardness measurement was performed using Mitutoyo HV-101 (load: 0.98N, duration time:15s). Microstructure observation were performed using Optical Microscopy (OM, OLYMPUS BX51M), Scanning Electron Microscopy (SEM, HITACHI S-3500H), Transmission Electron Microscopy (TEM, TOPCON EM-002B) and Scanning Transmission Electron Microscopy(STEM, Thermo Fisher Scientific Talos F200X G2).
As the result of hardness test, peak hardness increased with decreasing aging temperature and the time to reach peak hardness became shorter with increasing aging temperature.
As the result of TEM observation of sample aged at 473K for peak hardness, There were needle-shaped precipitates along <100>Al direction and granular-shaped precipitates. The distribution of needle-shaped precipitates and granular-shaped precipitates were different from place to place. We analyzed needle-shaped precipitates and granular-shaped precipitates with TEM and STEM.

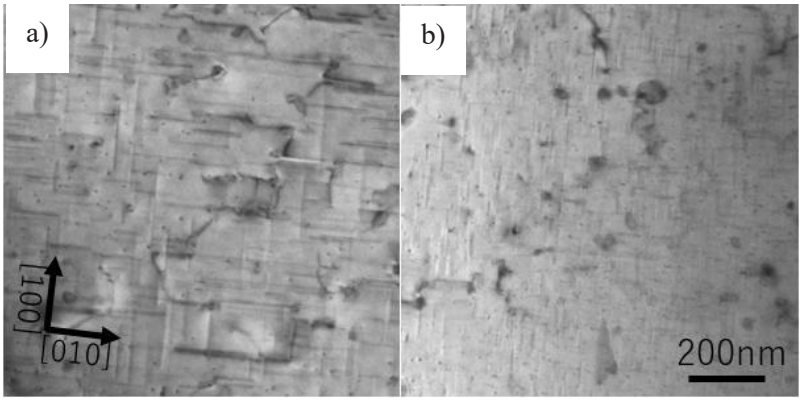

Fig. 1 TEM BF images in Al-Si-Mg alloy peak aged at 473K, (a) microstructure near eutectic Si,
(b) microstructure far from eutectic Si

Keywords: Al-Si alloy; Microstructure; Aging; Precipitates

Initial oxidation properties of nickel-based Al-Cr-Fe-Ni high entropy alloys under thermal shock conditions

Richard Gawel[1,*]
[1]Department of Physical Chemistry and Modelling, Faculty of Materials Science and Ceramics, AGH University of Krakow, Mickiewicza Ave. 30, 30-059 Krakow, Poland
Email: ragaw@agh.edu.pl

Abstract

The goal of this contribution is to identify chemical compositions of four-element Al-Cr-Fe-Ni high entropy alloys (HEAs) that allow for optimal high temperature oxidation properties and thermodynamic phase stability at elevated temperatures. To realize this, three different compositions were synthesized by melting individual elements (>99.9% purity) together in an induction furnace. As a result, the following nominal compositions were obtained (in at.%): 30%Al + 15%Cr + 15%Fe + 40%Ni ($Al_{30}Cr_{15}Fe_{15}Ni_{40}$), 25%Al + 15%Cr + 15%Fe + 45%Ni ($Al_{25}Cr_{15}Fe_{15}Ni_{45}$) and 20%Al + 10%Cr + 30%Fe + 40%Ni ($Al_{20}Cr_{10}Fe_{30}Ni_{40}$). These HEAs were then subjected to 100 h oxidation at 1273 K under thermal shock conditions (1 cycle = 2h heating + 10 min cooling). The mass changes were determined by systematically weighing the HEAs after a certain number of thermal shocks. The morphology, chemical and phase composition were identified and compared before and after the corrosion process by means of scanning electron microscopy combined with energy dispersive X-ray spectroscopy (SEM-EDS), and X-ray diffraction (XRD). Initially, the $Al_{25}Cr_{15}Fe_{15}Ni_{45}$ and $Al_{20}Cr_{10}Fe_{30}Ni_{40}$ HEAs consisted of a Ni-Cr-Fe-rich FCC phase and Ni-Al-rich ordered BCC (B2) structure, whereas the $Al_{30}Cr_{15}Fe_{15}Ni_{40}$ alloy is built of a Cr-Fe-rich disordered BCC (A2) structure and Ni-Al-rich B2 phase. The materials proved mostly capable of maintaining these dual-phase structures after prolonged high temperature exposure. The scales grown on the HEAs during the oxidation process contain large amounts of Al_2O_3, along with a Ni-Cr-Fe spinel oxide and Cr_2O_3 with Fe impurities. The most significant spinel content can be observed in the case of $Al_{20}Cr_{10}Fe_{30}Ni_{40}$. Conversely, $Al_{30}Cr_{15}Fe_{15}Ni_{40}$ exhibits a $(Cr,Fe)_2O_3$ inner layer and the highest mass gain. From this it can be concluded that high Fe concentration is detrimental to selective Al_2O_3 growth. Aluminium content above 25 at.% can also lead to less selective alumina formation, and consequently, inferior oxidation properties.

Keywords: high entropy alloys; high temperature oxidation; phase composition analysis

Influence of Laser Texturing on the Surface Properties of Magnesium Alloy

Jirayu Hemwat[1], Viboon Saetang[1], Patcharapit Promoppatum[2], Phromphong Pandee[1,*]
[1]Department of Production Engineering, Faculty of Engineering, King Mongkut's University of Technology Thonburi, 126 Pracha Uthit Road, Bang Mod, Tung Khru, Bangkok 10140, Thailand
[2]Department of Mechanical Engineering, Faculty of Engineering, King Mongkut's University of Technology Thonburi, 126 Pracha Uthit Road, Bang Mod, Thung Khru, Bangkok 10140, Thailand
Email: phromphong.pan@kmutt.ac.th
*Corresponding author

Abstract

Magnesium alloys are attractive for biomedical and lightweight structural applications due to their biodegradability and high specific strength; however, their poor surface properties limit broader use. This study investigates laser-based surface texturing as a strategy to enhance the surface integrity and wettability of WE43 magnesium alloy sheets. A nanosecond pulsed laser (1064 nm) was employed with varying power levels (5–25 W), pitch distances (50–150 µm), and numbers of passes (N = 1–3). Surface characterization included optical profilometry, topography analysis, and roughness parameters (Ra, Rz, Rp, Rv), while wettability was evaluated using static contact angle measurements. The results demonstrate that laser surface texturing significantly influences surface roughness and wettability. Groove width and depth increased with laser power, whereas pitch distance and the number of passes strongly affected roughness. Single-pass processing with wider pitch distances produced the lowest Ra values, while multiple passes induced remelting, resulting in increased Ra and Rz. Contact angle measurements revealed that the textured surfaces exhibited improved hydrophilicity compared with the as-received condition. These findings highlight the potential of laser surface texturing to tailor surface properties of magnesium alloys, providing a promising pathway for their use in future biomedical and structural engineering applications.

Keywords: WE43; Contact angle; Hydrophilicity; Surface roughness; Wettability

Effect of Processing Parameters on the Densification of Magnesium Alloy Fabricated by Laser Powder Bed Fusion

Khettawan Panchamat[1], Montian Sukprasert[2], Patcharapit Promoppatum[2], Phromphong Pandee[1,*]
[1]Department of Production Engineering, Faculty of Engineering, King Mongkut's University of Technology Thonburi, 126 Pracha Uthit Road, Bang Mod, Tung Khru, Bangkok 10140, Thailand
[2]Department of Mechanical Engineering, Faculty of Engineering, King Mongkut's University of Technology Thonburi, 126 Pracha Uthit Road, Bang Mod, Thung Khru, Bangkok 10140, Thailand
Email: phromphong.pan@kmutt.ac.th
*Corresponding author

Abstract

Magnesium (Mg) is a lightweight metal with mechanical properties comparable to cortical bone and excellent biocompatibility. When alloyed with suitable elements and processed using advanced manufacturing techniques, Mg can yield alloys with enhanced performance, making it highly attractive for biomedical implants. Among them, the WE43 alloy, specifically developed for improved properties, has gained increasing attention for biomedical applications. To fully exploit its potential, Laser Powder Bed Fusion (L-PBF) offers the capability to fabricate complex Mg components; however, achieving high density and full interlayer bonding requires careful optimization of process parameters. This study investigates the densification behavior of WE43 fabricated by L-PBF across a range of laser powers (50–200 W) and scan speeds (500–2000 mm/s). Porosity was quantified using two complementary techniques: the Archimedes method and optical microscopy image analysis. At low porosity levels, both methods exhibited consistent trends; however, image analysis method reported slightly lower density values because powder-filled voids were removed during polishing, leaving only continuous pores visible. Increasing volumetric energy density improved relative density by reducing lack of fusion and stabilizing pore morphology. Nevertheless, excessive energy input beyond the optimal window induced melt pool instability and gas entrapment, resulting in keyhole porosity. This study demonstrates the complementary roles of the Archimedes method and optical microscopy image analysis in reliable density quantification of L-PBF processed WE43 alloy. The findings provide valuable process–structure insights to guide parameter optimization and advance the development of Mg-based implants with improved structural integrity.

Keywords: Archimedes; Additive manufacturing; Porosity; WE43; L-PBF

Microstructure, mechanical properties and wear resistance of in-situ cast TiC/A356 composites

Wojciech Maziarz[1*], Paweł Kurtyka[2], Ganna Chyzhyk[1], Sebastian Sobula[3], Robert Chulist[4], Anna Wójcik[4], Ewa Olejnik[2,3*]
[1]Institute of Metallurgy and Materials Science of the Polish Academy of Sciences, Krakow, Poland
[2]Innerco Sp. z o.o., Krakow, Poland
[3]Faculty of Foundry Engineering, AGH University of Krakow, Krakow, Poland
[4]Faculty of Metals Engineering and Industrial Computer Science, AGH University of Krakow, Krakow, Poland.
Email: w.maziarz@imim.pl
*Corresponding author

Abstract

Aluminium based metal matrix composites (AMMC) have been widely used in various applications such as automotive, defense, marine, electronics and automobile sectors because of its excellent strength and stiffness to weight ratio, with better resistance to wear and corrosion. In this study, A357 Al alloy was used as the matrix material for the AMMCs. This alloy is known for its excellent machinability, good wear resistance and favorable fatigue strength. To investigate the influence of the matrix alloy's purity on the mechanical properties and abrasive wear resistance of AMMCs, A357 was sourced in different forms: commercially pure, scrap, and machining chips. As strengthening phase the TiC particles in volume fraction of 10% were in-situ synthesized during casting process. Microstructure characterization in particular in terms of describing the interfaces between the individual phases in the composites were preformed using advanced characterization techniques including X-Ray synchrotron radiation diffraction, (S)TEM-HREM and SEM. The study evaluated how the purity of the matrix influences the tensile strength, ductility, and wear resistance of the AMMCs (Fig. 1).

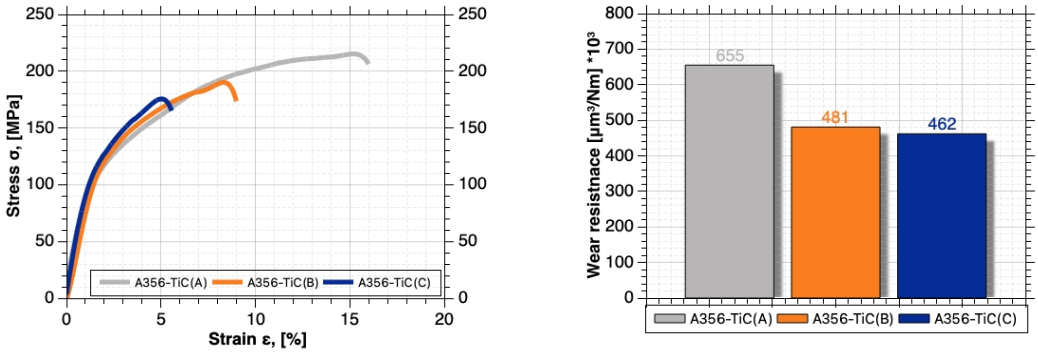

Fig. 1. Tensile test stress-strain curves and wear resistance results for different TiC/A356 composites varies of purity of matrix.

Acknowledgment
Financial support of the National Science Centre, Poland (project no. 2021/43/B/ST8/03271) is greatly acknowledged.

Effect of TiC volume fraction on the mechanical response and structure and microstructure evolution of Al-based composites

R. Chulist[1*], W. Maziarz[2], A. Wojcik[1], G. Chyzhyk[2], P. Kurtyka[3], S. Sobula[4], N. Schell[5] and E. Olejnik[3,4]
[1]Faculty of Metals Engineering and Industrial Computer Science, AGH University of Krakow, Krakow, Poland
[2]Institute of Metallurgy and Materials Science of the Polish Academy of Sciences, Krakow, Poland
[3]Innerco Sp. z o.o., Krakow, Poland
[4]Faculty of Foundry Engineering, AGH University of Krakow, Krakow, Poland
[5]Institute of Materials Physics, Helmholtz-Zentrum Hereon, Max-Planck-Strasse 1, D-21502 Geesthacht, Germany
Email: rchulist@agh.edu.pl
*Corresponding author

Abstract

The fabrication of metal matrix composites (MMCs) via the in-situ casting technique has garnered significant attention due to its notable advantages over ex-situ methods. These include finer particle size, cleaner interfaces, improved wettability between the reinforcement and matrix, and a more homogeneous distribution of the reinforcement phase. In this study, the effect of TiC volume fraction on the mechanical properties, structural changes, and microstructural evolution, including grain refinement and texture modification, of in-situ synthesized TiC/A1000 composites is investigated. Additionally, the relationship between hardness and wear resistance in the context of structural heterogeneity is assessed. Using advanced characterization techniques such as synchrotron X-ray diffraction, scanning/transmission electron microscopy with high-resolution imaging ((S)TEM-HREM), and scanning electron microscopy with electron backscatter diffraction (SEM-EBSD), two distinct types of aluminum solid solutions were identified within the dendritic grains of the A1000 matrix. These differ in lattice parameters and grain size, which is attributed to the presence of unreacted titanium. This unreacted titanium locally forms a supersaturated solid solution containing nanoprecipitates (~10 nm in size) with reduced lattice parameters compared to titanium-free regions. Furthermore, fractographic analysis revealed a clear correlation between mechanical strength and wear resistance in TiC/A1000 composites with TiC volume fractions ranging from 5% to 15%. For composites containing more than 10 vol.% TiC, particle clustering led to increased strength; however, this occurred at the cost of reduced ductility, due to weakened interfacial bonding and non-uniform stress distribution during deformation.

Acknowledgment
Financial support of the National Science Centre, Poland (project no. 2021/43/B/ST8/03271) is greatly acknowledged.

Effect of Mo Addition on Microstructural Evolution of Al–Si alloys Containing High Iron Impurity

Pongpat Phetchanasongkhram, Phromphong Pandee*
Department of Production Engineering, Faculty of Engineering, King Mongkut's University of Technology Thonburi, 126 Pracha Uthit Road, Bang Mod, Tung Khru, Bangkok 10140, Thailand
Email: phromphong.pan@kmutt.ac.th
*Corresponding author

Abstract

The increasing iron content in secondary aluminum sources promotes the formation of Fe-rich intermetallic phases in Al alloys. Among these, the β-Al_5FeSi phase, which predominates in Al–Si casting alloys, is particularly detrimental due to its needle-like morphology that degrades mechanical properties. In this study, the effect of molybdenum (Mo) addition on the microstructural evolution and mechanical properties of Al–7Si–2Fe alloys was systematically investigated. Mo was added in the range of 0.1–0.4 wt.% to evaluate its role in modifying Fe-rich intermetallics and enhancing alloy performance. Microstructural changes were examined using optical microscopy and scanning electron microscopy, while tensile testing was employed to assess mechanical properties. The results showed that Mo addition transformed the needle-like β-Al_5FeSi phase into more granular morphologies, thereby promoting a more uniform distribution of Fe-rich phases. At 0.1 wt.% Mo, both Chinese-script and blocky α-Al(Fe,Mo)Si phases appeared, accompanied by partial fragmentation of β-Al_5FeSi, marking the onset of phase transformation. Increasing the Mo content to 0.2 wt.% led to a microstructure dominated by compact blocky α-Al(Fe,Mo)Si phases. At higher Mo concentrations, coarse star-like α-Al(Fe,Mo)Si phases became prevalent. Correspondingly, tensile testing revealed a progressive improvement in both ultimate tensile strength and elongation with increasing Mo content. These findings demonstrate that Mo addition is an effective strategy to refine Fe-rich intermetallics and enhance the mechanical performance of Al–Si casting alloys with high Fe levels.

Keywords: Al–Si–Fe alloys; Fe-rich intermetallic; Molybdenum; Modification

Determination of Interaction Coefficient of La with Cr in Molten Iron and Analysis on Formation of La Compounds in High-Chromium Steel

Shinya OBA[1], Kengo KATO[2], and Hideki ONO[2,*]
[1]Graduate School of Science and Engineering, University of Toyama, Toyama, Japan
[2]Department of Materials Design and Engineering, Faculty of Sustainable Design, University of Toyama, Toyama, Japan
Email: ono@sus.u-toyama.ac.jp
*Corresponding author

Abstract

The demand for stainless steel is increasing year by year, and its cleanliness is becoming increasingly important. Oxygen and sulfur in molten steel adversely affect steel properties and must be removed during the refining process. However, the removal of oxygen and sulfur from molten high-Cr steel is more difficult than the removal of them from plain steel. Furthermore, residual oxygen and sulfur segregate during solidification and become the cause of cracking and fracture. Therefore, it is important to suppress the segregation of oxygen and sulfur during solidification. On the other hand, rare earth metals (REM) segregate during solidification along with oxygen and sulfur and precipitate as oxides and sulfides. Therefore, it is expected to suppress the segregation by controlling the precipitation of REM compounds. To control the formation of REM compounds in stainless steel, thermodynamic data on the interaction between REM and Cr in molten steel are required; however, available data are limited. This work focused on La as a rare earth metal, and the interaction coefficient of La with Cr in molten iron was measured at 1873 K using a chemical equilibration technique based on the liquid immiscibility between molten iron and silver phase. The La and Cr contents of molten Fe and Ag phases were analyzed by inductively coupled plasma emission spectrometry. It is found that the La content of the Ag phase increases with the increase of Cr content of iron. This result suggests that a repulsive force works between La and Cr in molten iron. The interaction parameter between La and Cr in molten iron at 1873 K was determined to be $\varepsilon^{\mathrm{Cr}}_{\mathrm{La(in\ Fe)}} = 6.24(\pm 1.31)$. Thermodynamic analysis of the formation of La compounds revealed that in high-chromium steel compared to plain steel, the formation of La oxide is suppressed, while the formation of La oxy-sulfide is enhanced.

Keywords: Rare earth metal; La; Stainless steel; Interaction parameter; Segregation.

Effects of Elemental Diffusion and Intermetallic Phases on the Microstructure, Mechanical Properties of Ti/Ti-6Al-4V Dissimilar Welding

Nguyen Van Hieu[1], Vu Trung Kien[1], Nguyen Tien Dung[2], Nguyen Thanh Dat[2], Nguyen Anh Xuan[3], Nguyen Duong Nam[3], Nguyen Hong Hai[1], Ha Minh Tan[1], Do Minh Duc[1], Vu Ngoc Hai[4], Lee Soo Yeol[2], Lee Seungwon[4], Kenji Matsuda[4], Pham Mai Khanh[1]*

[1] School of Materials Science and Engineering, Hanoi University of Science and Technology, Hanoi, Vietnam

[2] Department of Materials Science and Engineering, Chungnam National University, Daejeon, South Korea

[3] Vietnam Maritime University, Haiphong, Vietnam

[4] Department of Materials Science and Engineering, University of Toyama, Toyama, Japan

Email: khanh.phammai@hust.edu.vn

*Corresponding author

Abstract

This study focuses on clarifying the relationship between elemental diffusion and phase transformations that cause microstructural changes in Ti/Ti-6Al-4V dissimilar welding. Based on SEM-EDS analysis and hardness (HV) measurements, the difference in Al and V content was identified as the main reason for changes in microstructure and mechanical properties after welding.

Joints were produced by TIG (GTAW) using Ti-6Al-4V filler (W-Th₁ Ø2.4 mm), argon shielding 5 L·min⁻¹ (~12 MPa), and pulsed current 150/70 A. OM/SEM-EDS/TEM confirms the intermetallic phase in the fusion zone, including α′-martensite, Ti_3Al (α_2), and ω. The diffusion width of Al is markedly larger than that of V. Microhardness varies across the joint: ~225 HV in CP-Ti base metal, peaking at ~505 HV in the fusion zone, then decreasing toward the Ti-6Al-4V side (~458–442 HV).

These findings offer practical markers for weld quality assessment and for flagging regions that may be susceptible to embrittlement or cracking. They also open avenues for future work on refining welding parameters and post-weld heat treatment to balance strength and ductility across zones.

Keywords: Ti/Ti-6Al-4V dissimilar welding; Elemental diffusion; Microstructural transformation; Ti_3Al (α_2); ω phase; α′ martensite.

Hierarchical Si@T-Nb_2O_5 Core-Shell Confined within Conductive Carbon Nanofiber Scaffolds for High-Capacity Lithium-Ion Storage

Xiaochen Wu[1], Yongtao Zhao[1], Teng Long [1,*], Pengchao Si [1,*]
[1]State Key Laboratory of Coatings for Advanced Equipment, Key Laboratory for Liquid-Solid Structural Evolution and Processing of Materials (Ministry of Education), School of Materials Science and Engineering, Shandong University, Jinan, 250061, China.
Email: Pengchao Si: pcsi@sdu.edu.cn; Teng Long: tenglong@sdu.edu.cn
*Corresponding author

Abstract

Silicon has emerged as a promising anode material for next-generation lithium-ion batteries due to its exceptional theoretical capacity (4200 mAh g^{-1}), low working potential (~0.4 V vs. Li^+/Li), environmental friendliness, and natural abundance. However, its practical application is hindered by significant volume changes (~300%), unstable SEI formation, and poor reaction kinetics. To address these challenges, we developed a novel Si@T-Nb_2O_5@C-CCNF composite through hydrothermal synthesis, featuring a nitrogen-doped porous carbon shell encapsulating Si@T-Nb_2O_5 core. Theoretical simulations reveal that the T-Nb_2O_5 interphase facilitates Li^+ diffusion and lowers the energy barrier at carbon/Si interfaces. The optimized electrode delivers outstanding cycling stability and high rate capability. Full cell paired with LFP cathode demonstrates 150.4 mAh g^{-1} capacity after 80 cycles at 0.2C (98.3% retention). Notably, flexible pouch cells maintain stable LED illumination under repeated mechanical deformation, showcasing excellent practical potential.

Keywords: silicon anode; T-Nb_2O_5; structural design; coaxial electrospinning

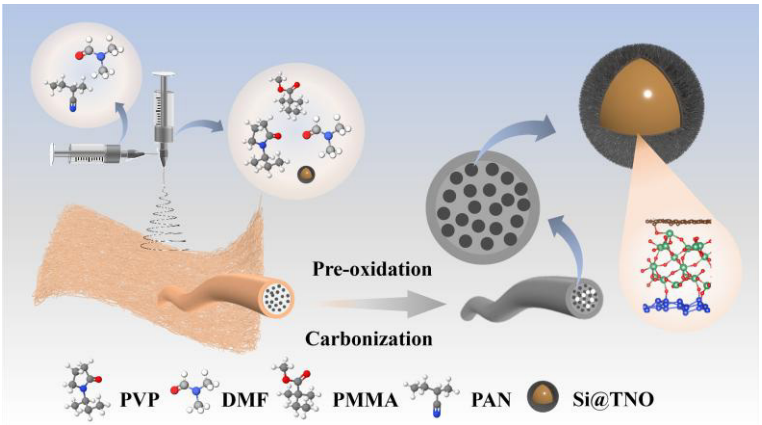

Anion-Tailored Solvation Clusters in Methyl Acetate Electrolyte: Achieving Concurrent Low Temperature Operation and High Voltage Stability

Jiaxuan Feng[1], Pengchao Si[*]
[1]State Key Laboratory of Coatings for Advanced Equipment, Key Laboratory for Liquid-Solid Structural Evolution and Processing of Materials (Ministry of Education), School of Materials Science and Engineering, Shandong University, Jinan 250061, China
Email: pcsi@sdu.edu.cn
*Corresponding author

Abstract

The development of lithium-ion batteries (LIBs) under extreme operating conditions (high voltage > 5.0 V and ultra-low temperature < -20 °C) faces limitations imposed by poor interfacial stability of conventional carbonate-based electrolytes and slow Li^+ transport kinetics. Methyl acetate (MA) offers great low-temperature advantages as a carboxylic acid ester solvent with an ultra-low melting point and viscosity. However, its electrochemical instability affects the interfacial stability, and the exact mechanism has not been well elucidated. Based on this issue, we propose a novel localized high-concentration electrolyte (LHCE) system based on MA, engineered through solvation structure reconstruction and anion coordination chemistry, which establishes a ternary solvent system with enhanced Li^+ mobility and reduced viscosity. The designed electrolyte enables the Li/NCM811 cell to be stably cycled for 200 cycles at -20 °C and 4.7 V while maintaining 84.9 % of the initial capacity. It keeps excellent cycling performance at the ultra-low temperature of -60 °C (93.02 % retention). Furthermore, the G/NCM811 pouch cell injected with the designed electrolyte has a CE of 88.78 % for the first cycle at a high voltage of 5.2 V. The new electrolyte exhibits an ultra-high oxidation cut-off voltage (~ 5.63 V vs. Li/Li^+) and a conductivity of 5.894 mS cm^{-1} at -40 °C, offering a promising avenue for the development of high-voltage resistant electrolytes suitable for use in extreme environments.

Keywords: methyl acetate (MA); LHCE; high voltage; wide temperature range

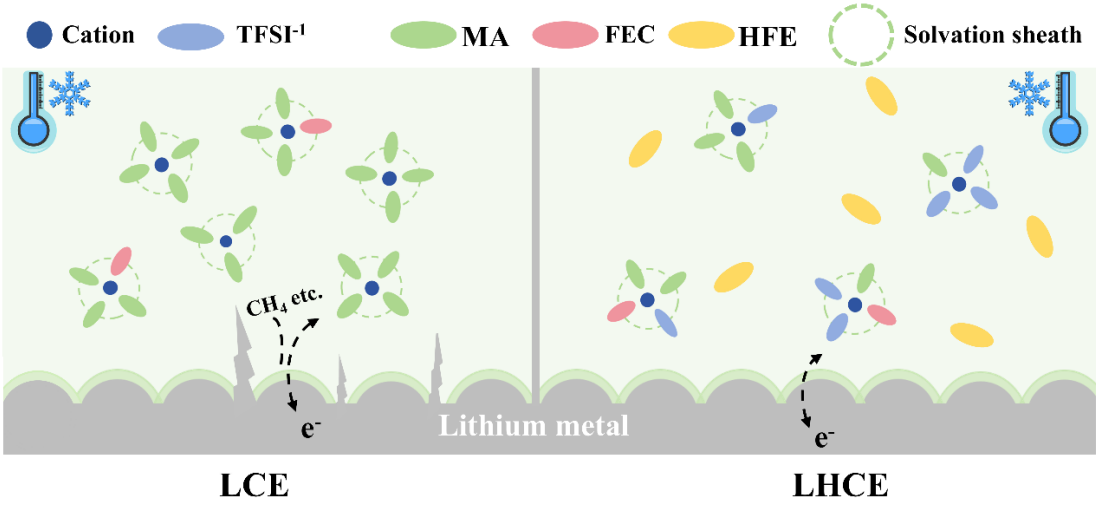

Effects of Process Parameters and Prior-Forming Process in Gaseous Ferritic Nitrocarburising of Low Carbon Steels

John Thomas Harry Pearce*[1], Sankum Nusen[1,2], Torranin Chairuangsri[1,2], Nipon Taweejun[3], Natnaree Senaweenin[3], Putthitorn Dechophop[3] and Teerapat Mungwattana[3]
[1]Department of Industrial Chemistry, Faculty of Science, Chiang Mai University, 50200 Thailand
[2]Centre of Excellence in Materials Science and Technology, Chiang Mai University, 50200 Thailand
[3]Thai Tohken Thermo Co. Ltd., Amata City, Chonburi, 20000 Thailand
E-mail address: jthp70@gmail.com
*Corresponding author

Abstract

Nitrocarburising produces a surface compound layer consisting of complex hard carbonitrides, increases the surface hardness and wear resistance, and improves fatigue and corrosion resistance of treated components. In gaseous ferritic nitrocarburising (GFNC), savings in production costs can be possible by reducing the amount of treatment gas used *via* reduction of gas flow rate into the treatment furnace, the treatment time, and the ammonia/reducing gases ratio used in the treatment gas mixture, while the correct characteristics, properties and overall quality of the nitrocarburized surfaces must be maintained. Also, it is well-known that prior processing before GFNC, such as hot forming or hot rolling, leads to surface oxide layer formation, and that some studies have reported that pre-oxidation before GFNC may form a thicker compound layer with more uniform and higher hardness.
In the present work, it is of interest to improve the efficiency of commercial GFNC treatment of plain low carbon steel, JIS G3141 (SPCC steel), to counteract ever increasing energy and materials costs. This group of steels is the largest requiring nitrocarburising treatment, particularly to improve the performance of mainly thinner-sectioned engineering and automotive parts. Any change to normal process operations will impact on the resultant microstructure and properties of the compound layer and its supporting substrates. Hence, a design of experiments approach using Analysis of Variance (ANOVA) was used to assess the effects of experimental treatment time, gas flow rate and ammonia/reducing gaseous ratio during GFNC of SPCC steel. Also, it is of interest to study possible effects of prior-forming on GFNC by comparing the GFNC treatment of cold-rolled SPCC steel with that of hot-rolled SPHC steel having similar composition. The results will be discussed based on the hardness depth profile obtaining from Vickers microhardness and nano-hardness tests, as well as thickness, porosity, microstructure and elemental distribution in the compound and diffusion layers obtaining from optical microscopy (OM), scanning electron microscopy (SEM) and wavelength dispersive X-ray spectroscopy (WDS).

Keywords: Gaseous Ferritic Nitrocarburising (GFNC); SPCC steel; SPHC steel; Microstructure; Hardness

A Self-Assembled Metal-Organic Framework Network-Reinforced Solid Electrolyte via In Situ Polymerization for Lithium Metal Batteries

Jianwei Qiu[1], Pengchao Si[1,*]
[1] State Key Laboratory of Coatings for Advanced Equipment, Key Laboratory for Liquid-Solid Structural Evolution and Processing of Materials (Ministry of Education), School of Materials Science and Engineering, Shandong University, Jinan 250061, China
Email: pcsi@sdu.edu.cn
*Corresponding author

Abstract

Solid electrolytes face the challenge of simultaneously achieving rapid ion transport and stable interfacial contact, as the optimal coordination environment for Li^+ conduction often conflicts with ideal interfacial chemistry. Herein, a composite polymer electrolyte (CPE) was constructed through the in situ polymerization of 1,3-dioxolane (DOL) electrolyte within a customized three-dimensional interconnected metal-organic framework (MOF)-modified porous polyimide (PI) framework to synergistically enhance ion transport kinetics and interface stability. The MOF selectively anchors anions via coordination effects and steric hindrance, which not only establishing continuous fast lithium ion channels but also promoting anions to participate in the formation of a stable derived SEI layer. Furthermore, the in situ formed poly-DOL within the porous framework ensures intimate electrode-electrolyte contact, significantly reducing interface impedance and enhancing ion migration efficiency, thereby effectively extending the Sand's time for lithium dendrite nucleation. The battery assembled based on this CPE exhibits excellent electrochemical performance, and this work provides valuable insights into addressing the challenges of ion transport and interfaces in solid-state lithium batteries.

Keywords: metal-organic framework; polyimide; in-situ polymerization; Lithium metal battery

Improved High-Temperature Performance of Al–Ce–Ni Alloys via Mg Solid-Solution Strengthening

Abid Abdu Mohammed, Phromphong Pandee*
Department of Production Engineering, Faculty of Engineering, King Mongkut's University of Technology Thonburi, Bangkok, 10140, Thailand
Email: phromphong.pan@kmutt.ac.th
*Corresponding author

Abstract

The remarkable thermal stability of Al–Ce alloys makes them promising candidates for structural applications at elevated temperatures. However, further improvement in their mechanical properties is essential for practical deployment. Microalloying offers a viable approach to enhance the mechanical performance of Al–Ce alloys by tailoring their strengthening mechanisms. In this study, a series of Al–10Ce–5Ni–xMg alloys (x = 0, 0.1, 0.3, 0.5, and 0.7 wt.%) were synthesized to investigate the influence of Mg addition on phase stability, microstructural evolution, and hardness. X-ray diffraction revealed Al, $Al_{11}Ce_3$, and Al_3Ni as the phases present across all compositions. SEM/EDS and optical microscopy confirmed that no Mg-containing intermetallics formed, consistent with Pandat thermodynamic predictions. Polarized optical microscopy indicated notable grain refinement, with an approximately 21% reduction in average grain size at 0.7 wt.% Mg. Vickers microhardness measurements showed increased hardness in both as-cast and thermally exposed conditions, primarily attributed to Mg-induced solid-solution strengthening. Overall, Mg microalloying effectively enhances the mechanical performance of Al–Ce–Ni alloys while retaining their excellent thermal stability.

Keywords: Pandat; Solid solution strengthening; Al-Ce-Ni-Mg; Thermal stability

Preparation and properties of polymer hydrogel from boric acid-crosslinked PVA for urea slow-release fertilizer

Wanida Wongla, Wilaiwan Simchuer, Pattranuch Pongsuk*
Department of Chemistry, Faculty of Science and Technology, Loei Rajabhat University, Loei, 42000
Email: pattranuch.pon@lru.ac.th
*Corresponding author

Abstract

In this study, polymer hydrogels were prepared from polyvinyl alcohol (PVA) and crosslinked with boric acid at 5% and 15% (w/w). The hydrogels were characterized using scanning electron microscopy (SEM), X-ray diffraction (XRD), and Fourier-transform infrared spectroscopy (FTIR) to elucidate their structural and chemical properties. The swelling behavior and the ability to release urea fertilizer were investigated. The results found that the PVA hydrogel crosslinked with 5% boric acid exhibited the highest swelling capacity as 1124.48 ± 0.047%. SEM analysis revealed that this hydrogel showed a highly porous multilayer structure, which is beneficial for water absorption and nutrient loading, while FTIR spectra confirmed the formation of crosslinking interactions between hydroxyl groups of PVA and borate ions. Urea release experiments, performed using a microplate reader (SPECTROstar Nano). It was found that the PVA–5% boric acid hydrogel provided a sustained and controlled release of urea for more than 84 hours. In contrast, pure urea showed an immediate and rapid release within just 1 hour. Furthermore, biodegradation studies indicated that the PVA–5% boric acid hydrogel decomposed completely in soil within 42 days, highlighting its environmental compatibility. In conclusion, the developed PVA–boric acid/urea hydrogel represents a promising and eco-friendly material for slow-release fertilizer applications in agriculture and horticulture.

Keywords: hydrogel; slow- release fertilizer; polyvinyl alcohol (PVA); crosslinking; boric acid

Improved Efficiency and Stability in $MAPbI_3$ Perovskite Solar Cells through Bulk Defect Passivation with Benzyl Trimethylammonium Tribromide

Bhabani Sankar Swain[1], Hiba Shahulhameed[1], Abdul Kareem Kalathil Soopy[1], Afna Manaf[1], Nail Ibrahim[2], Adel Najar[1,*]
[1] Department of Physics, College of Science, UAE University, Al Ain, Abu Dhabi, United Arab Emirates
[2] Department of Chemistry, College of Science, UAE University, Al Ain, Abu Dhabi, United Arab Emirates
Email: adel.najar@uaeu.ac.ae
*Corresponding author

Abstract

Perovskite materials offer a promising future for solar cells due to their high-power conversion efficiency, carrier transport properties, and low-temperature solution processability[1], however, require appropriate defect management in the bulk and at the surface and interface[2]. Bulk passivation is a technique for reducing defect density in perovskite film, improving efficiency and stability. Solution-processed halide perovskites have a large variety of defects arising from less formation energy and rapid growth process during spin coating process. Herein, we introduce benzyl trimethyl ammonium tribromide (BTMATB) in the precursor of perovskite solution to passivate uncoordinated defects in the bulk and at the grain boundary of perovskite film. The BTMATB incorporated to the precursor solution regulates the growth of the film's quality, effectively passivating the Pb2+ and X- associated defects in the bulk and at the grain boundaries of MAPbI3 perovskite films.
In addition to that the passivated films show better morphologies and crystallinity compared to the pristine films. The BTMATB-treated planar perovskite solar cell achieved an efficiency of 19.65%, exceeding the pristine device's efficiency of 17.84%. Moreover, the hydrophobic benzyl chain improves the device stability by which the device retains 90% of PCE after 600 hr.

Keywords: Perovskite; solar cell, defects; passivation

Synthesis of Low Carbon Polymorph Belite Cement: A Comparison of Pure Oxides and Lignite Bottom Ash

Chadapohn Tashingkam[1], Maneerat Thala[1], and Kedsarin Pimraksa[1,2,3]*
[1]Department of Industrial Chemistry (Faculty of Science, Chiang Mai University, 50200, Thailand)
[2]Center of Excellence in Materials Science and Technology (Faculty of Science, Chiang Mai University, 50200, Thailand)
[3]Materials Science Research Center (Faculty of Science, Chiang Mai University, 50200, Thailand)
Email: kedsarin.p@cmu.ac.th
*Corresponding author

Abstract

This research investigates the synthesis of belite (C_2S, Ca_2SiO_4) cement doped with boron oxide to observe polymorph of C_2S. Belite cement is claimed to be environmentally friendly cement or alternative cement due to its lower temperature production and lower greenhouse emission than ordinary Portland cement. In this study, calcium carbonate and silica are used as CaO and SiO_2 sources, respectively. Lignite bottom ash (BA) is used as CaO and SiO_2 source as a comparison. The proportion of the starting materials is based on the stoichiometry of belite cement with CaO/SiO_2 molar ratio of 2.0. The excess molar ratios have also been studied when BA is used. The firing temperatures (1200˚C, 1300˚C, and 1400˚C) with a rapid air-cooling are varied. The rapid air-cooling and slow cooling are investigated as a comparison at 1200˚C. Various contents of 0-1.5 wt% of B_2O_3 are studied at 1200˚C with a slow cooling condition. The synthesized cement quality is determined from their mineralogical compositions using X-ray diffractometer. In addition, the synthesized cement quality under different firing temperatures with rapid air-cooling and slow cooling is determined using particle size distribution and surface morphology. For pure oxide system, with undoped and rapid air-cooling conditions, C_2S contains β-C_2S as a major phase after firing at 1200˚C. For firing at higher temperatures (1300˚C and 1400˚C), γ-C_2S is a major phase. Particle sizes of the synthesized cement slightly increase when compared to their starting raw mix. With an increase in B_2O_3 content up to 1 wt% of B_2O_3 and rapid air-cooling, belite cement has a larger particle size than undoped belite cement due to more sintering effect and shows a promotion of α'$_L$–C_2S when firing temperature increases. Interestingly, γ-C_2S phase tends to increase when a fast cooling is applied. In other words, β-C_2S is enhanced with slow cooling. The synthesis of belite cement using BA is more influential by intermediate gehlenite ($Ca_2Al_2SiO_7$) and β-C_2 S, reflecting the complex chemistry of waste-derived raw materials. When CaO/SiO_2 molar ratio is increased from 2.0 to 2.5, gehlenite tends to decrease with an enhancement in β-C_2S and α'L–C2S phases, demonstrating the possibility of utilizing such an industrial waste for cement production, contributing to sustainable construction material development.

Keywords: Belite cement; Beta belite; Gamma belite; Alpha belite; Lignite Bottom Ash

Application of Impurity Removal through Selective Extraction and Phase Separation to the recovery of Al from Cast Al alloy

Kengo Kato[1,*], Sadanori Kajitani[2], Hideki Ono[1]
[1]Deprtment of Materials Science and Engineering, Faculty of Sustainable Design, University of Toyama, Toyama, Japan
[2]Aluminum Research Center, University of Toyama, Takaoka, Japan
Email: kato@sus.u-toyama.ac.jp
*Corresponding author

Abstract

The smelting process of aluminum ore requires a large quantity of electric energy, whereas the melting and recycling of used aluminum products consumes less energy. Therefore, aluminum recycling can reduce energy consumption to less than 1/10 of primary aluminum production. Accordingly, the recycling of aluminum is important. However, impurity elements are inevitably contained in the Al scrap recovered from society, and most of them are difficult to remove by the current pyro-metallurgical processes. Therefore, the aluminum scraps are mainly recycled into the cast alloys, which have a high tolerance level of impurities. Silicon is usually added to cast Al alloy to improve the fluidity of molten aluminum, whereas the silicon content of wrought aluminum alloy is controlled to be less than 1 mass%. Therefore, silicon removal is necessary to recycle cast aluminum scraps into wrought aluminum alloys. The authors proposed a new technology to remove Si with the application of the pyrometallurgical knowledge of extraction and phase separation. Aluminum can dissolve in molten tin, whereas Si cannot. The difference in the dissolution behavior of Al and Si into molten tin can be utilized for the selective extraction of aluminum from aluminum scraps, and aluminum can be separated from the residues consisting of Si. Furthermore, when the molten Sn-Al alloy is cooled to the melting point of tin, aluminum with low impurity content will precipitate. In this study, the principle of Si removal was applied to recover Al from a cast Al alloy using a bench-scale testing furnace. The possibility of Al recovery through the selective extraction and phase separation was examined.

Keywords: Al recycling; Silicon removal; Selective Extraction and Phase Separation; Cast aluminum alloys

Investigation on Dehydroxylation Temperature of Clay Minerals Affecting Mechanical Properties of Limestone-Calcined Clay Cement

Ketsarin Ariya[1], Sunatcha Seerat[1], Maneerat Thala[1], Worapong Thiemsorn[1,2] and Kedsarin Pimraksa [1,2,*]

[1]Department of Industrial Chemistry (Faculty of Science, Chiang Mai University, Chiang Mai, 50200, Thailand)

[2]Center of Excellence in Materials Science and Technology (Faculty of Science, Chiang Mai University, Chiang Mai, 50200 Thailand)

[3]Materials Science Research Center (Faculty of Science, Chiang Mai University, Chiang Mai, 50200 Thailand)

Email: Kedsarin.p@cmu.ac.th

Abstract

Two kaolinitic clays (1:1 phyllosilicate structure) from Thailand, with different crystallinity are investigated under thermal and mechanical activations in terms of their physical and mineralogical changes. Montmorillonitic clay (2:1 structure) is also investigated as a comparative study. The thermal activation is performed at 600, 700, 800, and 900 °C for the kaolinitic clays and at 730, and 830 °C for the montmorillonite, according to their physical and chemical changes using thermogravimetric analysis. Dehydroxylation changes of the thermally activated clays are characterized using x-ray diffraction, fourier transformed infrared spectrometry, and particle size distribution. The difference in the effect of the dehydroxylation temperature on the local Si and Al environments of kaolinitic clay has been studied by solid-state nuclear magnetic resonance spectroscopy. After thermal treatment, the calcined clay undergoes mechanical activation using ball mill to obtain the particle size less than 10 µm. The observation on the reactivity of the calcined clays is performed with a replacement of Portland cement (PC) clinker using the composites comprising of 50 wt% clinker, 30 wt% calcined clay, 15 wt% limestone, and 5 wt% gypsum at curing periods of 7, and 28 days. The highest compressive strength could be obtained at 800 °C, and at 830 °C, which kaolinitic and montmorillonitic structures are completely collapsed, respectively. The results show that after calcination, kaolinite with higher crystallinity provides a slightly lower strength (48 MPa) than that with lower crystallinity containing 49 MPa, while the calcined montmorillonite shows the highest strength (54 MPa) amongst them. The calcined clays undergo pozzolanic reaction combined with the hydration of the PC to form calcium (alumino)silicate hydrate, monocarboaluminate and ettringite minerals as binding phases. After hydration, calcined kaolinite with lower crystallinity provides higher calcium aluminosilicate hydrate than that with higher crystallinity. The calcined montmorillonite containing higher SiO_2 content shows the highest calcium silicate hydrate binding phases supporting the highest strength development. In addition, the finer particle size of montmorillonite plays an additional role on the strength development.

Keywords: Kaolinite; Montmorillonite; Dehydroxylation; Cement hydration

Influence of Short-Range Order and Precipitates on the Mechanical and Magnetic Properties of Multicomponent Alloys

Anna Wojcik[1*], Robert Chulist[1], Arkadiusz Szewczyk[1], Nikodem Poręba[1], Łukasz Hawełek[2], Wojciech Maziarz[3]
[1]Faculty of Metals Engineering and Industrial Computer Science, AGH University of Krakow, Krakow, Poland
[2]Lukasiewicz Research Network—Institute of Non-Ferrous Metals, 5 Sowinskiego Str., Gliwice 44-100, Poland
[3]Institute of Metallurgy and Materials Science of the Polish Academy of Sciences, Krakow, Poland
Email: anwojcik@agh.edu.pl
*Corresponding author

Abstract

Multicomponent alloys, particularly high-entropy alloys (HEAs), have been extensively investigated due to their exceptional mechanical and physical properties. This includes outstanding toughness at both room and cryogenic temperatures, excellent strength and ductility, high resistance to fatigue and creep, superior corrosion resistance, remarkable damage tolerance, and even superconductivity. Such a wide range of unique properties makes HEAs highly promising for diverse applications in energy, environmental technologies, electrocatalysis, thermoelectrics, and energy storage.
In this study, we examined different microstructural design strategies, focusing particularly on the influence of short-range order (SRO) which is reflected in a large change of lattice parametres (Fig. 1), as well as nano- and micro-scale precipitates, on the balance between strength and ductility, as well as on the magnetic properties of multicomponent alloys. The analysis was carried out using high-energy X-ray diffraction, along with scanning and transmission electron microscopy.
Our findings demonstrate that the formation of short-range order significantly affects the mechanical and magnetic performance of these materials and serves as a key factor in optimizing both chemical composition and heat treatment protocols.

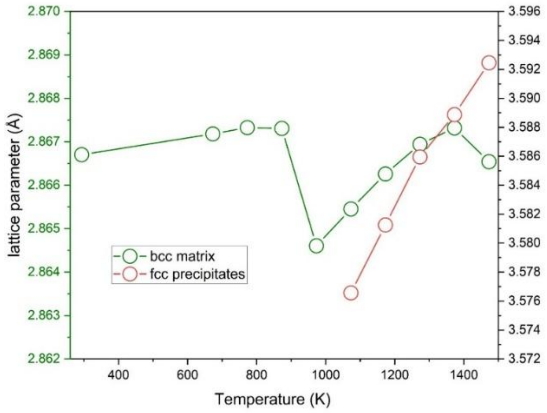

Fig. 1 Variation of lattice parameters with heat treatment temperature in the CoFeAlCr multicomponent alloy.

Acknowledgment
Financial support of the National Science Centre, Poland (project no. 2022/47/B/ST8/03298) is greatly acknowledged.

Design of Porous Carbon/Organic Polymer Composites as Cathode Materials in Li–S Batteries

Kittiputh Kunniyom[1,2], Orapim Namsar[1,3], Wittawat Punyaarthansakun[1], Waewwow Yodying[1], Chawin Yodbunork[3,4], Thanapat Autthawong[3,5], Natthawat Semakul[1,3], Montawat Wiboon[6], Jaturon Kumchompoo[6], Jyh-Tsung Lee[6], and Thapanee Sarakonsri[1,2,3,*]

[1] Department of Chemistry, Faculty of Science, Chiang Mai University, Muang, Chiang Mai 50200, Thailand.

[2] Center of Excellence for Innovation in Chemistry (PERCH-CIC), Faculty of Science, Chiang Mai University, Muang, Chiang Mai 50200, Thailand.

[3] Material Science Research Center, Faculty of Science, Chiang Mai University, Muang, Chiang Mai 50200, Thailand.

[4] Office of Research Administration, Office of the University, Chiang Mai University, Muang, Chiang Mai 50200, Thailand

[5] Department of Industrial Chemistry, Faculty of Science, Chiang Mai University, Muang, Chiang Mai 50200, Thailand

[6]Department of Chemistry, National Sun Yat-Sen University, Kaohsiung 80424, Taiwan

* Correspondence: thapanee.s@cmu.ac.th

Abstract

Lithium–sulfur (Li–S) batteries are attractive next-generation energy storage systems owing to their high theoretical capacity and energy density. However, the insulating nature of sulfur, the large volume expansion of lithium polysulfides, and the shuttle effect limit their commercialization. To address these challenges, porous carbon (PC) is often employed as a sulfur host due to its high surface area and conductivity, but its polysulfide retention relies only on weak physisorption. Porous organic polymers provide stronger chemical interactions but typically suffer from low sulfur content. In this work, a composite of porous carbon and disulfide-based porous organic polymer (POPDS) was developed to integrate the advantages of both components. PC was derived from biomass via KOH activation and pyrolysis, while POPDS was synthesized through an azo coupling reaction. The composite (SFPC/POPDS) was then subjected to inverse vulcanization with elemental sulfur to increase the sulfur content, yielding SFPC/POPDS-S(x). Structural characterization by XRD confirmed amorphous phase of SFPC and POPDS, while crystalline sulfur peaks were observed in the vulcanized composites. FTIR and XPS analyses verified the coexistence of functional groups and enhanced sulfur incorporation. Electrochemical studies demonstrated that SFPC/POPDS-S(x) delivered higher discharge capacities and lower charge-transfer resistance compared to the pristine components, while GITT analysis revealed fast lithium-ion diffusion. These results highlight SFPC/POPDS-S(x) composites as promising cathode materials that combine high conductivity, efficient sulfur confinement, and enhanced electrochemical performance for advanced Li–S batteries.

Keywords: Porous carbon; Porous Organic Polymers; Biomass; Inverse vulcanization; Lithium-sulfur battery

Development of Anode from Zinc Powder with Polyvinyl Alcohol Binder for Solid-state Zinc-air Batteries

J. Khemtong [1], K. Boulloy[1], J. Pumsusak[1,2], S. Nusen[1,2], J. T.H. Pearce[1], T. Chairungsri[1,2]
[1] Department of Industrial Chemistry, Faculty of Science, Chiang Mai University, Chiang Mai 50200, Thailand
[2] Center of Excellence in Materials Science and Technology, Chiang Mai University, Chiang Mai 50200, Thailand
*Corresponding Author e-mail address: nusen.san@gmail.com (Sankum Nusen)

Abstract

Anodes for potential use in solid-state zinc–air batteries were fabricated using zinc powder and a polyvinyl alcohol (PVA) binder.1 Various weight ratios of zinc powder to binder were investigated, including 1:0.2, 1:0.1, 1:0.05, and 1:0.025 ratio. The binder solution was prepared by dissolving 10 wt% PVA in water and adding 25 vol% glutaraldehyde (GA) as a crosslinking agent, with a GA-to-PVA ratio of 6:1. The resulting zinc–binder mixture was poured into a mold with dimensions of 3 × 3 × 0.3 cm^3 and allowed to dry at room temperature for 24 hours. A commercial zinc plate was included as an additional reference electrode. The anode performance of the solid-state metal-air battery was tested in a single cell metal-air battery. The battery cell consisted of an anode (zinc powder mixed with PVA binder) and a cathode (oxygen from the air), with a stainless-steel grid as a current conductor. A PVA/Polyvinylpyrrolidone (PVP) blend in a mass ratio of 1:0.5, cross-linked with glutaraldehyde, was immersed in a 7.0 M aqueous KOH solution for use as a solid electrolyte. Manganese oxide was coated onto the Gas diffusion layer (GDL) plate as a catalyst. The battery was discharged at a current density of 2 mA/cm^2. Morphology of the anodes before and after was analyzed using scanning electron microscopy (SEM, Hitachi, SU3000) equipped with energy dispersive x-ray spectroscopy (Oxford) for conducting the local chemical analysis. The experimental results for the zinc powder anode 1:0.2 ratio showed that the open-circuit voltage (OCV) of the battery was approximately 1.56 V, the specific capacity of the battery was around 900 mWh/g, the specific capacity of the battery was around 824.85 mAh/g, calculated from the theoretical zinc loss and a discharge time of 290 minutes. This indicates that the binder quantity had no significant effect on the specific capacity of the battery. It was noted that the zinc powder anode exhibited smaller oxide particles, which provided a larger reactive surface area, resulting in better performance compared to that of the zinc plate.

Keywords: Zinc powder anode, PVA binder, Zinc-air battery, Discharge performance

Removal of Impurities from Die-cast ADC12 Aluminum Alloy Via Molten Tin

Satoshi IWASAWA[1,2], Kengo KATO[3], Hideki ONO[3,*]
[1]Department of Materials Design and Engineering, School of Sustainable Design, University of Toyama, Toyama, Japan
[2]Materials Technology Section, Fundamental Technology Department, Sankyo Tateyama, Inc., Toyama, Japan
[3]Department of Materials Design and Engineering, Faculty of Sustainable Design, University of Toyama, Toyama, Japan
Email: ono@sus.u-toyama.ac.jp
*Corresponding author

Abstract

To achieve carbon neutrality, reducing CO_2 emissions is essential. CO_2 emissions from recycled aluminum can be limited to 3% of those from natural resources. In Japan, only about 10% of wrought Al alloys are produced from recycled aluminum. To expand the use of recycled aluminum in producing wrought Al alloys, various impurities contained in scrap derived from cast Al alloys must be removed. To recycle scrap derived from high-impurity die-cast ADC12 alloy into wrought alloys 6061 and 6063, the removal of Si, Fe, and Cu is necessary. This study focused on the principle of removing Si, Fe, and Cu from ADC12 alloy, which utilizes the differences in solubility between Al and these impurity elements in molten Sn (Sn(l)). In Sn(l) at 600°C, Si and Fe hardly dissolve, Cu dissolves at about 30 mass%, while Al dissolves at about 50 mass%. On the other hand, at 300°C, Si, Fe, Cu, and Al hardly dissolve in Sn(l). Therefore, Si, Fe, and Cu can be removed at 600°C, and Al crystallized at 300°C can be recycled into wrought alloys. In this work, the removal elements and their reduction limits were investigated when ADC12 alloy was dissolved in Sn(l). The alloy melt with a Sn/Al ratio of 3.86, prepared by dissolving ADC12 alloy in Sn(l), was held at 560°C for 0, 0.5, 1, and 5 h. Compounds containing Si, Fe, Mn, Cr, and Ti were floating in the molten alloy. Therefore, it was suggested that the removal of these elements is possible. The chemical composition in regions with low impurity concentrations was analyzed by inductively coupled plasma atomic emission spectrometry (ICP-AES). The analysis revealed that the impurity concentrations lowered their reduction limits at an early stage.

Keywords: Aluminum recycling; impurity removal; molten Sn; ADC12 alloy.

Enhanced Photocatalytic Activity of Zn-MOF and TiO_2 Nanocomposite for Methyl Orange Removal

Pemika Chaichana[1], Saranphong Yimklan[2], Yothin Chimupala[3]*
[1]Department of Industrial Chemistry and Doctor of Philosophy Program in Industrial Chemistry and Innovation, Faculty of Science Chiang Mai University, Thailand
[2]Department of Chemistry, Center of Excellence in Materials Science and Technology, and Materials Science Research Center, Faculty of Science, Chiang Mai University, Thailand
[3]Department of Industrial Chemistry, Center of Excellence in Materials Science and Technology, and Materials Science Research Center, Faculty of Science, Chiang Mai University, Thailand
Email: yothin.chimupala@cmu.ac.th
*Corresponding author

Abstract

Effective wastewater management is vital for mitigating the environmental impact of organic pollutants such as dyes and pesticides that threaten aquatic ecosystems. Among various treatment technologies such as advanced oxidation processes (AOPs), particularly photocatalysis. Photocatalysis process have attracted considerable attention due to their environmental compatibility and cost effectiveness. Titanium dioxide (TiO_2) is one of the most commonly used materials for photocatalytic applications due to its stability, non-toxicity, and strong oxidation ability. However, its photocatalytic efficiency is limited by narrow light absorption and rapid electron–hole recombination. Therefore, this study aims to enhance the photocatalytic performance of TiO_2 by constructing a zinc-based metal–organic framework (Zn-MOF)/TiO_2 heterostructure and clarifying its underlying mechanism through combined experimental and theoretical analyses. The Zn-MOF was synthesized via a microwave-assisted method using 4,4′-bipyridine and succinic acid as organic linkers, followed by co-precipitation of TiO_2 nanoparticles (P25 and anatase nanorods) onto the Zn-MOF surface. X-ray diffraction (XRD) confirmed the high crystallinity and uniform dispersion of TiO_2 within the composite, while SEM observations revealed a uniform coating of TiO_2 on the Zn-MOF surface, validating the successful construction of the Zn-MOF/TiO_2 heterostructure. The photocatalytic activity was evaluated via methyl orange (MO) degradation under UVC irradiation, where Zn-MOF, Zn-MOF/P25 and Zn-MOF/TiO_2 nanorods achieved degradation efficiencies of 24.56%, 34.34%, and 48.76%, respectively. The result demonstrates a pronounced synergistic effect between both components. To gain further insight, a Zn-MOF/ TiO_2 heterostructure model was developed by placing a Zn-MOF unit on the TiO_2 (101) surface, the most thermodynamically stable facet. Band-structure calculations revealed a type-II heterojunction, and work function analysis (5.14 eV for Zn-MOF and 5.37 eV for TiO_2) confirmed electron transfer from Zn-MOF to TiO_2, generating an internal electric field that facilitates charge separation. The heterostructure operates via a Z-scheme mechanism, preserving strong redox potential while enhancing charge transport. Overall, the microwave-synthesized Zn-MOF/TiO_2 composite demonstrates superior photocatalytic efficiency and holds strong potential as a sustainable photocatalyst for wastewater treatment applications.

Keywords: Photocatalysis; Titanium dioxide; Metal Organic Framework and Composite material

Magnesium removal from Al-Mg alloy through molten salt electrolysis using LiCl-KCl-$MgCl_2$ at 723K

Hikaru FUJIOKA [1], Kengo KATO [2], and Hideki ONO [2,*], Hirokazu KONISHI[3]
[1]Graduate School of Science and Engineering, University of Toyama, Toyama, Japan
[2]Department of Materials Design and Engineering, Faculty of Sustainable Design, University of Toyama, Toyama, Japan
[3]Department of Materials Design and Engineering, National Institute of Technology, Suzuka College, Mie, Japan
Email: ono@sus.u-toyama.ac.jp
*Corresponding author

Abstract

Recycling Al alloy is important to mitigate CO_2 emissions. However, the contents of alloying elements need to be reduced when the aluminum alloy scraps are recycled into other types of aluminum alloys. The A5000 series Al alloy, used for can lids, contains 5 mass% magnesium, whereas the other types of aluminum alloy typically contain less than 1 mass%. Therefore, the Mg content needs to be reduced to utilize the A5000 series Al scrap. This study proposes a removal method of Mg from Al-Mg alloy through molten salt electrolysis using LiCl-KCl-$MgCl_2$. Because magnesium is less noble than aluminum, it can be dissolved into molten salt by controlling the electric potential of the Al-Mg alloy and recovered at the cathode. Electrolysis experiments of Al-3 mass% Mg alloy were performed at 723 K in LiCl-KCl-$MgCl_2$ molten salt, and the possibility of Mg removal was investigated. A glass container equipped with 3 electrodes was used as an electrolysis cell. The sample alloy and glassy carbon rod were connected to the anode and cathode electrodes, respectively. The 58.5 mol% LiCl-41.5 mol% KCl+1mol%$MgCl_2$ molten salt was used for electrolyte. A reference electrode was prepared using a glass tube containing the molten salt with 1 mol%AgCl and silver wire. The electrodes and thermocouple were inserted, and Ar gas was introduced to the glass container. The samples were subsequently heated to 723 K, and the electrolysis was performed at -1.2 V (vs. Ag+/Ag) for 6h. After the electrolysis, the sample was withdrawn from the container and cooled in air. The Mg distribution in the Al-Mg alloy after the electrolysis was analyzed by SEM-EDS. Comparing the Mg content of the samples before and after electrolysis, it was found that the average Mg concentration in the Al-Mg alloy can be decreased from 2.60 mass% to 0.30 mass%.

Keywords: Electrochemistry; Molten salt electrolysis; Aluminum recycling; Al-Mg alloy
Electrochemistry; Molten salt electrolysis; Aluminum recycling; Al-Mg alloy

Wear Behavior of Ti6Al4V Titanium Alloy Against Steel Balls Under Dry Sliding Conditions

Phutawan Camput[1], Thanyarat Lerdratchatasirithon[1], Nutthanun Moolsradoo[1,*]
[1]Department of Production Technology Education, King Mongkut's University of Technology Thonburi, Bangkok, Thailand
Email: nutthanun.moo@kmutt.ac.th
*Corresponding author

Abstract

The tribological behavior of Ti6Al4V titanium alloy under dry sliding conditions was investigated using a ball-on-disk tribometer. The tests were conducted against steel balls under normal loads of 1 N, 3 N, and 5 N. The sliding speed was maintained at 3.14 cm/s for a total of 3,000 revolutions. Wear characteristics of both the Ti6Al4V disks and the steel balls were evaluated in terms of wear track morphology, wear scar diameter, and wear volume. The coefficient of friction (COF) was also monitored throughout the tests to examine the effect of applied load on tribological performance. The results reveal that both the wear rate and friction coefficient increase with increasing normal load, indicating stronger adhesive and abrasive interactions at higher contact pressures. Moreover, the wear on the Ti6Al4V surface exhibited features typical of mild adhesive wear at low load, transitioning to severe wear at higher loads. These findings provide useful insights into the dry contact wear behavior of Ti6Al4V alloy when paired with steel counterparts, supporting its practical applications in mechanical components subjected to dry sliding environments.

Keywords: Ti6Al4V; Steel balls; Dry sliding; Wear mechanism; Coefficient of friction

Surface-Enhanced Sharp-Edged Gold Microneedles on Pencil Graphite Microelectrodes as an Efficient Electrochemical Platform for NADH Detection

Mani Arivazhagan[1] and Jaroon Jakmunee[1,2*]
[1]Research Laboratory for Analytical Instrument and Electrochemistry Innovation, Department of Chemistry, Faculty of Science, Chiang Mai University, Chiang Mai, 50200, Thailand
[2]Research Laboratory on Advanced Materials for Sensor and Biosensor Innovation, Materials Science Research Center, and Center of Excellence for Innovation in Chemistry, Faculty of Science, Chiang Mai University, Chiang Mai, 50200 Thailand
Corresponding Author E-mail: jaroon.jakmunee@cmu.ac.th (J. Jakmunee)

Abstract

Electrochemical (EC) detection of NADH levels plays a critical role in the diagnosis and management of conditions ranging from metabolic disorders to neurodegenerative diseases. Thus, there is a need for sensitive electrochemical sensors based on nanostructured electrode materials employed for diverse concerns such as biological, biomedical, biotechnological, clinical and medical diagnostics, environmental and health monitoring, and food industries [1]. In this work, we developed the miniaturized sharp-edged hyper-branched gold microneedles (Au MNDs) decorated with pencil graphitic microelectrodes (PGME) via a single-step, green electrochemical deposition strategy in the absence of any redox mediators, organic solvents and enzymes, etc. This morphology, combined with the unique surface features, fosters highly ideal conditions for the rapid electron transfer from NADH to the Au MNDs @PGME. The nanostructures improve the mobility directly influencing the speed and efficiency of electronic charge carriers, which accelerates the rate of electron transfer [2]. This enhances the electrochemical kinetics of the system, contributing to rapid and sensitive detection of NADH. These attributes indicate that Au MNDs-modified microsensor holds great potential for high sensitivity (62.80 μA/μM cm^{-2}), wider linear ranges from 0.1 μM to 54.5 μM, fast response (<2 sec), and lower LOD for the reliable NADH detection. Notably, the current micro sensing platform, which is based on Au MNDs @PGME, has proven to be useful in clinical diagnostics by successfully testing for NADH sensing in human serum and urine samples in biomedical application.

Keywords: Electrochemical; Clinical diagnosis; Microelectrodes; Microneedles; NADH; Pencil graphite; Miniaturization.

References:

[1] Mani Arivazhagan, Brij Mohan, Jaroon Jakmunee, Green Analytical Chemistry, 2024,10, 100127
[2] Mani Arivazhagan, Pavadai Rajaji, Nagaraj Murugan, Jaroon Jakmunee. Analytical Methods. 2024, 16 (38), 6474-6486.

PEI-Capped Osmium Nanoclusters (Os NCs) for Dual-Mode Fluorescence and Electrochemical Detection of Cyanide: A Robust Platform for Environmental Sensing

Raheel Akram[1], S. Lokeswara Reddy[1], Anila Arshad[2], Jaroon Junsomboon[3], Serena Arnaboldi[4], Jaroon Jakmunee[1, *]

[1]Research Laboratory for Analytical Instrument and Electrochemistry Innovation, Department of Chemistry, Faculty of Science, Chiang Mai University, Chiang Mai, 50200, Thailand

[2]School of Agriculture Engineering, Jiangsu University, Zhenjiang 212013, PR China

[3]National Institute of Reference Laboratories, Department of Science Service, Ministry of Science and Technology, Bangkok 10400, Thailand

[4]Department of Chemistry, University of Milan, Via Golgi 19, 20133 Milan, Italy

Email: jaroon.jakmunee@cmu.ac.th

*Jaroon Jakmunee

Abstract

Cyanide (CN^-), a pervasive and highly toxic industrial pollutant, poses acute environmental and health risks due to its high bioavailability and disruption of cellular respiration. Conventional detection methods often lack sensitivity, portability, or real-time applicability, underscoring the need for advanced sensing technologies. Herein, we report the development of polyethyleneimine (PEI)-capped osmium nanoclusters (Os NCs) as a dual-mode sensor for highly sensitive fluorescence and electrochemical detection of CN^-. The PEI-assisted synthesis yielded biocompatible, solvent-free Os NCs with uniform ultrasmall sizes (2–3 nm, confirmed by TEM) and remarkable stability (up to 3 months) exhibiting with detection limits of 12 nM (fluorescence) and 12.93 nM (electrochemistry), with broad linear ranges of 0.03–24.0 µM and 0.01–200 µM, respectively. The detection mechanism is based on electrostatic interaction between the positively charged amine groups ($–NH_2$) of PEI and the negatively charged CN^-, forming a conjugated structure that quenches fluorescence via metal to ligand charge transfer (MLCT) while enhancing electrochemical current. The electrochemical sensor was successfully applied to real samples, including roof tiles leachates, with validation of results by ion chromatography (IC). Additionally, CN^- recoveries from spiked food and biological samples ranged from 93.65–102.66 % and 89.46–97.43 %, respectively. This work is based on our published article in *Talanta* (2026, 297, 128667) and establishes Os NCs as a cost-effective, robust platform for sustainable CN^- monitoring in environmental and biological matrices.

Keywords: Cyanide detection; osmium nanoclusters; dual-modal sensor; fluorescence-electrochemistry; environmental monitoring

Development of high-stability aluminum-air battery for next-generation energy storage system

Jesada Punyafu[1,*], Suphitcha Moonngam[2], Chaiyasit Banjongprasert[1,3]
[1] Materials Science Research Center, Faculty of Science, Chiang Mai University, 239 Huaykaew Road, Suthep, Chiang Mai 50200, Thailand
[2] Research Administration Center, Office of the University, Chiang Mai University, 239 Huaykaew Road, Suthep, Chiang Mai 50200, Thailand
[3] Department of Physics and Materials Science, Faculty of Science, Chiang Mai University, 239 Huaykaew Road, Suthep, Chiang Mai 50200, Thailand
Email: jesada.punyafu@gmail.com
*Corresponding author

Abstract

The growing demand for renewable energy has accelerated the development of advanced energy storage systems. Among them, aluminum–air batteries show great promise due to their high energy density, lightweight, and recyclability. To enhance battery performance, previous studies have focused on alloy development and microstructural refinement of aluminum anodes. In particular, severe plastic deformation (SPD) has been shown to improve anode stability and efficiency by refining the grain structure and altering the corrosion behavior [1]. Among SPD techniques, friction stir processing (FSP) is considered a scalable technique for fabricating large areas with uniform, fine-grained microstructures [2]. However, industrial implementation is limited by excessive heat generation during processing. This study addresses this challenge by introducing in-process cooling, which enables a continuous FSP process. Electron microscopy showed that in-process cooling further reduced the grain size compared to the non-cooled condition. Anode discharge testing revealed the relationship between microstructure characteristics, such as grain size and grain orientation, and anode performance. Furthermore, an aluminum–air battery prototype was developed, and the assembled cells were capable of powering small electronic devices. This work demonstrates a scalable strategy for fabricating high-performance aluminum–air batteries, supporting their potential for next-generation energy storage applications.

Keywords: Metal-air battery; Aluminum alloys; Severe plastic deformation; Microstructure refinement; Electron microscopy

References:

[1] S. Linjee, S. Moonngam, P. Klomjit, N.S. Pålsson, C. Banjongprasert, Corrosion behaviour improvement from the ultrafine-grained Al–Zn–In alloys in Al–air battery, Energy Reports 8 (2022) 5117–5128.
[2] S. Moonngam, C. Banjongprasert, Enhancing the electrochemical performance of aluminum-zinc alloy anodes by friction stir process for aluminum–air batteries, J Alloys Compd 1018 (2025) 178784.

Humidity-Sensitive ZnO–SnO_2 Films and Correction Modeling for Reliable Low-Cost $PM_{2.5}$ Monitoring

Teerasil Kumpika[1,2], Pisith Singjai[1,2*]
[1]Department of Physics and Materials Science, Faculty of Science, Chiang Mai University, Chiang Mai 50200, Thailand
[2]Materials Research Center, Faculty of Science, Chiang Mai University, Chiang Mai 50200, Thailand
*Corresponding author Email: pisith.s@cmu.ac.th

Abstract

Accurate measurement of fine particulate matter ($PM_{2.5}$) is essential for effective air quality management; however, low-cost optical sensors often suffer from humidity-induced bias and long-term signal degradation. Since relative humidity strongly influences light scattering and sensor stability, developing a sensitive and reliable humidity-sensing material is critical for improving measurement accuracy and correction modeling.
To address this challenge, ZnO–SnO_2 composite thin films were fabricated using a magnetic-field-assisted spark discharge technique, offering a simple, vacuum-free, and scalable approach to produce high-performance sensing materials. The application of a 450 mT magnetic field during sparking confined plasma species and guided charged molten droplets via the Lorentz force, leading to enhanced nanoparticle uniformity, crystallinity, and surface morphology. The resulting films exhibited excellent humidity-sensing performance ($\Delta R/R_0 \approx 120\%$) with rapid response and recovery (12.4 s/5.1 s).

Keywords: Light Scattering $PM_{2.5}$ sensor; Humidity Sensor; ZnO–SnO_2 composite; Magnetic field; Polynomial Correction Model

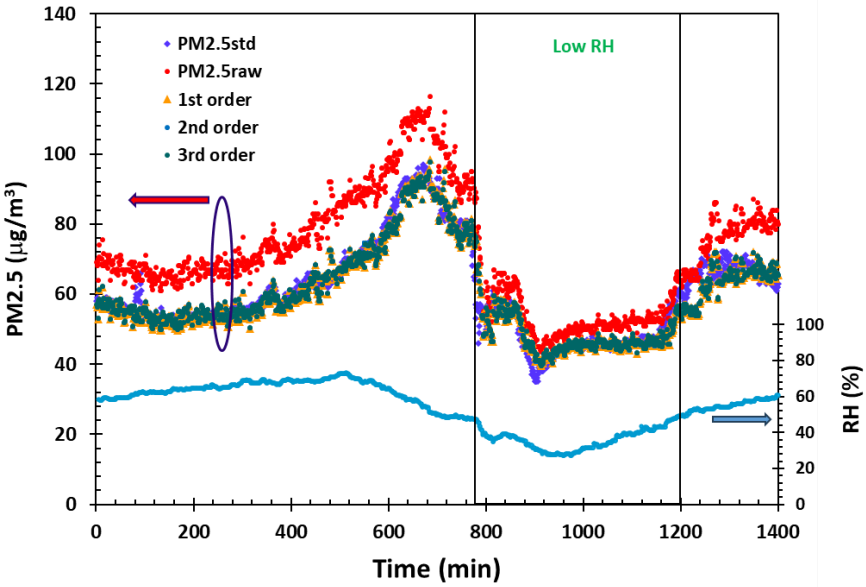

Comparison of PM2.5 measurements from raw sensor data (PM2.5raw), corrected values using first order, second order, and third order calibration models, and reference measurements (PM2.5std)

Utilization of Biomass for Nanostructured Silicon-Based Anodes Toward High-Efficiency Energy Storage

Orapim Namsar[1,2], Chawin Yodbunork[1,2,3], Waewwow Yodying[1], Kittiputh Kunniyom[1,4], Thanapat Autthawong[2,5], Mitsutaka Haruta[6], Thapanee Sarakonsri[1,2,4,*]
[1]Department of Chemistry, Faculty of Science, Chiang Mai University, Muang, Chiang Mai 50200, Thailand
[2]Materials Science Research Center, Faculty of Science, Chiang Mai University, Muang, Chiang Mai 50200, Thailand
[3]Office of Research Administration, Office of the University, Chiang Mai University, Muang, Chiang Mai 50200, Thailand
[4]Center of Excellence for Innovation in Chemistry (PERCH-CIC), Faculty of Science, Chiang Mai University, Muang, Chiang Mai 50200, Thailand
[5]Department of Industrial Chemistry, Faculty of Science, Chiang Mai University, Muang, Chiang Mai 50200, Thailand
[6]Institute for Chemical Research, Kyoto University, Uji, Kyoto 611-0011, Japan
Email: thapanee.s@cmu.ac.th (T. Sarakonsri).
*Corresponding author

Abstract

Biomass is an abundant resource in Thailand. However, open burning remains a common disposal method in many areas, significantly contributing to air pollution through the release of fine particulate matter (PM2.5), greenhouse gases, and other harmful emissions. These pollutants are linked to severe environmental degradation and adverse health effects, including respiratory and cardiovascular diseases. To mitigate these impacts, this study proposes a sustainable strategy to upcycle biomass into high-value materials for energy storage applications. Specifically, nanostructured silicon (Si)-based anodes for lithium-ion batteries (LIBs) were derived from biomass. To improve electrochemical performance and structural integrity, flexible carbon materials with varying content were incorporated into the composites. The carbon material served as mechanical buffers to accommodate volume expansion of Si-based materials during cycling. Experimental results revealed that sufficient carbon content significantly enhanced rate capability and long-term cycle stability of Si-based nanocomposite anodes, owing to improved Li ion diffusion and robust structural support. This work presents an effective solution to environmental pollution and energy sustainability by transforming biomass into high-performance anode materials for next-generation LIB technologies.

Keywords: Energy storage; Anode materials; Nanostructure; Biomass, Sustainable

Understanding Ion Intercalation Behavior of Layered Materials in "Water-in-Salt" Electrolytes

Sirintra Arayawate[1,2], Napaporn Kareeklina[2,3], Thanit Saisopha[4] , Prayoon Songsiriritthigul[5], Pawin Iamprasertkun[2,3,*]

[1] Department of Biotechnology, Faculty of Engineering and Industrial Technology, Silpakorn University, Nakhon Pathom 73000, Thailand

[2] School of Bio-Chemical Engineering and Technology, Sirindhorn International Institute of Technology, Thammasat University, Thailand

[3] Research Unit in Sustainable Electrochemical Intelligent, Thammasat University, Thailand

[4] Department of Applied Physics, Rajamangala University of Technology Isan, Thailand

[5] School of Physics, Suranaree University of Technology, Nakhon Ratchasima, 30000, Thailand

Email: pawin@siit.tu.ac.th

*Corresponding author

Abstract

Two-dimensional transition metal dichalcogenides (TMDs) such as MoS_2 offer unique opportunities for developing safe and efficient aqueous energy storage systems. Their layered structure enables ion intercalation within interlayer galleries, and this process can be significantly enhanced by modifying the solvation environment of aqueous ions. In this work, exfoliated MoS_2 was employed as a model electrode to investigate the influence of electrolyte concentration, temperature and ion species on intercalation behavior. Lithium-based aqueous electrolytes including LiTFSI, $LiNO_3$, Li_2SO_4, and LiCl were systematically compared across a wide concentration range, spanning from conventional "salt-in-water" to super-concentrated "water-in-salt" regimes. Electrochemical measurements revealed that the 5 m LiTFSI system exhibited the highest specific capacitance (205 F g^{-1} at 5 mV s^{-1}) and excellent ion mobility under ambient conditions. Temperature-dependent studies further identified a shift in optimal electrolyte performance with increasing concentration, associated with changes in ion dynamics and electrochemical stability windows. These results demonstrate the critical role of electrolyte composition and concentration in controlling charge storage mechanisms in layered materials and provide valuable insights for the rational design of next-generation aqueous supercapacitors.

Keywords: water-in-salt electrolytes; ion intercalation; layered material electrodes

Hydroxybenzaldehyde Derivatives as Dual-Functional Passivators for Efficient and Stable Perovskite Solar Cell

Sukhanidhan Singh[1,2], Woraprom Passatorntaschakorn[1], Warunee Khampa[2], Chukwuebuka Emmanuel Usulor[1], Wongsathon Musiksan[2], Isaac Chinaza Ogbuagu[2], Pipat Ruankham[1,3], Duangmanee Wongratanaphisan[1,2,3] *

[1]Department of Physics and Materials Science, Faculty of Science, Chiang Mai University, Chiang Mai 50200, Thailand

[2]Materials Science Research Center, Faculty of Science, Chiang Mai University, Chiang Mai, 50200, Thailand

[3]Thailand Center of Excellence in Physics (ThEP Center), Ministry of Higher Education, Science, Research and Innovation, Bangkok 10400, Thailand

*Email: duangmanee.wong@cmu.ac.th

Abstract

Carbon electrode-based perovskite solar cells (C-PSCs) have attracted considerable interest owing to their excellent photovoltaic characteristics. Nevertheless, attaining both high power conversion efficiency (PCE) and long-term stability in C-PSCs remains difficult because of the numerous defects present within the perovskite layer. Surface passivation provides a straightforward and cost-effective strategy to efficiently mitigate these defects and improve the overall film quality. This study explores the use of two small organic molecules, 4-hydroxy-3-methylbenzaldehyde (4H3MBA) and 4-hydroxybenzaldehyde (HBA), as surface passivation agents for perovskite films to minimize defects and enhance film quality. The work further elucidates the influence of molecular polarity on the effectiveness of perovskite surface passivation. The aldehyde (–CHO) functional group present in both molecules interacts with undercoordinated Pb^{2+} ions, effectively reducing trap-state density, suppressing non-radiative recombination, and thereby improving the overall device performance. With Spiro-OMeTAD as HTL, 4H3MBA and HBA enhance the PCE from 13.85% to 14.19% and 14.66%, respectively, under 1 Sun illumination (0.09 cm^2). This work highlights a promising approach toward developing low-cost, high-performance solar cells for practical photovoltaic applications.

Keywords: Surface passivation; Small organic molecules; non-radiative recombination; Low-cost photovoltaics.

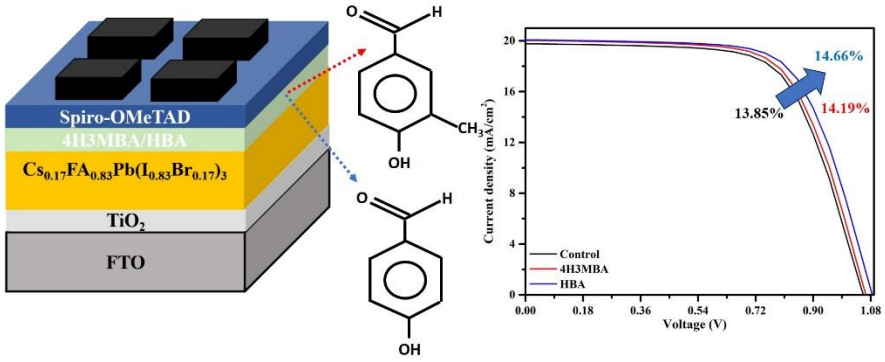

Intelligent Point-of-Care Monitoring of 5-FU Using a Pseudorotaxane/MXene-Based Sensor

Dulyawat Doonyapisut[1], David J. Harding [1], Phimphaka Harding [1*]
[1] School of Chemistry, Institute of Science, Suranaree University of Technology, Nakhon Ratchasima, Thailand
Email: phimphaka@g.sut.ac.th
*Corresponding author

Abstract

The rapid development of point-of-care (POC) diagnostic devices has drawn considerable interest in the medical sector, driven by the necessity for fast, precise, and economical analysis. Electrochemical point-of-care systems, especially those utilizing modified screen-printed electrodes, provide significant benefits in precision and detection speed. Nonetheless, difficulties arise with selectivity and interference management due to the intricate redox environment of biological samples. This study emphasizes the potential of functionalized pseudorotaxanes/MXenes for the modification of screen-printed electrodes (SPE), which can enhance the selective detection of 5-fluorouracil (5-FU) in samples. Moreover, the incorporation of artificial intelligence (AI) into POC devices is suggested to provide accurate, real-time data analysis and reduce dependence on expert interpretation. These integrated strategies have the potential to significantly enhance the reliability and clinical efficacy of point-of-care diagnostics for 5-FU monitoring.

Keywords: Anti-cancer drug monitoring; pseudorotaxanes; MXenes

References:

[1] R. Díaz-Torres, G. Chastanet, E. Collet, E. Trzop, P. Harding, D. J. Harding Bidirectional photoswitchability in an iron(III) spin crossover complex: Symmetry-breaking and solvent effects, Chem. Sci., 2023, 14, 7185.
[2] G.-R. Han, A. Goncharov, M. Eryilmaz, S. Ye, B. Palanisamy, R. Ghosh, F. Lisi, E. Rogers, D. Guzman, D. Yigci, S. Tasoglu, D. Di Carlo, K. Goda, R. A. McKendry, A. Ozcan Machine learning in point-of-care testing: innovations, challenges, and opportunities. Nat Commun, 2025, 16, 3165.

Development of Antioxidant and Antibacterial PLA-Curcumin Composite Film with Dual Metal-Doped CuO Nanoparticles

Gopinath Kasi[1], Sarinthip Thanakkasaranee[1,2,3], Kittisak Jantanasakulwong[1,2,3], Pornchai Rachtanapun[1,2,3]*
[1]Division of Packaging Technology, School of Agro-Industry, Faculty of Agro-Industry, Chiang Mai University, Mae Hia, Chiang Mai 50100, Thailand.
[2]Center of Excellence in Agro Bio-Circular-Green Industry (Agro BCG), Chiang Mai University, Chiang Mai 50100, Thailand.
[3]Center of Excellence in Materials Science and Technology, Faculty of Science, Chiang Mai University, Chiang Mai 50200, Thailand.
E-mail: pornchai.r@cmu.ac.th:
*Correspondence: Pornchai Rachtanapun

Abstract

This study developed a polylactic acid (PLA) - curcumin (CCM) composite film incorporated with silane-functionalized dual metal (silver and magnesium)-doped copper oxide (SF-M-CuO) nanoparticles to enhance antioxidant and antibacterial properties. PLA composite films were prepared by the solution casting method with CCM content varying from 1 to 4%. Among these, the 4% CCM formulation demonstrated the best compatibility. Furthermore, SF-M-CuO nanoparticles (1-4%) were incorporated into this optimal PLA-4%-CCM matrix. The films were characterized using FTIR, XRD, and SEM, and evaluated for their antioxidant and antibacterial activities. The composite film containing 3%-SF-M-CuO nanoparticles exhibited optimal physicochemical properties, as evidenced by FTIR-confirmed interfacial interactions, enhanced crystallinity, and a uniform, well-dispersed morphology. The antioxidant activity of the composite films increased with higher nanoparticle concentrations. The 3%-SF-M-CuO film also exhibited potent antibacterial efficacy, achieving a 100% reduction in growth against both Gram-positive (*Staphylococcus aureus*) and Gram-negative (*Escherichia coli*) bacteria. The developed composite film shows high potential and can be used as a dual-functional material for antibacterial packaging and biomedical applications.

Keywords: Copper oxide; Interfacial interaction; Silane; Solution casting

Synthesis and Characterization of Durian Rind–Derived Carboxymethyl Cellulose for Hydrogel Films Development

Kanticha Pratinthong[1], Rangsan Panyathip [2], Sarinthip Thanakkasaranee [1,3,4], Kittisak Jantanasakulwong[1,3,4], Pornchai Rachtanapun[1,2,3*]
[1] Division of Packaging Technology, School of Agro-Industry, Faculty of Agro-Industry, Chiang Mai University, Mae Hia, Chiang Mai 50100, Thailand
[2] Division of Physics, Faculty of Science and Technology, Rajamangala University of Technology Thanyaburi, Pathum Thani 12110, Thailand
[3] Center of Excellence in Agro Bio-Circular-Green Industry (Agro BCG), Chiang Mai University, Chiang Mai 50200, Thailand
[4] Center of Excellence in Materials Science and Technology, Faculty of Science, Chiang Mai University, Chiang Mai 50200, Thailand
Email: pornchai.r@cmu.ac.th
*Correspondence Pornchai Rachtanapun

Abstract

This study investigates the synthesis and characterization of carboxymethyl cellulose (CMC) derived from durian rind for hydrogel films preparation and biomedical applications. The effect of sodium hydroxide (NaOH) concentration, varied between 10%-60% (w/v), on the degree of substitution, yield, and crosslinking efficiency of CMC-based hydrogels was systematically examined. As the NaOH concentration increased within this range, the degree of substitution and product yield initially improved, indicating enhanced cellulose activation and substitution efficiency. However, at higher NaOH concentrations, these properties began to decline, likely due to cellulose degradation and decreased substitution performance. The hydrogel synthesized using 30% NaOH exhibited the most favorable characteristics, including superior crosslinking efficiency, high swelling capacity, and strong water absorption, reflecting a well-developed polymer network. Furthermore, the optimized hydrogel demonstrated a sustained release of methylene blue, confirming its potential for controlled drug delivery and wound dressing applications. Overall, this study emphasizes the significance of optimizing alkaline conditions in CMC synthesis and highlights durian rind as a valuable, sustainable source for producing high-quality biodegradable hydrogels.

Keywords: Agricultural waste; Biomaterials; Hydrogel synthesis; Sustainable materials

Modification of Smart Bio-Composite Cassava Starch/Carboxymethyl Cellulose/Sodium Carbonate Films Using Cold Plasma Treatment for Sustainable CO_2 Capture

Itchaya Thinnakorn[1], Sarinthip Thanakkasaranee[1,3], Pornchai Rachtanapun[1,2,3], Kittisak Jantanasakulwong[1,2,3*]
[1] Faculty of Agro-Industry, Chiang Mai University 50100, Thailand.
[2] Center of Excellence in Materials Science and Technology, Faculty of Science, Chiang Mai University, Chiang Mai, 50200, Thailand.
[3] Center of Excellence in Agro Bio-Circular-Green Industry (Agro BCG), Chiang Mai University, Chiang Mai 50100, Thailand.
Email: kittisak.jan@cmu.ac.th
*Corresponding author

Abstract

CP treatment is an innovative, chemical-free, and scalable green technology for developing sustainable and biodegradable carbohydrate-based films for applications in safe food packaging and health protection. This approach focuses on modifying the bio-based materials to enhance CO_2 capture efficiency to responsible consumption through waste reduction and help mitigate climate change by lowering plastic pollution and carbon footprint. Biofilm was developed from a blend of cassava starch (CS) and carboxymethyl cellulose (CMC) in a 60:40 ratio. CS/CMC was treated with cold plasma (CP) for varying times to enhance the reaction and its mechanical properties. CP treatment induced structural changes, as confirmed by the FTIR and ^{1}H-NMR spectra. FT-IR spectra of CS/CMC and CS/CMC/CP revealed the characteristic peaks of both components with no new bands. Therefore, ^{1}H-NMR spectroscopy was used to study the structural changes. ^{1}H-NMR spectra of CS/CMC/CP revealed a significant decrease peak intensity at 3.21–3.89 ppm indicated that plasma treatment affected the main chain of starch. And 5.3 ppm corresponding to –OH-8 and –OH-9. This decrease indicates a loss of –OH groups in the modified starch owing to intermolecular cross-linking. The optimum CP treatment time was 5 min, resulting in significantly improved mechanical properties, including a tensile strength of 30 MPa and elongation at break of 25%. The swelling ratio of the CS/CMC/CP films was 2.5 times (670%) higher than untreated CS/CMC films (275%). CP treatment enhanced hydrophobicity and thermal stability owing to crosslinking. The knowledge gained from developing plasma-modified materials can be further applied to create next-generation packaging with effective carbon dioxide adsorption capability.

Keywords: Smart bio-composite films; Cassava starch; Carbon capture; Cold plasma; Low-carbon society

Effect of Catalyst Loading and Argon Cold Plasma Treatment on Degree of substitution in Starch Esterification

Pattraporn Changsuwan[1], Pornchai Rachtanapun[1,2,3], Sarinthip Thanakkasaranee[1,2], Kittisak Jantanasakulwong[1,2,3,*]

[1] Division of Packaging Technology, Faculty of Agro-Industry, Chiang Mai University, Mae-Hea, Mueang, Chiang Mai 50100, Thailand.

[2] Center of Excellence in Materials Science and Technology, Faculty of Science, Chiang Mai University, Chiang Mai, 50200, Thailand.

[3] Center of Excellent in Agro Bio-Circular-Green Industry (Agro BCG), Faculty of Agro-Industry, Chiang Mai University, Chiang Mai 50100, Thailand.

Email: kittisak.jan@cmu.ac.th

*Corresponding author

Abstract

This study examines the effect of catalyst loading on the degree of substitution (DS) in starch esterification, comparing conventional chemical methods with argon cold plasma-assisted modification. Cassava starch was esterified using fatty acid derivatives under varying potassium carbonate (K_2CO_3) concentrations (0.5 – 7.0 mol% based on anhydroglucose unit, AGU) as catalyst. FTIR was used to estimate DS via carbonyl-to-hydroxyl absorbance ratios, while ^{1}H NMR provides precise DS values through proton signal integration. TGA assessed thermal stability, showing that higher DS correlated with increased decomposition temperatures. Results revealed a nonlinear relationship between catalyst loading and DS, with optimal substitution around 5 mol% based on AGU. Excess catalyst reduced efficiency due to side reactions and hydrolysis. Plasma-treated samples achieved comparable or higher DS at lower catalyst levels, indicating enhanced surface reactivity and reduced chemical input. This approach supports scalable, eco-friendly biopolymer development, offering a robust analytical framework for monitoring substitution and improving material performance in sustainable packaging.

Keywords: Cassava starch; Palm oil; Catalyst loading; Potassium carbonate; Argon Cold plasma

Optimization of Laser Remelting Parameters for the Microstructure and Hardness of Arc-Sprayed Ni-Cr-Al-Mo Coating

Sirinapa Shuecamlue[1], Chaiyasit Banjongprasert[1,2,3,*]
[1]Materials Science Research Center, Faculty of Science, Chiang Mai University, Mueang Chiang Mai, Chiang Mai, Thailand
[2]Center of Excellence in Materials Science and Technology, Chiang Mai University, Mueang Chiang Mai, Chiang Mai, Thailand
[3]Department of Physics and Materials Science, Chiang Mai University, Mueang Chiang Mai, Chiang Mai, Thailand
Email: chaiyasit.b@cmu.ac.th
*Corresponding author

Abstract

This research focuses on the optimization of laser remelting parameters to improve the microstructural characteristics and mechanical property of Ni-Cr-Al-Mo (PMET) coatings deposited by arc spraying. The study analyzed the influence of laser power and overlap percentage on coating integrity, interfacial bonding, and hardness. Arc-sprayed coatings typically exhibit porous and heterogeneous splat structures, which limit their mechanical properties. Laser remelting was therefore employed as a post-treatment technique to refine the microstructure and enhance coating–substrate adhesion.

Experimental results demonstrated that laser powers in the range of 400–600 watt (W) combined with 50% overlap produced the most effective results. Under these conditions, the coating layer was completely remelted, resulting in a dense and uniform microstructure with excellent metallurgical bonding to the substrate. Importantly, the diffusion of Fe from the substrate into the coating was found to be minimal, preserving the chemical integrity of the Ni-based layer. Despite these improvements, a reduction in hardness was observed after remelting. This decrease was associated with the full remelting of the coating, which modified the distribution of strengthening phases. In particular, the formation of Mo_2Si phases was identified as a key factor influencing the hardness response, with their morphology and distribution playing a significant role. Overall, this study highlights the critical influence of laser power and overlap percentage in optimizing the microstructure and hardness of arc-sprayed Ni-based coatings. The findings provide valuable insights into parameter optimization techniques for enhancing the performance of thermally sprayed coatings in demanding applications.

Keywords: Laser remelting; Arc spraying; Ni-Cr-Mo-Al coating

Age-hardening behavior of the BCC Ti-20Fe alloy

Sayori Fujimura[1], Takuya Ishimoto[2,3,*], Kazuhisa Sato[4], Masato Fukushima[5], Takayoshi Ishimoto[5], Tomoyo Manaka[2]
[1]Graduate School of Science and Engineering, University of Toyama, Toyama, Japan
[2]School of Sustainable Design, University of Toyama, Toyama, Japan
[3]Aluminium Research Center, University of Toyama, Toyama, Japan
[4]Research Center for UHVEM, The University of Osaka, Ibaraki, Japan
[5]Graduate School of Advanced Science and Engineering, Hiroshima University, Higashihiroshima, Japan
Email: ishimoto@sus.u-toyama.ac.jp
*Corresponding author

Abstract

1. Introduction
In Ni-based superalloys, strengthening is achieved by the precipitation of ordered phases. On the other hand, the strengthening of Ti-based alloys is mainly due to solid solution strengthening and grain refinement. The understanding of the mechanisms of precipitation strengthening is insufficient. In Ti-alloys, the β phase with a BCC structure can contain an ordered B2 (CsCl structure) phase. The aim of this study is to clarify the precipitation behavior of the B2 phase within the β-matrix and the associated changes in strength.
2. Materials and Methods
Alloy ingots of Ti-20Fe (at%) which can contain the TiFe-B2 phase were prepared by an arc-melting. After solution treatment in the β-phase region, aging was carried out for up to 48 h to precipitate the B2 phase. The constituent phases were evaluated by XRD, and mechanical properties were assessed via Vickers hardness testing. Microstructures were analyzed using SEM and TEM. The structural stability was estimated using first-principles calculations.
3. Results and Discussion
By aging for 2 h, the hardness reached its maximum value, after which it monotonically decreased with increasing aging time (Fig. 1). Interestingly, however, no distinct formation of a secondary phase was detected by XRD after 2 h of aging. Electron diffraction revealed the presence of diffuse scattering around the positions where B2 superlattice reflections should appear, suggesting the formation of short-range order (SRO) with a B2-type atomic arrangement. First-principles calculations indicated that, due to the strong bonding between Ti and Fe, SRO can form more stably than random atomic configurations. These results suggest that the formation of SRO is the key strengthening mechanism in this alloy.

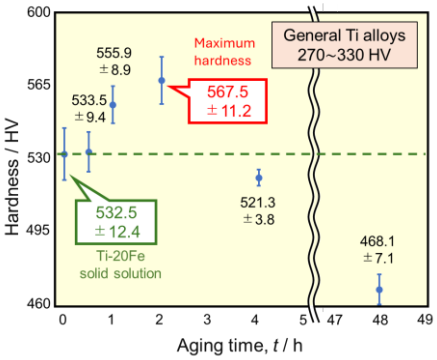

Fig. 1 Hardness variation as a function of aging time for Ti-20Fe alloy.

This work was supported by JSPS-KAKENHI (JP24K01194, JP21H05197) and Research funding from the Light Metal Educational Foundation.

Keywords: BCC-Ti; Hardening; Short-range order

Proposal of a strengthening approach for Ti-TRIP alloys through the introduction of Chemical Boundaries

Shion Shimizu[1], Takuya Ishimoto[2,3,*], Tomoyo Manaka[3]
[1]Graduate School of Science and Engineering, University of Toyama, Toyama, Japan
[2]Aluminium Research Center, University of Toyama, Toyama, Japan
[3]School of Sustainable Design, University of Toyama, Toyama, Japan
Email: ishimoto@sus.u-toyama.ac.jp
*Corresponding author

Abstract

1. Introduction

Transformation induced plasticity (TRIP) effects offer excellent ductility and notable work hardening through stress-induced phase transformation, resulting in a favorable strength–ductility balance for structural applications. However, TRIP-Ti alloys often show low yield strength due to low transformation stress. This study proposes introducing compositional heterogeneity during solidification to form chemical boundaries, which are expected to increase transformation stress similar to grain refinement. The aim of the present study is to evaluate whether this approach can improve the strength of TRIP-Ti alloys without compromising their ductility.

2. Experimental Methods

Ti-10V-2Fe-3Al which shows TRIP behavior was used as a reference alloy. The new alloy compositions were designed such that a portion of the segregation-induced modulated composition would traverse the vicinity of Ti-10V-2Fe-3Al, where TRIP is anticipated to occur. The compositional transition was estimated by the Modified Scheil-Gulliver calculation. Alloy ingots were prepared by arc melting under an Ar atmosphere. Two conditions were studied: as-cast (CH: Chemically heterogeneous) and homogenized (HM) as a comparison. Homogenization was performed in a vacuum, followed by rapid quenching into ice water to retain the β-phase structure. Microstructures and elemental distributions were examined using OM, SEM, and EPMA. Tensile tests were conducted, and local deformation behavior was analyzed through EPMA mapping after deformation to understand composition–mechanical response relationships.

3. Results and Discussion

CH samples exhibited clear compositional heterogeneity, including β regions susceptible to TRIP, while HM samples showed uniform composition. Both conditions reached ~1000 MPa ultimate tensile strength, but the HM alloy yielded at 200–300 MPa. In contrast, the heterogeneous alloy showed a 200–400 MPa increase in yield strength while maintaining elongation. Post-deformation analysis revealed distinct localized deformation patterns (Fig. 1), corresponding precisely to compositional variations, thereby demonstrating the effectiveness and strengthening role of chemical boundaries in controlling phase transformation behavior.

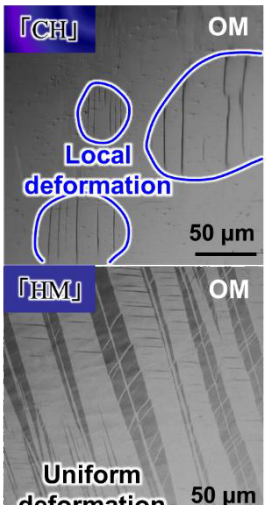

Fig. 1 Initial deformation structures in CH vs. HM materials.

This work was supported by JSPS-KAKENHI (JP24K01194, JP21H05197) and Research funding from the Light Metal Educational Foundation.

Keywords: TRIP; Chemical heterogeneity; Titanium; Yield strength

Influence of Zr and Hf substitution for Ti solvent on the mechanical properties of Ti-6Al-4V

Yusuke Nomura[1], Tomoyo Manaka[2], Abrar Ahmed[3], Taiki Tsuchiya[2],
Kenji Matsuda[2,3], Takuya Ishimoto[2,3,*]
[1]Graduate School of Science and Engineering, University of Toyama, Toyama, Japan
[2]School of Sustainable Design, University of Toyama, Toyama, Japan
[3]Aluminium Research Center, University of Toyama, Toyama, Japan
Email: ishimoto@sus.u-toyama.ac.jp
*Corresponding author

Abstract

In the fields of orthopedics and dentistry, there is an urgent need to develop low-stiffness implants that suppress the stress shielding. This study aims to partially replace the solute Ti in Ti-6Al-4V alloy, a frequently used bone implant material, with homologous elements Zr and Hf. The objective is to enhance strength through improved solid solution strengthening and to improve other mechanical properties by utilizing the β-phase stabilizing effect that Zr/Hf possesses, albeit to a lesser extent.

X-ray diffraction analysis revealed that both α and β phases were present in Ti-6Al-4V and the designed alloys. With increasing Zr/Hf content, diffraction peaks shifted toward lower angles, which corresponds to an increase in lattice constant. This behavior is consistent with Vegard's law for substitutional solid solutions, supporting the successful formation of solid solutions. Fig. 1 shows stress-strain curves. Tensile tests demonstrated that alloys with 4–10% substitution (ZH4 and ZH10) exhibited higher yield strengths than Ti-6Al-4V, indicating effective solid solution strengthening. However, alloys with 20% and 30% substitution (ZH20 and ZH30) showed a marked reduction in yield stress accompanied by significant work hardening. Furthermore, Young's modulus decreased systematically with higher Zr/Hf content, and the ZH30 alloy reached an exceptionally low value of about 54 GPa. After deformation, additional diffraction peaks corresponding to the α″ martensite phase appeared, suggesting that a deformation-induced martensitic transformation occurred, providing evidence of the TRIP effect.

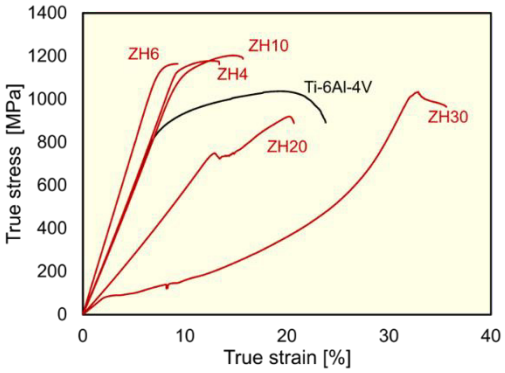

Fig. 1 Variation of tensile stress-strain curves depending on the amount of Ti-solvent substitution with Zr and Hf.

This work was supported by JSPS-KAKENHI (JP24K01194, JP21H05197), JST-SPRING (JPMJSP2145), and Research funding from the Light Metal Educational Foundation.

[1] Y. Nomura, T. Ishimoto, et al.: Materials, 17 (2024) 2548.

Keywords: titanium; bone biomaterial; solid solution strengthening; phase stability; low modulus-high strength trade-off

Effects of La_2O_3 on the Structure and Durability of Alkali Zirconium Silicate Glasses

A. Denprawat[1,*], P. Kidkhunthod[2], N. Laorodphan[3], and W. Thiemsorn[1]
[1]Department of Industrial Chemistry, Faculty of Science, Chiang Mai University, Muang District, Chiang Mai, 50200, Thailand
[2]Synchrotron Light Research Institute (Public Organization), 111 University Avenue, Muang District, Nakhon Ratchasima, 30000, Thailand
[3]Department of Industrial Chemistry Innovation, Faculty of Science, Maejo University, San Sai District, Chiang Mai, 50290, Thailand
Email: ativit_de@cmu.ac.th
*Corresponding author

Abstract

Alkali zirconium silicate glasses containing 0–1.5 mol% La_2O_3 were synthesized using the conventional melt-quenching technique. The effects of La_2O_3 incorporation on the structure, chemical durability, and weathering resistance of the glass samples were investigated by X-ray diffraction (XRD), Raman spectroscopy, ^{29}Si MAS NMR, X-ray absorption spectroscopy (XAS), and inductively coupled plasma optical emission spectrometry (ICP-OES). XRD confirmed the homogeneous incorporation of La_2O_3 into the glass matrix. XAS demonstrated that La^{3+} ions were present in the +3 oxidation state and were coordinated by seven O^{2-} ions. Raman spectroscopy revealed that increasing La_2O_3 concentration promoted the formation of Q^2(La) and Q^3(La) units, accompanied by a decrease in Q^3(Na, Li) and Q^4 units. These results suggest that La^{3+} ions are incorporated into the glass network through Si–O–La linkages, observed as Q^2(La) and Q^3(La) units in the Raman spectra. The ^{29}Si MAS NMR analysis indicated a reduction in Q^2 units and an increase in Q^4 units, attributed to Na^+ ions acting as charge compensators near $[LaO_7]^{4-}$ groups, thereby converting Q^2 into Q^4 units. Chemical durability tests indicated that Na^+ leaching from samples immersed in solutions of varying pH decreased with increasing La_2O_3 content, while weathering tests demonstrated a reduction in Na^+ accumulation on the glass surface, from 3.06 to 1.29 μg/cm^2. These improvements in durability are attributed to La^{3+} ions, which enhance network rigidity and alter the role of Na^+ ions from network modifiers to charge compensators, thereby reducing ion exchange with H^+ ions.

Keywords: Lanthanum oxide (La_2O_3); Chemical durability; Chemical weathering; Glass structure.

Comparison of Cutting Performance for a Bulk Metallic Glass Blade via AFM Analysis

Sejin Jang[1], Seong-Hoon Yi[1*]
[1]Materials Science and Metallurgical Engineering, Kyungpook National University, Daegu, Korea
Email: yish@knu.ac.kr
*Corresponding author

Abstract

Excellent sharpness, strength, and durability are critical factors for a blade to achieve precise and clean cuts. A sharp blade allows for higher quality incisions and applies less cutting force to tissue compared to a dull one.

Stainless steel and carbide materials are among the most widely used materials for commercial blades. However, the presence of grain boundaries can lead to easy chipping during grinding. As a result, particles can detach near the cutting edge, creating a wavy surface on the incision. Amorphous alloys, due to rapid cooling, have a non-crystalline structure without grain boundaries. This characteristic allows them to maintain high hardness and prevents chipping during polishing. In particular, Fe-based amorphous alloys boast high mechanical properties, with a hardness of 1000 HV and a yield strength of 3.5 GPa, and are expected to provide exceptional sharpness.

To demonstrate the superiority of the amorphous blade, this study conducted an AFM analysis. A comparative analysis of the roughness values and artifacts on the incision surfaces created by both amorphous and crystalline blades was performed. The results showed that the surface cut by the amorphous blade had a significantly lower average roughness and smaller step-height artifacts. This clearly demonstrates the superior cutting performance of the Fe based amorphous alloy. Furthermore, a silicone cutting test was conducted to additionally evaluate the durability of the blades.

Keywords: Amorphous alloy; Incision Surface; AFM

Phosphorus-Enhanced Fe-Based Amorphous Catalysts for Green Hydrogen Production

Moosung Kim[1], Juneyoung Lee[1], Seonghoon Yi[1*]
[1]Materials Science and Metallurgical Engineering, Kyungpook National University, Daegu, Korea
Email: yish@knu.ac.kr
*Corresponding author

Abstract

The growing dependence on fossil fuels has accelerated global warming and intensified climate anomalies, driving the urgent need for carbon-neutral strategies such as RE100 and the development of sustainable energy technologies. Among these, seawater electrolysis has emerged as a promising route for large-scale hydrogen production. Unlike freshwater electrolysis, this approach directly utilizes seawater which accounts for nearly 97% of the Earth's water resources, and can be coupled with renewable energy sources such as solar and wind. Furthermore, seawater electrolysis enables the production of green hydrogen without carbon dioxide emissions, in contrast to blue or grey hydrogen. However, the presence of impurities such as chloride ions induces side reactions during electrolysis, leading to electrode degradation and the evolution of toxic by-products. In addition, platinum-group catalysts, although highly active, remain limited in practical application due to their high cost and scarcity. These challenges have motivated extensive research into alternative catalysts based on the earth-abundant transition metals.
In this study, we focused on the design and fabrication of Fe-based amorphous alloy as cost-effective and corrosion-resistant electrocatalysts. Amorphous alloys, owing to their disordered atomic structures, provide uniform distribution of catalytic elements and abundant active sites. Phosphorus (P) was introduced as a key alloying element to enhance glass-forming ability (GFA) and modify the surface electronic structure. Alloy compositions were systematically designed with varying P contents, considering both thermodynamic and electrochemical factors. Master alloys were prepared by arc melting, followed by rapid solidification via melt-spinning to produce thin amorphous ribbons. The resulting samples were characterized using X-ray diffraction (XRD) to confirm amorphous structures and differential thermal analysis to evaluate thermal stability. Electrochemical performance was assessed in mixed acid-seawater electrolytes through hydrogen evolution reaction (HER) and oxygen evolution reaction (OER) measurements.

Keywords: Seawater electrolysis; Green hydrogen; Fe-based amorphous alloys; Phosphorus; Electrocatalyst

Enhanced Corrosion Resistance of Fe-based Amorphous Catalysts by Chromium Addition

JuneYoung Lee[1], Moosung Kim[1], Seonghoon Yi [1]*
[1] Department of Materials Science and Engineering, Kyungpook National University, Daegu, Republic of Korea
Email: yish@knu.ac.kr
*Corresponding author

Abstract

Green hydrogen production through water electrolysis has emerged as a key strategy for sustainable energy technologies. While platinum (Pt) catalysts exhibit high activity, their scarcity and cost hinder widespread adoption. As a promising alternative, Fe-based amorphous alloys have attracted attention due to their structurally rich active sites and excellent catalytic efficiency. However, their chemical stability is limited in highly corrosive environments, such as acidic seawater, which compromises both catalytic performance and structural durability.

In this study, Fe-based amorphous ribbons with varying chromium (Cr) contents were prepared to investigate the effect of chromium on their corrosion resistance and catalytic stability. The alloy compositions were designed to optimize glass-forming ability (GFA), electrochemical activity, and mechanical strength. Using arc melting and melt spinning techniques, the alloys were rapidly cooled, and their structural and thermal properties were evaluated using X-ray diffraction (XRD) and differential thermal analysis (DTA). Electrochemical performance was evaluated in acidic seawater using a conventional three-electrode configuration, and surface morphology and compositional changes before and after testing were analyzed by scanning electron microscope (SEM) and energy-dispersive spectroscopy (EDS).

Keywords: Amorphous alloy; Corrosion resistance; Seawater electrolysis; Green Hydrogen

Enhancement of Magnetic Properties through Control of Heat Treatment Conditions in Fe-Based Soft Magnetic Amorphous Alloys

Jongil Lee[1], Seonghoon Yi[1*]
[1]Materials Science and Metallurgical Engineering, Kyungpook National University, Daegu, Korea
Email: yish@knu.ac.kr
*Corresponding author

Abstract

In recent years, information and communication technology, electric vehicles, renewable energy systems, and high-frequency power devices have increasingly demanded higher frequencies and greater efficiency, yet conventional crystalline materials face limitations due to significant energy losses caused by domain wall motion and coercivity. In contrast, amorphous and nanocrystalline alloys, with their fine atomic structures and homogeneous compositions, enable easier domain wall motion and exhibit lower coercivity, thereby significantly reducing power loss. This translates into highly efficient power conversion, the miniaturization and lightweighting of components, and stable operation in high-frequency environments. Furthermore, in an era that calls for energy savings and carbon emission reduction, the use of soft magnetic alloys with low coercivity serves as a critical foundation for reducing power loss and driving the development of environmentally friendly technologies. Achieving low coercivity requires grain refinement to below 20 nm. In this study, Cu was added to the alloy to induce heterogeneous nucleation sites through clustering, thereby promoting microstructural refinement. The behavior of Cu clusters and their impact on magnetic properties were examined under various heat treatment conditions, leading to the identification of the optimal heat treatment process.

In this study, high-Fe-content alloys (Fe > 80 at%) were designed to achieve a magnetic flux density of 1.6 T and Cu was added to improve magnetic properties by optimizing crystal grain size. The Cu-added ribbons were annealed under various heat treatment conditions. Their microstructural and magnetic properties at each temperature were systematically analyzed using X-ray Diffraction (XRD), Differential Scanning Calorimetry (DSC), Vibrating Sample Magnetometry (VSM), and DC loop tracer measurements. This study provides valuable insights into the optimization of composition and heat treatment processes for Fe-based amorphous soft magnetic materials, enabling the development of high-performance materials suitable for high-frequency applications.

Keywords: Soft Magnetic; Fe-based amorphous alloys

Soft Magnetic Properties of High C Amorphous Alloys

Mingyo Jeong[1], Moosung Kim[1], Seonghoon Yi[1*]
[1]Materials Science and Metallurgical Engineering, Kyungpook National University, Daegu, Korea
Email: yish@knu.ac.kr
*Corresponding author

Abstract

In conventional steelmaking processes, multiple refining steps are typically carried out to produce steel from high-grade raw materials. However, in certain processes, refining is minimized, and low-grade raw materials are utilized to produce hot metal. This hot metal often contains various elements generally considered undesirable in the steel industry. If such hot metal can be directly used in industrial applications, bypassing extensive refining can reduce unnecessary energy consumption and processing time, thereby lowering production costs. Furthermore, process simplification can enhance productivity and establish a stable supply suitable for large-scale manufacturing, while also meeting current industrial demands for resource efficiency and carbon emission reduction. In this study, Fe-based amorphous alloys were inspired by High C Hot metal as a base, and evaluated their magnetic properties. In addition, the effect of varying carbon content on the magnetic properties and crystallization behavior is also investigated.
The alloys were synthesized via arc-melting followed by melt-spinning to produce flexible amorphous ribbons. To further improve their properties, the ribbons were heat-treated at various temperature ranges to optimize annealing conditions. Controlled annealing promoted nanocrystallization within the amorphous matrix, thereby enhancing the magnetic properties. Structural and thermal characterizations were conducted using X-ray diffraction (XRD), and Differential Scanning Calorimetry (DSC). Magnetic properties were examined using Vibrating Sample Magnetometry (VSM) and DC loop tracer measurements. Our results indicate soft magnetic properties of High C Fe-based amorphous alloys, while controlled nanocrystallization through optimized heat treatment provides further enhancement of magnetic properties. These findings highlight the feasibility of developing functional soft magnetic materials from low-cost industrial resources.

Keywords: Hot metal; Soft Magnetic; Fe-based amorphous alloys

TSV filling using Ag through Electroplating to Improve Electrical Conductivity

J.Y.Shin[1], I.J.Son[1,*]
[1]Department of Materials Science and Metallurgical Engineering, Kyungpook National University, Daegu, Korea
Email: ijson@knu.ac.kr

Abstract

With the increasing demand for high-density and high-performance semiconductor devices, the importance of Though-silicon via (TSV) technology, a key enabler for three-dimensional integrated circuits (3D ICs), has been growing significantly. TSV facilitates vertical interconnections between chips, thereby reducing signal transmission distance, lowering power consumption, and enhancing integration density. In order to achieve the aforementioned advantages, it is imperative to possess the capability to achieve uniform metal filling in high-aspect-ratio TSV structures. This is due to the fact that incomplete filling or void formation can have a significant effect on device reliability.

In this study, the effect of organic additives on TSV filling behavior and deposition quality will be investigated. Ag filling of TSV structures with a diameter of 5 μm and a depth of 25 μm (aspect ratio 1:5) was carried out using electrodeposition in a cyanide-based Ag electrolyte bath. The electroplating process was performed at a current density of 5 mA/dm^2 for 50 minutes at room-temperature. The influence of organic additives, including 2-Mercaptobenzothiazole (MBT) on via filling behavior and deposition characteristics was investigated by introducing them into the electrolyte at various concentrations. As a result, the optimal concentration was ascertained, and the via holes were successfully filled.

Cross-sectional morphologies and filling efficiency under different additive concentration were assessed by using Field-Emission Scanning Electron Microscopy (FE-SEM). In addition, Linear Sweep Voltammetry (LSV) experiments were utilized to analyze the influence of additives on the electrochemical characteristics of the plating bath. This work aims to elucidate the relationship between additive agents and process parameters, providing a foundation for optimizing high-quality Ag filling in TSV applications.

Keywords: TSV; Electroplating; Ag plating; Advanced Packaging

Microstructure, Wear, and Fatigue of Iron Alloy and Nickel Alloy Coatings on Rail Steel via Laser Cladding and High Velocity Oxygen Fuel Thermal Spray Techniques

Korn Pongthiya[a], Nunticha Wiratpruk[a], Suphatchagon Phongteerasirikul[a], Hataipat Koiprasert[b], Chaiyasit Banjongprasert[a,c*]
[a] Department of Physics and Materials science, Faculty of Science, Chiang Mai University, Thailand
[b] National Science and Technology Development Agency, Pathum Thani, Thailand
[c] Materials Science Research Center, Faculty of Science, Chiang Mai University, Thailand
Email: chaiyasit.b@cmu.ac.th
*Corresponding author

Abstract

Railway transportation serves as an essential infrastructure in many countries due to its high efficiency in both passenger and freight services. However, the continuous operation under heavy loads over long periods often leads to a major issue known as Rolling Contact Fatigue (RCF), which can cause significant rail damage. In addition, certain areas experience high traction or drag forces that further accelerate this damage, a phenomenon referred to as the slip ratio arising from differences in velocity between the wheel and the rail.
This study explores alternative maintenance methods for railway infrastructure. While welding is commonly used, its high heat input often leads to microstructural changes in the material, known as the Heat Affected Zone (HAZ). As a result, laser cladding (LC) and thermal spray (TS) via high-velocity oxy-fuel (HVOF) present promising alternatives. LC offers precise heat control, minimizing unwanted changes, while TS involves minimal heat input, making it a suitable option for reducing thermal impact. To simulate the welding process, Höganäs 3650 stainless steel powder with NiCr was applied, reflecting the typical use of stainless steel as a weldment material.
The study revealed significant differences in microstructure and mechanical properties depending on the processing method. To simulate real railway operating conditions, a Twin Disc test was conducted using a 1200 N load and a 5% slip ratio. These conditions helped demonstrate the effectiveness of the alternative maintenance processes.

Keywords: Rail; Laser cladding; HVOF; RCF

TEM observation of two step aged Al-Mg-Ge alloy

Yusuke Ishiguro[1], Seungwon Lee[2], Taiki Tsuchiya[2], Abrar Ahmed[3], Susumu Ikeno[4], Kenji Matsuda[2,*]

[1]Graduate School of Science and Engineering for Education, University of Toyama, Toyama, 930-8555, Japan

[2]Graduate School of Science and Engineering for Research, University of Toyama, Toyama, 930-8555, Japan

[3]Advanced Aluminum International Research Center, University of Toyama, Toyama, 930-8555, Japan

[4]Professor Emeritus, University of Toyama, 930-8555, Japan

Email: matsuda@sus.u-toyama.ac.jp

*Corresponding author

Abstract

Al-Mg-Ge alloys, are treated as Al-Mg2Ge pseudo-binary type alloys and have been researched to analyze aging precipitation of Al-Mg-Si alloys. There are several reports on the aging precipitation process of Al-Mg-Ge alloys, and it is basically the same as that of Al-Mg-Si alloys, i.e., supersaturated solid solution → G.P. zone → β" phase → β' phase → β phase (Mg2Ge). In the actual manufacturing process using Al-Mg-Si alloy of alloy, a so-called two-stage aging treatment is performed, in which the product is kept at room temperature (hereinafter referred to as natural aging) before the aging treatment and then aging treatment is carried out at high temperature. It is known that when this two-stage aging treatment is applied, a "negative effect" is occured in which the peak hardness is lower than the peak hardness of the single aging treatment. There are currently few reports on the effect of natural aging time on precipitates in Al-Mg-Ge alloy during two step aging treatment. In this study, Al-1.0Mg2Ge-0.4Ge (mass%) alloy are used and hardened by natural aging for 6 months. Measurement and microstructure observation were performed. In the hardness measurement, when the two-stage aging treatment was applied, the peak hardness of excess Ge alloys was lower than that of the single aging treatment. In the microstructure observation at peak hardness, the needle-shaped and rod-shaped precipitates mainly observed in the Al-Mg-Si Al alloys were observed. In the microstructure observation aged at room temperature, precipitate contrast of less than 2 nm were observed.

Keywords: Al-Mg-Ge; natural aging; Aging precipitation; TEM

Effect of Combined Fe and Cu Additions on the Mechanical Properties and Microstructure of 6000 Series Al Alloys

Yukito Suzuki[1], Yuto Nakagawa[1], Seungwon Lee[2], Taiki Tsuchiya[2], Abrar Ahmed[3], Toshiya Shibayanagi[2,3], Susumu Ikeno[4], Kenji Matsuda[2,3*]
[1]Graduate School of Science and Engineering for Education, University of Toyama, Toyama, Japan
[2]Graduate School of Science and Engineering for Research, University of Toyama, Toyama, Japan
[3]Advanced Aluminum International Research Center, University of Toyama, Toyama, Japan
[4]Professor Emeritus, University of Toyama, Toyama, Japan.
Email: matsuda@sus.u-toyama.ac.jp
*Corresponding author

Abstract

Al-Mg-Si alloys, known as 6000 series aluminum alloys, are produced by adding small amounts of magnesium (Mg) and silicon (Si) to aluminum (Al). In practical applications, the contamination of transition elements is often unavoidable due to variations in the purity of the base aluminum. Previous studies have investigated the influence of additional elements on the properties of 6000 series alloys. However, there are relatively few reports directly comparing the effects of Fe and Cu when added individually with those observed under combined addition. This study, therefore, aimed to clarify the influence of Fe, Cu, and their combined addition on an excess-Si alloy by evaluating mechanical properties and microstructural features. Vickers hardness testing, scanning electron microscopy (SEM), and transmission electron microscopy (TEM) were employed as the primary methods.

The results of the hardness tests revealed distinct effects of the alloying elements: the addition of Fe to the base alloy resulted in a decrease in hardness, whereas the addition of Cu led to an increase in hardness. Interestingly, when Fe and Cu were added simultaneously, the alloy exhibited a slightly higher hardness than the base alloy, without showing the pronounced reduction in hardness observed in Fe-only alloys. SEM observations revealed the presence of Si-containing intermetallic compounds, and the quantity of these compounds varied depending on alloy composition. TEM bright-field imaging provided further insight into the morphology of precipitates. Precipitates elongated along the <010>Al and <001>Al directions were observed from side views, while cross-sectional views along the <100>Al direction were also detected. Based on the number density and length of these precipitates, their contribution to hardness was evaluated.

In conclusion, the combined addition of Fe and Cu had a mitigating effect on the negative influence of Fe on hardness. While Fe alone significantly reduced the Vickers hardness, the presence of Cu counteracted this effect, resulting in alloys with hardness comparable to or slightly higher than the base alloy. These findings provide important insights into the role of combined transition element additions in controlling the balance between mechanical properties and microstructure in 6000 series aluminum alloys.

Keywords: Al-Mg-Si alloy; Transition metal addition; SEM; TEM;

Evaluation of rust preventative performance using water screen test in the AZ91D magnesium alloy/water-soluble cutting oil system

Masahiko Hatakeyama[1*], Kenta Makizaki[2], Takuya Morita[2], Mochisuke Kume[2], Satoshi Sunada[1]

[1] Graduate School Material of Science and Engineering for Research, University of toyama, 3190 Gohuku Toyama, 930-8555, JAPAN

[2] Graduate School of Material Science and Engineering for Education, University of toyama, Gohuku Toyama, 930-8555, JAPAN

Masahiko Hatakeyama, Email: hatake@sus.u-toyama.ac.jp

*Corresponding author

Abstract

The present study evaluated the rust preventive performance of water-soluble cutting oils in bulk magnesium alloy materials using a water screen test. Water-soluble cutting oils are classified into the emulsion type (micelle size 10–0.1 μm), the soluble type (micelle size 0.1–0.001 μm). In this study, the emulsion type and the soluble type oils were examined. The water screen test is a method for evaluating the rust preventive performance of oil films by forming a water screen on oil-coated specimens using a corrosive solution and examining self-excitation of the electrical potential oscillation. Water screen tests in a 0.35 wt% NaCl solution revealed distinct differences in corrosion inhibiting performance depending on the behavior of the oil film and the associated potential. With emulsion type cutting oils, self-excitation of the electrical potential oscillation was observed. This behavior correlated with enhanced rust preventive performance, confirmed by the extended time to rust formation. In contrast, soluble type cutting oils did not exhibit self-excitation of the electrical potential oscillation and provided only limited protective effects. Polarization curve measurements revealed that the emulsion type cutting oil reduced the corrosion current density, indicating suppression of the cathodic oxygen reduction reaction. Conversely, the soluble type cutting oil showed no improvement in corrosion resistance compared to the sample without cutting oil. These results suggest that the rust preventive performance of water-soluble cutting oils strongly depends on micelle size, with emulsion type cutting oils demonstrating superior protective effects. Furthermore, the water screen test is considered an effective method for evaluating the rust preventive performance of water-soluble cutting oils. While previous studies had only confirmed the effectiveness of the water screen test in systems using sintered steel and non-water-soluble oils, this research confirmed self-excitation of the electrical potential oscillation even in systems using bulk material without voids and water-soluble oil.

Keywords: Water screen test; Water-soluble cutting oil; Mg alloy; Corrosion; Open circuit potential; Self-excitation of the electrical potential oscillation

Effect of Mo addition on the pitting corrosion resistance of martensitic steels in 0.5 M H_2SO_4 + 0.5 M NaCl solution

Masahiko Hatakeyama[1*], Kenta Makizaki[2], Ryodai katayama[2],Daichi Nakato[2], Satoshi Sunada[1], Takahiro Onoe[3], Kazunari Tanii[3]
[1]Graduate School of Material Science and Engineering for Research, University of Toyama，3190 Gofuku Toyama 930-8555, Japan
[2]Graduate School of Material Science and Engineering for Education, University of Toyama, 3190 Gofuku Toyama 930-8555, Japan
[3]Nippon Koshuha Steel Co., 3-10-15 Hachiman-cho Imizu Toyama 934-8502, Japan
Email: m24c1605@ems.u-toyama.ac.jp
*Corresponding author

Abstract

The effect of Mo addition on the pitting corrosion resistance of martensitic stainless steels was investigated by potentiodynamic polarization tests in 0.5 M H_2SO_4 + 0.5 M NaCl solution. The pitting potential (E_{pit}) increased with Mo content, confirming that Mo enhances resistance to localized corrosion. At low Mo levels, the pitting current density (I_{pit}) remained comparable, indicating stable passive film properties. However, excessive Mo addition resulted in higher I_{pit} and degradation of film stability. Microstructural observations revealed δ-ferrite precipitation in high-Mo steels and preferential dissolution around it. These results demonstrate that moderate Mo addition improves the pitting corrosion resistance of martensitic stainless steels, while excessive content adversely affects passive film stability due to δ-ferrite formation.

Keywords: Martensitic stainless steel; Molybdenum (Mo) addition; Pitting corrosion resistance

Effect of Inclusions and δ-Ferrite on the Corrosion Behavior of SUS316L Stainless Steel Fabricated by Electron Beam Powder Bed Fusion

Masahiko Hatakeyama[1]*, Kenta Makizaki[2], Shota Otaki[2], Yoshino Fukui[2], Tatsuya Yamamoto[2], Satoshi Sunada[1], Ryotaro Yamamoto[3], Manabu Noguchi[3], Hiroaki Nakamoto[3]
[1]Graduate School of Material Science and Engineering for Research, University of Toyama，3190 Gofuku Toyama 930-8555, Japan
[2]Graduate School of Material Science and Engineering for Education, University of Toyama, 3190 Gofuku Toyama 930-8555, Japan
[3]EBARA corporation, 4-2-1 Honfujisawa, Fujisawa-shi, Kanagawa 251-8502, Japan
Email: hatake@sus.u-toyama.ac.jp
*Corresponding author

Abstract

This study investigates the influence of inclusions and δ-ferrite on the corrosion behavior of SUS316L stainless steel fabricated by electron beam powder bed fusion (EB-PBF). Bulk SUS316L prepared by conventional processing was used as a reference material, and five types of specimens with varying inclusion contents were prepared by arc remelting mixtures of EB-PBF material and bulk material in controlled fractions. Microstructural characterization and compositional analysis confirmed that all specimens contained a comparable area fraction of δ-ferrite, while the inclusion content increased with increasing EB-PBF fraction. Potentiodynamic polarization tests were performed in 20 mass% H_2SO_4 solution. The corrosion current density (I_{corr}) was found to increase significantly with increasing inclusion content. Tafel extrapolation revealed that this increase was primarily attributed to an enhanced anodic reaction. To further elucidate the corrosion behavior, polarization tests were interrupted at I_{corr}, and the specimen surfaces were examined using confocal laser scanning microscopy (CLSM). The results confirmed that both δ-ferrite and inclusions were preferentially dissolved at this stage.

Keywords: electron beam powder bed fusion; SUS316L stainless steel; inclusions; δ-ferrite

In-situ SEM Heating for Correlative Microscopy of Steels

Ondřej Ambrož[1,*], Petr Horodyský[2], Jan Čermák[1], Šárka Mikmeková[1]
[1]Electron Microscopy, Institute of Scientific Instruments of the CAS, Brno, Czech Republic
[2]Crytur, Turnov, Czech Republic
Email: ondrej@isibrno.czs
*Corresponding author

Abstract

Correlative microscopy provides a powerful framework for understanding microstructural evolution by combining complementary techniques. In this work, in-situ heating experiments were performed in a scanning electron microscope (SEM) to investigate structural transformations in metallic materials and subsequently correlated with light microscopy and microanalysis. The approach enabled the direct observation of thermally induced changes, supported by ex-situ characterization for detailed interpretation. Three representative case studies are presented. (1) Crystal structure evolution was studied by monitoring the recrystallization of plastically deformed steel during heating, revealing grain boundary migration and the nucleation of new grains. (2) Precipitation phenomena were investigated in duplex stainless steel, where the formation of sigma phase was followed in real time and correlated with phase mapping. (3) Controlled oxidation under low vacuum conditions demonstrated color tinting effects on duplex steel surfaces, providing a novel way to visualize microstructural features. The combination of in-situ SEM heating with correlative microscopy techniques provides unique insights into phase transformations, precipitation processes, and oxidation behavior. This methodology not only bridges the gap between dynamic in-situ experiments and conventional ex-situ analysis but also highlights new possibilities for developing advanced metallographic approaches.

Keywords: in-situ SEM heating; correlative microscopy; recrystallization; precipitation; oxidation

Enhanced Hydrogen Evolution by Exsolved Ag Nanoparticles on $AgNbO_3$

Gyeongbok Yang[1, a], Seonhwa Park[2, b] and Yuho Min[1, c]
[1] Materials Science and Metallurgical Engineering, Kyungpook National University, Daegu, Republic of Korea
[2] RLRC of Smart Energy System, Kyungpook National University, Daegu, Republic of Korea
Email: yuhomin@knu.ac.kr

Abstract

Exsolution represents a robust strategy for fabricating stable and efficient catalysts, where metal ions migrate from the bulk lattice to the surface under reducing conditions and evolve into nanoparticles strongly anchored to the oxide. In this study, Ag nanoparticles were exsolved from $AgNbO_3$ using ascorbic acid as a mild reducing agent, enabling the controlled formation of surface-decorated nanoparticles with strong interfacial bonding.
The resulting Ag nanoparticles exhibited remarkable stability against detachment and agglomeration. Furthermore, their surface plasmon resonance (SPR) effect enhanced light absorption, while the intrinsic piezoelectricity of $AgNbO_3$ facilitated efficient charge separation and transfer under mechanical stress. This cooperative interaction among exsolution, plasmonic photocatalysis, and piezocatalysis significantly promoted the hydrogen evolution reaction (HER).
The catalyst was thoroughly characterized using XRD, SEM, EDS, TEM, and UV–Vis spectroscopy. Electrochemical properties were evaluated through LSV, EIS, and CA tests, and hydrogen generation was quantitatively confirmed by gas chromatography (GC). Ongoing efforts are directed toward elucidating the exsolution mechanism and structural evolution.
This research provides a comprehensive design strategy that combines exsolution with piezo-photocatalytic effects, highlighting a promising pathway for durable and high-performance catalysts in sustainable hydrogen energy applications

Keywords: Exsolution; Perovskite; Piezocatalysis; Hydrogen evolution reaction (HER)

Enhanced Depolymerization of Polyethylene Terephthalate via Glycolysis Using CaO-Modified $CoFe_2O_4$ Magnetic Catalysts

Chanyeong Lee[1, a], Seonhwa Park[2, b] and Yuho Min[1, c]
[1] Materials Science and Metallurgical Engineering, Kyungpook National University, Daegu, Republic of Korea
[2] RLRC of Smart Energy System, Kyungpook National University, Daegu, Republic of Korea
Email: yuhomin@knu.ac.kr

Abstract

Polyethylene terephthalate (PET) waste has emerged as a major environmental concern due to its exceptional chemical stability and low degradability. Glycolysis using ethylene glycol (EG) represents a promising chemical recycling route to depolymerize PET into bis(2-hydroxyethyl) terephthalate (BHET), a valuable monomer for polymer regeneration. In this study, we developed a novel magnetic catalyst $CoFe_2O_4$ modified with calcium oxide ($CoFe_2O_4$@CaO) to significantly enhance PET glycolysis efficiency. The catalyst was synthesized through a solvent-free dry-mixing followed by calcination, enabling high surface basicity while maintaining magnetic separability. Systematic catalytic evaluations revealed that $CoFe_2O_4$@CaO exhibited a markedly higher BHET yield and superior reusability compared to pristine $CoFe_2O_4$. The improved performance is attributed to the synergistic effect of dual-active sites and structural stability. These results demonstrate the potential of recyclable CaO-coated magnetic catalysts as sustainable and efficient platforms for PET chemical recycling.

Keywords: PET Glycolysis; Magnetic Catalyst; CaO Surface Modification; BHET Yield; Chemical Recycling

Study of Corrosion Behavior of Rust Layers in Weathering Steels Grade 3Ni and Q420NH

Kanyanat Srisom[1], Chaiyasit BanJongprasert[1], Pranpreeya Wangjina[2], Benjawan Moonsri[2], Wanida Pongsaksawad[2]*
[1]Department of Materials Science, Faculty of Science, Chiang Mai University, Chiang Mai, Thailand
[2]Corrosion Technology Research Team (CTT), Rail and Modern Transport Research Group (RMT), National Metal and Materials Technology Center (MTEC), National Science and Technology Development Agency (NSTDA), Thailand Science Park, Pathum Thani, Thailand
Email: wanidap@mtec.or.th ; wanida.pon@mtec.or.th
*Corresponding author

Abstract

This study aims to investigate the rust layers formed on weathering steels, specifically grades 3Ni and Q420NH, under actual service environments. Understanding the corrosion characteristics of these materials is crucial for extending the service life of steel structures exposed to highly corrosive atmospheres. This research is significant for developing and selecting materials with superior corrosion resistance for structural steel applications. Exposure tests under C3 marine environment were conducted between the two steels for 24 months, and the elemental distribution within the rust layers was examined using Electron Probe Micro Analysis (EPMA). The analysis revealed that the 3Ni steel contained alloying elements that promote the formation of a more stable protective film, effectively reducing the penetration of chloride ions (Cl^-) into the substrate and thereby enhancing its corrosion resistance. In contrast, the Q420NH steel exhibited noticeable chloride ion penetration into the metallic substrate, which accelerated localized corrosion under humid or saline conditions. In conclusion, the results demonstrate that the 3Ni grade exhibits superior corrosion resistance compared to Q420NH under real environmental conditions. These findings highlight the potential of 3Ni weathering steel for use in structural applications exposed to aggressive atmospheric environments, such as railway infrastructures and steel bridges.

Keywords: Weathering steel; 3Ni steel; Q420NH steel; Corrosion behavior; EPMA; Chloride penetration; Protective film

The Role of Iron oxide in the Color and Stability of blue-green Heritage Thai Glass Mosaic Mirrors

Supapon Deechob[1], Susheela Noikae[1], Surapich Poolprasroed[1], Kamonpan Pengpat[1,2*], Sukum Eitssyeam[1], Arnon Kraipok[3], Pratthana Intawin[4], Surapong Panyata[5], Ekarat Meechoowas[6], Terd Disayathanoowat[7], Pinit Kidkhunthod[8], Phakkhananan Pakawanit[8], Jintara Padchasri[8], Manlika Kamnoy[9], Thapanee Srichoompong[9], Tawee Tunkasiri[1]
[1]Department of Physics and Materials Science, Faculty of Science, Chiang Mai University, Chiang Mai 50200, Thailand
[2]Center of Excellence in Materials Science and Technology, Chiang Mai University, Chiang Mai 50200, Thailand
[3]Budget Bureau, The Prime Minister's Office, Bangkok 10400 Thailand
[4]Division of Physics, Faculty of Science and Technology, Rajamangala University of Technology Thanyaburi, Pathum Thani 12110, Thailand
[5]Faculty of Industrial Technology, Rambhai Barni Rajabhat University, Chanthaburi 22000, Thailand
[6]Division of Engineering Materials, Department of Science Service, Bangkok 10400, Thailand
[7]Department of Biology, Faculty of Science, Chiang Mai University, Chiang Mai 50200, Thailand
[8]Synchrotron Light Research Institute, 111 University Avenue, Muang District, Nakhon Ratchasima 30000, Thailand
[9]Office of the University, Chiang Mai University, Chiang Mai 50200, Thailand,
Email: kamonap.p@cmu.ac.th
*Corresponding author

Abstract

This study examines the influence of iron oxide (Fe_2O_3) on the chemical and optical properties of blue-green lead silicate glass, with relevance to both historical Thai glass mosaic mirrors and modern conservation materials. Traditional samples from northern, central, and southern Thailand were analyzed using WDS, XRF, and LA-ICP-MS, UV-Vis spectroscopy, and XRD. Results showed that (Co) and (Cu) were key to blue and green hues, while corrosion phases varied by environment PbO and $2PbCO_3 \cdot Pb(OH)_2$ in older inland samples and $NaPb_2(CO_3)_2(OH)_2$ in younger coastal samples suggesting more severe environmental degradation possibly due to salt exposure.

To extend these findings, experimental glass was fabricated with a fixed CuO:CoO ratio (~40:1) and varying Fe_2O_3 levels (0, 0.8, 2.7 wt%). UV-Vis and colorimetry revealed that higher Fe_2O_3 increased light transmittance, shifted color toward yellow-green, and reduced the energy band gap. Moderate Fe_2O_3 (0.8 wt%) improved melt homogeneity, while higher levels introduced visual color defects.

The combined results highlight how transition metal oxides particularly iron affect both visual and structural properties of lead slilicate glass. These insights support conservation efforts and inform new formulations for colored glass in art and architecture.

Keywords: Thai glass mosaic mirrors; Lead silicate glass; Iron oxide; Glass degradation; Heritage materials

Synthesis and thermoelectric characterization of Fe_3GeTe_2

Hyojin Jun,[1] Hyoju Son,[1] Joseph Ngugi Kahiu,[1] Suhyeon Woo,[2] Samuel Kimani Kihoi,[3] Ho Seong Lee[1,2,3*]
[1]School of Materials Science and Engineering, Kyungpook National University, 80 Daehak-ro, Buk-gu, Daegu, 41566, Republic of Korea
[2]Department of Materials Science and Metallurgical Engineering, Kyungpook National University, 80 Daehak-ro, Buk-gu, Daegu, 41566, Republic of Korea.
[3]Research Institute of Automotive Parts and Materials, Kyungpook National University, 80 Daehak-ro, Buk-gu, Daegu, 41566, Republic of Korea.
E-mail: hs.lee@knu.ac.kr
*Corresponding author

Abstract

Thermoelectric materials enable direct conversion between thermal and electrical energy, and their performance is characterized by the dimensionless figure of merit, $ZT=S^2\sigma T/\kappa$, where S is the Seebeck coefficient, σ is the electrical conductivity, and κ is the thermal conductivity. Achieving a high ZT value typically requires either enhancing the power factor ($S^2\sigma$) or suppressing the lattice thermal conductivity.
Among known thermoelectric materials, Bi_2Te_3 has been widely utilized at room temperature owing to its layered crystal structure and intrinsically low lattice thermal conductivity. Inspired by this, we aimed to explore novel layered compounds with potentially low thermal conductivity and promising thermoelectric performance.
In this study, we investigated Fe_3GeTe_2, which has recently been reported to possess a layered structure similar to Bi_2Te_3. We synthesized Fe_3GeTe_2 and examined the effects of Ni substitution on its structural, electrical, and thermoelectric properties. X-ray diffraction confirmed that Fe_3GeTe_2 crystallizes as a single phase, while Ni_3GeTe_2 forms predominantly as a two-phase system centered on the Ni_3GeTe_2 structure. Furthermore, the power factor of Ni_3GeTe_2 was found to increase with temperature, suggesting its potential applicability as a thermoelectric material at elevated temperatures.
This presentation will discuss the synthesis behavior, phase stability, and thermoelectric characteristics of Fe_3GeTe_2 upon Ni substitution, providing insights into the design of layered thermoelectric compounds with tunable properties.

Keywords: thermoelectric; layered structure; Fe_3GeTe_2;

A Model for Formation of Interfacial Structure in Dissimilar A1070 Aluminum and TP340 Titanium Joint during Disc Friction Joining

Miyu Yamazaki[1] and Toshiya Shibayanagi[2,*]
[1]Graduate School of Science and Engineering, University of Toyama, 180 Futagami-machi Takaoka Toyama 933-8588, Japan
[2]Aluminum Research Center, University of Toyama, 180 Futagami-machi Takaoka Toyama 933-8588, Japan
Email: m24c1631@ems.u-toayama.ac.jp
*Corresponding author

Abstract

Disk friction joining (DFJ) is a solid-state welding technique in which workpieces are pressed against both sides of a rotating disk to generate frictional heat, softening part of the base material. Upon disk withdrawal, additional pressure is applied, resulting in the formation of the joint interface. DFJ has been applied to both similar and dissimilar combinations such as Al/Al, Al/PET, and Al/Mg. A common characteristic of these joints is the presence of fine interfacial undulations, often referred to as "hooks," which are expected to enhance joint strength through an anchoring effect. Nevertheless, the interfacial formation mechanism in DFJ has not yet been sufficiently clarified, making the understanding of this mechanism an important issue. The present study aims to investigate dissimilar joining between A1070 commercially pure aluminum and TP340 commercially pure titanium and to propose an interfacial formation model for DFJ.

Stop-action observations were conducted to capture the transient states of the joining process. This method allowed direct observation of the sequence from disk withdrawal to the completion of interfacial formation, including the development of interfacial undulations.

The results revealed the presence of unbonded regions on both the welding-direction and normal-direction planes, existing from the disk periphery to the contact point between the two materials. Furthermore, four distinct plastic flow modes were identified: (i) heating and burr extrusion during disk contact, (ii) plastic deformation immediately after disk withdrawal, (iii) formation of interfacial undulations prior to bonding, and (iv) compression, buckling, and diffusion following the initiation of bonding. The proposed DFJ joint interface formation model is expected to serve as a foundation for achieving even higher-reliability joints through future quantitative analysis, leading a guidance for optimizing joint parameters in DFJ.

Keywords: Disc Friction Joining; Aluminum; Titanium; Joining mechanism

Hydrogen Reduction of Black Mass Recovered from NCM-based Spent Lithium-ion Batteries

Jae-Ho Hwang[1], Sang-Yeop Lee[1], Ho-Sang Sohn[1,*]
[1]Kyungpook National University (Department of Materials Science and Metallurgical Engineering, School of Materials Science and Engineering, Daegu, Korea)
Email: jaeho9834@naver.com
*Corresponding author

Abstract

NCM($LiNi_xCo_yMn_zO_2$)-based Li-ion batteries (LIBs) for electric vehicles contain critical metals, such as Li, Ni, Co, and Mn. The black mass recovered from spent LIBs contains a large amount of carbon. Therefore, it is necessary to recover valuable metals from spent LIBs to prevent resource depletion. In this study, we investigated the reduction behavior of cathode materials when a black mass was heated in a H_2 atmosphere. When the black mass was heated up to 1,100 °C in a H_2 atmosphere, emission of a large amount of CO led to rapid weight loss from approximately 780 °C by the Boudouard reaction. During the isothermal reaction in a H_2 atmosphere, the weight loss rate and final weight loss of the sample increased with the reaction temperature. Significant amounts of CO were emitted in the region of rapid weight loss. Above 400 °C, NiO was reduced to Ni; above 890 °C, MnO was reduced, and a $MnNi_3$ phase was observed. Li_2CO_3 was produced at temperatures above 300 °C although the reaction occurred in a hydrogen atmosphere. When the reduced black mass was treated with water, Li and Al were detected in the leaching residue. The product recovered from the water leaching solution contained $LiAl_2(OH)_7{\cdot}(H_2O)_2$ together with Li_2CO_3. When the reduction temperature was above 400°C, the Li recovery ratio was approximately 90 % regardless of the temperature. To improve the Li recovery ratio, it is necessary to control the production of complex hydroxides of Li and Al.

Keywords: lithium-ion battery; black mass; hydrogen reduction; recycling; water leaching

Reduction Behavior of NCM-Based Lithium-Ion Battery Black Mass in CO Atmosphere

Sang-Yeop Lee[1], Jae-Ho Hwang[1], Ho-Sang Sohn[1*]
[1]Kyungpook National University, Department of Materials Science and Metallurgical Engineering, Daegu, Republic of Korea.
Email: sohn@knu.ac.kr
*Corresponding author

Abstract

Efforts to combat the climate crisis are driving a shift from fossil fuels to green energy, rapidly growing the electric vehicle market. Lithium, essential for EVs, is in high demand. Recovering lithium from spent $Li(Ni_xCo_yMn_z)O_2$ (NCM) batteries is crucial, with reduction roasting using CO gas being an effective method.

The samples were heated to 1,000°C in step of 100 °C, monitoring weight changes and exhaust gas concentrations in real time at Ar and Ar-CO atmosphere. The roasted samples were water-leached, and the leachate was dried to recover lithium as Li_2CO_3 powder.

Above 600 °C, Ni and Co are fully reduced to metallic forms by CO gas. But Mn remained in oxide because of thermodynamically impossible to reduced. Li_2CO_3 was synthesized by reacting Li_2O with CO_2 gas above 500°C. Leaching experiments show that higher reduction roasting temperatures improve lithium recovery rates. The highest recovery rates were achieved at reduction roasting temperatures of 700°C and 800°C, with recovery rates exceeding 90% and purity over 98%.

Structural, magnetic and spin-reorientation of Nd-doped $ErFeO_3$ polycrystalline ceramics

Ashwini Kumar[1,*], Poorva Sharma[1], Fujun Qiu, Jin Cui[1], Yong Gong[1]
[1]School of Electrical and Electronics Engineering, Luzhou Vocational and Technical College, Luzhou, Sichuan, China - 646000
Email: ashu.dhanda2@hotmail.com
*Corresponding author

Abstract

Rare earth orthoferrites ($RFeO_3$), have a perovskite structure and have attracted significant interest due to their intriguing magnetic, ferroelectric, and multiferroic properties, making them promise for applications in data storage, catalysis, and spintronics [1-4]. In this study, pristine and Nd-doped $ErFeO_3$ ($Er_{1-x}Nd_xFeO_3$, x = 0.0, 0.01) polycrystalline ceramics were synthesized via the solid-state reaction method. We used X-ray diffraction (XRD), Raman spectroscopy (Raman), and X-ray photoelectron spectroscopy (XPS). A Physical Property Measurement System (PPMS) was utilized to assess the magnetic properties of $ErFeO_3$ polycrystalline ceramics. Rietveld-refined X-ray diffraction (XRD) confirmed the formation of a single-phase orthorhombic structure. Magnetic characterization using a Physical Property Measurement System (PPMS) revealed temperature-dependent antiferromagnetic ordering in all samples, with a transition to a fully antiferromagnetic state near 81 K. The pristine $ErFeO_3$ sample exhibited spin reorientation (T_{SR}) in the range of 85–98 K. It was noted that the polycrystalline ceramic $ErFeO_3$ underwent a transition in its magnetic configuration from Γ_4(Gx, Ay, Fz) to Γ_2(Fx,Cy, and z). The magnetic hysteresis loops at temperatures before and after spin reorientation were examined. Nd doping significantly influenced the magnetic interactions, modifying coercivity and net magnetization at low temperatures. These findings provide insights into the tunability of magnetic properties in rare-earth orthoferrites through elemental substitution.

References

[1] X.W. Li, M. Bamba, N. Yuan, Q. Zhang, Y.G. Zhao, M.L. Xiang, K. Xu, Z.M. Jin, W. Ren, G.H. Ma, S.X. Cao, D. Turchinovich, J. Kono, Science, 2018, 361, 794–797.
[2] T. Suemoto, K. Nakamura, T. Kurihara, H. Watanabe, Magnetization-free measurements of spin orientations in orthoferrites using terahertz time domain spectroscopy, Appl. Phys. Lett.,2015, 107, 042404.
[3] H.J. Zhao, L. Bellaiche, X.M. Chen, J. Iniguez, Improper electric polarization in simple perovskite oxides with two magnetic sublattices, Nat. Commun.,2017, 8, 14025.
[4] H. Das, A.L. Wysocki, Y.N. Geng, W.D. Wu, C.J. Fennie, Bulk magnetoelectricity in the hexagonal manganites and ferrites, Nat. Commun., 2014, 5, 29–98.

Structural, optical, and magnetic properties of Nb-doped $YbFeO_3$ polycrystalline ceramics

Poorva Sharma[1,*], Ashwini Kumar[1], Fujun Qiu, Jin Cui[1], Yong Gong[1]
[1]School of Electrical and Electronics Engineering, Luzhou Vocational and Technical College, Luzhou, Sichuan, China - 646000
Email: poorva@lzy.edu.cn
*Corresponding author

Abstract

Rare-earth orthoferrites ($RFeO_3$, R = rare-earth element) are widely explored for their multifunctional properties, particularly in spintronic, magnetic data storage and energy efficient device applications [1-3]. In this study, we investigate the effects of Nb^{5+} substitution at the Yb^{3+} site in $YbFeO_3$ ceramics, with compositions $Yb_{1-x}Nb_xFeO_3$ (x = 0.00, 0.02, 0.05), synthesized via the solid-state reaction method. X-ray diffraction (XRD) analysis confirms the retention of the orthorhombic distorted perovskite structure (*Pbnm*) with slight variations in lattice parameters due to the ionic radius difference between Nb^{5+} (0.64 Å, CN = 6) and Yb^{3+} (0.868 Å, CN = 6). Rietveld refinement suggests that Nb doping induces lattice distortion, modifying the Fe-O-Fe bond angles and bond lengths, which strongly influence the magnetic exchange interactions. Magnetic measurements reveal that the spin reorientation transition ($\Gamma_4 \rightarrow \Gamma_2$) occurs in the temperature range of 6 K $\leq T_{SR} \leq$ 8 K for undoped $YbFeO_3$, while Nb doping shifts this transition to higher temperatures. The observed changes suggest that Nb^{5+} doping disrupts the delicate balance of 3*d*–4*f* magnetic interactions, leading to modifications in the spin dynamics and overall magnetic anisotropy [4]. To examine the influence of Nb doping on optical properties, UV-Visible spectroscopy was performed. The bandgap energy, estimated using Tauc's relation, was found to be approximately 1.8 eV, indicating strong absorption in the visible region. The observed tuning of optical and magnetic properties with Nb doping highlights the potential of these ceramics for applications in spintronic memory devices, where controlled magnetic transitions and tailored optical properties are crucial for device performance.

References

[1] H. Das, A.L. Wysocki, Y.N. Geng, W.D. Wu, C.J. Fennie, Nat. Commun., 2014, 5, 29.
[2] J. F. Scott, Nat. Mater., 2007, 6, 256.
[3] Y. K. Jeong, J.-H. Lee, S.-J. Ahn, S.-W. Song, H. M. Jang, H. Choi, J. F. Scott, J. Am. Chem. Soc., 2012, 134 (3), 1450-1453.
[4] Q. Li, J. Zhou, J. Shang, H. Shen, L. Li, F. Wang, X. Shen, T. Tian, A.M. Kalashnikova, A. Wu, J. Xu, J. Cryst. Growth, 2025, 649, 127939.

Green Aerogel-Enhanced Chitosan/Mung Bean Composite Films: Miscibility and Potential as Solid Polymer Electrolytes

Aunchisa Buasuk[1], Manat Jaimasith[1], Wanrudee Kaewmesri[1,*]
[1]Division of Chemistry, School of Science, University of Phayao, 19 Moo. 2 Mae-Ka, Muang, Phayao, Thailand 56000
Email: wanrudee.ka@up.ac.th
*Corresponding author

Abstract

This study explores the development of bio-based composite films as potential solid polymer electrolytes (SPEs) for metal-air battery applications. Chitosan and mung bean starch were selected as the polymer blend matrix. However, due to the use of different solvents, the resulting films exhibited immiscibility and surface roughness. To overcome these limitations, aerogel silica was synthesized from sugar cane leaf ash, an abundant agro-waste, using the sol-gel method and incorporated as a reinforcing agent. A chitosan/mung bean solution with a 2:1 volume ratio, containing 1 %w/v of glycerol and 5 %v/v of citric acid, was blended with varying concentrations of aerogel silica (0.5, 1.0, and 3.0 %w/v) followed by solvent evaporation to form composite films. The prepared films were systematically characterized in comparison with neat polymer films. The composites demonstrated resistance in 6M KOH for nearly 20 hours, indicating improved alkaline stability. FT-IR spectra confirmed crosslinking interactions between hydroxyl and carboxyl groups, while electrochemical impedance spectroscopy (EIS) revealed Nyquist plots with spike-like features attributed to the electrode blocking effect, without semicircle relaxation processes. The bulk resistance was measured at 1.79 Ω, and Bode plots exhibited a single time constant with phase signal peak in the 0.1-50 Hz range and a frequency shift to the kHz region, confirming the homogeneity of phase and impedance response influenced by the electrode-electrolyte interface. Morphological analysis using digital image correlation showed smoother surface in the composite films, particularly at 3 %w/v aerogel silica, compared to the neat films. These finding demonstrate the potential of green aerogel-reinforced chitosan/mung bean composite films as eco-friendly SPE candidates with enhanced structural and electrochemical performance, contributing to the advancement of sustainable materials for metal-air batteries.

Keywords: Aerogel silica; Bio-composite film; Chitosan; Metal-air batteries; Solid polymer electrolyte

Effect of Cu Addition on the Thermal Stability and High-Density SPS Consolidation of Fe-Based Amorphous Alloy

Seongjun Kim[1], Seonghoon Yi[1,*]
[1]Department of Materials Science and Engineering, Kyungpook National University, Daegu, Republic of Korea
Email: kim5516566@naver.com, yish@knu.ac.kr
*Corresponding author

Abstract

Fe-based amorphous alloys have been considered as attractive soft magnetic materials owing to their high saturation magnetization, low coercivity, and economic advantages. In this study, the role of Cu addition was emphasized with respect to its effect on both the glass-forming ability and the first crystallization temperature (Tx1) of α-Fe. Variations in Cu content were found to influence the thermal stability of the amorphous phase, thereby altering the appropriate consolidation window during spark plasma sintering (SPS).
Amorphous ribbons with different Cu contents were fabricated by rapid solidification and bulk samples were subsequently consolidated by SPS under tailored conditions. During SPS, concurrent nanocrystallization occurred, resulting in the controlled precipitation of α-Fe nanocrystals within the amorphous matrix.
The consolidated samples were characterized by X-ray diffraction (XRD) for phase analysis and their magnetic properties were evaluated using vibrating sample magnetometry (VSM), a DC B-H loop tracer and an AC magnetic analyzer.

Keywords: Soft magnetic properties; Amorphous alloy; Nanocrystallization

Enhanced Thermoelectric Characteristics and Performance of Bi_2Te_3 Modules via Ni–P Electroless and Ag Electrodeposition

Anh Doan Tien[1], Khanh Dang Quoc[2], Son Injoon[1,*]
[1] School of Materials Science and Engineering, Kyungpook National University, Daegu, 41566, South Korea
[2] School of Materials Science and Engineering, Hanoi University of Science and Technology, Hanoi, 100000, Vietnam
Email: ijson@knu.ac.kr
*Corresponding author

Abstract

Bi–Te-based thermoelectric (TE) materials are among the most promising candidates for low-temperature (≤200 °C) energy conversion, where heat can be directly converted into electricity and vice versa. However, their practical application is limited by interfacial degradation between TE legs and Cu electrodes. Conventional Sn-based soldering often produces brittle Sn–Te intermetallic compounds, which reduce both efficiency and mechanical reliability. To overcome this limitation, we propose an interfacial engineering strategy combining electroless nickel–phosphorus (Ni–P) plating with silver (Ag) electroplating. Bi_2Te_3 elements (n-type and p-type) were first coated with a 1 μm Ni–P diffusion barrier at 80 °C, followed by Ag electroplating of controlled thicknesses (1–6 μm) at room temperature. The coated legs, sized 3 × 3 × 2 mm, were assembled into TE modules using lead-free solder paste and reflow soldering. Coating thickness was verified by X-ray fluorescence (XRF), and the modules were evaluated in terms of cooling capability, power generation performance, and resistance. The results indicate that optimizing Ag coating thickness balances mechanical integrity and thermoelectric efficiency, thereby enhancing output power and durability. This scalable approach offers a practical pathway for improving the reliability of Bi–Te-based thermoelectric devices in low-temperature energy conversion applications.

Keywords: Thermoelectric material; Bismuth-Telluride; Power performance; Electroless Ni-P; Ag Electrodeposition

Influence of Holding Time on the Properties of Porous Alumina Fabricated by Pulse Electric Current Sintering

Anh Duc Hoang Chu[1], Hong Minh Duong[1], Dung Phuong Thi Nguyen[1], Truong Xuan Truong [2], Khanh Quoc Dang[1,3,*]
[1]School of Materials Science and Engineering, Hanoi University of Science and Technology, Hanoi, Vietnam
[2]School of Chemistry and Life Sciences, Hanoi University of Science and Technology, Hanoi, Vietnam
[3]Laboratory of Metals, Alloys and Composite, School of Materials Science and Engineering, Hanoi University of Science and Technology, Hanoi, Vietnam
Email: khanh.dangquoc@hust.edu.vn
*Corresponding author

Abstract

In the context of growing global air pollution concerns, porous Al_2O_3 ceramic emerges as an advanced material with exceptional properties, including high-temperature resistance, low density, large specific surface area, and excellent thermal stability. To optimize environmental treatment performance, porous Al_2O_3 ceramic requires precise microstructure with controlled porosity, optimized pore size distribution, and enhanced pore interconnectivity tailored to specific environmental applications. In this study, pulse electric current sintering (PECS) was employed as an advanced consolidation technique to fabricate porous Al_2O_3 ceramics with tailored microstructures while preserving mechanical integrity. The influence of holding time on the microstructure and compressive strength of porous Al_2O_3 fabricated by PECS process was systematically investigated. The results revealed that total porosity decreased with increasing sintering time and applied pressure, indicating enhanced densification. Conversely, the compressive strength showed a positive correlation with both pressure and sintering time, with the lowest value of 7.02 MPa observed at 20 MPa and sintering for 3 minutes. These findings demonstrate the critical role of sintering parameters in optimizing the structural and mechanical properties of porous Al_2O_3 ceramics for environmental applications.

Keywords: Al_2O_3; porosity; PECS; holding time

Cloisonné Using Blue Laser with Heater Assistance

Shuntaro Arakawa[1], Takashi Hashizume[1*], Atsushi Saiki[1], Shoto Isizaki[2]
[1]School of Sustainable Design, Univ. Toyama, Toyama, Japan
[2]Nikon corporation, Tokyo, Japan
Email: hasizume@sus.u-toyama.ac.jp
*Corresponding author

Abstract

In traditional cloisonné, it is essential to apply glaze onto a metal plate and fire it at high temperatures. However, this process requires long firing times and high-temperature environments. As a result, improvement in work efficiency is limited. Recently, laser technology has attracted attention for its ability to perform high-precision and high-speed processing. This study proposes the application of laser technology to the firing process of cloisonné. Compared to conventional electric kiln firing, this method enables the formation of fine patterns in a shorter time. It also allows for the creation of precise color expressions and textures. To establish optimal laser firing conditions, the study evaluated the color development characteristics and crack formation behavior. In the experiment, four types of glazes were used. Each glaze is mainly composed of lead, silicates, and metal oxides. The glazes were ground to approximately 40–50 μm. They were then applied to copper plates. The samples were placed near a heater to remove moisture. After complete drying, they were preheated on a 350°C heater for three minutes. This ensures uniform thermal distribution. Laser irradiation was then performed. The temperature was maintained during this process. Since the laser alone did not provide sufficient thermal energy, a heater was used in combination. This resulted in a uniform glassy surface. High color reproducibility was observed across the glazes. The surface hardness and smoothness of the laser-fired samples were confirmed. These properties were comparable to those produced by electric kiln firing. Furthermore, the boundaries between different glaze colors were also clearly visible. The result demonstrated the potential for more precise design expression than conventional methods.

Keywords: Cloisonné; Glaze; Laser

Microstructure of Al–Sn and Al–Sn–In Alloys Produced by Severe Plastic Deformation for Anode Applications

Pornpan Wanna[1] and Chaiyasit Banjongprasert[1,*]
[1]Department of Physics and Materials Science, Faculty of Science, Chiang Mai University, Chiang Mai, 50200, Thailand
E-mail: chaiyasit.b@cmu.ac.th
*Corresponding author

Abstract

Aluminum-air batteries have a potential energy density of roughly 8.1 kWh/kg, regarding as one of the most promising options for future energy storage. These batteries are economical and eco-friendly since aluminium is plentiful, lightweight, affordable, and recyclable. However, the severe self-corrosion and high hydrogen evolution of pure aluminium anodes severely restricts their practical application. This study examines how aluminium anodes made from Al–Sn and Al–Sn–In alloys can perform better electrochemically by using Equal Channel angular Pressing (ECAP) and Friction Stir Processing (FSP). ECAP and FSP create ultrafine grains and ensure uniform dispersion of alloying components by introducing strong plastic deformation. In contrast to coarse-grained aluminium, prior research has demonstrated that finer microstructures greatly increase energy density and corrosion resistance. This investigation involves the preparation of three alloys: Al–0.1Sn, Al–0.1Sn–0.05In, and Al–0.1Sn–0.1In. ECAP was conducted by route Bc. Using a straight hexagonal pin tool, FSP is used to treat the samples following casting and homogenization. Grain refinement and elemental distribution are examples of microstructural changes that are characterized by optical microscopy, SEM–EDS, and EBSD. In addition, electrochemical characteristics are assessed using potentiodynamic polarization tests. The results are intended to shed light on the connection between alloy microstructure, composition, and electrochemical performance. The findings will help develop high-performance aluminium anode designs, which will progress the development of affordable, environmentally friendly, and effective Al-air batteries for use in upcoming energy purposes.

Keywords: Aluminum-air battery; Anode; Friction stir processing; Microstructure; Electrochemical properties; Al-Sn alloys; Al-Sn-In alloys

First Principles Study of $L1_2$-Type Al_3Zr Precipitates in Aluminum Alloys

Yuma Matsuzaki[1,*], Norio Nunomura[2]
[1]Graduate School of Science and Engineering, University of Toyama, Toyama, Japan
[2]Department of Materials Design and Engineering University of Toyama, Toyama, Japan
Email: m25c1626@ems.u-toyama.ac.jp
*Corresponding author

Abstract

The mechanical properties of aluminum alloys are strongly influenced by the formation of precipitates induced by minor alloying additions, particularly transition metal elements. Among these, $L1_2$-type compounds, which exhibit good coherency with the Al matrix, are well-known strengthening phases. However, the detailed relationship between their electronic structures, stability, and resulting mechanical properties remains incompletely understood. In this study, we focus on $L1_2$-type compounds and investigate representative examples using first-principles calculations with AkaiKKR, analyzing their electronic densities of states and elastic properties. Our initial results for Al_3Zr indicate that strong orbital hybridization between aluminum and zirconium leads to the formation of a pseudo-gap in the electronic structure, suggesting a potential correlation between the Fermi level position relative to this pseudo-gap and the compound's stability. Moving forward, we aim to systematically examine the effect of alloying additions on the Fermi level and the stability of the $L1_2$ phase. We will extend our calculations to $Al_3Zr_xTM_{1-x}$ (TM: Transition metals) compounds, varying the concentration of transition metal elements to tune the electronic structure and shift the Fermi level toward the bottom of the pseudo-gap. By analyzing the resulting electronic structures and formation energies, we aim to establish design principles that utilize $L1_2$-type precipitates to enhance both the electronic stability and overall performance of aluminum alloys, ultimately providing guidance for the design of $Al_3Zr_xTM_{1-x}$ alloys with improved mechanical properties and durability.

Keywords: density functional theory; aluminum alloys; $L1_2$ structure; KKR-CPA; AkaiKKR

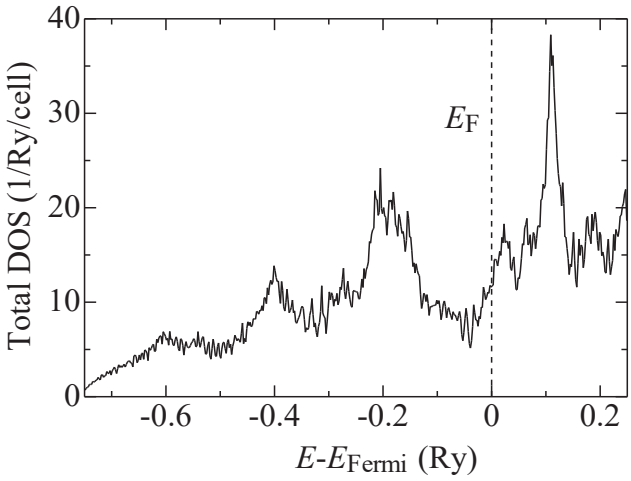

Fig.1. Total electronic density of states (DOS) of Al_3Zr

First-principles calculation of electron transport influenced by Fe adsorption on graphene nanoribbons (GNRs)

T. Yoshida[1*], N. Nunomura[2]
[1] Graduate School of Science and Engineering, University of Toyama, Toyama, Toyama, Japan
[2] Department of Materials Design and Engineering, University of Toyama, Toyama, Toyama Japan
Email: m24c1633@ems.u-toyama.ac.jp

Abstract

Graphene nanoribbons (GNRs) are one-dimensional materials derived from graphene, a carbon-based material known for its exceptional electrical conductivity and atomic-scale thinness. In addition to inheriting graphene's unique properties, GNRs exhibit tunable electronic and magnetic characteristics depending on their edge structure, making them highly promising for a wide range of technological applications. Although graphene is intrinsically non-magnetic, theoretical studies have demonstrated that its magnetic properties can be significantly enhanced through the adsorption of iron atoms—a phenomenon that also applies to GNRs. This type of functionalization holds strong potential for spintronics applications, which utilize the spin degrees of freedom of electrons. Given their atomic-scale thinness and tunable electronic properties, GNRs are expected to play a crucial role in the development of next-generation electronic components and semiconductor devices.
This study investigated the electronic transport properties of GNRs and examined the effect of Fe atom adsorption on the GNR structure. Furthermore, we explored how structural parameters such as GNR width (vertical) and length (lateral) influence their electronic behavior. We performed our calculations using spin-polarized density functional theory (DFT) with the OpenMX package. The energy cutoff was set to 100 Ry. 1×7×7 k-point sampling grid was used, along with a convergence threshold of 1×10^{-7}.
Our calculations indicate that the structural stability of GNRs, which are indexed in order of increasing width, increases with width. However, when normalized per Fe atom, it was found that the work function efficiency sharply declines beyond a certain width.

Keywords: Density functional theory; Graphene surface; Metal adsorption; Electron transport

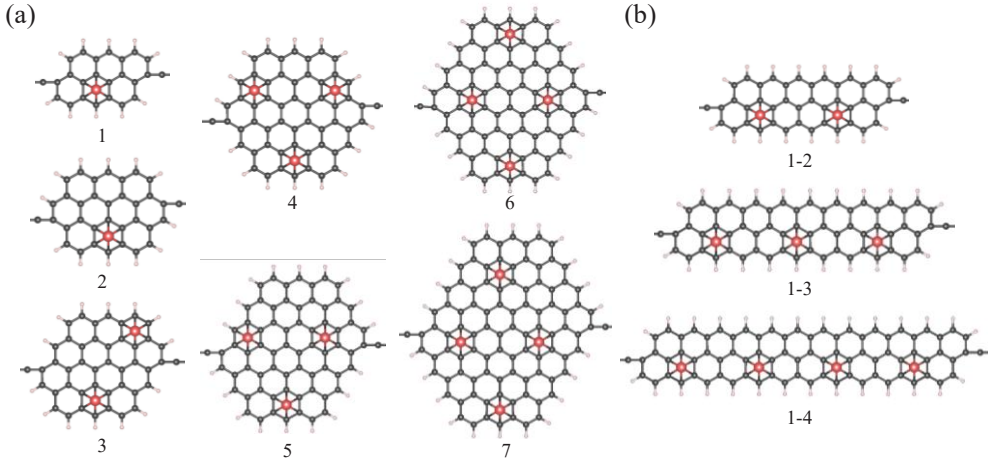

Fig.1 Top view of a GNR structure with adsorbed Fe atoms. Carbon atoms are shown in black, Fe atoms in red, and hydrogen atoms in white. (a) shows the structure with extended width (vertical), while (b) shows the structure with extended length (horizontal).

Towards Safer, Reproducible and Smarter Metallographic Sample Preparation through Collaborative Robotics and Computer Vision

J. Čermák[1,*], O. Ambrož[1], Š. Mikmeková[1]
[1]Electron Microscopy, Institute of Scientific Instruments of the Czech Academy of Sciences, Královopolská 147, 612 00 Brno, Czech Republic
Email: cermak@isibrno.cz
*Corresponding author

Abstract

Despite decades of instrument development, metallographic sample preparation remains only partially automated. Individual subprocesses—such as sectioning, grinding, polishing, or surface contrasting—are typically handled through instrument-level automation, but they are rarely integrated into a seamless automated workflow. This fragmented approach maintains flexibility, yet the overall degree of automation remains limited.

Recent advances in collaborative robotics, artificial-intelligence-driven computer vision, and modern sensor technologies offer an opportunity to move beyond isolated steps towards holistic automation. Instead of replacing the operator, these systems are intended to complement human expertise. Collaborative workstations with intuitive cobot programming interfaces can merge human decision-making with robotic precision, enabling safer, more reproducible, and less labor-intensive sample preparation.

Such a synergistic setup not only reduces repetitive workload and minimizes operator risks but also allows full digital traceability of the preparation procedure. Recording preparation parameters and outcomes provides metadata that can be reused for reproducibility, shared within research teams, or linked to FAIR data repositories as part of open science initiatives.

This contribution outlines how combining collaborative robotics, advanced vision systems, and user-friendly automation strategies can transform metallographic practice. By addressing both stochastic variability and operator workload, the approach paves the way towards safer, more standardized, and future-ready specimen preparation.

Keywords: metallography; sample preparation; automation; collaborative robotics

Effect of Double-Diffusive Convection on the Solidification Microstructure in the Solidification of Molten Al–Si Alloys

Kensuke Shimode[1], Takeshi Yamane[2], Toshiya Shibayanagi[2,*]
[1]Graduate Student, University of Toyama, 3190 Gofuku, Toyama, 930-8555, Japan
[2]Aluminum Research Center, University of Toyama, 180 Futagami-machi, Takaoka, Toyama, 933-8588, Japan
Email: toshiya@sus.u-toyama.ac.jp
*Corresponding author

Abstract

In the solidification process of multicomponent molten systems, solute convection driven by the density differences of the solutes released into the liquid phase coexists with thermal convection caused by the release of latent heat during solidification and by cooling. When certain conditions are met, double-diffusive convection occurs. This flow phenomenon is characterized by the formation of multiple convection cells with concentration discontinuities. In double-diffusive convection, complex flows arise due to the differing diffusivities of heat and solute. This phenomenon has been demonstrated through visualization experiments using a eutectic NH_4Cl-H_2O solute and solidification experiments with Sn-Pb melts, and has also been investigated numerically. However, the effects of double-diffusive convection during solidification of metals, and the quantitative conditions under which it occurs, remain unclear. Therefore, numerical simulations and metal solidification experiments were carried out to elucidate the relationship between this convection and the solidified microstructure. The numerical code used in this study has also been validated. Numerical simulations were carried out for the Al-10wt%Si alloy, and horizontal unidirectional solidification experiments were conducted using the ADC12 alloy. The effects of double-diffusive convection on the solidification microstructure were examined through microstructural observation and concentration analysis using EPMA. Numerical simulations revealed the formation of multiple vertical convection structures within the liquid phase during solidification, along with discontinuous regions where concentration stagnated. In the metal solidification experiments, a distinctive microstructure was observed in the specimens as a result of controlled cooling rates, which may have been caused by double-diffusive convection.

Keywords: Solidification; Double-diffusive convection; Numerical simulation; Aluminum alloys

Si Removal from Molten Al-Mg-Zn Alloy through the Precipitation of Intermetallic Compounds

Mikoto KOJIMA[1], Kengo KATO[2], Hideki ONO[2,*]
[1]Department of Materials Design and Engineering, School of Sustainable Design, University of Toyama, Toyama, Japan
[2]Department of Materials Design and Engineering, Faculty of Sustainable Design, University of Toyama, Toyama, Japan
Email: ono@sus.u-toyama.ac.jp
*Corresponding author

Abstract

To achieve carbon neutrality, it is required to reduce CO_2 emissions. Aluminum is widely used in automotive parts, window frames, and other applications due to its low density and high corrosion resistance. The energy required to produce recycled Al ingots is significantly lower than that required to produce Al ingots from natural resources. Accordingly, CO_2 emissions from recycled aluminum can be limited to 3% of those from natural resources. Therefore, recycling aluminum scraps is extremely important. In Japan, almost all cast Al alloys are produced from recycled aluminum, although only about 10% of wrought Al alloys are produced from it. To expand the use of recycled aluminum in producing wrought Al alloys, various impurities contained in the scrap must be removed. This study focused on Si removal through Mg addition. The authors reported that the Si content can be reduced through the precipitation of Mg_2Si by adding Mg into molten aluminum. In this work, the solubility of Si in molten Al-Mg-Zn alloys was investigated to decrease the Si content. When the Al-20mass%Mg-3mass%Zn-Si alloy was melted at 873K, the precipitation of Mg_2Si was observed. The Al-Mg-Zn alloy was equilibrated with Mg_2Si, preliminarily made from regent-grade Mg and Si, and the effect of Zn on the Si solubility in the molten Al-Mg alloy was investigated.

Keywords: Aluminum recycling; Si removal; Al-Mg-Zn alloy; Thermodynamics

High-Quality Graphene for Advanced Applications in Electron Microscopy

Ivo Konvalina[1], Lukáš Průcha[1], Eliška Materna Mikmeková[1*]
[1]Department of Electron Microscopy, Institute of Scientific Instruments of the CAS, v. v. i., Brno, Czech Republic
Email: eliska.mikmekova@isibrno.cz
*Corresponding author

Abstract

Graphene, with its unique combination of atomic thinness, electrical conductivity, mechanical stability, and chemical inertness, provides a powerful platform for advancing electron microscopy. We produce high-quality graphene by chemical vapor deposition (CVD) on copper substrates, followed by exfoliation using our proprietary ultra-clean method. This approach enables precise control of layer number, large-area coverage of smooth substrates up to 3 × 3 cm, and the preparation of robust free-standing membranes up to 300 µm. Such membranes serve as stable TEM supports and effectively suppress electron beam aberrations, thereby improving imaging conditions. Graphene-coated TEM grids minimize background scattering, enhance contrast, and enable reliable imaging of beam-sensitive samples with high fidelity.
In addition, exfoliated graphene of exceptional quality is applied as a protective coating for electron detectors, where it reduces contamination, prevents degradation of sensitive surfaces, and improves sensitivity and efficiency under low accelerating voltages. Graphene also serves as a protective barrier against oxidation, corrosion, and environmental contamination, extending sample lifetime and preserving intrinsic structure and chemistry. These results highlight graphene's versatility not only as a support film or protective layer but also as an enabling material for novel experimental setups. Future developments may include graphene-based EDS windows, encapsulation layers for in situ liquid and gas TEM cells, and integration with cryo-electron microscopy workflows. Our work establishes a reliable methodology for ultra-clean graphene preparation and demonstrates its transformative role in the next generation of electron microscopy.

Keywords: graphene; electron microscopy; CVD deposition

Acknowledgement: The research was supported by the Lumina Quaeruntur Fellowship of the Czech Academy of Sciences (grant no. LQ100652201) and by the Technology Agency of the Czech Republic (grant no. TN02000020).

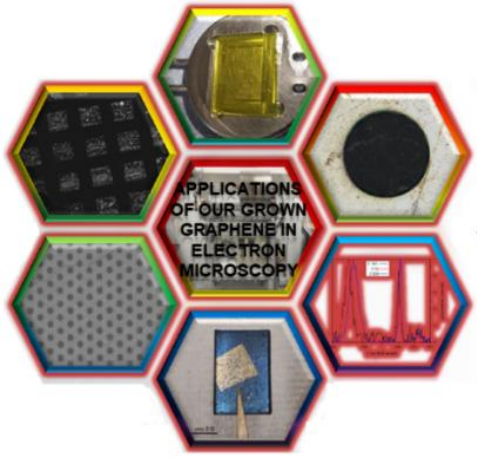

Rational Interface Design of Zinc Powder Anodes with rGO and PAA for High-Performance Aqueous Zinc-Ion Batteries

Jinhyeong Yoon[1], Jihong Kim[1], Hak-Sung Kim[2], Heejoon Ahn[1,3,*]
[1]Department of Battery Engineering, Hanyang University, Seoul, South Korea
[2]Department of Mechanical Engineering, Hanyang University, Seoul, South Korea
[3]Department of Organic and Nano Engineering, Hanyang University, Seoul, South Korea
Email: ahn@hanyang.ac.kr
*Corresponding author

Abstract

Aqueous zinc-ion batteries (ZIBs) are promising next-generation energy storage systems owing to their intrinsic safety, low cost, and environmental compatibility. Zinc powder anodes, with high surface area and scalable processability, offer significant advantages but suffer from dendrite growth, surface passivation, and binder instability, which limit their practical viability. Here, we present a dual-interface engineering strategy that integrates reduced graphene oxide (rGO) encapsulation with a polyacrylic acid (PAA) binder to realize durable zinc powder anodes. The rGO shell not only suppresses dendrite formation and parasitic reactions by shielding the Zn surface from direct electrolyte contact but also provides electronic conductivity. Simultaneously, the hydrophilic PAA binder enhances electrode–electrolyte affinity and ensures uniform Zn-ion deposition, while hydrogen bonding with rGO functional groups prevents binder dissolution. This synergistic design enables exceptional electrochemical stability: symmetric cells exhibit >670 h of cycling at 33% depth of discharge, and full cells with vanadate cathodes deliver 147 mAh g^{-1} at 20 A g^{-1} with 80% retention after 2000 cycles. These results highlight the effectiveness of rational interface engineering in achieving high-performance, long-life aqueous ZIBs and offer practical guidelines for scalable, binder-integrated anode architectures.

Keywords: Zinc powder anode; Interface engineering; Reduced graphene oxide (rGO); Zinc-ion batteries

Sonochemical-assisted deposition synthesis and characterization of metallic Au nanoparticles modified thin Bi_2WO_6 nanoplates for enhanced visible-light-driven photocatalytic reaction

Anukorn Phuruangrat[1,*], Yothin Chimupala[2], Budsabong Kuntalue[3], Titipun Thongtem[4,5] and Somchai Thongtem[4,6]

[1] Division of Physical Science, Faculty of Science, Prince of Songkla University, Hat Yai, Songkhla 90112, Thailand

[2] Department of Industrial Chemistry, Faculty of Science, Chiang Mai University, Chiang Mai 50200, Thailand

[3] Advanced Scientific Instruments Unit (ASci Unit), Faculty of Science, Chiang Mai University, Chiang Mai 50200, Thailand

[4] Materials Science Research Center, Faculty of Science, Chiang Mai University, Chiang Mai 50200, Thailand

[5] Department of Chemistry, Faculty of Science, Chiang Mai University, Chiang Mai 50200, Thailand

[6] Department of Physics and Materials Science, Faculty of Science, Chiang Mai University, Chiang Mai 50200, Thailand

Email: phuruangrat@hotmail.com

*Corresponding author

Abstract

Au/Bi_2WO_6 nanocomposites as visible-light-driven photocatalyst were synthesized by a sonochemical-assisted deposition method and used for rhodamine B (RhB) degradation under visible light irradiation. Phase, morphology, surface area, atomic vibration, oxidation state of elements and optical properties of as-prepared Bi_2WO_6 and Au/Bi_2WO_6 were characterized by X-ray diffraction, scanning electron microscopy, transmission electron microscopy, Fourier transform infrared spectroscopy, Raman spectrophotometry, nitrogen adsorption–desorption isotherm, UV-Visible diffuse reflectance spectroscopy, Brunauer–Emmett–Teller surface area analysis and X-ray photoelectron spectroscopy. The results identified that metallic Au nanoparticles were supported on the surface of thin Bi_2WO_6 nanoplates to create heterostructure Au/Bi_2WO_6 nanocomposites. The Au/Bi_2WO_6 nanocomposites show strong absorption range of visible light in 450-700 nm. The heterostructure 5% Au/Bi_2WO_6 nanocomposites exhibited the photodegradation for RhB with excellent efficiency of 97.91% under visible light irradiation for 150 min due to the Schottky interface of Au nanoparticles and Bi_2WO_6 nanoplates and surface plasmon resonance (SPR) effect of metallic Au nanoparticles. The role of active species in degrading RhB over 5% Au/Bi_2WO_6 nanocomposites was investigated and a photocatalytic mechanism was proposed and explained according to the experimental results.

Keywords: Au/Bi_2WO_6; Photocatalysis; Nanocomposites

Changes in Battery Capacity Due to the Application of a Magnetic Field to Lithium-Ion Batteries

Yoshiki YAMASHITA[1], Takashi HASHIZUME[1], Atsushi SAIKI[1], Ryusei TANIMOTO[2], Ren Sato[3]
[1]School of Sustainable Design, University Of TOYAMA, Toyama, Japan
[2]JTEKT Corp., Aichi, Japan
[3]Rent Corp., Shizuoka, Japan
Email: hasizume@sus.u-toyama.ac.jp
*Corresponding author

Abstract

The recycling of lithium-ion batteries has increased in recent years. In the recycling process for used lithium-ion batteries, these batteries are disassembled. The battery's cathode is then placed into a high-temperature furnace and melted. In our research, we attempted to extend the lifespan of lithium-ion batteries. In this study, degraded lithium-ion batteries were subjected to charge–discharge cycling under an applied magnetic field, and their state of health (SOH) was compared with that of batteries cycled without a magnetic field. The charge–discharge rate was set to 1C in both cases. Subsequently, the internal resistance of each battery was measured, and the negative electrodes were observed in order to investigate the influence of the magnetic field on the anode. After ten charge–discharge cycles under a magnetic field, the SOH decreased from approximately 67% to 60%, whereas the SOH of the batteries cycled without a magnetic field decreased from about 65% to 39%. Furthermore, the internal resistance was measured, showing values of 0.375 Ω for the battery cycled under the magnetic field and 0.575 Ω for the battery cycled without the magnetic field. In addition, the negative electrode surfaces of both types of batteries were analyzed by SEM and EDS. It was found that less metallic lithium was deposited on the negative electrode surface of the battery cycled under a magnetic field compared to that cycled without a magnetic field. From these experimental results, it was demonstrated that applying a magnetic field during charge–discharge cycling can suppress the degradation of lithium-ion batteries. Moreover, it was clarified that battery degradation is caused by the increase in internal resistance due to the growth of metallic lithium deposits on the negative electrode.

Keywords: magnetic field; anode; SOH

Properties of Corn Stalk Rind Compressed Pads

Seephapa Siriprakaikoon, Linda Thiraphattaraphun*
Division of Packaging Technology, Faculty of Agro-Industry, Chiang Mai University,
Chiang Mai 50100, Thailand
Email: linda.t@cmu.ac.th
*Corresponding author

Abstract

Packaging pads provide several functions, such as serving as protective inserts, partition within a box, and stabilizing the product. Commonly, polymeric foam, paper, paperboard, and corrugated paper are used to produce packaging pads. Corn stalk rind is an agricultural residue that can be used to produce packaging pads by compression molding. Two difference sizes (1 and 2 mm) of corn stalk rind were used. The corn stalk rind compressed pads exhibited a brown color. The density, water solubility (60 min.), and residue weight at 700 °C of the corn stalk rind compressed pads were 0.26-0.27 g/cm^3, 5.6-5.8% and 22.6-22.7% respectively. The puncture resistance of the corn stalk rind compressed pads increased with the number of layers (from 1 to 3 layers) in both sizes of corn stalk rind. These corn stalk rind compressed pads could be used as alternative bio-packaging pads for environmentally friendly packaging.

Keywords: corn stalk rind; pads; packaging

High-Density Amorphous Compacts with High B and Gd Contents for Neutron Shielding

Hyeseong Choi[1], Seong-Hoon Yi[1*]
[1]Materials Science and Metallurgical Engineering, Kyungpook National University, Daegu, Korea
Email: yish@knu.ac.kr
*Corresponding author

Abstract

The safe management of radioactive waste generated from nuclear power plants and research facilities requires the development of highly reliable radiation shielding materials. The stable isotope ^{157}Gd is well known for its excellent thermal neutron absorption, with a capture cross-section of 254,000 barns. This value is about 66 times higher than that of ^{10}B (3,840 barns). However, both B and Gd show low solid solubility in Fe alloys, and high additions result in the formation of secondary phases, leading to poor mechanical properties and corrosion resistance.

In this study, Fe-B-Mo-Gd-Al amorphous alloys were designed to maintain high B and Gd contents while achieving excellent glass-forming ability. The as-cast were prepared by arc melting, and bulk metallic glasses were produced using suction casting. High-density amorphous compacts were fabricated through hot pressing and spark plasma sintering. Thermal behavior was evaluated using differential scanning calorimetry. Phase evolution and microstructure were analyzed by X-ray diffraction and scanning electron microscopy. Mechanical properties were examined by Vickers hardness testing.

The results show that Fe-based amorphous alloys containing high B and Gd possess a wide supercooled liquid region, enabling the fabrication of 1 mm diameter bulk metallic glasses and dense amorphous compacts. The compacts maintained a fully amorphous structure, achieved ~98% relative density compared to as-cast, and exhibited superior mechanical properties. These findings suggest that the proposed alloys are strong candidates for next-generation neutron shielding materials in radioactive waste storage and nuclear safety systems.

Keywords: Bulk metallic glass; Fe-based amorphous alloy; Neutron shielding; High density Sintered compact

Void-Free TSV Filling by Copper Electroplating with Thioflavin T Additive

Nayoung Kim, Injoon Son*
Materials Science and Engineering, Kyungpook National University, Daegu, Korea
Email: ijson@knu.ac.kr
*Corresponding author

Abstract

In this study, we successfully achieved void-free filling of through-silicon vias (TSVs) with an aspect ratio of 1:5 through a copper electroplating process using an additive system based on Thioflavin T.
TSV technology is a key enabler for high-density 3D semiconductor packaging, providing high-density vertical interconnections between different layers and chips by filling deep and narrow vias with conductive materials such as copper. The quality of TSV filling directly affects the electrical performance and reliability of the packaging, and achieving a stable and uniform filling process remains a critical challenge in 3D packaging technologies.
In this study, copper electroplating was performed using a step current method, where a low current density was initially applied and then switched to a higher current density after certain period to fill the TSVs. A copper sulfate-based electrolyte was used, and an additive system based on Thioflavin T was applied. Experimental results confirmed that Thioflavin T contributed to the improvement of TSV filling performance. To verify this, cross-sectional samples were prepared, and the filling profiles were observed using scanning electron microscopy (SEM). Additionally, electrochemical measurements using linear sweep voltammetry (LSV) were performed to analyze the copper ion reduction behavior influenced by the additive.
Unlike conventional TSV filling processes that often require complex additive systems and advanced pulse plating conditions, this study presents a distinctive approach by achieving significant improvement in TSV filling characteristics through a relatively simple additive combination and a step current method. This study demonstrates a promising strategy for simplifying the TSV filling process, with strong potential for practical implementation in advanced semiconductor packaging technologies.

Keywords: Copper; Electroplating; Thioflavin T; Through-silicon via (TSV)

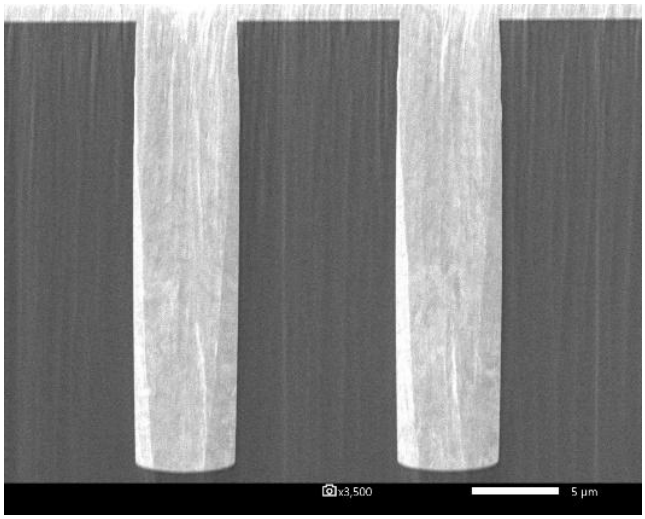

Eye doses measurement with BeO in nuclear medicine

Natch Rattanarungruangchai[1], Busayakorn Na ranong[1], Tossawat Autila[1],
Hasana Laewoharn[1], Waraporn Sudchai[1,*]
[1]Thailand Institute of Nuclear Technology (Public Organization), Nakhon Nayok, Thailand
Email: newsudchai18@gmail.com
*Corresponding author

Abstract

To reduce the risk of cataracts, lens of the eye dose measurements using personal dosimeters have been implemented in accordance with standards established by the International Atomic Energy Agency (IAEA), ensuring both radiation worker safety and regulatory compliance. Crystal-based devices were once used as personal dosimeters that employed crystalline materials to measure ionizing radiation. When exposed to radiation, the crystal traps electrons. Upon stimulation with light, the crystal releases these electrons, which emit light proportional to the amount of radiation absorbed. The Beryllium oxide (BeO) material, a commercial crystal has been introduced in recent years. The development of new materials may also contribute to advances in personal dosimetry. BeOSL Eye Lens Dosimeter is designed to be a compact and is capable of detecting both photon and beta radiation. It offers the advantage of being nearly tissue-equivalent. In this study, BeOSL was calibrated in term of lens of eye doses, $H_p(3)$, the personal dose equivalent at a depth of 3 mm using a head-shaped phantom. BeOSL dosimeters were calibrated at the Secondary Standard Dosimetry Laboratory (SSDL), TINT, using beam qualities from both a gamma-ray source (^{137}Cs) and a beta radioactive source ($^{90}Sr/^{90}Y$). True dose measurements were performed with delivered air kerma values ranging from 0.5 to 2 mGy at angles of incidence of 0 and 60 degrees. This value was traceable to the Physikalisch-Technische Bundesanstalt (PTB) in Germany. The dosimeters were inserted into the cylindrical phantom holes representing an eye. The irradiated BeOSL dosimeters were read out using a BeOSL reader. Radiological performance parameters such as linearity, energy dependence, and angular response were evaluated to ensure the suitability of BeOSL for nuclear medicine applications. The correction factors for Hp(3) for radionuclides such as I-131, Tc-99m, and Ga-68 beta particles were determined. The BeOSL dosimeter demonstrated performance capable of achieving an accuracy of approximately 10% at the 95% confidence level under good laboratory conditions.

Keywords: Beryllium oxide; The lens of the eye dose; Nuclear Medicine

Study on Hardness and Microstructure of The Electroplated Silver-Antimony Alloy Layer

Son Injoon*
[1] School of Materials Science and Engineering, Kyungpook National University, Daegu, 41566, South Korea
Email: ijson@knu.ac.kr
*Corresponding author

Abstract

Pure silver is an excellent conductor of electricity but has low hardness. Numerous scientific studies have used various methods to enhance the hardness of silver. In this study, the electrochemical deposition of silver-antimony (Ag-Sb) alloys is applied to investigate the effect of Sb alloying on the hardness, mechanical properties, and microstructure with different concentration (ranging from 0 to 20,000 ppm) and different temperatures (75°C, 125°C, and 175°C). Through systematic experimentation, we clarify the optimal conditions that promote the formation of a fine-grained, homogeneous structure, significantly contributing to increased hardness. X-ray diffraction (XRD), scanning electron microscopy (SEM), electron backscatter diffraction (EBSD), and Vickers hardness (HV) analyses reveal the phase composition and morphological characteristics of the alloy, while microhardness testing quantitatively assesses the mechanical improvements achieved. Results indicate that higher Sb content correlates with increased hardness, even after 3 weeks of heating. The results demonstrate that an increase in Sb content leads to a rise in hardness, from approximately 132 to 160 HV. Additionally, heating further enhances the hardness. This study highlights the potential of Ag-Sb alloy coatings as an effective solution for applications demanding superior wear resistance and long-term durability.

Keywords: Hardness; Electroplating; Ag-Sb alloy; Ag Electrodeposition

Study on the improvement of heat generation performance of aluminum powder by forming Self-Assembled Monolayers(SAMs) using thiol-based substances.

Seoyoung An[1], Injoon Son[1,*]
[1]Kyungpook National University Department of Materials Science and Metallurgical Engineering, Kyungpook National University, Daegu, Republic of Korea
Email: ijson@knu.ac.kr
*Corresponding author

Abstract

Aluminum powder provides excellent mass-volume calorific value upon oxidation, but the exothermic reaction is hindered by the dense Al2O3 oxide film that forms immediately upon exposure to air. In this study, we proposed process conditions for suppressing reoxidation and enhancing exothermic performance by etching the Al2O3 oxide film in a 3 wt% HF solution and then immersing the thiol-based materials 1-Octadecanethiol (ODT) and 1-Dodecanethiol (DDT) in 2 g/L aqueous solutions. This process involves forming self-assembled monolayers (SAMs). This process involves immersing the 7 μm Al powder in an ODT or DDT aqueous solution, removing the oxide film, and then drying the powder. The exothermic enthalpy and oxidation onset temperature were analyzed by TGA-DSC at 10°C/min in an air atmosphere. Field-effect scanning electron microscopy (FE-SEM/EDS), XPS, and FT-IR analyses were used to confirm the presence of -SH groups. As a result, the exothermic enthalpy value of the Al powder forming SAMs was improved by 160% compared to the powder without -SH groups adsorbed, and the exothermic onset temperature was also lowered. This suggests that the SAMs layer including the Al-S bond suppresses re-oxidation, and the thermal decomposition and gas evolution of the SAMs during heating induce microcracks, which increase the O2/Al diffusion path, thereby improving the exothermic performance. In addition, the effect of the difference in CHn length (ODT vs DDT) of the SAMs layer on the improvement of exothermic performance was compared and discussed.

Keywords: Aluminium powder; Enthalpy; Thiol; SAMs

Development of Biodegradable Medical-Grade PLA Monofilaments for 3D Printing in Compliance with ISO 13485

Manasanan Namhongsa[1,2], Tanyaluck Mekpothi[3], Tawan Chiwan[3], Donraporn Daranarong[4], Kulrachart dung-u-kos[5], Apirat chaitan[5], Gareth M. Ross[6], Sukunya Ross[6], and Winita Punyodom[1,2,4]*

[1] Bioplastics Production Laboratory for Medical Applications, Faculty of Science, Chiang Mai University, Chiang Mai, 50200, Thailand

[2] Center of Excellence in Materials Science and Technology, Chiang Mai University, Chiang Mai 50200, Thailand2,

[3] Office of Research Administration, Chiang Mai University, Chiang Mai 50200, Thailand

[4] Multidisciplinary Research Institute, Chiang Mai University, Chiang Mai 50200, Thailand

[5] IRPC Public Company Limited, Mueang District, Rayong 10900, Thailand

[6] Center of Excellence in Biomaterials, Department of Chemistry, Faculty of Science, Naresuan University, Phitsanulok 65000, Thailand

E-mail: winita.punyodom@cmu.ac.th

*Corresponding author

Abstract

This research supports Thailand's goal of becoming a regional medical hub by developing biodegradable, medical-grade polylactic acid (PLA) monofilaments for fused deposition modeling (FDM). Resorbable biomaterials represent a high-value sector of the bioplastics industry; however, Thailand currently depends on imported medical-grade polymers for device manufacturing, especially for biomedical monofilament applications. With funding from PMU-C (2023–2024) and in collaboration with IRPC Public Company Limited, a prototype PLA monofilament was produced at the Bioplastics Research Laboratory for Medical Applications, Chiang Mai University, in accordance with ASTM F1925-17 standards. To enable industrial application by 2025, the project will focus on process validation to ensure reproducibility, accuracy, and product quality, with documentation prepared to generate a Validation Report per ASTM F1925-17 and toward ISO 13485 compliance. This effort is expected to decrease dependence on imports, strengthen domestic manufacturing capacity, and expand healthcare options in Thailand.

Keywords: Medical-grade PLA monofilament; Fused deposition modeling (FDM); Process validation.

Superconcentration Electrochemistry Reveals Halide Redox Control over Water Splitting Kinetics

Sagar Ingavale, Pawin Iamprasertkun*
School of Bio-Chemical Engineering and Technology, Sirindhorn International Institute of Technology, and Research Unit in Sustainable Electrochemical Intelligent, Thammasat University, Pathum Thani, Thailand
Email: pawin@siit.tu.ac.th
*Corresponding author

Abstract

Electrochemistry involving super-concentrated electrolytes has rapidly gained attention as a transformative approach in electrochemical processes. The electrochemical hydrogen evolution reaction (HER) and oxygen evolution reaction (OER) are fundamental processes in energy conversion and storage technologies. This study investigates the electrochemical activity of platinum electrodes in lithium-based electrolytes for advancing energy storage and conversion technologies. The HER and OER kinetics in a super-concentrated electrolytes performed to address challenges related to stability and efficiency in high-concentration ionic environments. Highly concentrated electrolytes characterized by their unique solvation structure and extended electrochemical stability potential window, offer promising avenues for enhancing energy storage and conversion applications. Through cyclic voltammetry and linear sweep voltammetry, we analyze key parameters such as redox reactions, overpotentials, and kinetic reactions. This study explores the interaction between platinum and highly concentrated aqueous electrolytes to elucidate its influence on catalytic performance. The results provide insights into optimizing platinum-based electrocatalysis for next-generation sustainable energy solutions, highlighting the role of electrolyte composition in dictating reaction kinetics, potential window and overall electrochemical performance.

Keywords: Super-concentrated electrolytes; Oxygen evolution reaction; Hydrogen evolution reaction; Platinum electrode; Potential window keyword.

Electrochemical Creatinine Sensor Based on Bimetallic Cu@Co-on-Graphene

Pantipa Sawatmuenwai[1,2], Keerakit Kaewket,[1,2] Théo Claude Roland Outrequin,[3] Somrudee Deepaisarn,[3] Jinnapat Wijitsak,[1,2] Pachanuporn Sunon,[1,2] Kamonwad Ngamchuea[1*]
[1]School of Chemistry, Institute of Science, Suranaree University of Technology, 111 University Avenue, Suranaree, Muang, Nakhon Ratchasima, 30000, Thailand
[2]Institute of Research and Development, Suranaree University of Technology, 111 University Avenue, Suranaree, Muang, Nakhon Ratchasima, 30000, Thailand
[3]Sirindhorn International Institute of Technology, Thammasat University, Pathum Thani, Thailand
[*]Corresponding author: Kamonwad Ngamchuea, School of Chemistry, Institute of Science, Suranaree University of Technology, 111 University Avenue, Suranaree, Muang, Nakhon Ratchasima, 30000, Thailand.
Email: kamonwad@g.sut.ac.th ; Tel: +66 (0) 44 224 637

Abstract

Creatinine, a crucial biomarker for renal function, presents a significant challenge for direct electrochemical detection due to its non-electroactive nature. To meet the urgent demand for low-cost, portable point-of-care testing (POCT), this study introduces a novel electrochemical sensor built upon self-fabricated screen-printed electrodes (SPEs). The sensor's active surface is engineered using a tri-component nanocomposite of copper, cobalt, and graphene. This advanced modification strategy utilizes the superior conductivity of graphene and the synergistic properties of the dual-metal (copper and cobalt) system, which forms stable complexes with creatinine. This combination significantly enhances the electron transfer kinetics and the overall electrochemical signal. The developed platform demonstrates enhanced sensitivity and notable selectivity against key biological interferences found in urine.

Keywords: Creatinine; Electrochemical Sensor; Screen-Printed Electrode; Copper; Cobalt

Non-invasive electrochemical sensors for guanosine and guanine analyses

Jinnapat Wijitsak[1], Bunrat Tharat[2], Suwit Suthirakun[3], Kamonwad Ngamchuea[3,*]
[1]Institute of Research and Development, Suranaree University of Technology, 111 University Avenue, Suranaree, Muang, Nakhon Ratchasima 30000, Thailand
[2] High-Performance Computing Unit (CECC-HCU), Center of Excellence on Catalysis and Catalytic Reaction Engineering (CECC), Chulalongkorn University, Bangkok 10330, Thailand
[3]School of Chemistry, Institute of Science, Suranaree University of Technology, 111 University Avenue, Suranaree, Muang, Nakhon Ratchasima 30000, Thailand
Email: kamonwad@g.sut.ac.th
*Corresponding author: Kamonwad Ngamchuea, School of Chemistry, Institute of Science, Suranaree University of Technology, 111 University Avenue, Suranaree, Muang, Nakhon Ratchasima, 30000, Thailand.

Abstract

Guanosine, a purine-derived nucleoside, is a potential biomarker of oxidative stress and central nervous system diseases. In the present study, its oxidative behavior is examined using voltammetric techniques on both stationary and hydrodynamic electrodes at the macro- and micro-scales, supported by density functional theory (DFT) calculations. This integrative approach provides comprehensive insight into the complex reaction pathways of guanosine that are relevant in biological contexts. In addition to elucidating the underlying mechanism, the study reports the development of an electrochemical sensor for guanosine detection based on a carbon fiber microelectrode. The sensor demonstrates effective performance in media with low ionic strength and operates without the addition of a supporting electrolyte. It exhibits two linear ranges: 0.0067–0.12 mM and 0.12–1.00 mM, with sensitivities of 1.40 ± 0.03 nA mM^{-1} and 0.05 ± 0.003 nA mM^{-1}, respectively, and a detection limit ($3s_B/m$) of 0.002 mM. Validation in synthetic urine samples yielded a recovery of $99.71 \pm 4.02\%$ (RSD = 4.95%), confirming the sensor's suitability for direct quantification of guanosine in complex matrices.

Keywords: Guanosine; Biomarker; microelectrode; Voltammetry

Optimization of Plasma-Activated Hydrogel by Factorial Design for Enhanced Antimicrobial Efficacy on Animal Skin

Kochakon Moonsub[1,2], Phisit Seesuriyachan [3], Wassanai Wattanutchariya[1,2,*]
[1]Advanced Technology and Innovation Management for Creative Economy Research Group (AIMCE) Chiang Mai University, Chiang Mai:50200, Thailand.
[2]Department of Industrial Engineering, Faculty of Engineering Chiang Mai University, Chiang Mai:50200, Thailand.
[3]Division of Biotechnology, Faculty of Agro-Industry, Chiang Mai University Chiang Mai:50100, Thailand.
Email: wassanai@eng.cmu.ac.th
*Corresponding author

Abstract

Plasma-Activated Hydrogel (PAH) was successfully developed and optimized in this investigation to overcome the short half-life of critical reactive species, like hydrogen peroxide (H_2O_2), by enhancing and stabilizing its generation, thereby offering a practical and sustained antimicrobial solution for animal wound care, a limitation previously seen with Plasma-Activated Water (PAW). Moreover, related technologies such as micro/nanobubbles (MNB), Ultraviolet (UV) light, and Ultrasonication (US) are also incorporated to enhance the PAH system. The study employed a 2^k factorial design to systematically analyze how PAH treatment time (ranging from 0 to 20 minutes) and gel ratio (from 1:5 to 3:5) influenced key physicochemical properties: Oxidation-Reduction Potential (ORP), Electrical Conductivity (EC), and pH. Analysis revealed significant interaction effects for ORP, with both factors substantially elevating EC and extended exposure significantly lowering pH. Multiple response optimization, aiming to maximize ORP and EC while minimizing pH, pinpointed the most desirable profile at a gel ratio of 3:5 and a PAH treatment time of 10 minutes, yielding optimal values of ORP (278.90 mV), EC (263.75 µS/cm), and pH (5.325). Crucially, the optimized PAH formulation demonstrated 1.5 times higher H_2O_2 concentration (29.38 ppm) compared to PAH alone, and this concentration remained stable for 24 hours, attributed to the gel's enhanced surface area for reaction, retention of precursor species, and superior stabilization of H_2O_2. These findings validate the significant potential of the optimized PAH as an efficacious, long-acting antimicrobial agent for veterinary wound healing.

Keywords: Plasma Technology; Plasma-Activated Water; Plasma-Activated Hydrogel; Microbubbles/Nanobubbles; Ultraviolet; Ultrasonication; Disinfection

Development of a Rapid and Sensitive Electrochemical Immunosensing of TNF-α for Personalized Medicine Applications

Napolean Bonaparte Thanapaul [1], Polina Istomina [2], Thae Thae Min [2], Piyanut Pinyou [1*], Montarop Yamabhai [2*]

[1]School of Chemistry, Institute of Science, Suranaree University of Technology, Nakhon Ratchasima 30000, Thailand

[2]Molecular Biotechnology Laboratory, School of Biotechnology, Institute of Agricultural Technology, Suranaree University of Technology, Nakhon Ratchasima 30000, Thailand

E-mail: montarop@g.sut.ac.th, piyanutp@sut.ac.th

Abstract

Tumor necrosis factor alpha (TNF-α) is a key inflammatory cytokine and an important biomarker for various immune-related diseases. Rapid and accurate detection of TNF-α is crucial for early diagnosis and effective disease management. Point-of-care testing (POCT) enables on-site, real-time monitoring with minimal sample volume and handling. Recent advances in electrochemical immunosensors enable the detection of TNF-α at picogram levels with high sensitivity and specificity. These portable and rapid POCT platforms hold great potential for personalized medicine and timely clinical decision-making. In this study, we report the development of a highly sensitive electrochemical immunosensor capable of quantifying TNF-α at the picogram level in relevant human biofluids. The sensor platform comprises a bare gold electrode functionalized with linker molecules and immobilized recombinant antibody (adalimumab), integrated with a compact, palm-sized reader. Optimized concentrations of cross-linkers and antibody enable highly specific and reproducible real-time detection of the target antigen. Experimental evaluation demonstrated a sensitive and broad detection range of 1–20 pg/mL for recombinant TNF-α spiked in artificial biofluids, highlighting the sensor's precision and robustness. Compared to conventional enzyme-linked immunosorbent assays (ELISAs), which typically require 300 minutes, the proposed electrochemical immunosensor provides significantly faster analysis (90 minutes) while maintaining high sensitivity and specificity. The small sample volume, portability, and rapid response make this platform particularly suitable for on-site monitoring of TNF-α, supporting early detection of inflammation and enabling timely patient-specific therapeutic interventions. Overall, this electrochemical immunosensor represents a promising tool for point-of-care cytokine monitoring and demonstrates substantial potential in advancing personalized medicine by facilitating precise, real-time assessment of immune status.

Keywords: Electrochemical Immunosensor; Point-of-care testing; POCT; Tumor necrosis factor TNF-α; Immunodiagnostics

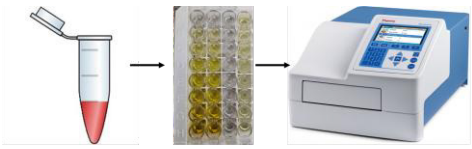

Total time for TNF-α detection using human body fluids with ELISA kit 300 min

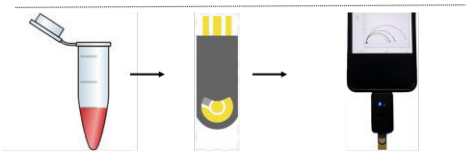

Total time for TNF-α detection using human body fluids with electrochemical immunosensor 90min

Competitive Electrochemical Immunosensor toward Signal Amplification via Electrocatalytic Reaction for Insulin Detection

Siriporn Anuthum[1], Jaroon Jakmunee[1,2], Kontad Ounnunkad[1,2,*]
[1] Department of Chemistry, Faculty of Science, Chiang Mai University, Chiang Mai 50200, Thailand
[2] Center of Excellence for Innovation in Chemistry, Faculty of Science, Chiang Mai University, Chiang Mai, 50200, Thailand
Email: *kontad.ounnunkad@cmu.ac.th, suriyacmu@yahoo.com

Abstract

Diabetes, characterized by elevated blood glucose levels, is one of the most prevalent chronic metabolic disorders affecting millions of people worldwide. Uncontrolled diabetes can lead to severe complications, including cardiovascular disease, neuropathy, and kidney failure. Therefore, early and accurate diagnosis is critical for effective diabetes management and prevention of its related complications. Insulin, a vital hormone responsible for regulating blood glucose, plays a central role in maintaining glucose homeostasis. Consequently, reliable and rapid quantification of insulin is essential for clinical diagnostics and diabetes monitoring. In this study, we present a competitive immunosensor strategy for insulin detection. The sensor was fabricated using a combination of two-dimensional (2D) materials, including graphene oxide (GO) and bimetallic molybdenum tungsten disulfide (2D $MoWS_2$), deposited onto the working area of screen-printed carbon electrodes (SPCEs) to enhance the active surface area. The insulin antigen was immobilized on the modified SPCE, forming the active bioelectrode. For signal amplification, a nickel metal-organic framework (Ni-MOF) conjugated with an anti-insulin antibody (anti-insulin/Ni-MOF) was employed as a nanotag. Ni-MOF exhibits excellent catalytic activity toward hydrogen peroxide (H_2O_2) electro-oxidation, enabling substantial amplification of the electrochemical signal. During the competitive assay, the chronoamperometric current decreased proportionally with increasing insulin concentration, reflecting the reduced catalytic activity and then allowing sensitive detection at the electrode surface. The sensor demonstrates a linear response over the dynamic range of 10–50,000 pg mL^{-1}, achieving a detection limit of 6.2 pg mL^{-1}. Furthermore, the fabricated competitive immunosensor offers high selectivity, robust stability, and good reproducibility. These features suggest its potential for practical applications in insulin monitoring and diabetes management.

Keywords: Competitive Immunosensor; Diabetes; 2D $MoWS_2$; Metal-organic framework; Insulin

Electrochemical Competitive Aptasensor for Alpha-Fetoprotein via Electrocatalytic Signal Amplification

Supakeit Chanarsa[1], Methawut Sirisom[1,2], Jaroon Jakmunee[1,2], Kontad Ounnunkad[1,2,*]
[1] Department of Chemistry, Faculty of Science, Chiang Mai University, Chiang Mai 50200, Thailand
[2] Center of Excellence for Innovation in Chemistry, Faculty of Science, Chiang Mai University, Chiang Mai 50200, Thailand
Email: kontad.ounnunkad@cmu.ac.th, suriyacmu@yahoo.com
*Corresponding author

Abstract

This work presents an electrochemical competitive aptasensor designed for detecting alpha-fetoprotein (AFP), a effective biomarker for liver cancer. The sensor uses a graphene oxide and graphitic carbon nitride (GO/C_3N_4) composite to modify the electrode surface. This combination improves electrical conductivity and provides more active sites for AFP binding. The modified electrode enhances electron transfer and increases sensitivity for AFP detection. For signal generation, an aptamer-loaed GO/NiO nanocomposite is prepared as a tag. The aptamer specifically binds to AFP, while the GO/NiO acts as an electrocatalyst that promoteshydrogen peroxide (H_2O_2) oxidation to generate measurable electrochemical signals. The sensing process follows a competitive principle thatfree AFP in the solution competes with electrode-confined AFP for limited aptamer binding sites on the tags, causing a decrease in current as the AFP concentration increases. The proposed aptasensor achieved a wide detection range from 0.10 to 50 ng mL^{-1}. The limits of detection were 3.6 pg mL^{-1} in phosphate buffer and 6.4 pg mL^{-1} in diluted human serum. The developed sensor shows excellent sensitivity, good stability, and strong potential for clinical diagnosis.

Keywords: Alpha-fetoprotein; Electrochemical competitive aptasensor; GO/C_3N_4 composite; GO/NiO tag

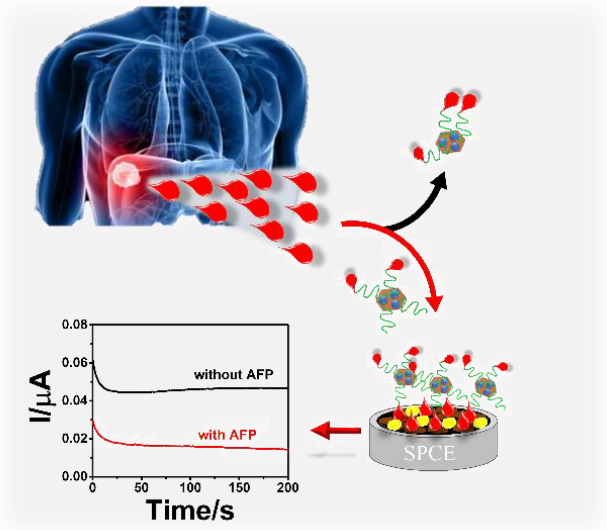

Graphical abstract of a competitive electrochemical aptasensor for AFP: aptamer–nanoprobe binding at a nanomodified SPCE catalyzes H_2O_2, yielding an amplified current inversely proportional to AFP.

Proceedings of The 19th International Conference on the Physical Properties and Application of Advanced Materials (ICPMAT2025)

1-4 December 2025, Chiang Mai Marriott Hotel, Chiang Mai, Thailand

Organized by

Department of Industrial Chemistry
Materials Science Research Center
Faculty of Science, Chiang Mai University

Early-stage cluster evolution and hardness measurement during natural aging in Al-Mg-Si alloys

Tran Sy Quan[a], Abrar Ahmed[b], Vu Ngoc Hai[a], Seungwon Lee[c], Taiki Tsuchiya[c], Susumu Ikeno[c], Kenji Matsuda[c]*

[a] *Graduate School of Science and Engineering for Education, University of Toyama, Toyama 930-8555, Japan*
[b] *Advanced Aluminium International Research Centre, University of Toyama, Takaoka, Toyama 933-8588, Japan*
[c] *Graduate School of Science and Engineering for Research, University of Toyama, Toyama 930-8555, Japan*

Corresponding Author E-mail: matsuda@sus.u-toyama.ac.jp

Abstract

The aim of this study is to investigate the effect natural aging on hardness evolution and clustering behaviour in Al-Mg-Si alloys with different Mg/Si ratio by using hardness measurement and scanning transmission electron microscopy (STEM). The results show that the hardness increases with exposure natural aging (NA) which is confirmed that the cluster is the main strengthening precipitates in early stage. The excess Si alloy is highest hardness compared to the excess Mg and Balance alloys, suggesting that the faster precipitates kinetic due to a higher cluster density. STEM images show clusters at 6ks that transformed into square structure after 600ks, indicating progressive atomic ordering even at room temperature. The correlation between hardness and number density of clusters demonstrates that the Mg/Si ratio strongly controls clustering kinetics. Thus, it is possible to optimize the alloy composition and heat treatment process in 6xxx series Al alloys.

Keywords: *Natural Aging, HAADF-TEM, cluster, Aluminium*

Introduction

The 6xxx series aluminium alloys, based on the Al-Mg-Si system are widely used in transportation and construction due to their excellent combination of strength, corrosion resistance, and good formability [1-3]. Their primary strengthening mechanism is precipitation hardening, where the formation of metastable precipitates such as β″, which significantly enhances mechanical properties [4-5]. The precipitation behaviour strongly depends on the ratio of Mg/Si

because the total amount of the supersaturated solid solution elements in the matrix by solution heat treatment (SHT) affected to the formation of cluster during aging [6]. A balanced Mg/Si ratio favors β″ phase formation, while excess Si accelerates clustering and hardness increase, and excess Mg slows hardening due to vacancy-solute interactions [7-8].

In addition, after SHT aluminium alloys are often subjected to a delay for assembly or transportation before being subjected to artificial aging [9]. During this waiting period, Natural Aging (NA) inevitably occurs and a high density of solute clusters forms, this phenomenon significantly changes the hardness response during the final aging process [10]. The Mg/Si ratio is the primary factor influencing NA. Previous studies have established that with a high solute content of Mg/Si > 1%, the negative of NA exerts a negative effect to strengthening at peak aging condition [11]. These are also reported that NA has a positive on the behaviour strengthening of AA with the content of Mg/Si < 1% [12]. Therefore, understanding the clustering behaviour during NA is essential for optimizing alloy composition and heat treatment process.

In this study, three Al-Mg-Si alloys with different Mg/Si ratios were investigated: a balanced, excess-Mg, and an excess-Si composition. Hardness measurements during natural aging revealed differences in hardening behaviour in three alloys. To understand the microstructure of three alloys, the scanning transmission electron microscopy (STEM) observations were conducted after 6ks (100 min) and 600ks (10000 min) of NA. This study provides more information into the influence of the difference Mg/Si ratio in early stage of precipitates kinetic and its impact on hardness evolution in 6000 series Al alloys.

Materials and Methods

Table 1: Chemical composition of the Al-Mg-Si alloy (mass%):

	Mg	Si	Al	Mg_2Si	Mg + Si
Bal.	0.98	0.59	Bal.	1.55	1.57
Ex. Mg	1.58	0.56	Bal.	1.54	2.1
Ex. Si	1.05	0.95	Bal.	1.66	2

In this experiment, high-purity ingots of aluminum (99.99%), magnesium (99.9%), and silicon (99.9%) were used as the starting materials. The melting was carried out in an electric resistance furnace at 720 °C. After the target temperature was reached, Mg and Si were added, and the melt was stirred thoroughly. Subsequent degassing and refining were performed, after which the alloy was cast into a steel mold at a pouring temperature of 700 °C. The casting process was carried out under normal atmospheric conditions, allowing the molten alloy to flow naturally into the mold cavity. The alloy designed as 1.6% Mg_2Si was used as the balance alloy. This composition corresponds to the Mg_2Si ratio, which is commonly treated as a quasi-binary system within the Al-Mg-Si phase diagram because Mg and Si combine preferentially to form Mg_2Si. In Al alloys, the solute additions of Mg and Si are often expressed in terms of their Mg_2Si equivalent, since this provides a meaningful basis for comparing the amount of Mg-Si strengthening phase available in the matrix. The actual mass fractions of the alloying elements were measured using an optical emission spectrometer, and the compositions of all alloys are listed in Table 1. Two additional alloys were prepared by adding Mg or Si to the balance composition. This was done to examine how an excess amount of Mg or Si, relative to the quasi-binary Mg_2Si baseline, influences the clustering behavior and subsequent microstructural evolution. As-cast ingots firstly homogenized at 575 ℃ for 36ks and rapidly quenched in ice-water. Following by hot rolled at 400℃ to make 10mm thick plate and cold rolled to make 1.5mm thickness sheet. The sheet was cut into 10mm long pieces which was solution treated at 575 ℃ for 3.6ks, immediately quenched in ice-water. Hardness measurement was conducted by using Mitutoyo HM-101 with a loading of 0.98N and holding time of 15s. The average of 10 points are generally used for hardness for each aging condition. The STEM samples were thinned using mechanical polishing down to thickness 0.08mm and punched out a disc sheet with a diameter of about 3mm, then were electronic polished by using twin-jet polishing machine with the solution containing a mixture of 1/3 nitric acid and 2/3 methanol. Microstructure observations were carried out by a Talos F200X G2 at 200KV.

Results and discussion

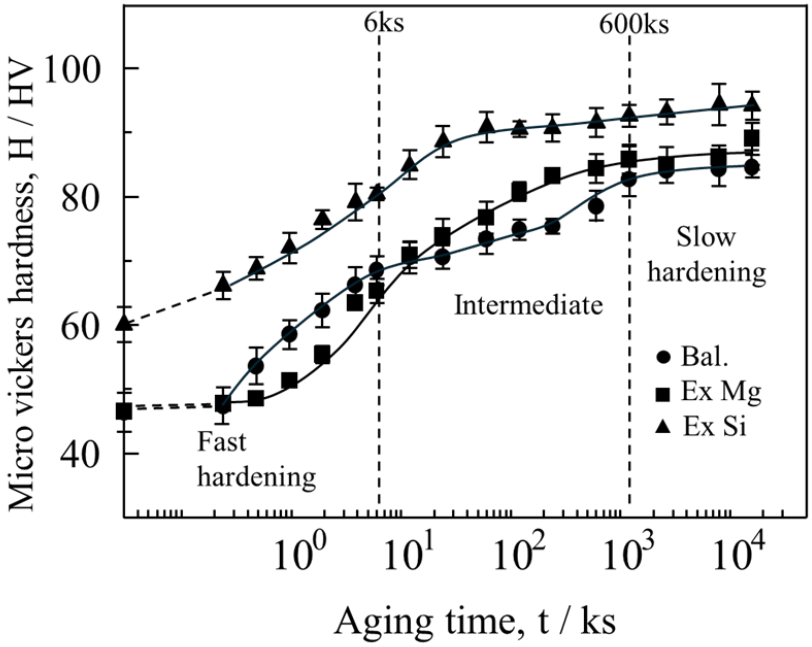

Fig. 1 Hardness evolution of alloys Bal., ex. Mg and ex. Si during NA at 20℃ after solution heat treatment and quenching.

The evolution of hardness for the three alloys during natural aging (NA) after solution heat treatment (SHT) is shown in Fig. 1. As observed, three distinct stages can be identified based on the hardening rate (R_H) [13] By using the Eq. (1):

$$R_H = \frac{HV_2 - HV_1}{t_2 - t_1} \qquad (1)$$

where HV_1 and HV_2 are the measured Vickers hardness values at aging times t_1 and t_2, respectively. In the early stage (0.24-6 ks), the calculated hardening rate reaches approximately 3-4 HV/ks for all alloys but decreases sharply to below 0.05 HV/ks at longer NA times, confirming the transition from rapid cluster formation to hardness stabilization. Accordingly, the NA process can be characterized by a fast-hardening stage at the beginning, followed by an intermediate stage, and finally a slow-hardening stage after longer NA times.

After SHT, ex. Mg and Bal. alloys show similar hardness values of approximately 46 HV, which increase to about 76 HV and 73 HV, respectively, after one week of NA. The hardness of ex. Si is from approximately ~60 HV (measured after SHT) to ~91 HV after one week and then became stable. Note that, the hardness of ex. Si alloy is higher than Bal. and ex. Mg alloys,

suggesting that the faster precipitates kinetic due to a higher cluster density. This tendency agrees well with previous reports that excess Si accelerates early cluster formation and hardening, while excess Mg slows it down due to lower diffusivity and delayed clustering [14-15].

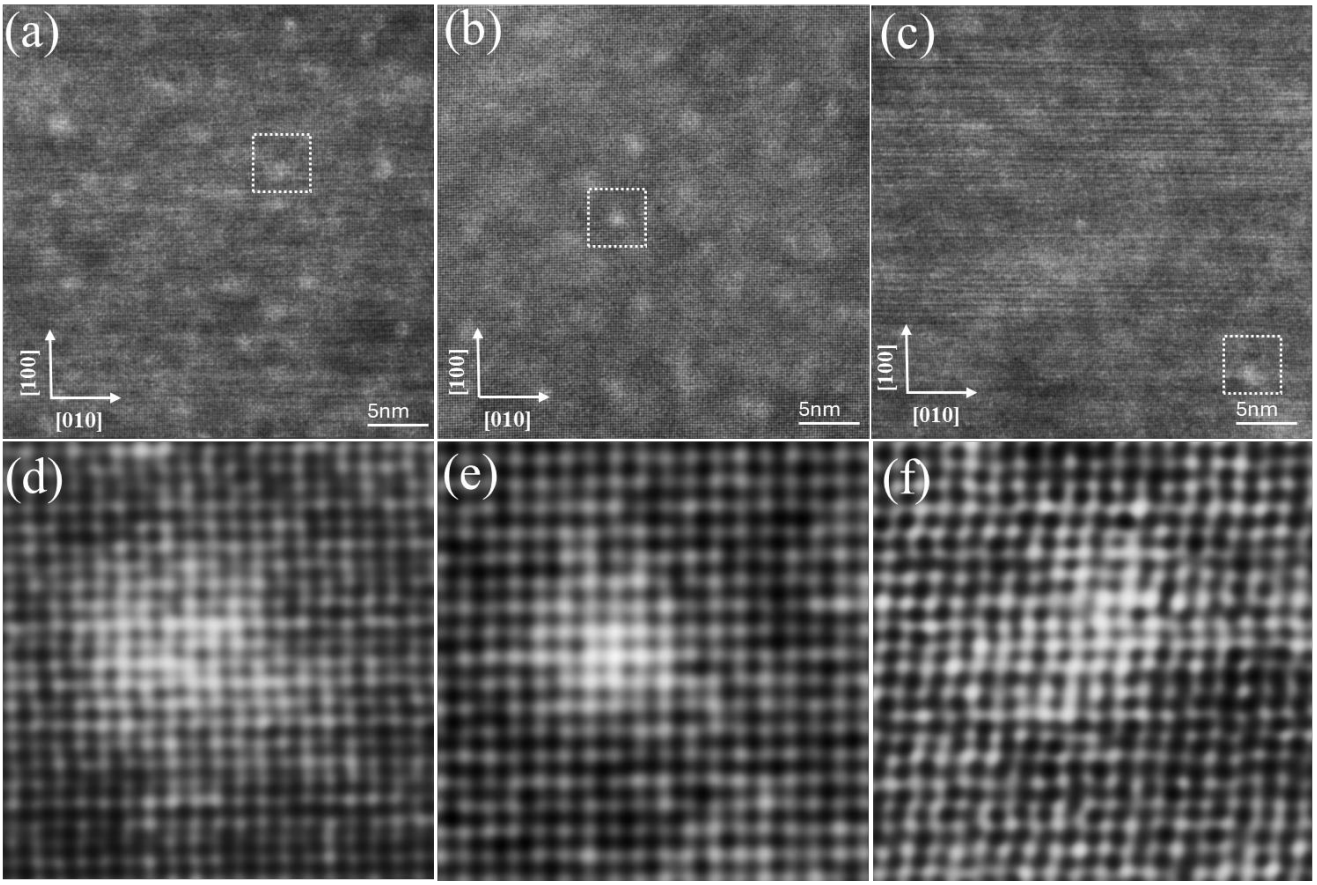

Fig. 2. STEM-HAADF images of cluster in the three alloys (a) ex. Si (b) Bal. and (c) ex. Mg after of 6ks of Natural Aging at 20°C. (d-f) corresponding magnified images and atomic-scale characterization convert by inverse FFT with the white squares area indicates selected regions

Fig. 2(a–c) show the HAADF-STEM images of the three alloys after 6 ks of natural aging. The contrast observed in these images is not determined by the elemental differences between Si, Al, Mg (atomic number: Si > Al > Mg). Instead, the bright atomic columns correspond to solute-enriched sites, confirming that Mg-Si ordering has already formed after 6 ks of natural aging at 20 °C as Si and Mg atoms begin to gather, they locally increase the solute and make these columns

appear brighter than the surrounding matrix. The measured cluster area densities are 4.65 × 10^4 pcs/μm², 3.33 × 10^4 pcs/μm², and 3.23 × 10^4 pcs/μm² for the ex. Si, Bal., and ex. Mg alloys, respectively, indicating that the ex-Si alloy contains the highest number density of early clusters.

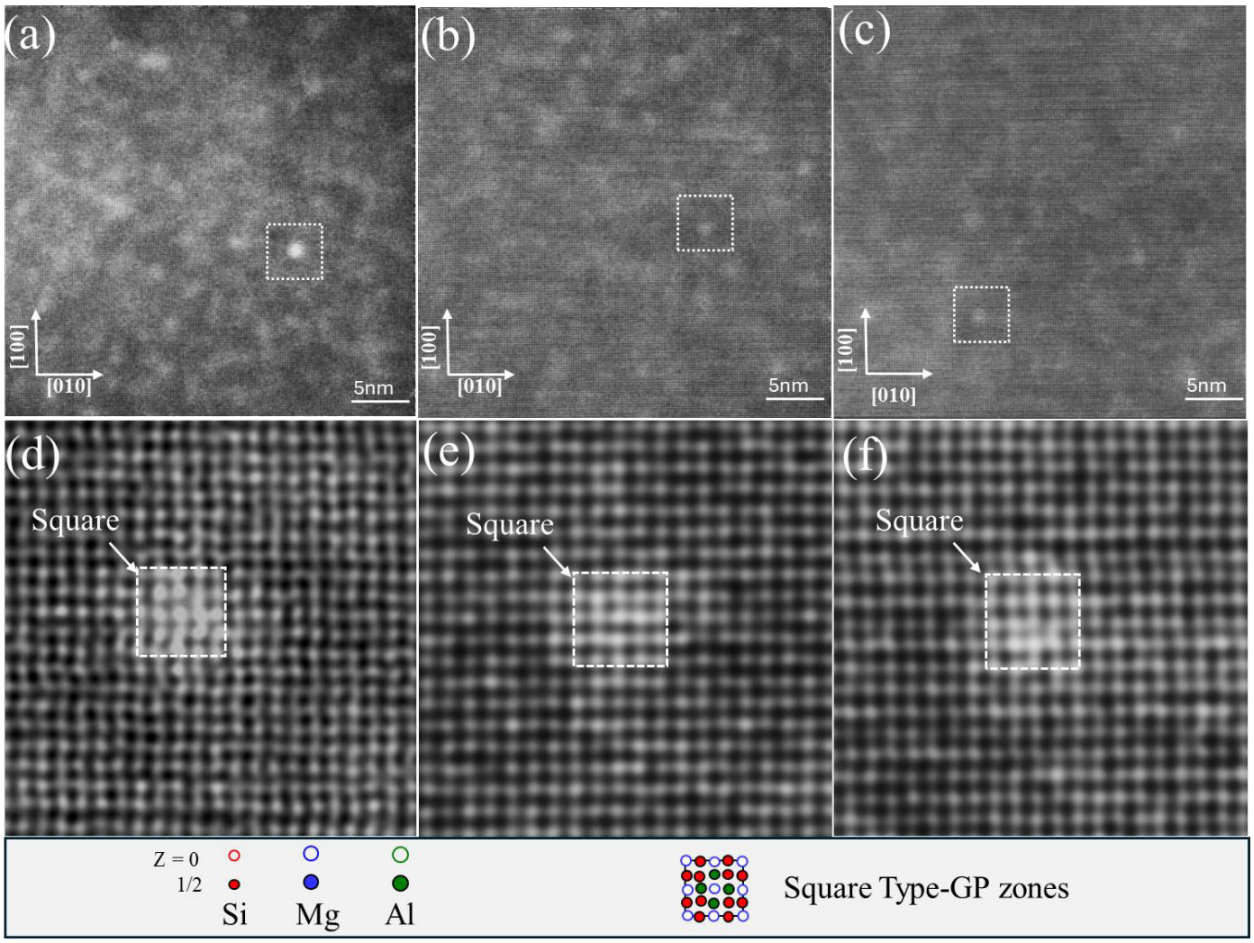

Fig 3. STEM-HAADF images of cluster in the three alloys (a) ex. Si (b) Bal. and (c) ex. Mg after of 600ks of Natural Aging at 20°C. Corresponding image by inverse FFT with 3 alloys show in figure (d-f) and atomic models draw in white squares as shown in the bottom vertical bar.

Fig. 2(d–f) show inverse FFT–filtered HAADF-STEM images taken from the selected regions in Figs. 2(a–c). These clustered features represent the earliest stage of precipitation at the atomic level and are present in all three alloys, demonstrating that initial Mg–Si clustering occurs regardless of the compositional variations. The morphology and arrangement of these clusters are

consistent with the early structures reported by Marioara et al. and Kawahara et al. [16,17], often described as Disordered Frank–Kasper (DFK)-type clusters.

Fig.3(a-c) shows HAADF-STEM and corresponding inverse FFT images of three alloys in Fig.3(d-f) after 600ks of NA, viewed along the $\langle 001 \rangle_{Al}$ direction. Compared to 6ks NA, the bright contrasts become more numerous, confirming a increase in the hardness in three alloys. In the ex. Si alloy, several regions exhibit short-range ordered features with a square-type configuration [18] highlighted in the inverse FFT images (see Fig.3d). Similar square features are also visible in the Bal. and ex Mg alloy. The consistent appearance of this structure across the three alloys suggests that, during extended NA, the early disordered clusters gradually evolve toward partially ordered configurations. This evolution is accompanied by an increase in number density of clusters, implying that continued atomic diffusion and vacancy movement contribute to the structural reorganization of solute clusters [6-17].

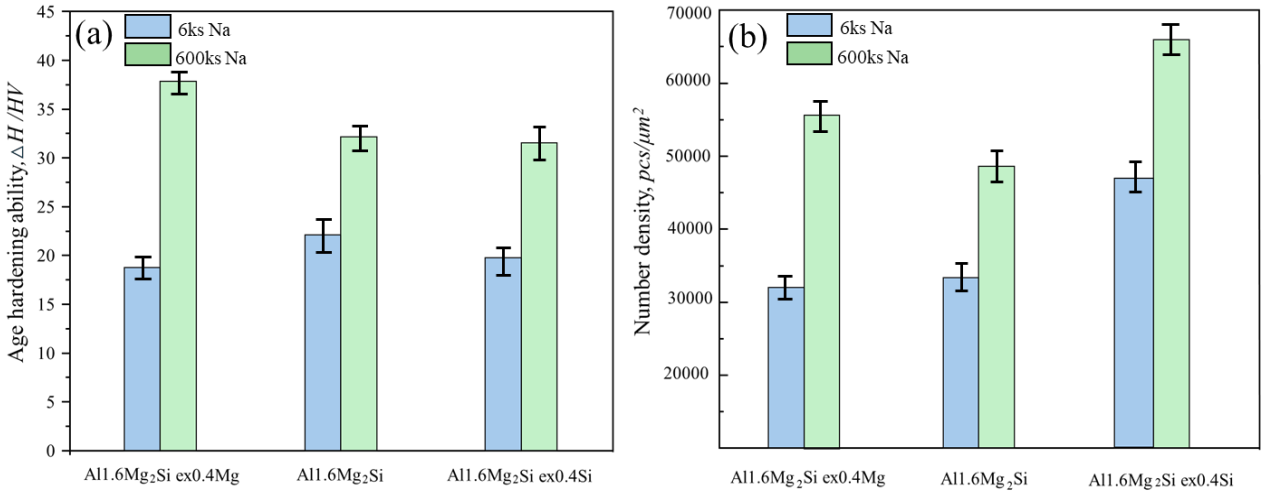

Fig. 4. The relationship between the ΔHV (a) and the number density of cluster (b) in three alloys with different NA.

The variation in of hardness and cluster number density of the three alloys after 6ks and 600ks of NA are summarized in Fig.4. with $\Delta HV = HV_{(60ks,6ks)} - HV_{(as.Q)}$. As the NA extends from 6ks to 600ks, both hardness and number densities significantly increase, confirming that the

accumulation and structural evolution of the clusters, which is the main strengthening precipitates during NA. This similar trend clearly demonstrates that the evolution of hardness is directly influenced by the clustering behaviour during NA from STEM observations further clarify the atomic-scale origin of this behaviour (see Fig.2 and Fig.3).

When NA extends to 600ks, the number density of clusters increases in all alloys (see Fig.4). Among them, the ex. Si alloy exhibits the highest cluster density, whereas the Mg-rich and Balance alloys show comparatively lower values. However, the ex. Mg alloy after 600ks exhibit the fastest and highest hardening response, which can be attributed to a relatively increase in cluster density during this stage. STEM images reveal that several clusters evolve into more ordered structures, showing square structure. This configuration implies that the structural configurations observed after NA not only clarify the clustering mechanism but also provide an important basis for evaluating the potential negative influence of NA on the artificial-aging response of the three alloys [19-20].

Conclusions

In this study, the effects of Mg/Si ratio on hardness evolution and clustering behaviour during natural aging (NA) in Al-Mg-Si alloys were systematically investigated by hardness testing and HAADF-STEM analysis. The following conclusions can be summarized:

a. NA enhances significant hardening in three alloys, both hardness and number densities increase continuously with increasing aging time, confirming that the early strength development originates from clustering.

b. After prolonged NA, the ex. Mg alloy exhibits the fastest and highest hardening response, corresponding to a substantial increase in cluster density. The ex. Si alloy also shows a strong hardening response due to its high cluster density, whereas the Bal. alloy displays the slowest hardness evolution. These results indicate that the Mg/Si ratio strongly governs clustering kinetics and the associated hardening behaviour during NA.

c. STEM observations confirmed that clusters form in all alloys at the early stage(6ks). After extended time(600ks), these clusters evolve into square configurations, demonstrating progressive short-range ordering and structural transformation even at room temperature.

Acknowledgment

We would like to express our sincere gratitude to the MEXT (Ministry of Education, Sports, Science and Technology) scholarship for providing financial support during Mr. Tran Sy Quan's studies at University of Toyama. This work was also supported by Advanced Aluminium International Research Center (ARC), University of Toyama.

Conflict of Interest

The authors declare that they have no known competing financial interests or personal relationships that could have appeared to influence the work reported in this paper.

References

1. Hirsch, J. (2014). Recent development in aluminum for automotive applications. *Transactions of Nonferrous Metals Society of China*, *24*(7), 1995–2002. https://doi.org/10.1016/s1003-6326(14)63305-7.

2. Gupta A, Lloyd D, & Court S. (2001). Precipitation hardening in Al–Mg–Si alloys with and without excess Si. *Materials Science and Engineering A*, *316*(1–2), 11–17. https://doi.org/10.1016/s0921-5093(01)01247-3.

3. Dumitraschkewitz P, Gerstl SSA, Stephenson LT, Uggowitzer PJ, & Pogatscher S. (2018). Clustering in Age-Hardenable aluminum alloys. *Advanced Engineering Materials*, *20*(10). https://doi.org/10.1002/adem.201800255.

4. Matsuda K, Naoi T, Fujii K, Uetani Y, Sato T, Kamio A, & Ikeno S. (1999). Crystal structure of the β″ phase in an Al–l.0mass%Mg2Si–0.4mass%Si alloy. *Materials Science and Engineering A*, *262*(1–2), 232–237. https://doi.org/10.1016/s0921-5093(98)00962-9.

5. Murayama M, & Hono K. (1999). Pre-precipitate clusters and precipitation processes in Al–Mg–Si alloys. *Acta Materialia*, *47*(5), 1537–1548. https://doi.org/10.1016/s1359-6454(99)00033-6.

6. Li C, Marioara CD, Hatzoglou C, Andersen SJ, Holmestad R, & Li Y. (2024). Chemical composition dependent atom clustering during natural aging in Al-Mg-Si alloys. *Scripta Materialia*, *257*, 116474. https://doi.org/10.1016/j.scriptamat.2024.116474.

7. Xiao Q, Liu H, Yi D, Yin D, Chen Y, Zhang Y, & Wang B. (2016). Effect of Cu content on precipitation and age-hardening behavior in Al-Mg-Si-xCu alloys. *Journal of Alloys and Compounds*, *695*, 1005–1013. https://doi.org/10.1016/j.jallcom.2016.10.221.

8. Fallah V, Korinek A, Ofori-Opoku N, Raeisinia B, Gallerneault M, Provatas N, & Esmaeili S. (2014). Atomic-scale pathway of early-stage precipitation in Al–Mg–Si alloys. *Acta Materialia*, *82*, 457-67. https://doi.org/10.1016/j.actamat.2014.09.004.

9. Banhart J, Liu M, Yong Y, Liang Z, Chang C, Elsayed M, & Lay M. (2012). Study of ageing in Al–Mg–Si alloys by positron annihilation spectroscopy. *Physica B Condensed Matter*, *407*(14), 2689–2696. https://doi.org/10.1016/j.physb.2012.03.028.

10. Hell CM, Søreide HS, Bjørge R, Marioara CD, Li Y, Holmestad R. Influence of natural aging and ramping before artificial aging on 6xxx Al alloys. (2022) *J. Mater. Res. Technol.,* 21,4224-4240. https://doi.org/10.1016/j.jmrt.2022.10.139.

11. Tao GH, Liu CH , Chen JH, Lai YX, Ma PP, Liu LM, (2015). The influence of Mg/Si ratio on the negative natural aging effect in Al–Mg–Si–Cu alloys. *Materials Science and Engineering A*, 642, 241-248. https://doi.org/10.1016/j.msea.2015.06.090.

12. Chang CST, Wieler I, Wanderka N , Banhart J. (2009) Positive effect of natural pre-ageing on precipitation hardening in Al–0.44 at% Mg–0.38 at% Si alloy. *Ultramicroscopy,* 109,585-592. https://doi.org/10.1016/j.ultramic.2008.12.002.

13. Tu W, Tang J, Ye L, Cao L, Zeng Y, Zhu Q, Zhang Y, Liu S, Ma L, Lu J, & Yang B. (2020). Effect of the natural aging time on the age-hardening response and precipitation behavior of the Al-0.4Mg-1.0Si-(Sn) alloy. *Materials & Design, 198, 109307.* https://doi.org/10.1016/j.matdes.2020.109307

14. Werinos M, Antrekowitsch H, Ebner T, Prillhofer R, Uggowitzer P, & Pogatscher S. (2016). Hardening of Al–Mg–Si alloys: Effect of trace elements and prolonged natural aging. *Materials & Design*, *107*, 257–268. https://doi.org/10.1016/j.matdes.2016.06.014

15. Aruga Y, Kim S, Kozuka M, Kobayashi E & Sato T. (2018). Effects of cluster characteristics on two-step aging behavior in Al-Mg-Si alloys with different Mg/Si ratios and natural aging periods, *Materials Science and Engineering A, 718,371-376.* https://doi.org/10.1016/j.msea.2018.01.086

16. Marioara CD, Andersen SJ, Jansen J, & Zandbergen, HW (2001). Atomic model for GP-zones in a 6082 Al–Mg–Si system. *Acta Materialia*, *49*(2), 321–328. https://doi.org/10.1016/s1359-6454(00)00302-5

17. Kawahara Y, Marioara CD, Hell CM, Thrane ES, Mørtsell EA, Røyset J, Holmestad R, Kaneko K (2025*).* Effect of Cu addition on atomic clusters and its influence on the dispersion of precipitates in Si-rich Al-Mg-Si alloys, *Materials Science and Engineering: A,*946-149121. https://doi.org/10.1016/j.msea.2025.149121

18. Li C, Marioara CD, Hatzoglou C, Andersen SJ, Holmestad R, Li Y *(*2024). Accelerating precipitation hardening by natural aging in a 6082 Al-Mg-Si alloy, *Acta Mater.* 281-120396. https://doi.org/10.1016/j.actamat.2024.120396

19. Cui Z, Jiang H, Zhang D, & Rong L. (2024). Inhibiting of the negative natural aging effect in Al–Mg–Si alloys. *Materials Science and Engineering A*, *894*, 146196. https://doi.org/10.1016/j.msea.2024.146196

20. Liu C, Lai Y, Chen J, Tao G, Liu L, Ma P, & Wu C. (2016). Natural-aging-induced reversal of the precipitation pathways in an Al–Mg–Si alloy. *Scripta Materialia*,*115*,150–154. https://doi.org/10.1016/j.scriptamat.2015.12.027

First Principles Study of $L1_2$ Type Al_3Zr Precipitates in Aluminum Alloys

Yuma Matsuzaki[a,*], Norio Nunomura[b]

[a] *Graduate School of Science and Engineering, University of Toyama, Toyama, Japan,*
[b] *Department of Materials Design and Engineering University of Toyama, Toyama, Japan,*

*Corresponding Author's E-mail: m25c1626@ems.u-toyama.ac.jp

Abstract

The mechanical properties of aluminum alloys are strongly influenced by the formation of precipitates induced by minor alloying additions, particularly transition metal elements. Among these, $L1_2$ -type compounds, which exhibit good coherency with the Al matrix, are well-known strengthening phases. However, the detailed relationship between their electronic structures, stability, and resulting mechanical properties remains incompletely understood. In this study, we focus on $L1_2$ -type compounds and investigate representative examples using first-principles calculations with AkaiKKR [1], analyzing their electronic densities of states and elastic properties. Our initial results for Al_3Zr indicate that strong orbital hybridization between aluminum and zirconium leads to the formation of a pseudo-gap in the electronic structure, suggesting a potential correlation between the Fermi level position relative to this pseudo-gap and the compound's stability. Moving forward, we aim to systematically examine the effect of alloying additions on the Fermi level and the stability of the $L1_2$ phase. We will extend our calculations to $Al_3ZrxTM1\text{-}x$ (TM: Transition metals) compounds, varying the concentration of transition metal elements to tune the electronic structure and shift the Fermi level toward the bottom of the pseudo-gap. By analyzing the resulting electronic structures and formation energies, we aim to establish design principles that utilize $L1_2$ -type precipitates to enhance both the electronic stability and overall performance of aluminum alloys, ultimately providing guidance for the design of $Al_3ZrxTM1\text{-}x$ alloys with improved mechanical properties and durability.

Keywords: density functional theory; aluminum alloys; $L1_2$ *structure; KKR-CPA; AkaiKKR*

Introduction

Aluminum (Al) alloys are critical for aerospace and automotive applications due to their high specific strength, achieved primarily through precipitation hardening [2], [3]. The stability and efficiency of strengthening precipitates, particularly those with the ordered $L1_2$ crystal structure (like Al_3Zr and Al_3Sc), determine the alloy's performance, especially at high temperatures. Notably, Al_3Zr forms a metastable $L1_2$ structure upon rapid solidification, which exhibits excellent thermal stability against coarsening [4]. While current research confirms the importance of precipitate stability, the precise electronic mechanisms governing this stability remain insufficiently understood for rational alloy design.

There is a significant gap in having a clear, predictive principle that directly links the alloy's adjustable parameters to the precipitate's electronic stability. Early studies have investigated the formation of metastable $L1_2$ phases in Al_3Zr-based ternary alloys [5], and dispersoid formation in Zr-containing aluminum alloys has also been examined in detail through experimental studies and process modeling [6]. Traditional alloying methods are inefficient.

The objective of this study is to establish a robust electronic design principle using first-principles calculations. We aim to: (1) elucidate the correlation between Valence Electron Concentration (VEC), the hybridization-induced pseudo-gap, and precipitate stability; (2) systematically investigate Sc and Y alloying in the $Al_3(Zr_{1-x}TM_x)$ ternary system to tune the electronic structure; and (3) identify the optimal composition that maximizes both electronic stability and structural compatibility.

This work provides atomistic-level guidance necessary to move beyond empirical alloy development. By confirming the electronic design principle and identifying the optimal $Al_3Zr_{0.5}Sc0.5$ composition, this study offers a new framework for developing high-performance Al alloys with enhanced thermal stability and long-term durability.

Materials and Methods

All reported results were obtained using first-principles calculations based on Density Functional Theory (DFT). The computational approach was hybridized, employing two distinct software packages based on the specific type of calculation required. The VASP [7] was used for initial structural relaxation, energy minimization, and mechanical property calculations of ordered binary compounds. For investigating the detailed electronic structure and modeling substitutional disorder in ternary alloys, the AkaiKKR package, based on the Korringa-Kohn-Rostoker (KKR) Green's function method and the Coherent Potential Approximation (CPA), was utilized. The generalized gradient approximation (GGA) parameterized by Perdew-Burke-Ernzerhof (PBE) was consistently applied across both codes to treat the exchange-correlation energy.

Structural relaxation and energy convergence calculations for the binary Al_3TM compounds (TM = Sc, Ti, Y, Zr, Nb) were performed using VASP. The plane-wave energy cutoff was set to 600 eV. Electronic convergence was strictly enforced with the energy difference between subsequent steps required to be less than 1.0×10^{-8} eV. Structural optimization included relaxation of both cell shape/volume and atomic positions using the conjugate gradient algorithm. A Monkhorst-Pack k-point sampling scheme was employed; a 9x9x9 k-point grid was used for structural relaxation and elastic properties, while a denser 18x18x18 grid was utilized for accurate Density of States (DOS) calculations. The smearing method was applied with a width of 0.2 eV.

Electronic structure and stability analyses for the binary compounds and the disordered ternary alloys ($Al_3(Zr_{1-x}TM_x)$, where TM = Sc, Y) were performed using AkaiKKR. The CPA method was essential for modeling the substitute disorder (Zr/TM mixing) on the Transition Metal (TM) sublattice. The concentration of the alloying TM element (x) varied from x=0 to x=1. The convergence threshold for the electronic self-consistency was set to 0.001. The resultant density of states at the Fermi level (D(EF)) was extracted and used as the primary metric for assessing the electronic stability of the disordered alloys.

Results and Discussion

The research findings are presented in three thematic parts: Binary Compound Characteristics, Electronic Stabilization Mechanism, and Ternary Alloy Optimization.

Al_3Binary Compound Characteristics:

The initial investigation focused on the $L1_2$ -type binary intermetallic compounds Al_3TM (TM = Sc, Ti, Y, Zr, Nb). Calculated formation enthalpies (ΔH , Table 1) indicated thatAl_3Zr (ΔH = -0.464 eV/atom) and Al_3Sc (ΔH = -0.461 eV/atom) exhibited the highest thermodynamic stability, suggesting they form the most robust precipitates. All compounds displayed high stiffness (high Bulk Modulus *B* and Young's Modulus *E*, Table 2) and an intrinsically brittle nature, characteristic of effective strengthening phases.

Table 1. Calculated lattice constant (a_0), bulk modulus (B_0), and formation enthalpy (ΔH) for Al_3TM compounds in the $L1_2$ structure.

	a_0 (Å)	B_0 (GPa)	ΔH (eV/atom)
Al_3**Sc**	4.103	88.92	-0.461
Al_3**Ti**	3.979	106.64	-0.39
Al_3**Y**	4.258	74.64	-0.426
Al_3**Zr**	4.104	102.79	-0.464
Al_3**Nb**	3.995	122.89	-0.262

Table 2. Calculated elastic constants ($C11$, $C12$, $C44$), derived moduli (B, G, E), and Poisson's ratio (v) for Al_3TM compounds (all values in GPa except v).

	C_{11}	C_{12}	C_{44}	B	G	E	G/B	v
Al_3**Sc**	175.45	46.25	66.84	89.32	65.94	158.75	0.74	0.204
Al_3**Ti**	191.11	63.95	74.90	106.34	70.14	172.51	0.66	0.230
Al_3**Y**	147.52	38.36	54.88	74.80	54.80	133.50	0.73	0.206
Al_3**Zr**	185.30	63.04	70.39	103.79	66.61	164.81	0.64	0.236
Al_3**Nb**	186.91	91.93	95.61	123.59	76.36	181.29	0.58	0.244

Electronic Stabilization Mechanism:
The thermodynamic variability observed across the Al_3TM series is strongly linked to the electronic structure of the compounds.

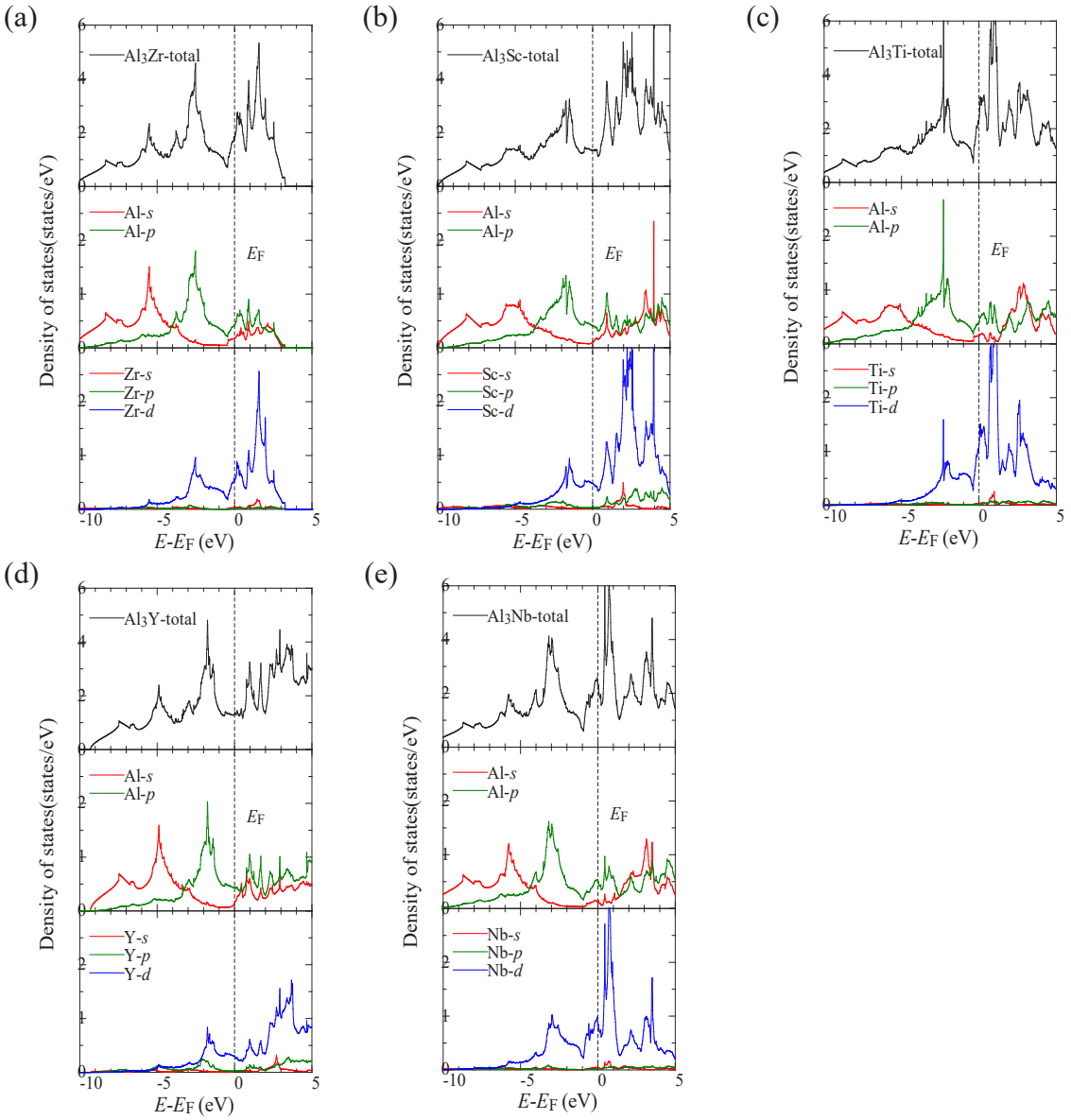

Figure 1. Calculated Total and Partial DOS for $L1_2$ -Al_3TM Compounds (a: Al_3Zr, b: Al_3Sc, c: Al_3Ti, d: Al_3Y, e: Al_3Nb)

All compounds exhibit a pronounced pseudo-gap near the Fermi level (E_f), resulting from the strong Al_3*p*-TM *d* orbital hybridization (Figure 1). This hybridization splits the electronic states into occupied bonding states and unoccupied antibonding states. Thermodynamic stability is maximized when E_f resides precisely at the minimum of this pseudo-gap, minimizing the occupation of destabilizing antibonding states.

This effect is controlled by the Valence Electron Concentration (VEC). The high-stability compounds (Al_3Zr, Al_3Sc) successfully position their E_f near the pseudo-gap minimum. Conversely, the high-VEC compound Al_3Nb shifts its E_f onto the steep slope of the antibonding states (Figure 1(e)), leading to a high density of states at the Fermi level ($D(E_f)$) and low stability (ΔH = -0.262 eV/atom). This establishes the electronic design principle: The stability of the $L1_2$ precipitate is directly proportional to the effective lowering of $D(E_f)$

Ternary Alloy Optimization:
To exploit the VEC-tuning principle, Sc (Group 3) and Y (Group 3) were systematically substituted into Al_3Zr (Group 4), forming $Al_3(Zr_{1-x}TM_x)$ solid solutions.

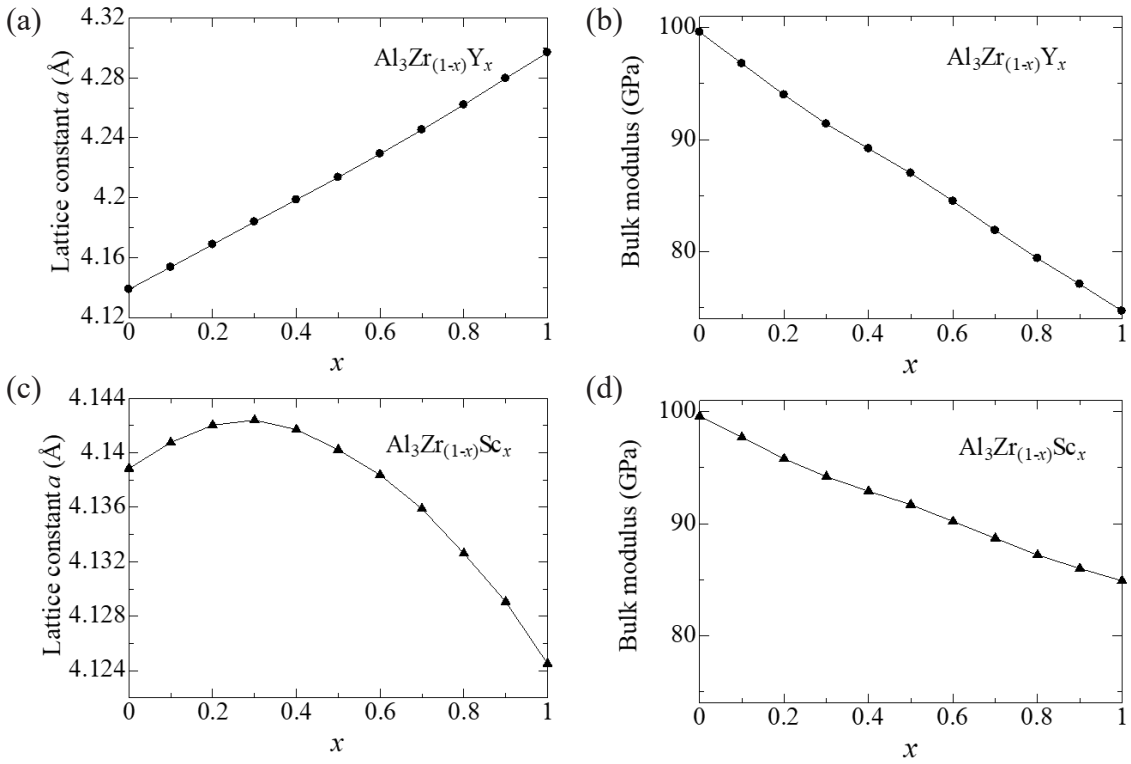

Figure 2. Composition Dependence of Lattice Constant and Bulk Modulus (a, c: lattice constant, b, d: bulk modulus)

Focusing on the composition dependence of the lattice constant (Figure 2(a) and (c)), the $Al_3Zr_{1-x}Y_x$ system shows significant lattice expansion with increasing Y concentration x, indicating increasing lattice mismatch with the Al matrix. In stark contrast, the $Al_3Zr_{1-x}Sc_x$ system is mechanically advantageous as the lattice constant remains within a minimal range across the entire composition (Figure 2(c)), confirming the maintenance of near lattice-matching. Notably, the composition optimized for electronic stability, x=0.5, exhibits a lattice constant nearly identical to that of Al_3Zr. This superior lattice compatibility is crucial for mitigating coherency strain and enhancing the precipitate's resistance to coarsening. Furthermore, although the bulk modulus exhibits a linear decreasing trend in both systems (Figure 2(b, d)), it maintains sufficient stiffness required for a strengthening phase even after alloying, due to its high initial value.

Electronic Optimization:

The change in electronic stability was tracked by the calculated D(EF) as a function of concentration x.

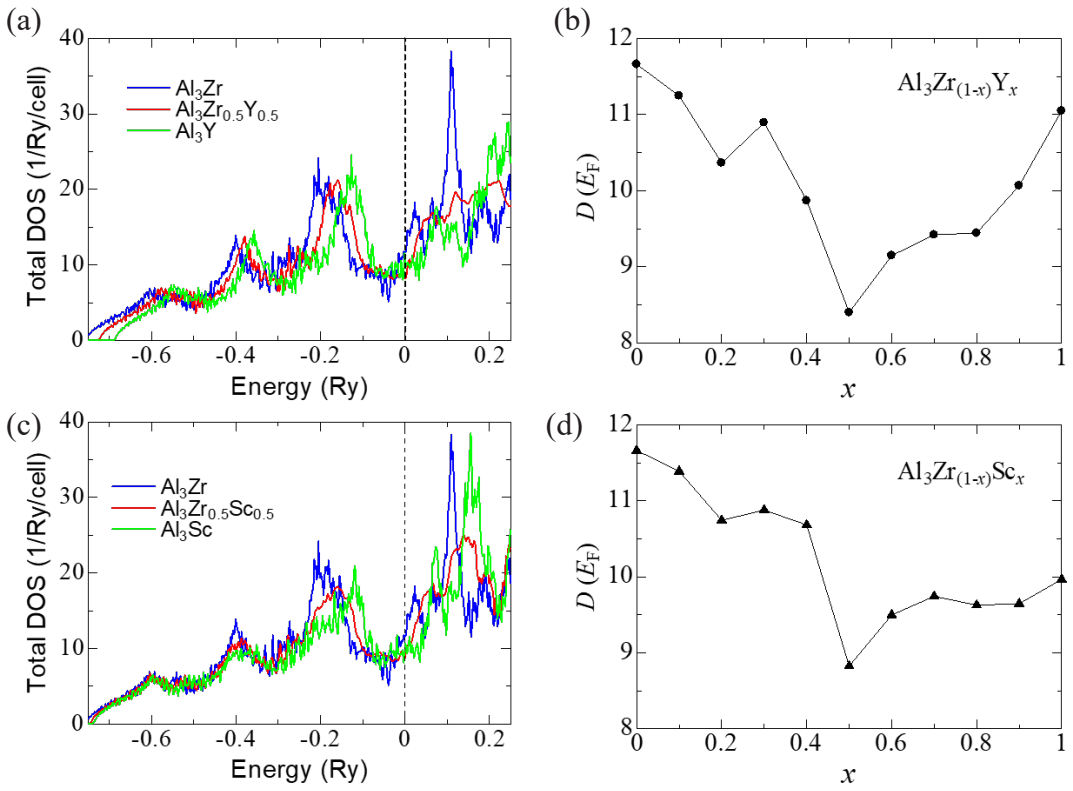

Figure 3. Electronic Stability and DOS Changes in Ternary $Al_3(Zr_{1-x}TM_x)$

The minimum D(EF) was clearly observed at an alloying concentration of approximately x=0.5 for both Sc and Y substitution (Figure 3(a, c)). This minimum directly confirms the successful electronic tuning; substituting Zr (Group 4) with a Group 3 element (Sc or Y) reduces the VEC, causing the EF to shift downward and settle at the deepest part of the pseudo-gap.

The total DOS plots (Figure 3(b, d)) visually validate this optimization, showing that the DOS curve at EF for the x=0.5 compositions drop significantly below the binary endmembers, thus achieving the maximum electronic stabilization.

Conclusion and Future Outlook The combined electronic and mechanical evidence identifies the $Al_3Zr_{0.5}Sc_{0.5}$ compound as the most promising precipitate. This composition simultaneously fulfils the primary requirement for stability (optimized electronic structure/minimized $D(E_F)$) and the key mechanical requirement for high performance (near lattice-matching).

Limitations of this 0 K DFT study include the lack of finite temperature analysis (ΔG) and kinetic modelling. Future research should prioritize calculating the Gibbs free energy for the $Al_3Zr_{0.5}Sc_{0.5}$ alloy and conducting experimental validation to confirm its predicted superior thermal stability and mechanical performance.

Conclusion

The mechanical performance of precipitation-hardened aluminum alloys is inherently tied to the stability of their $L1_2$ strengthening phases. Through comprehensive first-principles calculations, this study has successfully established a clear electronic design principle for maximizing this stability.

The stability of the $L1_2$ phase is demonstrably governed by the position of the Fermi level (E_F) relative to the hybridization-induced pseudo-gap. Optimal stability is achieved by precisely tuning the Valence Electron Concentration (VEC) to minimize the density of states at the Fermi level ($D(E_F)$).

Crucially, the $Al_3Zr_{0.5}Sc_{0.5}$ composition was identified as the ideal design candidate. It uniquely achieves maximum electronic stabilization (minimized $D(E_F)$) while simultaneously maintaining excellent lattice compatibility with the Al matrix, a prerequisite for sustained strengthening and high thermal stability. These findings provide essential, atomistic guidance for the design of new high-performance $Al_3Zr_xTM_{1-x}$ alloys, steering future alloy development efforts towards electronically informed materials selection for improved durability and performance.

Acknowledgments

There are no funding sources, grants, or scholarships to acknowledge. The authors acknowledge no contributions from individuals not listed as authors.

Conflict of Interest

The authors declare no conflict of interest.

References

[1] H. Akai, AkaiKKR (MACHIKANEYAMA) - A KKR-CPA program, Available from: http://kkr.issp.u-tokyo.ac.jp/jp/

[2] W.C. Hu, Y. Li, D.J. Li, X.Q. Zeng, C.S. Xu, First-principles study of phase stability and mechanical properties of Al_3X (X = Sc, Ti, Zr) intermetallic compounds, Phys. B Condens. Matter 427 (2013) 85–90.

[3] Z. Mao, W. Chen, D.N. Seidman, C. Wolverton, First-principles study of Al_3(Sc,Zr) alloys: Structural, elastic and electronic properties, Acta Mater. 59 (2011) 3012–3023.

[4] T. Ohashi, R. Ichikawa, Formation of metastable Al_3Zr precipitates in Al–Zr alloys, Metall. Trans. 3 (1972) 2300–2306.

[5] P.B. Desch, R.B. Schwartz, P. Nash, Metastable phase formation in rapidly solidified Al–Zr–X alloys, J. Less-Common Met. 168 (1991) 69–75.

[6] R.E. Sanders, E.A. Starke Jr., et al., Dispersoid precipitation and process modelling in zirconium-containing commercial aluminium alloys, Acta Mater. 49 (2001) 1187–1200.

[7] G. Kresse, J. Furthmüller, Efficient iterative schemes for ab initio total-energy calculations using a plane-wave basis set, Phys. Rev. B 54 (1996) 11169–11186.

First-principles calculation of electron transport influenced by Fe adsorption on graphene nanoribbons (GNRs)

T. Yoshida [a*], N. Nunomura [b]

[a] *Graduate School of Science and Engineering, University of Toyama, Toyama, Toyama, Japan*
[b] *Department of Materials Design and Engineering, University of Toyama, Toyama, Toyama Japan*

*Corresponding Author's E-mail: m24c1633@ems.u-toyama.ac.jp

Abstract

To investigate the initial electronic and magnetic properties of graphene nanoribbons (GNRs) with Fe atom adsorption, we performed density functional theory (DFT) calculations, focusing on how the structure influences electronic transport characteristics. The model system comprised hydrogen-terminated GNRs with a vacuum layer, where Fe atoms were adsorbed on the surface at regular intervals. Carbon atomic chains were employed to connect the electrodes.

DFT calculations were carried out using norm-conserving pseudopotentials and numerical pseudo-atomic orbitals (PAOs) as basis functions. For transport calculations involving electrodes, the non-equilibrium Green's function (NEGF) method was applied.

The results demonstrate that increasing the amount of Fe adsorption improves the stability of electron transport. However, detailed analysis revealed that the enhancement effect of Fe adsorption diminishes with increasing GNR width (vertical) but strengthens with increasing length (horizontal). These findings indicate that Fe adsorption activates the GNR surface for electronic transport, with its effectiveness strongly dependent on the adsorption site and the structural geometry.

Keywords: Density functional theory, Graphene surface, Metal adsorption, Electron transport

Introduction

Graphene is a two-dimensional material composed of carbon atoms arranged in a hexagonal lattice. It exhibits a variety of unique properties, including atomic-scale thickness, exceptional mechanical strength, and excellent electrical conductivity [1-3].

Due to these remarkable characteristics, graphene has attracted extensive research interest across a wide range of scientific fields. In particular, materials science has focused on its surface activity induced by metal adsorption [4-6].

Similar phenomena are observed in graphene nanoribbons (GNRs), which are narrow strips of graphene cut along specific crystallographic directions. In GNRs, electronic properties are influenced not only by graphene's intrinsic characteristics but also significantly by the edge structure, making precise control of these edges essential for tuning performance.

Although previous theoretical studies have demonstrated the influence of metal adsorption on graphene, the underlying mechanisms are still not fully understood.

The theoretical work by Hu et al. compared the effects of various metal atoms adsorbed on the graphene surface and revealed that Fe, in particular, induces strong magnetism throughout the entire structure [7]. Moreover, many of the metals that exhibit similarly strong magnetic properties are rare and costly, whereas Fe is inexpensive. Therefore, Fe is considered a highly practical candidate for future applications, and further developments are anticipated.

The objective of this study is to investigate the properties of graphene nanoribbons with adsorbed Fe atoms—known to exhibit high surface activity—using first-principles calculations. We evaluate the effects of Fe adsorption on GNRs connected to electrodes and analyze how variations in structural width (vertical) and length (horizontal) affect their electronic transport properties.

Materials and Methods

First-principles calculations were performed using the density functional theory (DFT) software package OpenMX [8-11]. Density functional theory (DFT) calculations employed norm-conserving pseudopotentials [12] and numerical pseudo-atomic orbitals (PAOs) as basis functions. For calculations involving electrodes, the non-equilibrium Green's function (NEGF) method was employed [8-9].

A cutoff energy of 100 Ry was used, and the k-point mesh was set to 1×7×7. The self-consistent field (SCF) convergence criterion was set to 1×10^{-7}, and the electronic temperature was fixed at 300 K. A bias voltage was applied along the x-axis. To eliminate the influence of periodic boundary conditions along the y- and z-directions, vacuum layers of 10 Å were introduced above and below the graphene nanoribbon (along the y-direction) and on both sides (along the z-direction). This vacuum spacing was sufficient to prevent interactions between adjacent Fe atoms and graphene layers. Fe atoms were adsorbed at the H-sites, corresponding to the centers of the graphene hexagons.

Results and Discussion

To validate the accuracy of the computational settings, calculations were first performed for body-centered cubic (bcc) iron. The optimized lattice constant was a = 2.760 Å, in good agreement with the experimental value of 2.867 Å [13].

Similarly, to verify the potential parameter for carbon atoms, calculations were conducted using a graphene structure. The optimized lattice constant was a = 2.58 Å, closely matching the experimental values of 2.46 Å, respectively [14]. These calculated values were subsequently used as input parameters in the main simulations.

Figure 1 illustrates the structural model, in which Fe atoms are adsorbed at regular intervals on a monolayer graphene nanoribbon with varying width (vertical) and length (horizontal). The spacing between Fe atoms corresponds to the most stable configuration reported in previous experimental studies on Fe adsorption on graphene [15].

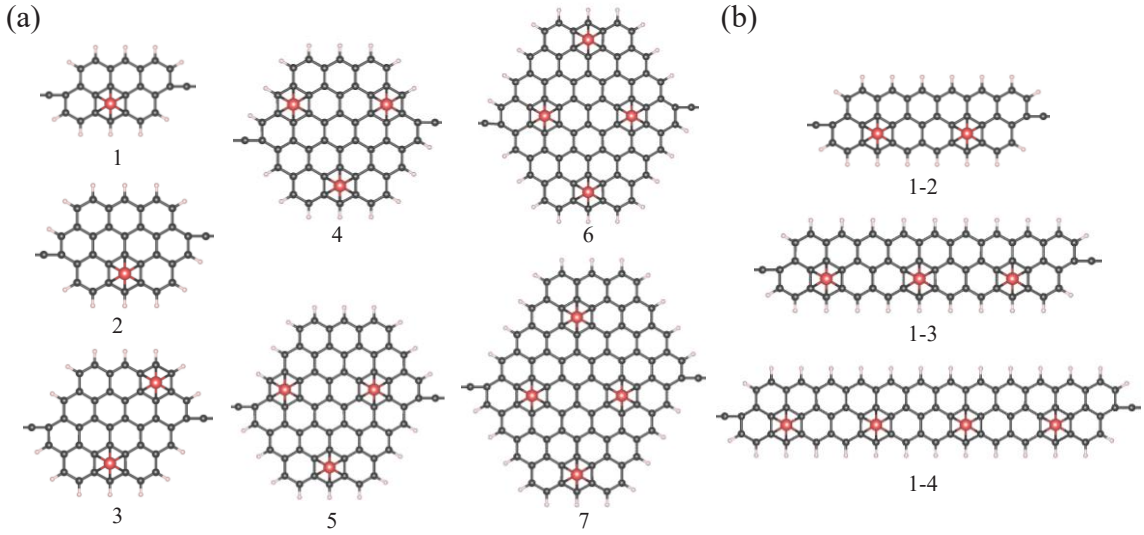

Fig.1 Top view of a GNR structure with adsorbed Fe atoms. Carbon atoms are shown in black, Fe atoms in red, and hydrogen atoms in white. (a) shows the structure with extended width (vertical), while (b) shows the structure with extended length (horizontal).

Figure 2 shows the electrode structure. The electrodes were configured to allow a bias voltage to be applied to the central region. The structure consists of several electrodes: two finite electrodes (L and R) located on the left and right sides, and one semi-infinite electrode (B). Electrodes L and R each comprise a carbon chain containing five carbon atoms, while electrode B consists of a carbon chain with three carbon atoms.

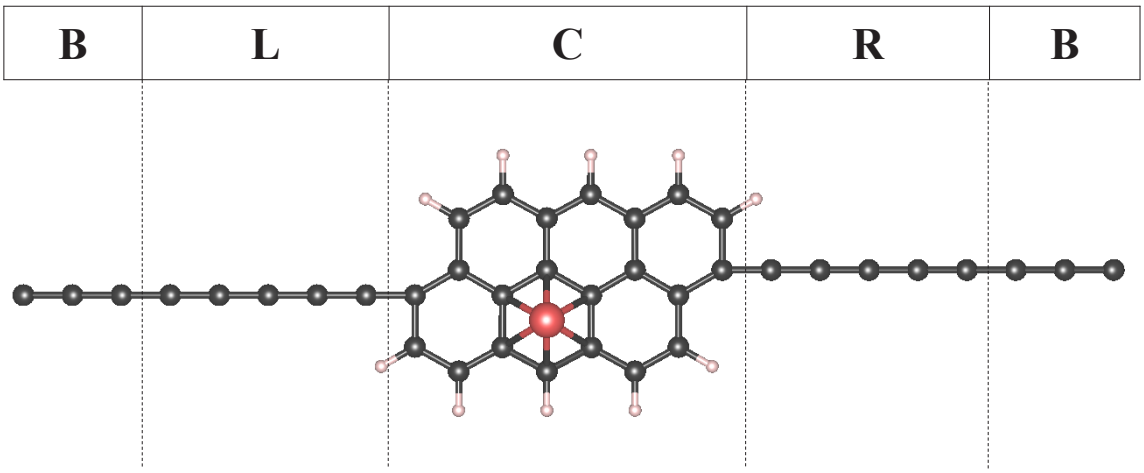

Fig.2 Top view of the structure of GNR with adsorbed Fe atoms, connected to an electrode positioned at the center of the structure.

Figure 3 illustrates the variation in the work function along the x-axis for each structural configuration. In all cases, the work function decreases toward the central region and reaches a

minimum at the center of the structure. Moreover, it was observed that increasing the number of adsorbed Fe atoms leads to a significant reduction in the overall work function. A similar decrease in the work function has also been observed when other metals are adsorbed on graphene [16]. This finding represents an important step toward understanding the role of Fe adsorption in modulating the electron transport properties in graphene nanoribbons.

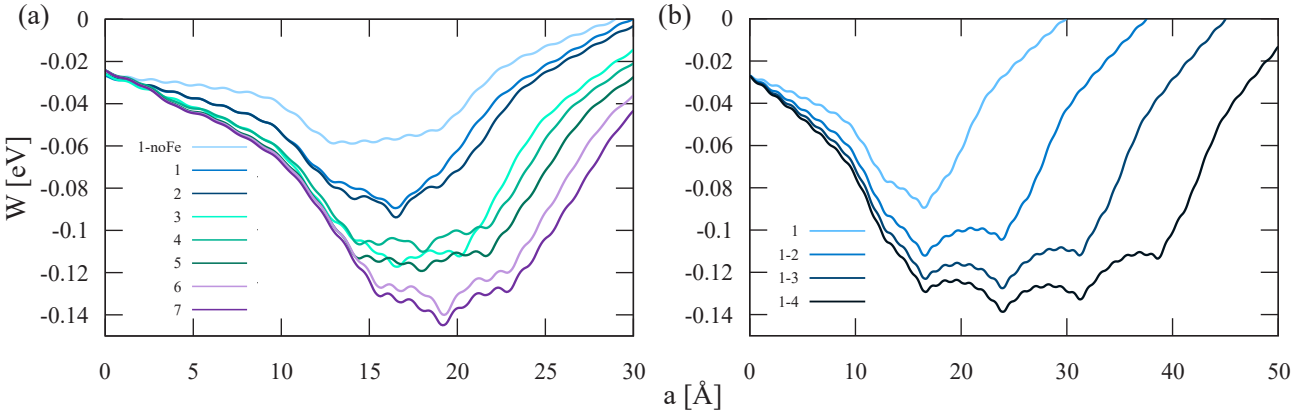

Fig.3 Relationship of work functions along the x-axis for each structure under 1.0 V. (a) shows the structure with extended width (vertical), while (b) shows the structure with extended length (horizontal).

Figure 4 presents a comparison of the work function reduction per adsorbed Fe atom, obtained by evaluating the difference between structures with and without Fe adsorption. Along the width (vertical) direction, the reduction tends to diminish with increasing width. In contrast, the reduction increases steadily with structural length (horizontal). Furthermore, upon applying an external voltage, the reduction tends to become more pronounced for all structures.

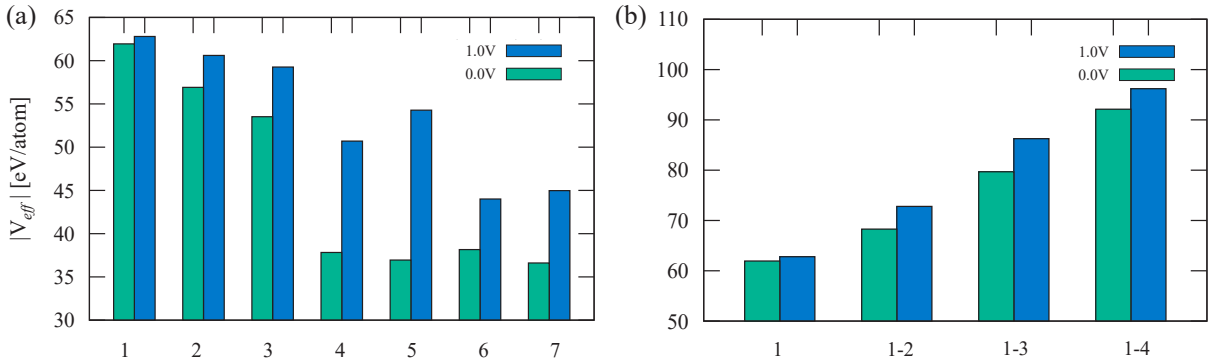

Fig.4 Comparison of the work function reduction per adsorbed Fe atom for each structure. (a) Comparison when the structure is stretched in width (vertical). (b) Comparison when the structure is stretched in length (horizontal).

Figure 5 shows the changes in conductance for each structure. Similar to the trend observed in the work function reduction, conductance decreases significantly from Structure 3 to Structure 4. A slight decrease is also observed when the structure is stretched horizontally.

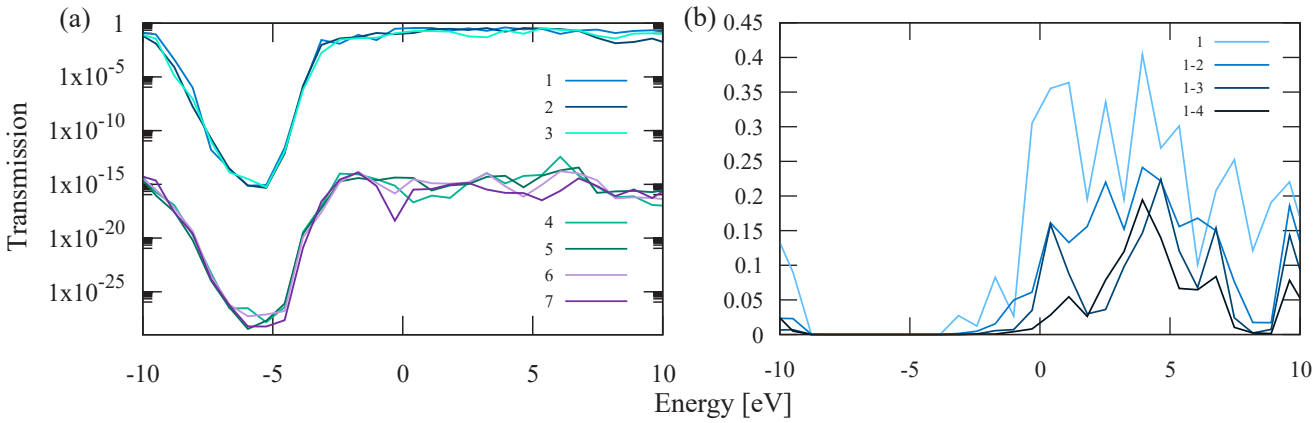

Fig.5 Comparison of the conductance for each structure. (a) Comparison when the structure is stretched in width (vertical). (b) Comparison when the structure is stretched in length (horizontal).

Figure 6 shows the work function reduction for each Fe atom in structure 6. The Fe atoms located at the edges of the GNR tended to exhibit a greater reduction than those at the center. Consequently, the vertically extended structure, with more Fe atoms at the center, showed a decrease in the overall work function reduction. In contrast, the horizontally extended structure, where Fe atoms were adsorbed at the GNR edges, exhibited an increase in the work function reduction.

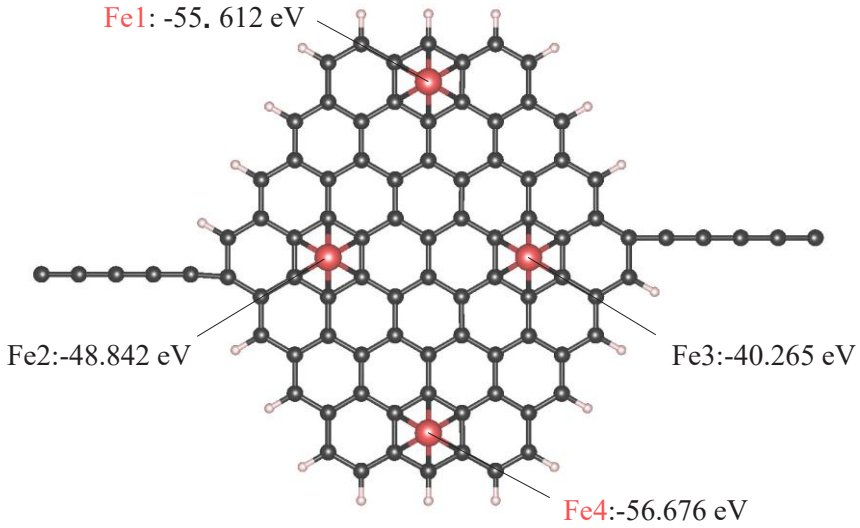

Fig.6 Effect of the work function on each adsorbed Fe in Structure 7.

Moreover, as shown in Figure 7, both the density of states (DOS) and the differential charge density distribution exhibit significant changes, particularly a localized change in electron density near the Fe atoms. This change has a pronounced effect on both the magnetic and electronic properties of the GNR. Similar changes have also been reported in other studies, indicating a consistent behavior of electron density redistribution around transition metal atoms [17-18].

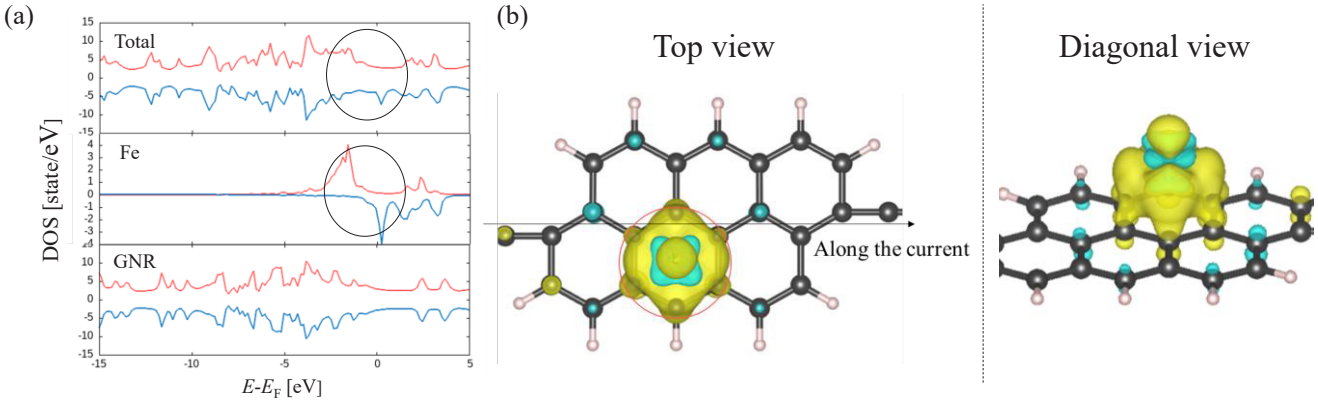

Fig.7 (a) Plot of the density of states (DOS) for structure 1 relative to energy of the entire structure minus the Fermi energy (E-E_F) (b) Current density dependence on Fe adsorption sites in GNRs, along with differential electron density distributions.

Conclusion

We investigated the electronic properties of the GNR–Fe surface under a constant voltage using first-principles calculations based on density functional theory. Our results demonstrate that Fe adsorption stabilizes the electronic transport characteristics of the system and leads to notable modifications in its electronic structure. In future work, we aim to achieve a more realistic understanding of the material's behaviour by incorporating structural features such as defects in the GNR into our calculations.

References

[1] A. K. Geim, Science 324, 1530-1534 (2009).
[2] Lee C, Wei X, Kysar JW, Hone J, Science 321, 385-388 (2008).
[3] Chen S et al, Nat Mater 11, 203-207 (2012).
[4] Sevinçli H, Topsakal M, Durgun E, Ciraci S, Phys Rev B 77, 195434 (2008).
[5] Deng X, Wu Y, Dai J, Kang D, Zhang D, Phys Lett A 375, 3890–3894 (2011).
[6] Sanjeev K. Gupta, Himadri R. Soni, Prafulla K. Jha, AIP Adv 3, 032117 (2013).
[7] Leibo Hu, Xianru Hu, Chenlei Du, Yunchuan Dai, Jianbo Deng, Density functional calculation of transition metal adatom adsorption on graphene, Physica. B 405, 3337-3341 (2010).
[8] T. Ozaki, K. Nishio, and H. Kino, Phys. Rev. 81, 035116 (2010).
[9] T. Ozaki, Phys. Rev. B 75, 035123 (2007).
[10] T. Ozaki and H. Kino, Phys. Rev. B 72, 045121 (2005).
[11] K. Lejaeghere et al., Science 351, aad3000 (2016).
[12] W.Kohn and L. Sham, Self-consistent equations including exchange and correlation effects, Phys Rev A 140, 1133-1138 (1965).
[13] http://webelements.com/
[14] Y. Ishizawa, Tanngennsisou graphite no seisitu to sono ouyou (in Japanease) [Properties of monoatomic layer graphite and its applications] Gypsum & Lime 247, 481-489 (1993).
[15] T. Yoshida, N. Nunomura, Arch. Metall. Mater. 70, 3, 1295-1299 (2025).
[16] M. Legesse, F. El Mellouhi, E. Bentria, M. E. Madjet, T. S. Fisher, S. Kais, and F. H. Alharbi, Appl. Surf. Sci. 394, 98–107 (2017).
[17] H. Sevinçli, M. Topsakal, E. Durgun, and S. Ciraci, Phys. Rev. B 77, 195434 (2008).
[18] K. T. Chan, J. B. Neaton, and M. L. Cohen, Phys. Rev. B 77, 235430 (2008).

Glaze Firing Using Blue Laser with Heater Assistance

Shuntaro Arakawa[1], Shoto Isizaki[2], Takashi Hashizume[1*], Atsushi Saiki[1]
[1]School of Sustainable Design, Univ. Toyama, Toyama, Japan
[2]Nikon corporation, Tokyo, Japan
Email: hasizume@sus.u-toyama.ac.jp
*Corresponding author

Abstract

Glaze firing is an important process in the decoration of ceramics and metal crafts. However, traditional cloisonne production require long firing times and high-temperature environments, resulting in low manufacturing efficiency. Recently, laser technology has attracted attention for its ability to perform high-precision and high-speed processing. This study proposes the application of laser technology to the firing process of cloisonné enamel. Compared to conventional electric kiln firing, this method enables the formation of fine patterns in a shorter time and allows for the creation of precise color expressions and textures. To establish optimal laser firing conditions, the study evaluated the color development characteristics and crack formation behavior. In the experiment, four types of glaze were used. It mainly composed of lead, silicates, and metal oxides. The glazes were ground to approximately 40–50 μm and applied to copper plates. The samples were placed near a heater to remove moisture. After complete drying, they were preheated on a 350°C heater for three minutes to ensure uniform thermal distribution. Laser irradiation was then performed while maintaining this temperature. Since the laser alone did not provide sufficient thermal energy, a heater was used in combination. This resulted in a uniform glassy surface. High color reproducibility was observed across the glazes. The surface hardness and smoothness of the laser-fired samples were confirmed to be comparable to those produced by electric kiln firing. Furthermore, the boundaries between different colors of glazes were clearly defined. The result demonstrated the potential for more precise design expression than conventional methods.

Keywords: Cloisonné; Glaze firing; Laser

Introduction

Glaze firing is an essential process in decorating ceramics and metal crafts. It imparts gloss and color by firing glaze at high temperatures (780–900°C) [1]. This technique originated in ancient Egypt and Western Asia. In Japan, it was established as cloisonné enamel during the Edo period [2]. Cloisonné developed uniquely in Japan. During the Edo period, it was used for armor and ornaments. In the Meiji era, it became a symbol of Japanese culture as an export craft. The use of multiple glazes and a transparent finish are key attractions of cloisonné. However, traditional production requires long firing times and high temperatures. This makes efficient manufacturing difficult. Today, technological innovation is advancing even in the craft field. New production techniques are in demand. Recently, laser technology has attracted attention for high-precision and high-speed processing. It is widely applied in metal and ceramic processing, as well as in medical and electronics fields [3][4]. The main feature of lasers is their ability to deliver high-density energy in a short time. Compared to conventional heating, this enables efficient processing. Laser parameters such as output, wavelength, and scanning speed can be precisely controlled. This allows localized processing and the creation of unique textures. Applying these characteristics to traditional crafts could enable new forms of expression. Such expressions were difficult to achieve with conventional techniques.

This study proposes introducing laser technology into the cloisonné firing process. The proposed "Laser Cloisonné" technique can create fine patterns in a shorter time. It also enables precise color expression and complex designs. This research examines the effects of laser firing on glaze properties. It evaluates color development, crack formation, and melting-solidification processes. The goal is to establish optimal laser firing conditions. The advantages and challenges of laser firing compared to conventional methods will also be clarified. This study aims to create new value by combining traditional crafts with advanced technology. It contributes to diversifying cloisonné techniques and developing new craft technologies. The potential of laser cloisonné extends beyond art and craft production. It may also apply to modern design, interior decoration, and decorative technologies in electronics. The findings of this study are expected to promote expansion beyond traditional craft boundaries.

Materials and Methods

To fire glaze, it is necessary to supply thermal energy exceeding its melting point. A laser can deliver high energy locally. However, heat supply by laser is characterized by rapid heating and rapid cooling. In glass, cooling rate has been reported to affect optical properties. When cooling is fast, optical transmittance tends to decrease, and transparency is impaired [5]. Rapid heating and cooling also generate large internal stress in the glaze. As a result, defects such as cracks may occur. Therefore, this study proposes a method of laser irradiation with heater assistance. This chapter examines the conditions required for firing glaze using a laser. It also considers conditions to maintain quality after firing based on thermal properties of the glaze. Glaze is generally made by mixing glass raw materials with red lead, soda, and borax. It is melted at a high temperature of 1300°C, taken out with a long iron spatula, and quenched in water. Metal compounds are then added for coloring to complete the glaze. Glazes that melt at 750–900°C are called low-fire glazes. Those melting at 1000–1150°C are medium-fire glazes, and those above 1200°C are high-fire glazes. Most ceramics fall into these categories [2]. In this experiment, a commercially available low-fire glaze mainly composed of lead was used. It is easier to fire even at low laser output. A blue laser (445 nm) was selected for this study. The reason is that blue laser has a short wavelength within the visible range. It is expected to have high absorption efficiency for glaze components and colorants based on metal oxides, especially cobalt oxide. Therefore, energy absorption on the surface occurs efficiently.

This enables effective localized heating. In addition, the short wavelength forms a relatively small beam spot. This makes irradiation of fine areas and adaptation to complex patterns easier. These characteristics are advantageous for cloisonné techniques requiring delicate expression. Furthermore, blue lasers are widely used in industrial applications. High-power and cost-effective models are readily available. This makes them a practical choice for introducing new cloisonné techniques. In this chapter, conditions for blue laser firing with heater assistance were examined. The aim was to suppress problems such as unmelted areas and cracks caused by rapid heating and cooling. It also aimed to ensure surface quality of the glaze. Commercial low-fire glazes (Kujaku brand cloisonné pigments) in yellow, orange, green, and blue were used. The glazes were ground with a mortar for firing. Generally, grinding glaze reduces transparency [1]. However, when particles are large or uneven, uniform firing by localized laser heating becomes difficult. Therefore, particle size was adjusted to approximately 40–50 μm. Copper plates with a thickness of 0.3 mm were used as substrates. They were cut into pieces of 2 × 4 cm. Then, they were immersed in sulfuric acid solution and washed with water to remove dirt and oil from the surface. Ground glaze was placed on the cleaned copper plate using a brush to form a square of 5 × 5 mm. The plate was then placed near a heater to evaporate moisture. After complete drying, it was quickly heated with the heater. The copper plate with glaze was heated at 350°C for 3 minutes using a heater. The temperature was set to 350°C because higher temperatures would change the color after firing.

Laser irradiation was performed while maintaining this temperature. The laser used was FABOOL Laser Mini (smartDIYs). Its wavelength was 445 nm, maximum output 3.5 W, and beam diameter 200 μm. Laser conditions were as follows:

- Scanning speed: 50, 75, 100 mm/min
- Number of scans: 1
- Output: 0.175–3.5 W

A schematic diagram of the laser firing process with heater assistance is shown in Fig. 1. Thermal analysis of the glaze was performed using TG-DTA (THERMOPLUS TG8120, RIGAKU). Surface evaluation was conducted using low-vacuum SEM (LVP-SEM Miniscope TM-3030, Hitachi High-Tech). Additionally, a digital microscope (VHX-700FSP1344, KEYENCE) was used for observation and analysis.

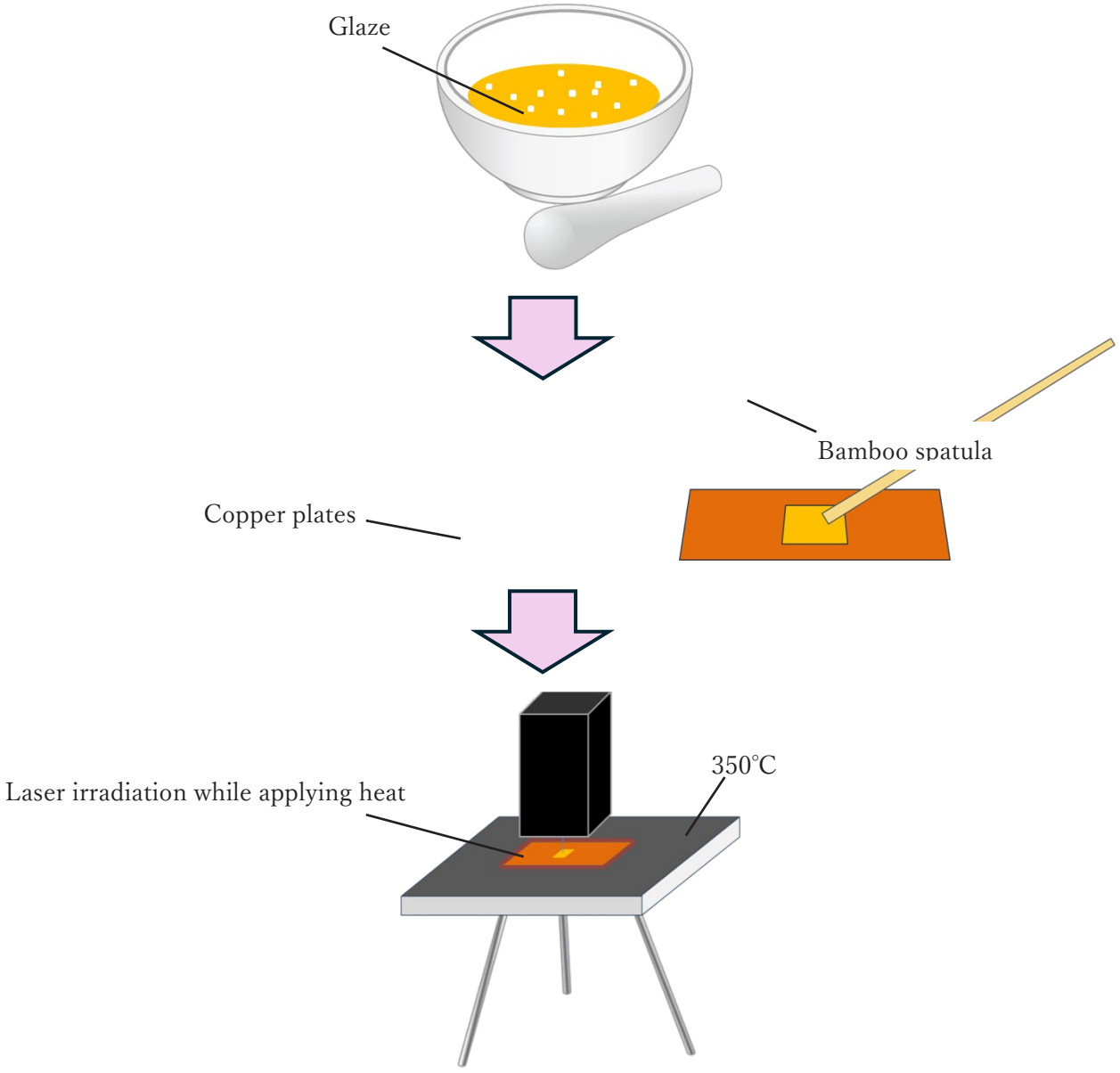

Fig. 1. Schematic of laser glaze firing with heater assistance

The laser was scanned back and forth across the sample. It was set to fire the entire glaze surface. The hatching width was set to 150 μm. This was slightly smaller than the laser beam diameter of 200 μm to avoid unmelted areas. A schematic diagram of the laser scanning direction is shown in Fig. 2. The results of glaze firing without heater assistance are shown in Fig. 3. The laser parameters were output 1.40 W and 1.93 W, with a scanning speed of 50 mm/min. At outputs below 1.23 W, no melting or firing of the glaze was observed. Melting was confirmed starting at 1.40 W. However, a uniform and smooth surface was not obtained under any condition. In the results without heater assistance, bead-like glassy regions were observed in several areas. This is considered to be traces where the laser light was converted into heat on the glaze surface and melted the glaze. The reason for the bead-like spherical shape is thought to be insufficient thermal energy. With rapid heating by the laser, part of the glaze melts. However, immediately after the laser passes, rapid cooling occurs. As a result, the glaze solidifies into a spherical shape due to surface tension. Furthermore, cavities were observed around the solidified spherical glaze. This is thought to occur because the melted glaze solidified while incorporating surrounding glaze. When the laser output was increased, the size of the glassy regions increased. However, even at the maximum output of 3.5 W, a uniform surface melted over the entire area was not obtained. Similar results were obtained for other colors used in this study. Optical photographs are shown in Fig. 4. From these results, it was concluded that firing glaze using only the laser is difficult due to insufficient thermal energy. Therefore, a method combining heater assistance with laser irradiation is proposed.

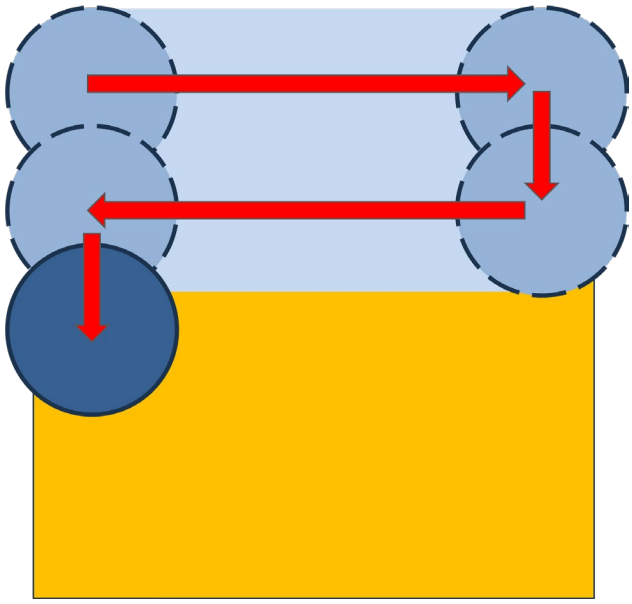

Fig. 2. Schematic of laser scanning direction

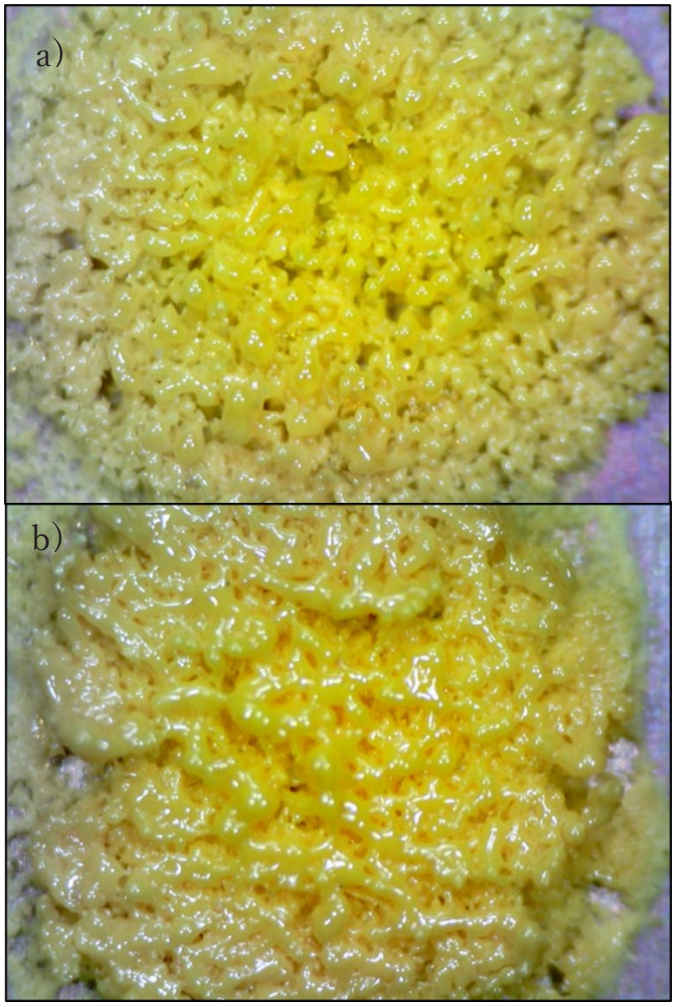

Fig. 3. Results of glaze firing without heater assistance. a) Laser output 1.40 W, scanning speed 50 mm/min; b) Laser output 1.93 W, scanning speed 50 mm/min

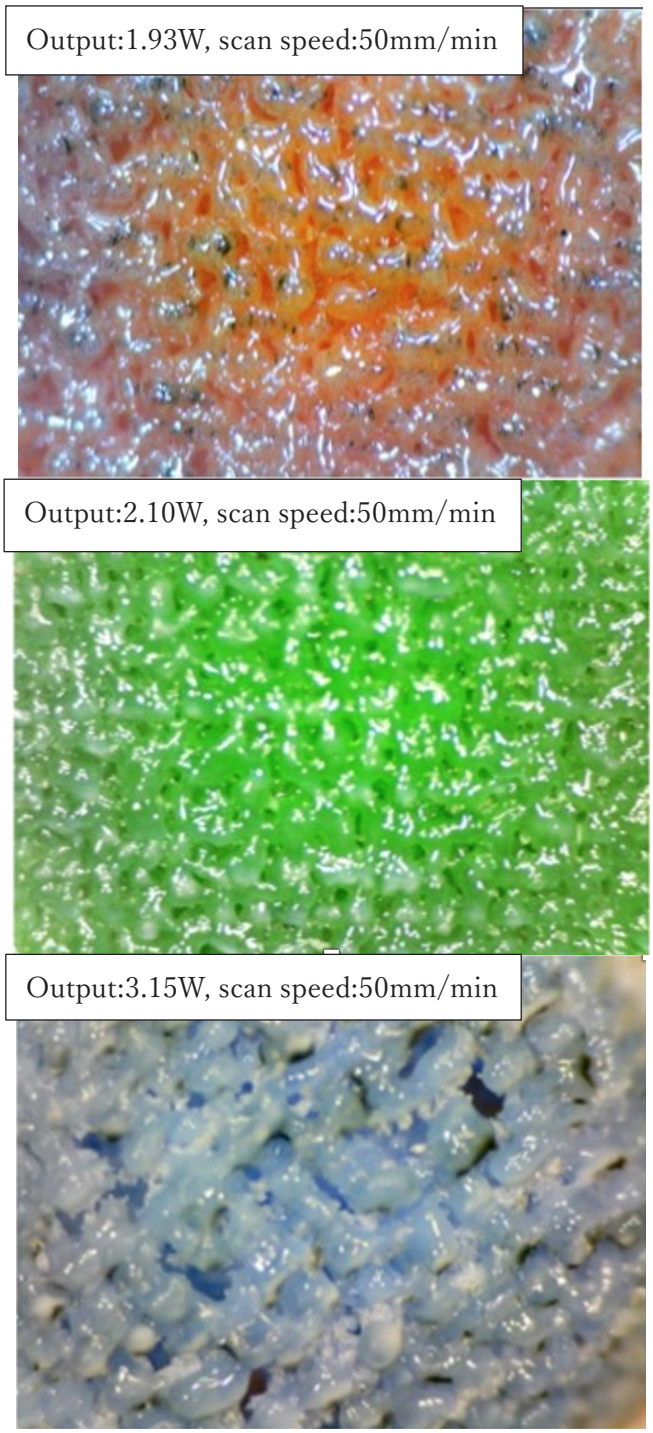

Fig. 4. Glaze firing results for different colors without heater assistance

A comparison image of yellow glaze at laser output 1.4 W and scanning speed 50 mm/min, with and without heater assistance, is shown in Fig. 5. In the sample with heater assistance, the glaze melted uniformly and a glassy surface was obtained. This occurred because the heater compensated for the thermal energy that was insufficient with the laser alone. As a result, the temperature exceeded the melting point of the glaze, enabling successful firing. The firing results for yellow glaze at various outputs and scanning speeds are shown in Fig. 6. The thermal energy supplied by the laser per unit time was also measured. At a scanning speed of 50 mm/min, no glassy surface was obtained below 0.7 W. At 75 mm/min, no glassy surface was

obtained below 1.23 W.
At 100 mm/min, no glassy surface was obtained below 2.1 W. From Fig. 6, it was confirmed that glaze firing is possible at all scanning speeds. However, when the output was low, holes appeared due to insufficient thermal energy. An SEM image of the inside of these holes is shown in Fig. 7. Unmelted glaze was observed, and bubble-like structures appeared on the surface. Adjacent glaze particles seemed to be connected. This suggests that the glaze attempted to melt but did not fully dissolve due to insufficient heat. The reason unmelted parts were exposed from the holes is that the interior did not reach the melting point, while the surface melted and solidified, pulling surrounding glaze during solidification. An illustration of this phenomenon is shown in Fig. 8. It was also confirmed that the number of holes increased in proportion to scanning speed. The reason is that even if the thermal energy per unit time is the same, the laser moves before sufficient heat penetrates the glaze interior. Therefore, as scanning speed increases, more holes appear on the surface and more unmelted areas remain inside. Furthermore, excessive output caused cracks and pitting. The cause is that high output generates large thermal energy, and rapid cooling after laser passage accumulates internal stress. When high-energy-density laser light irradiates for a short time, the glaze heats locally and instantly. The glaze melts rapidly, but cooling begins immediately after the laser passes.
This creates a steep temperature gradient inside the glaze, and internal stress accumulates during cooling, leading to cracks. In addition, at higher scanning speeds, lines were observed along the edges of the laser path. Increasing scanning speed reduces thermal energy per unit area, requiring higher laser output to melt the glaze. As a result, strong localized heat occurs on the surface, pushing molten glaze outward during irradiation, forming lines. To examine surface roughness of laser-fired glaze, measurements were taken using a digital microscope. 3D models of samples with holes (50 mm/min, 1.23 W) and smooth surfaces (50 mm/min, 1.40 W) are shown in Fig. 9. The surface with holes showed a maximum depression of 148 μm. The surface at 1.40 W showed slight unevenness, with a maximum bulge of 30.88 μm. This is considered to result from rapid heating and cooling, where molten glaze solidified while incorporating surrounding glaze. However, samples fired in an electric kiln also showed unevenness of 30–40 μm. Therefore, it was judged that laser firing can achieve smoothness comparable to electric kiln firing. Similar measurements were performed for other glaze colors, and the results are shown in Table 1. It was confirmed that at all scanning speeds, surface roughness was smallest when thermal energy per unit area was 0.34 J. Based on these results, the following conditions enable firing of yellow glaze:

- 50 mm/min at 1.40 W
- 75 mm/min at 2.07 W
- 100 mm/min at 2.80 W

However, considering stability of quality, 50 mm/min at 1.40 W was judged optimal. Keeping scanning speed at 50 mm/min, similar experiments were conducted for other colors. Optimal outputs were 1.75 W for orange, 2.10 W for green, and 3.15 W for blue. Yellow is complementary to blue and absorbs blue light easily. Therefore, yellow glaze effectively absorbed blue laser and melted at lower output. In contrast, blue glaze reflects most light near the blue laser wavelength. Thus, its absorption efficiency was very low, requiring higher output compared to other colors. The firing results for each color are shown in Fig. 10. Experiments were conducted under these conditions.

a)

b)

Fig. 5. Comparison of yellow glaze firing a)with and b)without heater assistance at laser output 1.40 W and scanning speed 50 mm/min

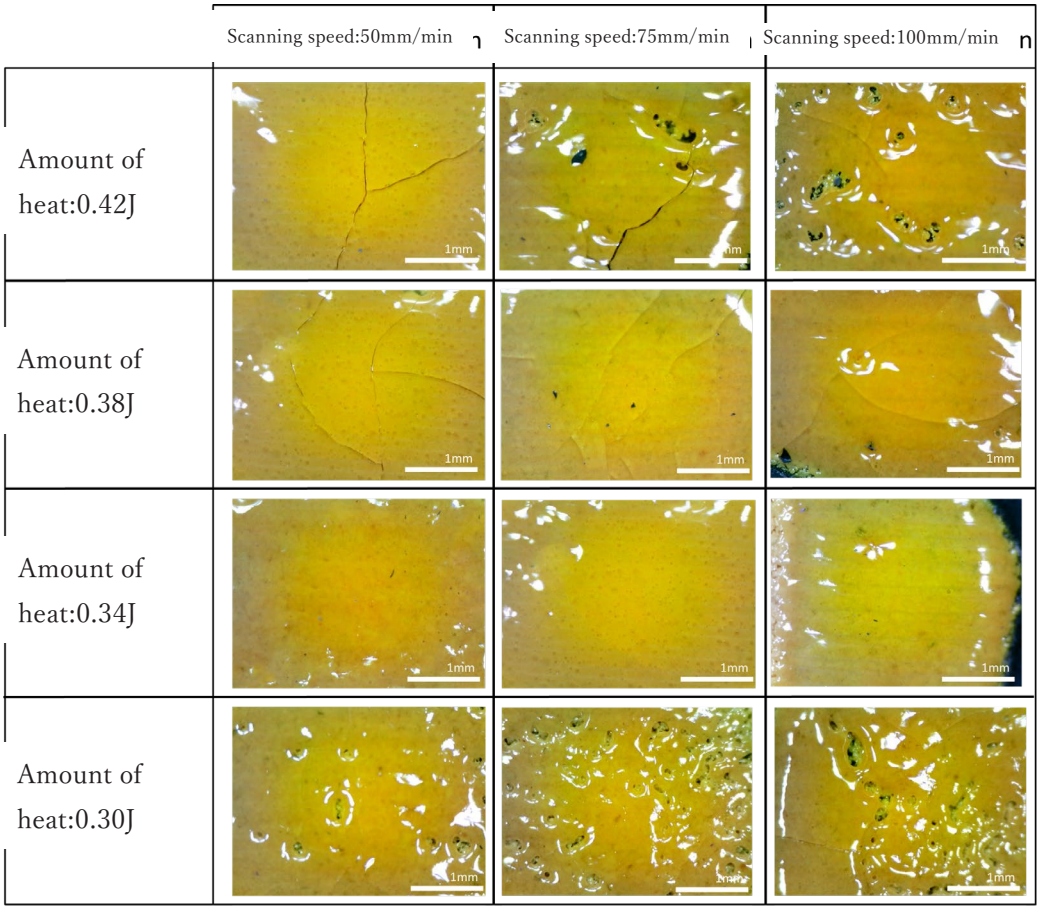

Fig. 6. Glaze firing results at various amounts of heat and scanning speeds

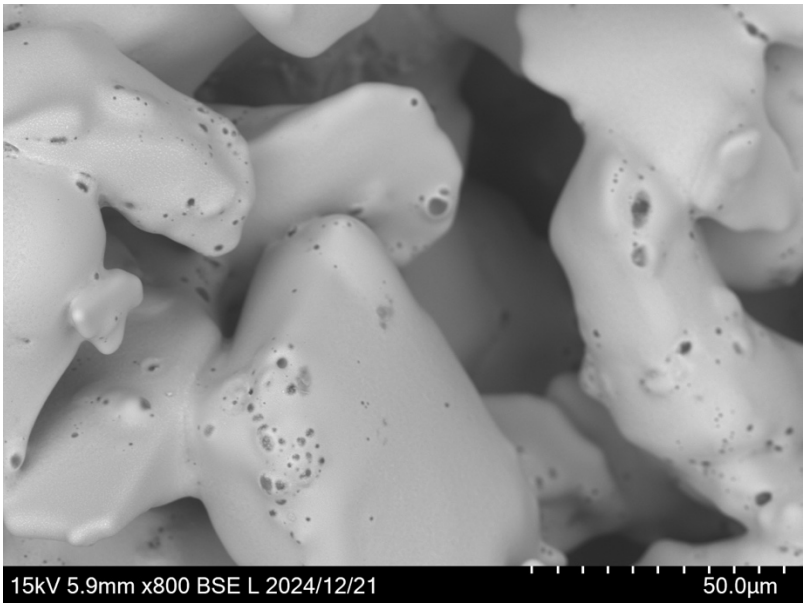

Fig. 7. SEM image of holes formed on the glaze surface after firing

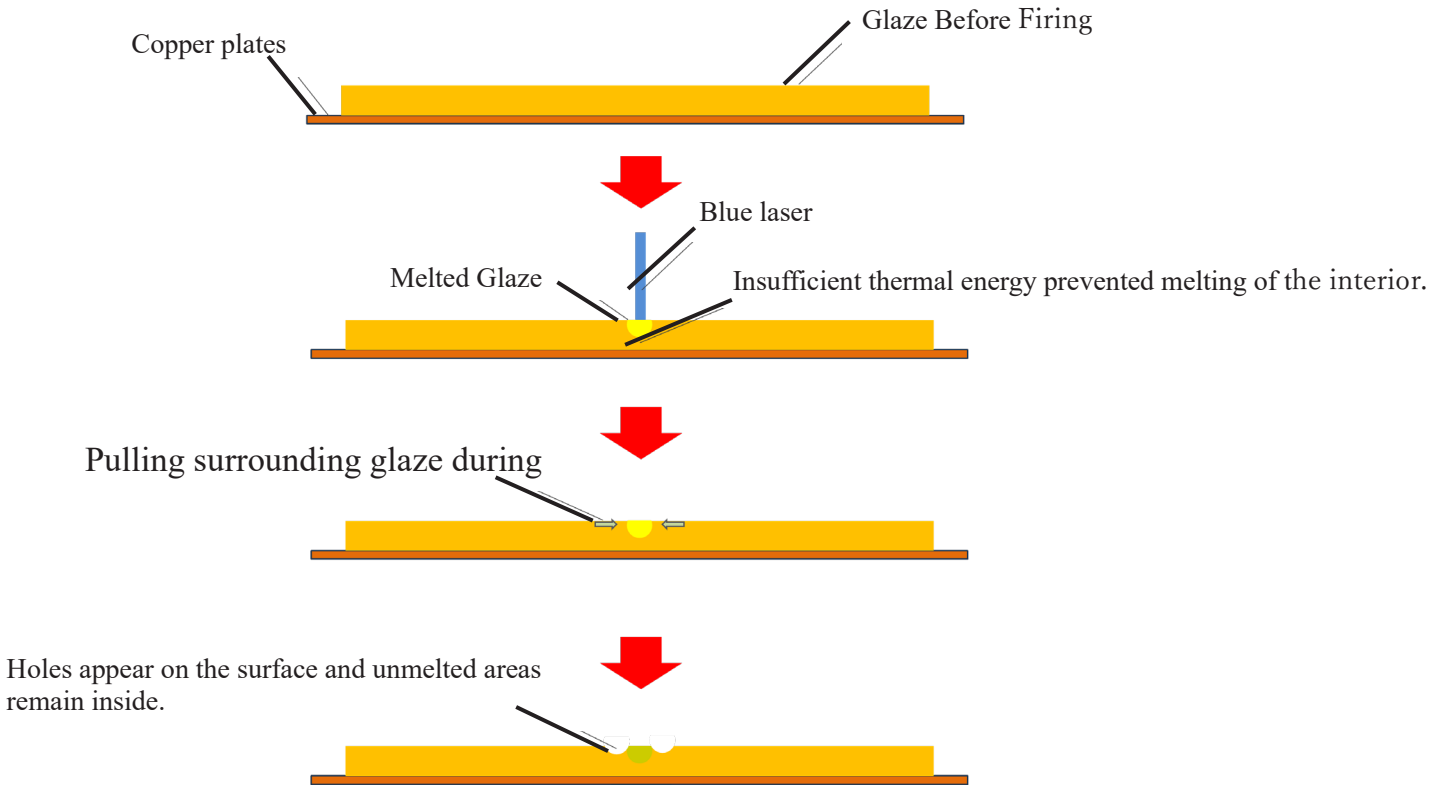

Fig. 8. Illustration of hole formation and unmelted material inside the glaze

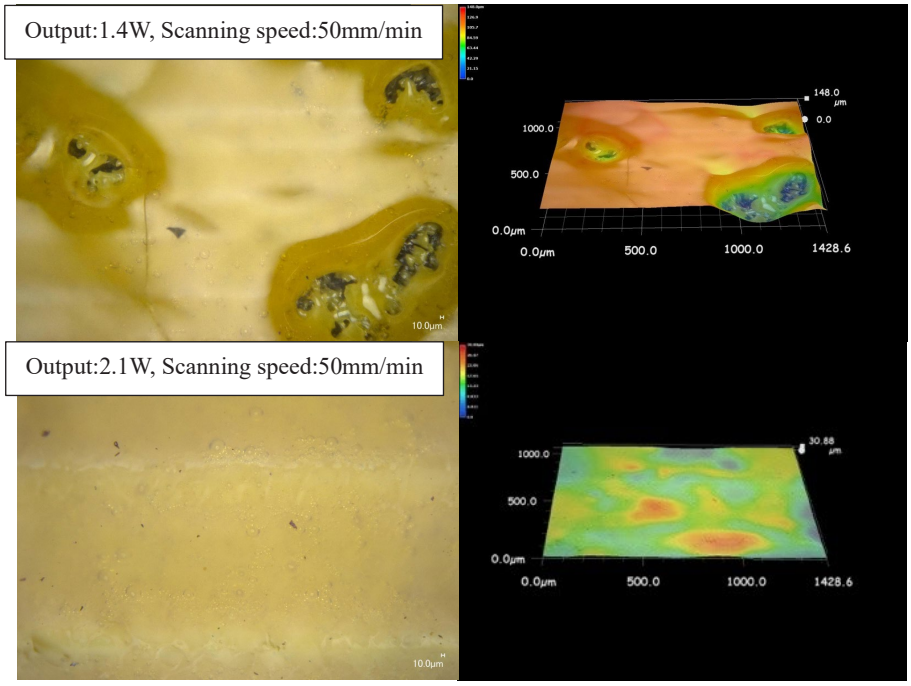

Fig. 9. Surface roughness of glaze after firing

Table 1. Surface roughness at amount of heat and scanning speeds

		Scan speed		
		50mm/min	75mm/min	100mm/min
Amount of heat	0.42J	102μm	170μm	162μm
	0.38J	69μm	33μm	56μm
	0.34J	31μm	29μm	36μm
	0.30J	148μm	184μm	166μm

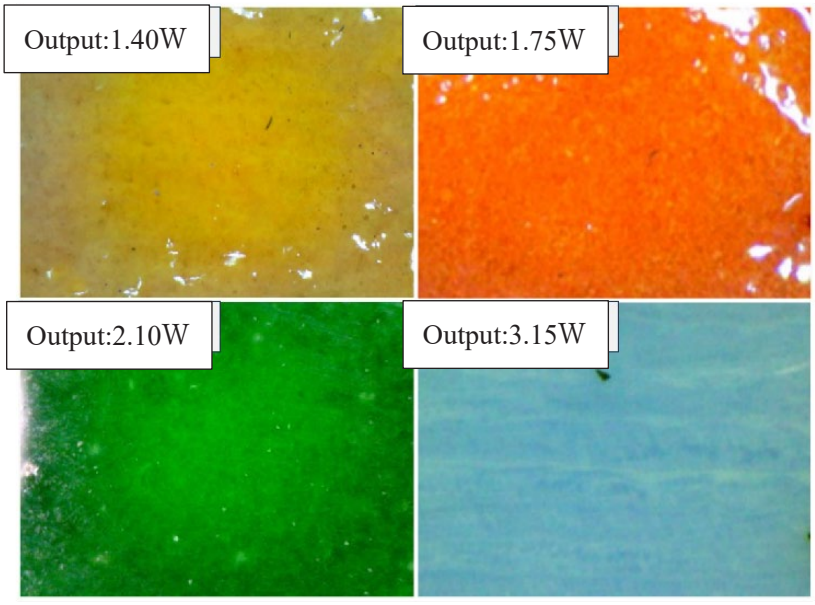

Fig. 10. Glaze firing results for different colors at a scanning speed of 50 mm/min

The effects of laser output and scanning speed on glaze firing were observed to determine optimal conditions. When only the laser was used, thermal energy was insufficient, and a uniform, smooth surface could not be obtained. By combining a heater with the laser, the thermal energy shortage was compensated, and glaze firing became possible. Heater assistance enabled the formation of a uniform glassy surface and significantly reduced unmelted areas on the glaze surface. Therefore, the approach of using both heater and laser is considered effective as a new glaze firing method. In particular, under the condition of 50 mm/min scanning speed and 1.40 W laser output, the most stable surface quality was achieved. Under this condition, unmelted areas and surface defects were minimized, and good smoothness was confirmed by roughness measurements using a digital microscope. From these results, it was clarified that heater assistance is useful for laser-based glaze firing. It was also confirmed that appropriate settings of laser output and scanning speed greatly affect quality. The findings of this study indicate new possibilities for applying laser firing techniques.

Results and Discussion

Glaze color changes before and after firing. This change occurs due to oxidation of coloring metals and variations in light reflection and refraction [7]. Therefore, differences in firing methods and conditions affect the final color tone. In this study, a spectrophotometer was used to compare samples fired in an electric kiln and those fired with a laser. Measurements were taken at five randomly selected points, and the average value was used for each sample. Electric kiln samples were prepared at 830°C for 2 minutes. The spectrophotometer results are shown in Table 2 and Fig. 11. From the L*a*b* color space diagram, yellow, orange, and green glazes showed values very close to those of electric kiln samples. In contrast, blue glaze shifted in the negative direction of b*, indicating a shift from yellow toward blue. The blue glaze used in this study contained cobalt. Cobalt is commonly used as a blue colorant, and its firing result is known to vary depending on oxygen concentration and temperature [8]. In this case, local oxygen deficiency during laser firing may have occurred, enhancing the blue color. An optical image of the blue glaze firing result is shown in Fig. 12. The stronger blue tone was also confirmed visually.

Table 2. Spectrophotometer measurement results

		L*	a*	b*	c*	h*
Yellow	Electric Kiln	59.3	12.1	53.2	54.6	77.1
	Laser	49.6	10.5	48.1	43.5	72.2
Orenge	Electric Kiln	46.5	42.6	44.0	61.2	45.9
	Laser	43.6	35.9	46.1	73.6	52.1
Green	Electric Kiln	25.3	-33.3	16.2	37.0	-25.9
	Laser	38.4	-30.4	17.3	35.0	-29.6
Blue	Electric Kiln	73.8	-1.1	-25.0	25.0	87.5
	Laser	60.8	1.7	-34.4	34.5	-87.2

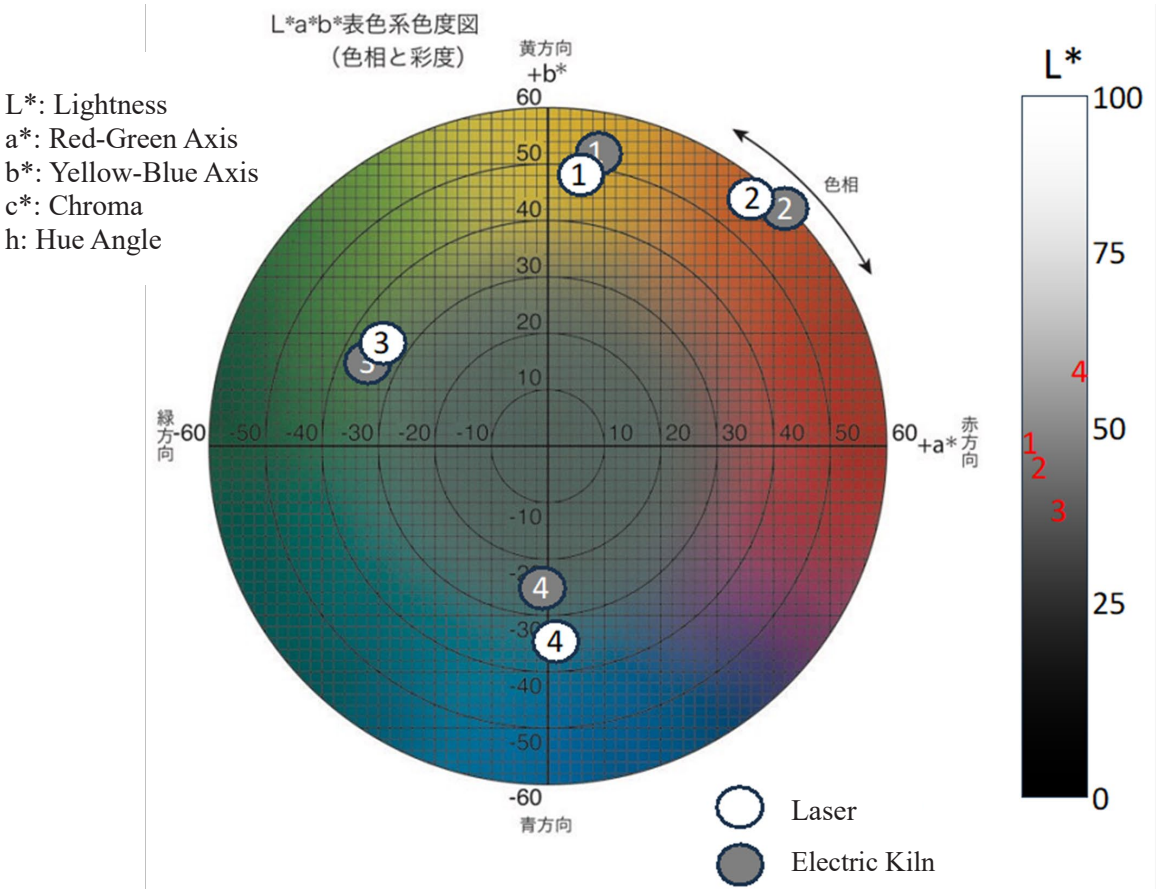

Fig. 11: Chromaticity Diagram in the L*a*b* Color Space Plotting the Results of Electric Kiln Firing and Laser Firing

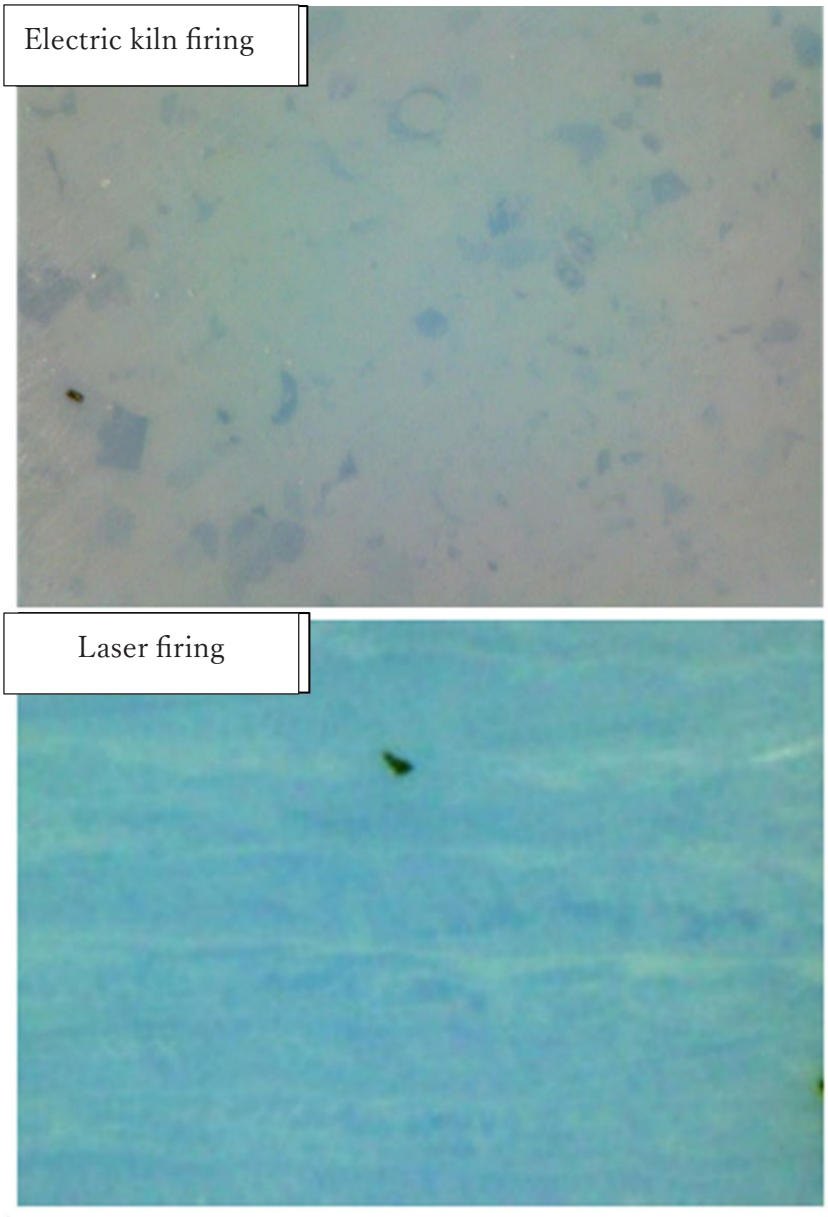

Fig. 12: Firing Results of Blue Glaze — a) Electric Kiln Firing, b) Laser Firing

A custom-made pencil hardness tester was used. The surface hardness of glaze fired by laser was compared with that of glaze fired in an electric kiln. The test was performed on fired glaze using pencils from 6H to 8H. The results are shown in Fig. 13. The test was conducted with pencils ranging from 3H to 8H. No scratches were observed at hardness levels of 6H or lower. From the test results, scratches appeared on the glaze surface starting from 7H for both laser-fired and electric kiln-fired samples. Therefore, the pencil hardness for both methods was determined to be 6H. It was confirmed that the surface hardness of glaze fired by laser was equivalent to that of glaze fired in an electric kiln. The main components of the glaze used were lead, silica, and metal oxides. These components are the primary factors determining the hardness of the glassy phase formed during melting and solidification. The reason why the hardness of laser-fired glaze was equivalent to that of kiln-fired glaze is considered to be the suppression of fine crystal formation due to rapid cooling during laser firing. As a result, the proportion of the glassy phase increased. This glassy structure was uniformly formed in both laser-fired and kiln-fired samples.

Therefore, no difference in hardness was observed. This result suggests that, under appropriate conditions, laser firing can achieve surface hardness comparable to electric kiln firing. The findings of this study provide useful fundamental data for the practical application of cloisonné production using laser technology.

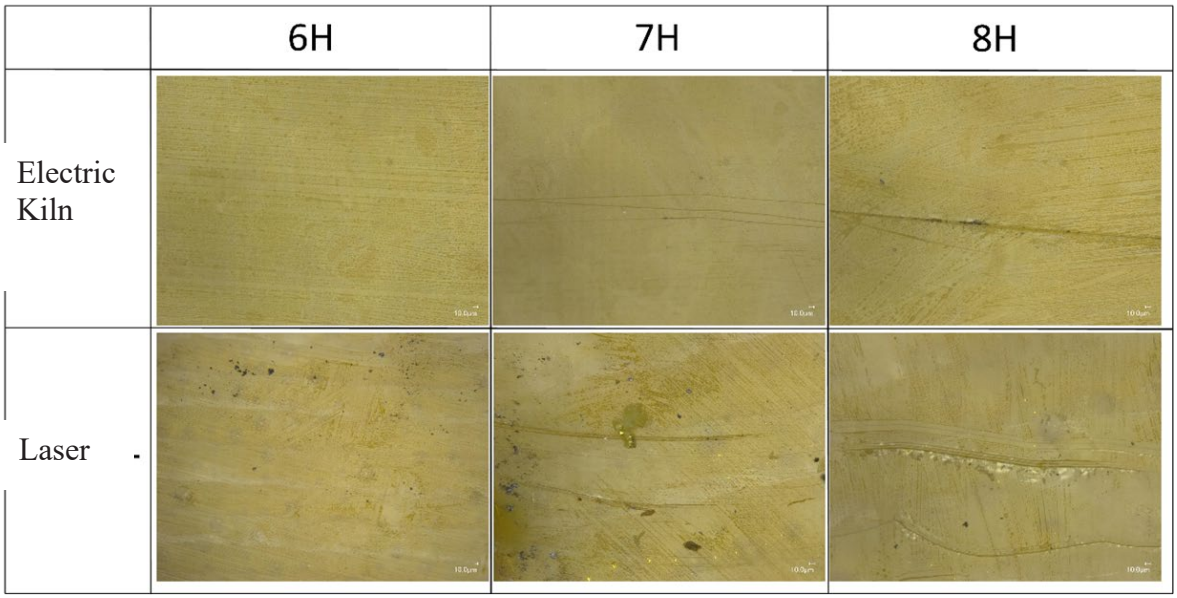

Fig. 13: Comparison of Electric Kiln Firing and Laser Firing Using a Pencil Hardness Tester

In general, cloisonné uses various colors to create patterns. Therefore, the boundary structure between different glazes fired by an electric kiln and by laser was observed using low-vacuum SEM. SEM images of the boundaries created by electric kiln and laser firing are shown in Fig. 14. Yellow glaze was used on the left side, and green glaze on the right side. In the sample fired in an electric kiln, it was confirmed that the glazes penetrated into each other. The boundary line was also found to be irregular. In an electric kiln, the entire surface melts slowly and remains at high temperature for a long time compared to laser firing. The specific gravity of the yellow glaze used was 3.14 g/cm^3, and that of the green glaze was 4.32 g/cm^3. Therefore, the melted glazes became fluid and promoted material diffusion at the boundary, causing the glazes to mix. On the other hand, in the boundary created by laser firing, the boundary line was clearly defined. Laser firing involves an extremely narrow heating area, and the time for mixing with adjacent glaze is very short. Thus, the color boundary became distinct. SEM observation confirmed that electric kiln firing formed boundaries where different glazes mixed, while laser firing produced clear boundaries. This result indicates that the localized heating characteristic of laser firing suppresses mixing and diffusion between glazes. This property enables precise design expression in cloisonné. It suggests that laser firing is useful as a new production technique.

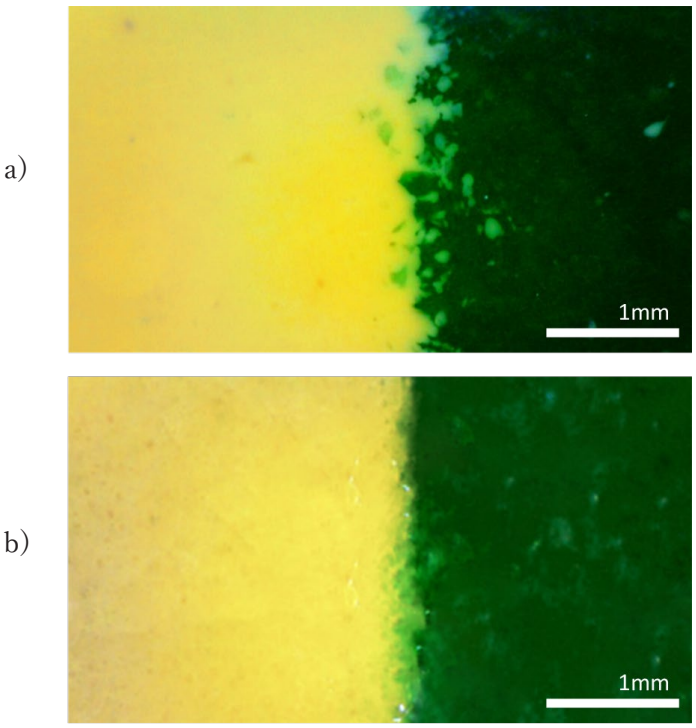

Fig. 14: Boundary Between Different Colors in a) Electric Kiln Firing and b) Laser Firing

The cross-sections of samples fired by laser and by electric kiln were observed using low-vacuum SEM. SEM images of the cross-sections are shown on Fig. 15. The samples were prepared using yellow glaze. Laser conditions were 1.4 W output and 50 mm/min scanning speed. In the sample fired in an electric kiln, no obvious voids were observed in the cross-section. In contrast, in the sample fired by laser, uniform voids were confirmed in the cross-section. These voids are considered to have formed because a surface layer solidified rapidly during firing, trapping internal bubbles. In electric kiln firing, heating and cooling occur gradually. Therefore, bubbles inside the glaze are slowly released, making void formation less likely. In contrast, in laser firing, cooling progresses rapidly. As a result, bubbles inside the glaze solidify before they can escape to the surface. This makes voids more likely to remain in the center. In addition, slight voids were observed near the copper plate even in electric kiln firing. This is because the glaze near the substrate melts less easily than the surface, causing bubbles to solidify before rising.

Furthermore, the small bubble size reduces buoyancy, which also contributes to this phenomenon. These results are attributed to differences in heating and cooling behavior during the firing process and to the behavior of gases inside the glaze. To suppress voids, improvements in glaze composition and optimization of firing conditions are important. The findings of this study provide useful insights into improving laser-based cloisonné firing technology. However, this paper focuses on exploring new possibilities for decorative items such as cloisonné. Surface color and roughness were found to be comparable to those of electric kiln firing. In terms of strength, pencil hardness tests confirmed adhesion to the substrate equivalent to electric kiln firing. Therefore, it was judged that there is no problem with functionality as a decorative item.

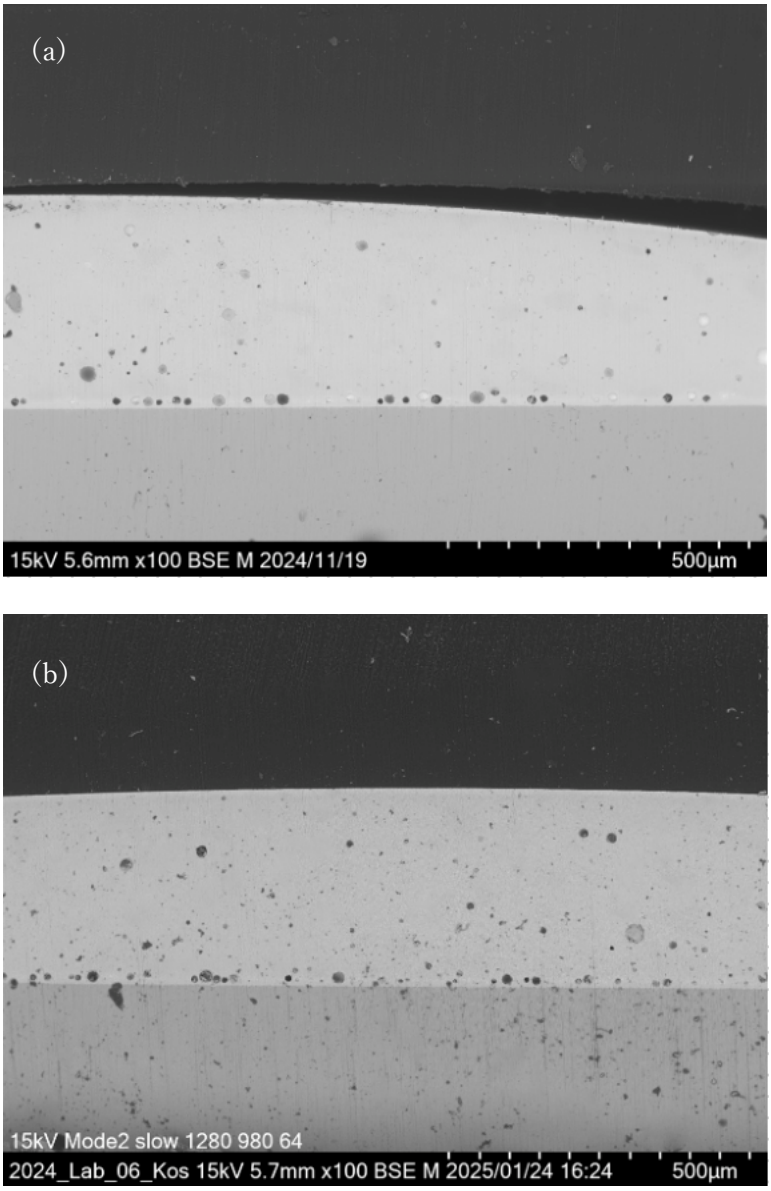

Fig. 15: SEM Images of Cross-Sections of Samples Prepared by (a) Electric Kiln Firing and (b) Laser Firing

A three-point bending test was conducted to evaluate the mechanical properties of the glaze and substrate and the interfacial bonding strength. The three-point bending test is a standard method for assessing bending strength and fracture behavior of materials. It is particularly suitable for evaluating the properties of brittle materials such as glaze. In this test, three samples fired in an electric kiln and three samples fired by laser were prepared. An illustration of the bending direction is shown in Fig. 16. The load-displacement curves obtained from the three-point bending test are shown in Fig. 17. For the electric kiln-fired samples, the load-time curve showed a linear increase immediately after the test began. After reaching a peak of 9.5–10.5 N, the load dropped sharply. This indicates that cracks occurred at the peak load and rapid fracture progressed because glaze is a brittle material. Afterward, the load remained around 7–8 N, and irregular waveforms were observed. This behavior is considered to result from progressive fracture of the glaze while the copper substrate continued plastic deformation at the center.

First, fracture occurred at the center where stress was concentrated. Then, as deformation progressed, fracture spread from the initial crack toward the edges in a chain-like manner. This mechanism is assumed to be the cause. For the laser-fired samples, the load-time curve increased linearly up to about 5 N. After that, the increase in load became gradual, and the load remained between 7–9 N. The linear region indicates elastic deformation. The subsequent gradual increase is considered to be due to plastic deformation of the substrate. SEM images of the cross-section revealed many voids near the substrate. However, no delamination was observed in the three-point bending test, suggesting that the effect of voids on adhesion was small. Although no delamination was confirmed in this test, an increase in voids could lead to delamination. Voids in the center of the glaze were more frequently observed in laser-fired samples. When voids exist, local stress concentration tends to occur inside the specimen. Especially under bending load, microcracks may initiate at voids and propagate, leading to early fracture. Therefore, this is considered one of the reasons why laser-fired samples showed lower strength compared to electric kiln-fired samples. SEM images of the glaze surface after the test are shown in Fig. 18. Laser-fired samples were confirmed to fracture in block-like patterns compared to electric kiln-fired samples. In laser firing, heat is transmitted locally from above and solidifies immediately after passing. Therefore, horizontal connectivity is weak, which is considered the reason for this fracture behavior. Furthermore, this block-like fracture pattern closely resembles that of tempered glass. Laser firing involves repeated rapid heating and cooling. This may have partially tempered the surface, creating a tempered glass-like structure.

This measurement was conducted as a preliminary study. Therefore, further tests are needed to determine whether the block-like fracture is due to partial tempering or weak horizontal connectivity caused by the laser firing process. From these results, it was confirmed that the bending strength of laser-fired glaze was about 5 N lower than that of electric kiln-fired glaze. This is due to rapid heating and cooling during laser firing, which weakened the bonding between adjacent glaze layers. In both electric kiln-fired and laser-fired samples, no delamination was observed. This result suggests that the interface bonding between glaze and substrate maintains sufficient strength even in laser firing.

This is an important factor for ensuring glaze stability during long-term use of decorative items.

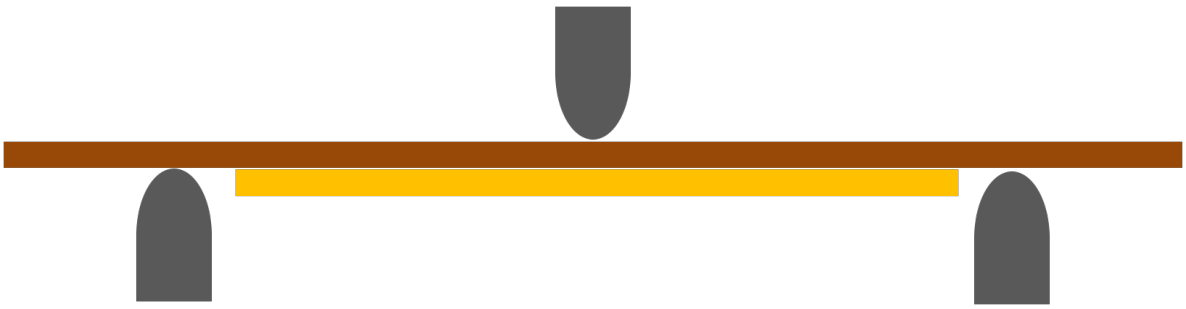

Fig. 16: Illustration of Bending Direction

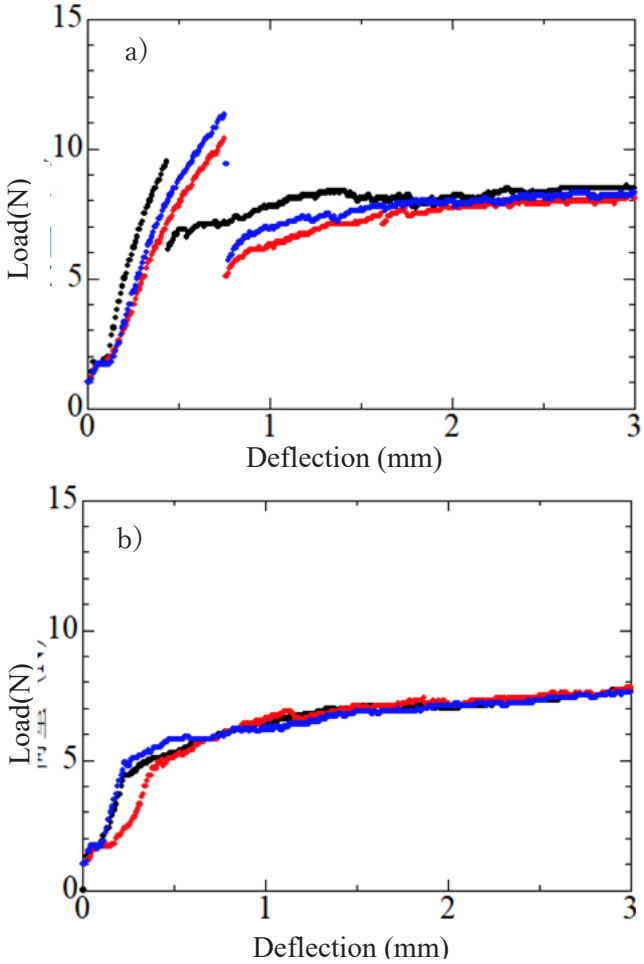

Fig. 17: Load–Deflection Curves Obtained from the Three-Point Bending Test — (a) Electric Kiln Firing, (b) Laser Firing

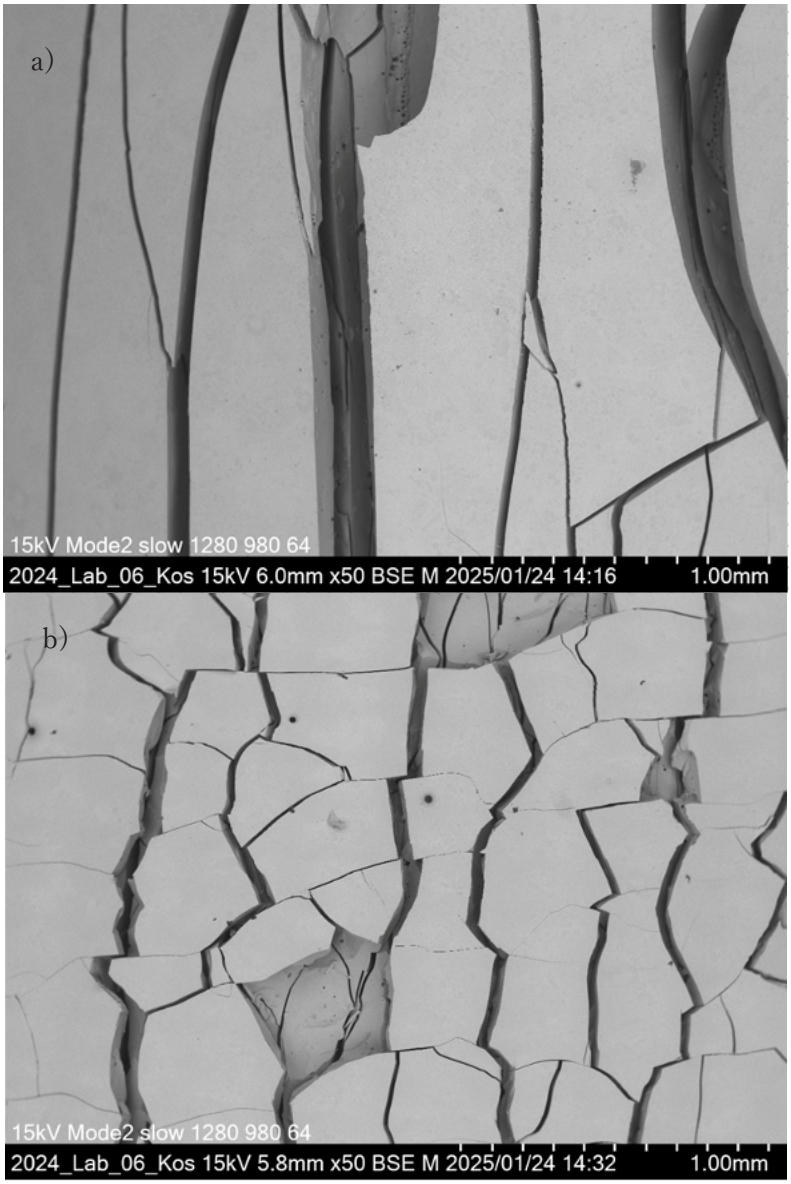

Fig. 18: SEM Images of the Glaze Surface After the Three-Point Bending Test for Samples Fired by (a) Electric Kiln and (b) Laser

The properties of laser-fired glaze were evaluated and compared with those of conventional electric kiln firing. The color tones of glazes fired by laser and by electric kiln were compared using a spectrophotometer. For yellow, orange, and green glazes, both firing methods produced almost identical color tones. In contrast, blue glaze showed a tendency for stronger blue coloration when fired by laser. This may have been caused by local oxygen deficiency during laser firing, which enhanced the blue color. In this experiment, color changes were particularly evident in blue glaze. However, other colors may also exhibit variations in color tone. The pencil hardness test showed that both laser-fired and electric kiln-fired glazes had a hardness of 6H. Equivalent surface hardness was confirmed for both methods. Low-vacuum SEM observation revealed that boundaries between different glazes were clear in laser-fired samples. In contrast, boundaries were ambiguous in electric kiln-fired samples, where mixing occurred. This suggests that the localized heating characteristic of laser firing suppresses mixing and diffusion between glazes. Such a property is considered useful for achieving precise design expression in cloisonné. Cross-sectional observation showed that voids were rarely observed

in electric kiln-fired samples. However, voids were confirmed in laser-fired samples. These voids are thought to result from rapid surface solidification during firing, which trapped internal bubbles. Nevertheless, appearance and strength were comparable to those of electric kiln-fired samples. Therefore, it was judged that there is no problem with functionality as a decorative item. On the contrary, the ability to create clear boundaries and fine patterns offers significant advantages for decorative applications.

Conclusion

In this study, the characteristics and potential of glaze firing using a laser were examined. Laser-based glaze firing was combined with heater assistance. This compensated for the thermal energy that was insufficient when using the laser alone. As a result, a uniform glassy surface was obtained. It was confirmed that the most stable surface quality was achieved under the condition of 50 mm/min scanning speed and 1.40 W laser output. In terms of color reproducibility, most glazes showed consistent results with electric kiln firing. However, for blue glaze, a shift from yellow toward blue was observed compared to samples fired in an electric kiln. Surface hardness was equivalent to that of electric kiln firing. This indicates that appropriate physical properties were maintained. Laser firing produced clear boundaries between different colors. This demonstrated that more precise design expression is possible compared to conventional electric kiln firing. However, voids were observed in the cross-section of laser-fired samples. This revealed challenges related to the cooling process and gas behavior during firing.

Acknowledgments

I would like to express my sincere gratitude to Professor Saiki and Associate Professor Hashizume for their invaluable advice and thoughtful guidance throughout the preparation of this thesis.

References

1. Yoshimura Y. My Handicraft Series New Cloisonné Techniques Playing with Colors. Tokyo: Mako-sha [in Japanese]; 1991.
2. Saito K. HOBBY GALLERY From cloisonné design to metal engraving cloisonné. Tokyo: Mako-sha [in Japanese]; 1990.
3. Merino RI, et al. Laser processing of ceramic materials for electrochemical and high temperature energy applications. Bol Soc Esp Ceram Vidrio. 2022; 61:19-39.
4. Zhu Y, et al. Recent advancements and applications in 3D printing of functional optics. Addit Manuf. 2022; 52:102682.
5. Liu J, et al. Effect of cooling rate on the crystallization and optical properties of silicate glasses containing ZnS. Ceram Int. 2023; 49:35414-35419.
6. Takaishi D. Recent study and development of glaze for pottery. NEW GLASS. 2020; 35:19-23.
7. Takeuchi N. Color and chemical state of metal elements in ceramic glaze. Chemistry & Education. 2008; 56:380-381.
8. Pinakidou F, et al. Transition metal chromophores in glass beads of the classical and Hellenistic period: Bonding environment and coloring role. Spectrochim Acta B. 2020; 171:105928.

ICPMAT 2025
1-4 December
Chiang Mai, Thailand
GOLD SPONSOR

2025 - 2026 INFORMATION

Faculty of Science

Chiang Mai University

คณะวิทยาศาสตร์

มหาวิทยาลัยเชียงใหม่

CMU
CHIANG MAI UNIVERSITY

FACULTY OF SCIENCE
CHIANG MAI UNIVERSITY

BE FUN TO THE FRONTIER
FUN
FUNCTIONAL
FUNDAMENTAL

International Collaboration

Number of MOUs / MOAs **119**

*Retrieved on 15 September, 2025

Chiang Mai, the prosperous city with natural resources and Lanna culture, is a 725-year-old city. The city's expansion is well-balanced, giving Chiang Mai its distinctive Thai character. Chiang Mai is one of the most popular tourist attractions. Since 2017, Chiang Mai has been a member of UNESCO's creative cities network under the "craft and folk art" branch.

In addition to being a city of culture and nature, Chiang Mai is a city of education, having institutes of all levels and national research institutes. This enables us the premier city for higher education. With the strengths of education, climate, geography, and biodiversity, we can learn and contribute to natural science research just by wandering around campus. It is possible to say that CMU is one of the greatest institutions for studying the natural sciences.

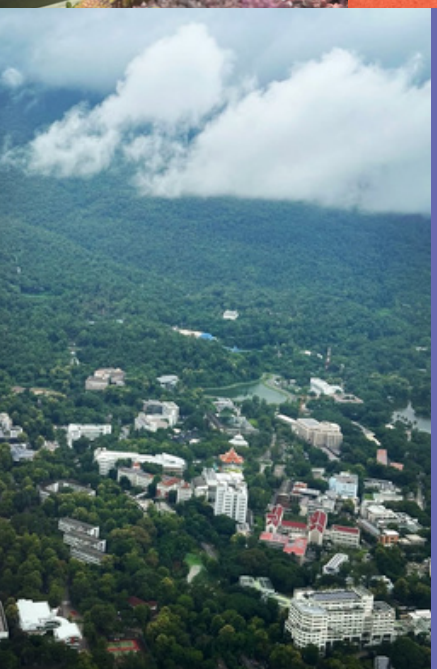

Contact Us

http://www.science.cmu.ac.th

Faculty of Science, Chiang Mai University

Science CMU Official

sci_cmu

sci_cmu

sci_cmu

@scicmu

Faculty of Science
Chiang Mai University
239 Huay Kaew Rd,
Suthep Sub-district, Mueang Chiang Mai District, Chiang Mai, 50200, Thailand
Tel : (+66) 53-222180
Fax : (+66)53-222268, (+66) 53-892274

Full version:
https://cmu.to/SciBrochure

English Version - Last updated : November 27, 2025
Published by Corporate Communication Affair
Faculty of Science, Chiang Mai University

ABOUT SCI CMU

The Faculty of Science as well as Chiang Mai University was established in 1964 along with two other pioneering faculties.

The Faculty currently consist of 33 fully equipped buildings occupying a total area of approximately 6 ha. Our mission is to produce global citizens with high quality education in both pure and applied science disciplines that serve local, national and international communities.

15 Bachelor's Degree Programs
- 14 Thai
- 1 International

17 Master's Degree Programs
- 1 Thai
- 11 Bilingual
- 5 International

A premier faculty driving sustainable development through science and innovation

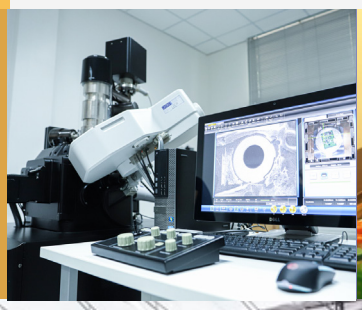

Science Society and Sustainability
Development of science, technology, and innovation applied for the benefit of communities and society, towards sustainable development.

FUN
At the Faculty of Science, we truly believe science can be both challenging and FUN and there are more to discover!

FUNCTIONAL
Science is everywhere! It is a functioning tool that is applicable toward everyday life, such as industries, innovation, technologies, creative communities and much more!

FUNDAMENTAL
We focus on investigation of fundamental science, leading to the deep science and deep technology, based on scientific knowledge.

Our departments

Currently, the Faculty of Science consist of 8 academic departments, 3 research centers and 2 service centers which drive our vision and mission based on faculty's values.






Departments: Chemistry, Industrial Chemistry, Biology, Physics and Materials Science, Geology, Mathematics, Statistics, Computer Science
Research Centers: Material Science Research Center (MSRC), Environmental Science Research Center (ESRC), Data Science Research Center (DSRC)
Service Centers: Science and Technology Service Center (STSC), Doi Suthep Nature Center (DSNC)

15 Doctoral Degree Programs
- 1 Bilingual
- 14 International

~ 2,500 Number of Bachelor's degree students (2024)

~ 250 Number of Bachelor's degree students (2024)

~ 200 Number of Doctoral degree students (2024)

~ 5MB Supported scholarship for undergraduate students (2024)

~ 200 Number of students through lifelong education system (2024)


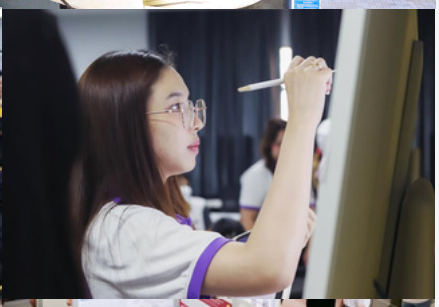


Research @Science CMU

The Faculty of Science focuses on international frontier research housed in laboratories equipped with advanced scientific apparatus. These facilities support both research and teaching and help to promote research excellence amongst our researchers.

Fundamental Research
- We investigate the state-of-art scientific knowledge which leads to the frontier researches. We also promote high-quality publications in the international academic journals.

Applied and Innovation Research
- We apply scientific knowledge to solve real-world problems via spinning off the researches to create innovations based on the strong fundamental science.

Targeted Research
- We aim to the goals set by the government and country policy. We also follow new research trends which lead to the future research directions.

Outreach Research
- We connect industries and users to obtain the research questions or connect the researches to users directly, which follow the sustainable development goals (SDGs).

≥550 Total number of research papers published in journal of SCOPUS database per year

≥45% Number of published paper in the first quartile of SCOPUS per year

230MB Internal and external research fund per year

~ 320 Number of academic staffs; More than 95% are PhD holders.

TOP 3 We are ranked in top 3 among Thailand's universities based on QS University Ranking.

ICPM 1-4 December Chiang Mai, Thailand 2025 GOLD SPONSOR

KEYENCE

KEYENCE products are engineered to be versatile,
so they can be used in every industry and solve a wide variety
of applications. We strive to offer the world's best products for today and
tomorrow's application needs.

3D Surface Profiler

VK-X3000 series

Digital Microscope

VHX-X1 series

Laser-based Elemental Analyzer

EA-300 series

KEYENCE (THAILAND) CO., LTD.
Tel: 02-078-1090 **Fax:** 02-369-2775 **Email:** info@keyence.co.th

KEYENCE

GOLD SPONSOR ICPMAT 1-4 December 2025 Chiang Mai, Thailand

3D Surface Profiler

Triple scan approach enables observation and measurement of any target

Highly accurate observation and measurement of any target is possible through the use of three different measurement principles: focus variation, laser confocal scanning, and white light interferometry.
Tasks that previously required multiple pieces of equipment can now be performed with a single device.

New product — 3D Surface Profiler VK-X3000

OBSERVATION AND IMAGING

Adaptive lighting and true-color imaging enables observation of samples under different lighting conditions, allowing minute surface defects to be identified. Magnification up to 28,800x allows for capturing of SEM-like images, with no sample prep.

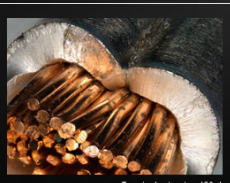
Terminal crimping (50×)

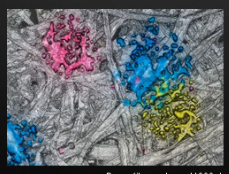
Paper fibrous toner (1000×)

MEASUREMENT AND ANALYSIS

Profile, roughness, film thickness, and additional 2D and 3D measurements can be performed for unprecedented surface analysis. Advanced programming capabilities streamline the measurement process, and ensure repeatable results.
Automatic comparison of samples across 42 roughness parameters provides clear and immediate analysis of how the sample surfaces differ.

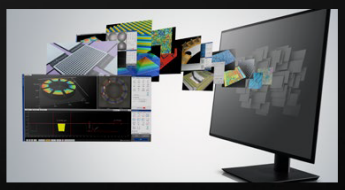

3D Surface Profiler - Triple Scan

Millimeter, micrometer, and nanometer measurements in one device

FOCUS VARIATION

Fast measurement over a large area

Up to 50 x 50 mm areas can be scanned, so the entire surface of the sample can be measured and analyzed.

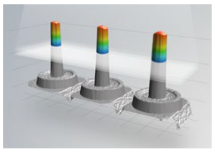

- Measurement results in seconds
- Analyze large height changes
- Guaranteed accuracy even at low magnification

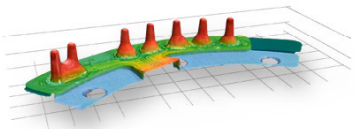

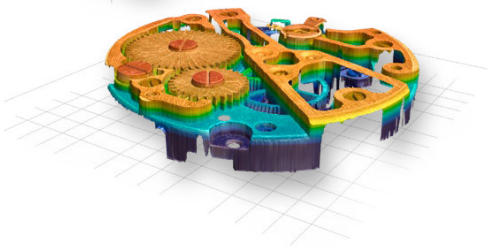

LASER CONFOCAL

Measure nearly any shape and material

Transparent, mirrored, and matte surfaces can be measured, as well as samples with steep angles or rough surfaces.

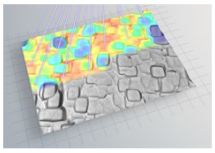

- Material independent results
- High lateral resolution
- Surface roughness quantification

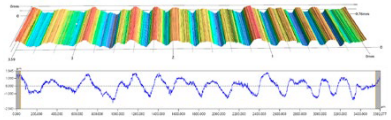

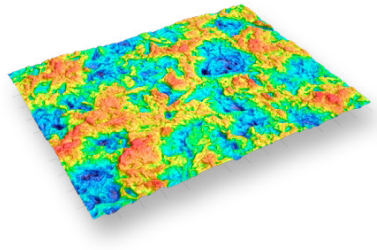

WHITE LIGHT INTERFEROMETRY

High-resolution data for high-precision surfaces

Accurately measure minute changes in shape at the nano level, even the finest surface features can be quantified.

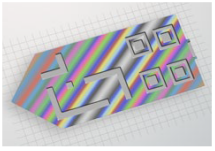

- 0.01 nm Z resolution
- Detect the smallest surface changes
- Measure flatness over a wide area

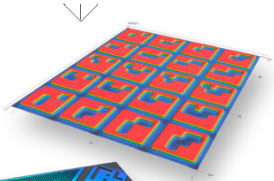

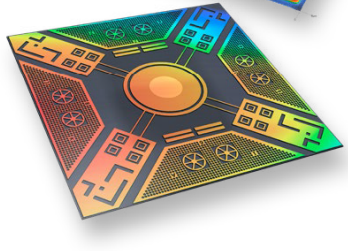

KEYENCE

CALL TOLL FREE TO CONTACT YOUR LOCAL OFFICE **1-888-KEYENCE** 1-888-539-3623

www.keyence.com

SAFETY INFORMATION Please read the instruction manual carefully in order to safely operate any KEYENCE product

CONTACT YOUR NEAREST OFFICE FOR RELEASE STATUS

KEYENCE CORPORATION OF AMERICA
500 Park Boulevard, Suite 200, Itasca, IL 60143, U.S.A. **PHONE:** +1-201-930-0100 **FAX:** +1-855-539-0123 **E-mail:** keyence@keyence.com

KEYENCE CANADA INC.
E-mail: keyencecanada@keyence.com

KEYENCE MEXICO S.A. DE C.V.
E-mail: keyencemexico@keyence.com

KA12-1109
VK3in1-KA-TG4-US 2061-1 611R37

ICPM 17 1-4 December 2025 Chiang Mai, Thailand **GOLD SPONSOR**

Bara Scientific

Solution of Success

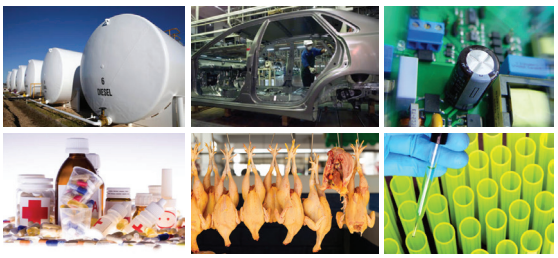

บริษัท พาราไชแอนติฟิค จำกัด เป็นบริษัทชั้นนำของประเทศ ในการนำเข้าและให้บริการแบบครบวงจร สำหรับเครื่องมือวิทยาศาสตร์ และเครื่องมือทดสอบด้านวิศวกรรม จากผู้ผลิตชั้นนำที่มีชื่อเสียงของโลก โดยเฉพาะอย่างยิ่งบริษัทฯ ได้เป็นตัวแทนจำหน่ายแต่เพียงผู้เดียวในประเทศไทย สำหรับเครื่องมือวิทยาศาสตร์ และเครื่องทดสอบของ **Shimadzu** ซึ่งเป็นบริษัทชั้นนำของประเทศญี่ปุ่น มานานกว่า 30 ปี

เพื่อให้ลูกค้าของบริษัทฯได้รับความพึงพอใจสูงสุด บริษัทฯได้มีการพัฒนาประสิทธิภาพในการให้บริการแก่ลูกค้า โดยได้มีการนำระบบ **คุณภาพมาตรฐาน ISO 9001:2015** มาใช้ในการบริหารงาน และบริษัทฯ ยังสามารถให้ **บริการสอบเทียบเครื่องมือตามมาตรฐาน ISO/IEC 17025 :2005** สำหรับเครื่อง UV-VIS Spectrophotometer และเครื่อง Universal Testing Machine และจะขยายขอบเขตเพื่อให้ ครอบคลุมการสอบเทียบเครื่องมือชนิดอื่นๆต่อไป

และการที่ บริษัท พาราไชแอนติฟิค จำกัด เป็นบริษัทใน **กลุ่มบริษัทพาราวินเซอร์ จำกัด** ซึ่งเป็นองค์กรขนาดใหญ่ชั้นนำของประเทศ ทำให้บริษัทฯ มีศักยภาพสูง สามารถให้บริการลูกค้าได้ทุกระดับ ซึ่งรวมถึงการจัดซื้อ ที่เป็นโครงการขนาดใหญ่

สำหรับลูกค้าของบริษัทฯ ได้ครอบคลุมทั้งกลุ่มลูกค้าราชการและเอกชน เช่น

- มหาวิทยาลัยและสถาบันการศึกษาต่างๆ
- กรม-กองของภาครัฐบาล
- สถาบันค้นคว้าวิจัยด้านวิทยาศาสตร์
- อุตสาหกรรมอาหารและการเกษตร
- อุตสาหกรรมยา
- อุตสาหกรรมปิโตรเคมี/โพลีเมอร์/เคมี
- อุตสาหกรรมยานยนต์
  อุตสาหกรรมไฟฟ้าและอิเลคทรอนิคส์

BSC Customer Support Center

ศูนย์บริการลูกค้าแบบครบวงจร (Customer Support Center)
บริษัท พาราไชแอนติฟิค จำกัด มาตรฐาน ISO 9001:2015 , ISO/IEC 17025:2005


Laboratory & Training Center


BSC Calibration Center


Technical Support Center


Rayong Branch


Sales & Marketing Center


Ayutthaya Branch


Collaboration Center

BARA SCIENTIFIC
Solution of Success

Bara Scientific Co., Ltd.
968 U Chu Liang Building Floor7
Rama 4 Road Silom Bangrak Bangkok 10500 Thailand
Tel : 02-6324300 (auto 20 lines) Fax : 02-6375496-7
www.barascientific.com

BARA SCIENTIFIC
Solution of Success

World Class Product Support for Science & Technology


SMX-1000 Plus

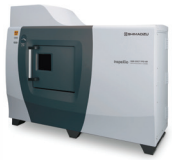
inspeXio SMX-225CT FPD HR


Universal Testing Machines


LCMS Q-TOF


Imaging Mass Microscope

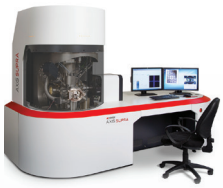
Imaging X-Ray Photoelectron Spectrometer

SHIMADZU
Excellence in Science

One Stop Shopping of Shimadzu Human Technology

Analytical Instruments

Spectrophotometric
- UV-VIS Spectrophotometer
- Atomic Absorption Spectrophotometer
- Inductively Coupled Plasma Spectrometer
- Inductively Coupled Plasma Mass Spectrometer
- Spectrofluorophotometer
- Fourier Transform Infrared Spectrophotometer
- Infrared Microscope

Chromatographic
- High Performance Liquid Chromatograph
- Gas Chromatograph

Mass Spectrometer
- LC-MS/MS (Triple Quadrupole)
- LCMS-Q-TOF MS
- LC-MS (Single Quadrupole)
- GC-MS/MS
- GC-MS

Life Science Research
- Imaging Mass Microscope
- MALDI TOF(/TOF) Mass Spectrometer
- Microorganism Identification (MALDI TOFMS)
- Microchip Electrophoresis (DNA/RNA Analysis)
- Functional Near-infrared Spectroscopy System for Research

Physical Properties Analyser
- Thermal Analyzer
- Particle Size Analyzer
- Total Organic Carbon Analyzer

Scientific Equipment

Elemental Analyzer Group
- Energy Dispersive X-Ray Fluorescence Spectrometer
- Optical Emission Spectrometer

Surface Analyzer Group
- Scanning Probe Microscope
- Electron Probe Micro Analyzer
- X-Ray Photoelectron Spectroscopy

Testing Machine
- Universal Testing Machines
- Fatigue Tester Machine
- Hardness Tester
- Viscosity Testers
- Special Purpose Tester

Non-Destructive Testing
- X-ray Fluoroscopy and CT System
- Microfocus X-Ray CT System
- Special X-Ray CT System

Informatics
- LabSolutions CS
- LabSolutions Bix
- Caliber LIMs

GL Sciences Inc.

GC & HPLC Accessories
GC & HPLC Column & Accessories
Equipment for VOCs & Positive List

DAICEL

CHIRALPAK® CHIRALCEL® CROWNPAK®
Chiral Stationary Phase

Shodex

Shodex HPLC Column
Sugar Analysis Column
GPC Column

MBRAUN

Inertgas Technology
Glove Box System
Solvent Purification System

KUBOTA

Centrifuges
Table-top Centrifuge
High Speed Refrigerated Centrifuge

EYELA

Laboratory Equipment
Rotary Evaporators
Low Temperature Circulator

TOKI SANGYO

Viscosity Measurement
Portable Viscometer
Digital Viscometer

TAITEC

Shaker Technology
Incubator Shaker
Water Bath

SIBATA

SIBATA
Mini pump is a small, light-weight, portable air sampling suction pump (air pump)

NMReady

Desk Top NMR
NMReady-60MHz : 1H, 7Li, 13B, 13C, 19F, 31P
NMReady-100MHz : 1H, , 13C, 19F, 31P

AS ONE

AS ONE
General Lab Equipment
Consumable & Supplies

Biotage

Sample Preparations, Purification and Chemical Synthesis
Automated Sample Preparation Instruments
Flash Purification Chromatography

IES

Isolate Extraction Systems Inc.
Supercritical Fluid CO2 Extraction
Commercial Series (10, 20, 40 L)

Greatwall

Greatwall
Glass Reactor
Rotary Evaporator

BARA SCIENTIFIC
Solution of Success

Bara Scientific Co., Ltd.
968 U Chu Liang Building Floor7
Rama 4 Road Silom Bangrak Bangkok 10500 Thailand
Tel : 02-6324300 (auto 20 lines) Fax : 02-6375496-7
www.barascientific.com

ICPM 1-4 December Chiang Mai, Thailand 2025 SILVER SPONSOR

"BRIDGING SCIENCE INSPIRING POSSIBILITIES."

Scan for Website

ITS (Thailand) Co., Ltd. an ISO 9001:2015 certified company, was founded in 1992 with the aim to help local communities progress through research and development. We do this by making high-quality research equipment readily available to the scientific community in Thailand.

OUR PARTNERS

KEM KYOTO ELECTRONICS MANUFACTURING CO.,LTD.

Automatic Potentiometric Titrator, Karl Fischer Moisture Titrator, Density/ Specific Gravity Meter, Electromagnetically Spinning Viscometer

BROOKFIELD AMETEK

Viscometer, Texture Analyzer

MERCK

Water Purification System

VACUUBRAND

Diaphragm pump, Rotary vane pump

BÜCHI

Freeze Dryer, Spray Dryer, Rotary Evaporator, Flash Chromatography

MICROTRAC PARTICLE CHARACTERIZATION

Particle Size and Shape Analyzer, Stability Analyzer, Surface Area and Pore Size Analyzer, Gas Pycnometer, Catalyst Analyzer

POROMETER

Pore Size Measurements of Porous Materials

SILVERSON

High Shear Mixer

OHAUS

Centrifuge, Hotplate

ABET TECHNOLOGIES Function Focused Innovation

Solar Simulators

AG! Asahi Glassplant Inc.

Short Path Evaporation System/ Glass Reactor

AMETEK SCIENTIFIC INSTRUMENTS

Materials Test and Electrochemical Analysis/ Potentiostat / Galvanostat, Battery Analyzer

BIOINICIA

Electrospinning & Electrospraying Equipment

elementar EXCELLENCE IN ELEMENTS

Elemental Analyzer CHNOS Cl / TOC and water Analyzer, Isotope Ratio Mass Spectrometer

inert

Glovebox System Solvent Purification System

C-THERM TECHNOLOGIES

Thermal Conductivity

setaram KEP TECHNOLOGIES

Thermal Analyzer (TGA, DTA, DSC,TMA)

Biometrics Quality of life

UV Spectrometer, Microwave Digestion System, Mini HPLC, Moisture balance

microlight3D

Micro Scale 3D Printing, Maskless Lithography for Rapid-Prototyping

SCS SPECIALTY COATING SYSTEMS A KISCO Company

Spin coater, Ionograph contamination Tester

RENISHAW apply innovation™

Raman Confocal Microscope Spectrometer, Raman Analyzer, SEM Raman Interface

tousimis

Critical Point Dryer

THALESNano

Benchtop Continuous Flow Chemistry Reactor

BRAND

Dispenser, Pipette

SUPERCRITICAL FLUID TECHNOLOGIES

Cannabis SFE SYSTEM

xplore

Twin-Screw Micro Compounder

GETINGE LANCER | ULTIMA

Washing Machine

LIEBHERR

Refrigerator

huber

Thermostat, Chiller

Teclis Scientific

Drop Tensiometer, Foam analyzer

memmert

Oven, Water bath

Nabertherm

Furnace

ITS (Thailand) Co., Ltd.
47/1 & 49/1 Soi Preeyanuch, Rama 9 Road, Bangkapi, Huaykwang, 10310 Bangkok, Thailand.
Tel: +66 2 3691793
Fax: +66 2 369 1794
Email: info@its-thailand.com

In-Situ correlative Raman spectroscopy and SEM analysis from Renishaw

Raman spectroscopy is a non-contact and non-destructive optical technique which is superior at providing detailed information on the identity and chemical structure of materials. Each molecule has its own unique Raman spectrum, which provides insights into various chemical bonds and their characteristics.

On the other hand, scanning electron microscopy (SEM) deploys an electron beam to probe the sample instead of a visible light source, it provides much higher magnifications and can resolve structures down to a few nanometers. In addition to producing highly detailed images, conventionally, SEM can be combined with energy-dispersive X-ray spectroscopy (EDS) to reveal the elemental composition of the sample. However, SEM-EDS does not provide information about chemical bonds or structure within a sample.

In this presentation, we would like to showcase recent technological advancement from Renishaw on the integration of a Raman spectroscopy system with a scanning electron microscope (SEM) and present several applications demonstrating the advantages of correlative microscopy using these technologies. The molecular information provided by Raman spectroscopy complements the ultrastructural details from SEM imaging, providing comprehensive insights into the chemistry and structure of the samples.

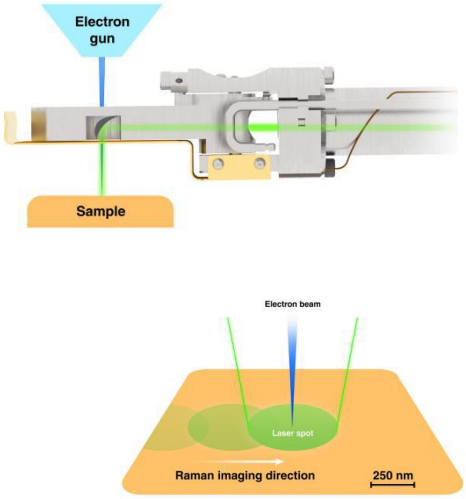

Speaker: Dr. Tan See Hua , Renishaw Plc.

ICPMAT 2025 1-4 December Chiang Mai, Thailand BRONZE SPONSOR

KINETICS *Your best partner in materials research*

EQUIPMENT FOR

Materials Research & Testing

CONTACT US

Kinetics Corporation Ltd.
T 02 515 8999 (ext.8940)
E mat@kinetics.co.th
W www.kinetics.co.th

THERMAL ANALYSIS INSTRUMENTS
(Dilatometer / Heating Microscope / TMA / TGA / DSC / ...)

THERMAL CONDUCTIVITY ANALYZERS
(Heat Flow Meter / THB Analyzer / LFA / ...)

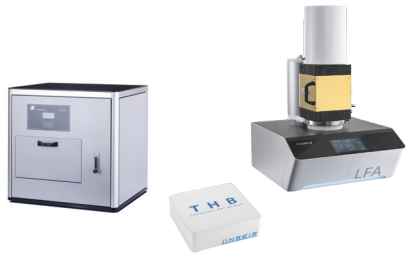

NANO-SCALE IMAGING AND SPECTROSCOPY
(SEM / AFM / AFM-IR / NANO-RAMAN / ...)

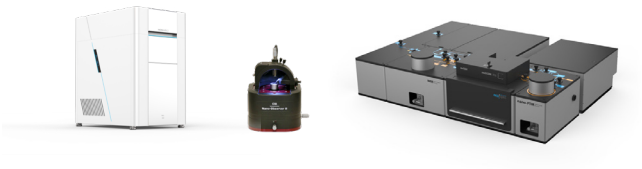

IMPEDANCE TUBE
(Sound absorption)

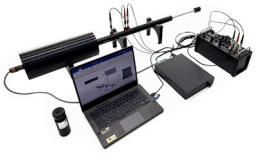

APPLICATION FIELDS

Ceramics
Building materials
Polymer / Rubber
Composites
Semiconductor
Thin film
Thermoelectric
Piezoelectric
Photovoltaic
Energy storage
Battery
...

PIEZOELECTRIC CHARACTERIZATION SYSTEM

SPARK PLASMA SINTERING (SPS) MACHINE

ELECTROSPINNING MACHINE

MORE PRODUCTS AVAILABLE

FEATURED PRODUCTS / FOR ADVANCED MATERIALS RESEARCH

nano-IR / nano-Raman

attocube
WITTENSTEIN group

A complete imaging and spectroscopic materials chatacterization system with 3-techniques in 3-scales

ระบบวิเคราะห์สมบัติเฉพาะวัสดุเชิงภาพและสเปกตรัมแบบครบวงจร
ด้วย 3 เทคนิค ใน 3 ระดับสเกล

attocube systems GmbH

Germany, Haar

Founded: 2001

IRa-SCOPE

IRa-SCOPE เป็นการผสานเทคนิคการวิเคราะห์ 3 รูปแบบ คือ LDIR, Raman และ nano-IR ไว้ด้วยกัน เพื่อให้ได้ข้อมูลเชิงโครงสร้าง และเคมีอย่างละเอียดภายในเครื่องเดียว

เหมาะกับการวิเคราะห์วัสดุหลายประเภท ตั้งแต่พอลิเมอร์ เซมิคอนดัคเตอร์ ไปจนถึงสารชีวภาพ ด้วยความแม่นยำสูง และการใช้งานที่สะดวกในสภาพแวดล้อมทั่วไป

SCALE : ***micron***

LDIR Spectroscopy

เทคนิค Laser Direct Infrared สแกนได้รวดเร็วเหมาะกับการใช้งานวิเคราะห์พื้นที่ตัวอย่างขนาดใหญ่ในระดับไมโครเมตร

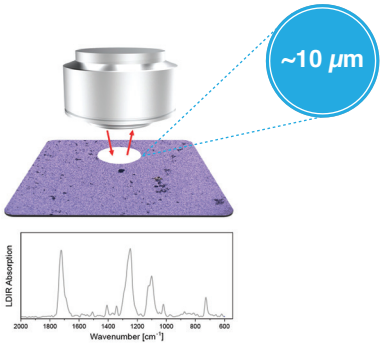

SCALE : ***sub-micron***

Confocal Raman

ระบบวิเคราะห์ raman ออกแบบเฉพาะสามารถวิเคราะห์สัญญาณอ่อนจากวัสดุ 2D material monolayers เช่น MoS_2

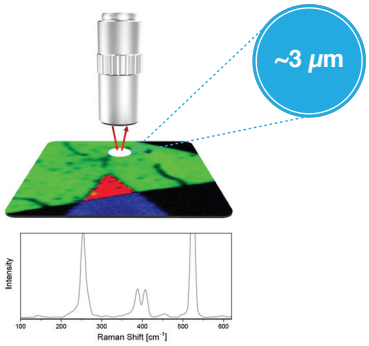

SCALE : ***nano***

nano-IR *(nano-FTIR / AFM-IR)*

เทคนิควิเคราะห์แสงอินฟราเรดระดับขั้นสูง 2 ชนิด สามารถวิเคราะห์ได้ทั้งวัสดุ organic และ inorganic ในสเกลระดับนาโน

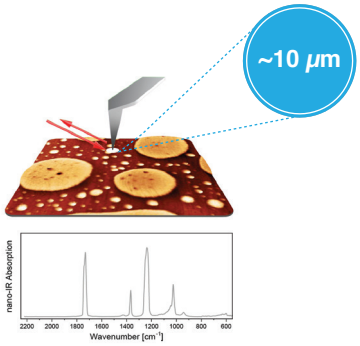

Correlative Raman & nano-IR Spectroscopy

สามารถวิเคราะห์สเปคตรัมรามานและอินฟราเรดในตำแหน่งเดียวกันบนตัวอย่างเดียว

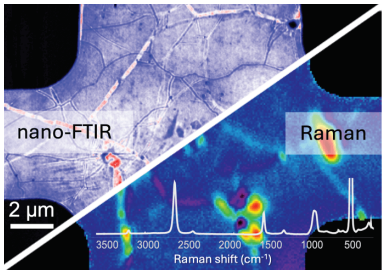

2D Materials

correlative analysis of graphene transistor device

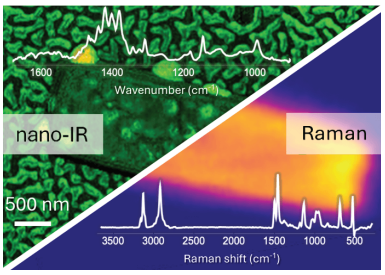

Catalysis

quality of micron-sized MOF crystallites

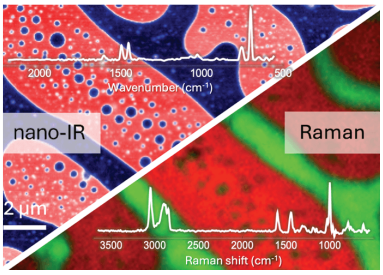

Polymers/nano-Plastics

interfaces of heterogeneous polymer blend

ICPMAT 2025 1-4 December Chiang Mai, Thailand

BRONZE SPONSOR

ESTD 2013

LAB CONNECTION

บริษัท แลบคอนเนคชั่น จำกัด

- จำหน่ายเครื่องมือและอุปกรณ์วิทยาศาสตร์
- ออกแบบ–ติดตั้งห้องปฏิบัติการครบวงจร (Turnkey Lab)
- บริการสอบเทียบ ซ่อมบำรุง และหลังการขาย
- ครบจบในที่เดียว สำหรับงานวิจัยและอุตสาหกรรม

THE CATALOG PORTAL

อัพเดตข่าวสาร FACEBOOK PAGE

LABCONNECTION LABORATORY CO.,LTD.

บริษัท ห้องปฏิบัติการแลบคอนเนคชั่น จำกัด

- ให้บริการรับทำวิจัย วิเคราะห์ และทดสอบทางวิทยาศาสตร์
- ให้เช่าเครื่องมือวิทยาศาสตร์
- ทีมผู้เชี่ยวชาญดูแล พร้อมให้คำปรึกษา
- สนับสนุนงานวิจัย พัฒนา และนวัตกรรม (R&D / QC)

www.labconnection.co.th
Tel: 052-000-452
Email: labcnt@hotmail.com

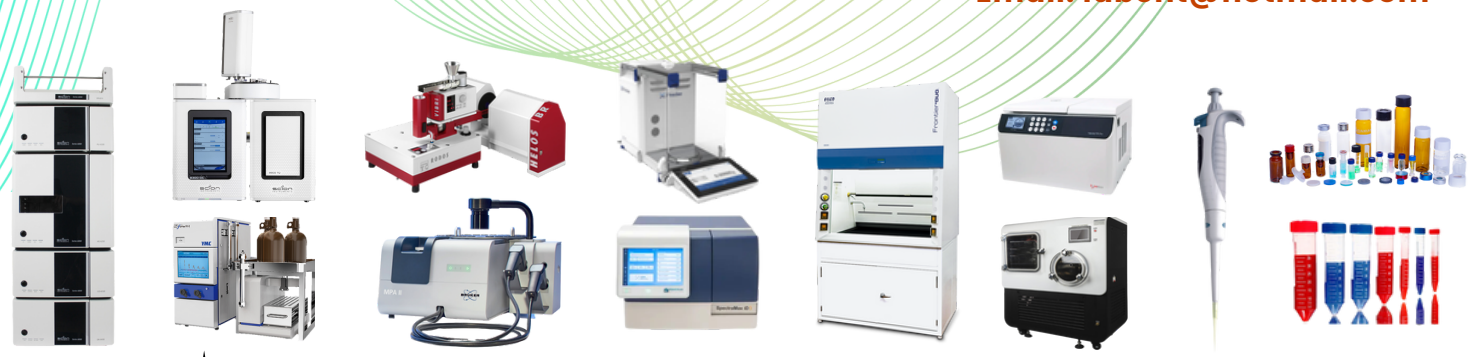

EXCLUSIVE

Equipment

- Exclusive Agent (best price, Solution, cover consumable to hi-end product.
- Service, PM, Repair, Validation

local applications

- ·ทีม application (Local, Center)
- ทีมที่ปรึกษา ISO17025
- ทีม back-upรวม method validation ได้

SERVICE

- one stop service
- เครื่องสำรอง ระหว่างรอซ่อม
- no travel cost ทั้งในประกันและหลังประกัน

ESTD 2013
LAB CONNECTION

analytikjena
An Endress+Hauser Company

LABCONNECTION
LABORATORY CO.,LTD.

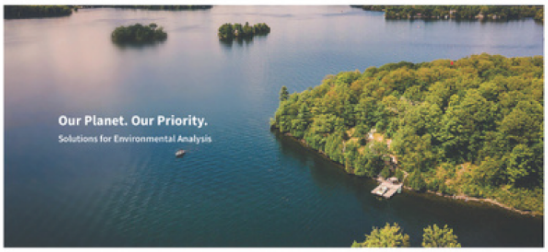

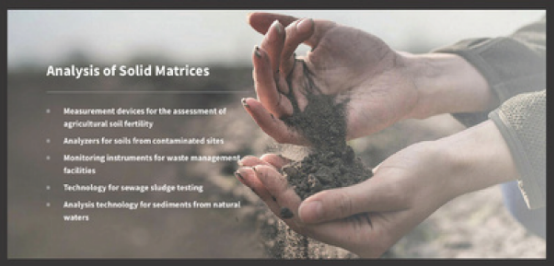

Innovative Analytical Solutions
Flexibility and Efficiency Across Applications

The Analytik Jena chemical analysis solutions provide you with highly sensitive, robust, and user-friendly devices for nearly every task in analytical chemistry. Our portfolio includes:

- Adsorbable organic halides (AOX)
- Carbon, nitrogen, sulfur, and chlorine analysis (CNSX)
- Atomic absorption spectrometry (AAS)
- Inductively coupled plasma mass spectrometry (ICP-MS)
- Inductively coupled plasma optical emission spectrometry (ICP-OES)
- UV/Vis spectroscopy
- TOC/TN_b analysis
- Sample handling and sample preparation

www.analytik-jena.com | email: sales@analytik-jena.co.th | Tel. 02-1062970

analytikjena
An Endress+Hauser Company

LC-ICP-MS
- Speciation: ใช้แยกสปีชีส์ของธาตุและประเมินระดับความเป็นพิษของธาตุแต่ละรูปแบบ
- authenticity/Origin verification: ยืนยันความแท้และแหล่งที่มาของตัวอย่าง จากลักษณะเฉพาะของอัตราส่วนไอโซโทปในธรรมชาติ (isotope ratio)

HR-ICP-OES PQ9200 Series
- **Fast device start-up** time of less than **ten minutes**
- log 6 Dynamic range
- **Argon-saving** up to 50 % lower gas consumption with stable, high-performance plasma.
- **robust plasma** and the **smallest footprint** on the ICP-OES market
- **Low detection limit** achieved through high-resolution optics, enabling precise analysis in complex matrices.

High-Resolution Continuum Source (HR-CS) AAS
ContrAA800 Series
- 1 lamp = 64 elements
- Fast multi-element analysis
- 10 Elements < 3 min.
- High-Resolution Optics
- Offers the best detection limit among all AAS techniques.

EA4000 C/S/ Cl Macro Analysis
Carbon species: TOC/TOC, TC,AC, OC, EC, BOC
in solids + (liquid)

www.labconnection.co.th
Tel: 052-000-452
Email: labcnt@hotmail.com

ICPMAT 2025 1-4 December Chiang Mai, Thailand
BRONZE SPONSOR

ICPM 2025 1-4 December Chiang Mai, Thailand

BRONZE SPONSOR

micromeritics®

SCIENCE AND TECHNOLOGY OF SMALL PARTICLES

MEGA MATT CO.,LTD.

MEGA MATT CO., LTD.
บริษัท เม็กกาแมทท์ จำกัด
Tel. +66 (0) 9 1953 5545
www.megamatt.co.th

SURFACE AREA AND POROSITY

- Pore size can be measured from 0.3nm to 300nm using a variety of different models

- Water vapor adsorption studies allow the investigation of a material's sensitivity towards water

POROSITY

- pore size, 3nm to 500 µm
- total pore volume
- total pore surface area
- percent porosity
- sample densities (bulk and skeletal)
- particle size

DENSITY

Combining data from these two techniques enables the determination of the percent porosity and total pore volume.

- true, absolute, and skeletal density
- apparent volume and density
- envelope volume and density bulk
- volume and density

PARTICLE SIZE

The SediGraph remains the global standard for particle size analysis by sedimentation after five decades, whether in a rugged production environment or a controlled laboratory setting.

POWDER RHEOMETER

- Resistance to flow in motion
- Shear strength
- Shear against the wall
- Bulk density
- Compressibility
- Permeability
- Aeration

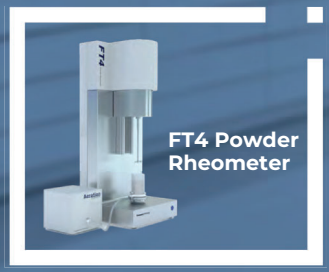

INTERACTIONS

Advance system for measurement of catalytic activity.

SURFACE AREA | POROSITY | DENSITY | PARTICLE INTERACTIONS | POWDER FLOW | PARTICLE SIZE

Carbon capture, utilization, and **storage,** CCUS, is an important portfolio of emissions reduction technologies. A clean energy future includes electric vehicles, **valorizing CO2** for synthethic fuels, and industrial plants using carbon capture.

CO_2 CAPTURE

Adsorbents, Membranes, and Catalysts

- Effect of water on performance
- Tailor pore size of membrane for application
- Optimize adsorption / desorption cycle to minimize cost

Applications

- Industrial Capture
- Amine Scrubber
- Direct Air Capture

CO_2 STORAGE

Adsorbents, Membranes

- Develop materials with high H2 adsorption
- Determine critical parameters to scale adsorbents
- Understand efficiency and lifetime of catalysts
- Maximize catalytic activity

Applications

- Metal Organic Framework
- Function-alized Porous Material
- Activated Carbon

CO_2 Utilization

Catalysts

- Optimize pore size of fuel cell membranes
- Use chemisorption to determine catalyst active area
- Adsorb/Desorb cycle optimization to minimize costs
- Study fuel cell efficiencies

Applications

- Synthetic Fuels
- Shipping E-NH_3, E-methanol
- Aviation E-kerosene

Hydrogen will play a key role in **decarbonization** as it supports **60%** of the **applications** with greenhouse gas (GHG) emissions.

HYDROGEN PRODUCTION

Adsorbents, Membranes, and Catalysts

- Optimize adsorption / desorption cycle to increase productivity and reduce cost
- Determine CO2 that can be adsorbed
- Maximize activity and lifetime of the catalyst
- Measure membrane pore size to optimize transport and reactivity

Applications

- Steam Reforming
- Biomass
- Green Electroylsis

HYDROGEN STORAGE

Adsorbents, Catalysts

- Develop materials with high H2 adsorption
- Determine critical parameters to scale adsorbents
- Understand efficiency and lifetime of catalysts
- Maximize catalytic activity

Applications

- Storage: MOFs, Zeolites, Carbon
- Synthesis CH_3OH, NH_3, HCOOH
- Hydrogenation LOHC, Metal Hydrides

HYDROGEN APPLICATION

Adsorbents, Membranes, and Catalysts

- Optimize pore size of fuel cell membranes
- Use chemisorption to determine catalyst active area
- Adsorb/Desorb cycle optimization to minimize costs
- Study fuel cell efficiencies

Applications

- Fuel Cells
- Ammonia, Fertilizer, Fuel
- Chemical Processes

Leica Metrology Products

Leica Visoria

Visoria P
Polarization Microscope

Visoria M
Material Microscope

Visoria B
Laboratory Microscope

Metal Industry Microscopy Solutions

Leica EM TXP
Polish cross-section

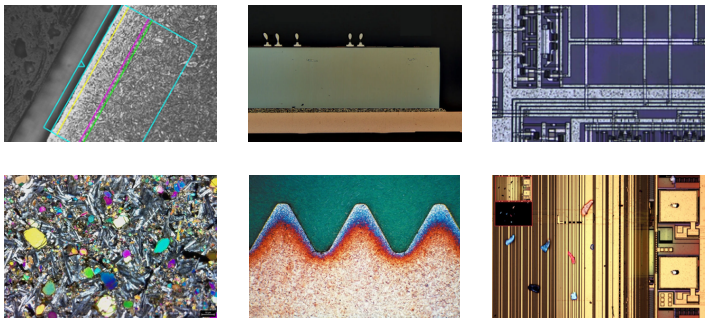

Leica EM TIC3X
Ion milling

Digital Microscope
DVM6

Leica DM8000,12000M
Wafer

Leica EM ACE200,600
Coating

HISTOCENTER
Beyond Instruments

HISTOCENTER (Thailand) Co., Ltd.
115, Rompo Mansion Building, Room A1, Rimthangrotfaisaipaknam Road, Klongtoey, Klongtoey, Bangkok 10110 Thailand.
T: +662 6713068 F: +662 6713069 Email : histothai@histocenter.com

ICPM 17 1-4 December 2025 Chiang Mai, Thailand BRONZE SPONSOR

Leica MICROSYSTEMS

Overview of industries and applications

R&D | Production | Quality | Failure analysis

Metals

Electronics & Electrical

Transportation

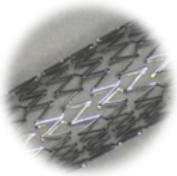

Medical Device

Academia & Research Institutes

Examples :

Microelectronic & Semiconductor :

- **Flat panel**
- **TFT displays**
- **Masks**
- **Wafer**
- **Solar cells**

Metals :

- **Multi sample analysis with the LAS X Steel Expert**

Transportation :

- **Multi sample analysis with the LAS X Cleanliness Expert**
- **Inspection of large samples**

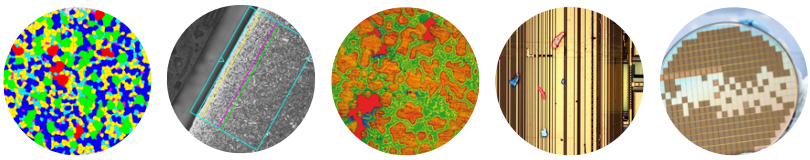

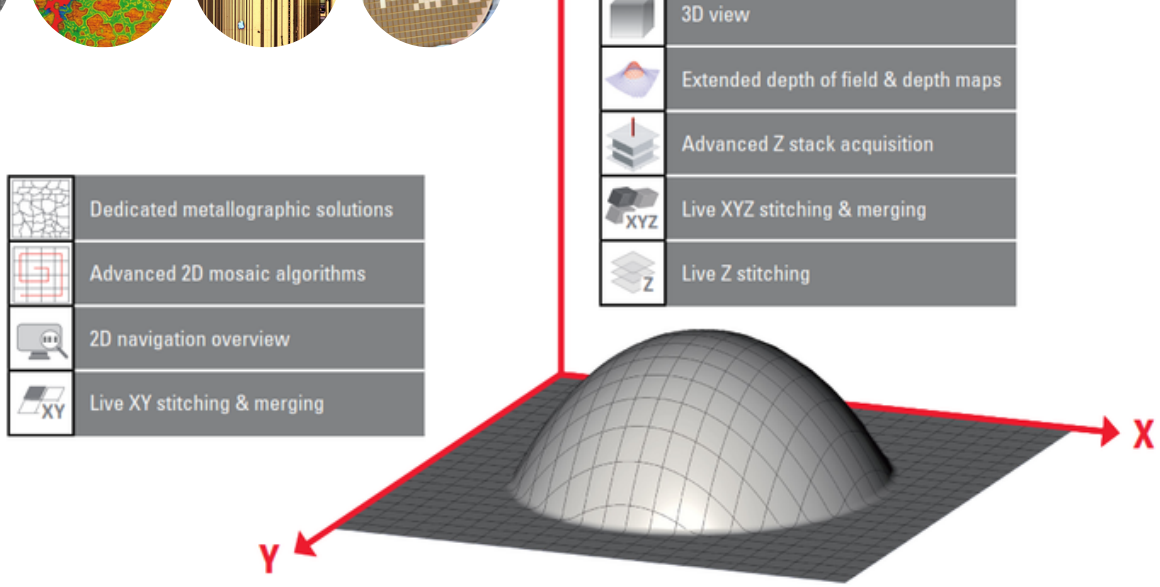

HISTOCENTER Beyond Instruments

HISTOCENTER (Thailand) Co., Ltd.
115, Rompo Mansion Building, Room A1, Rimthangrotfaisaipaknam Road, Klongtoey, Klongtoey, Bangkok 10110 Thailand.
T: +662 6713068 F: +662 6713069 Email : histothai@histocenter.com

Discover Together

By working with our customers to develop new approaches, Gatan and EDAX believe there are endless opportunities to explore the boundaries of electron microscopy and uncover new insights into your research. Let's discover together how to achieve your next breakthrough.

EDAX Orbis II Micro-XRF System

The EDAX® Orbis™ II micro-x-ray fluorescence (micro-XRF) system delivers non-destructive, high performance elemental analysis with unmatched flexibility and ease of use.

- Custom x-ray window technology enables the detection of light elements
- Proprietary coaxial light and x-ray optics precisely targets specific regions – eliminating x-ray interference from adjacent areas
- Maximizes throughput by collecting spectra 2.5x faster and spectral maps >3x faster
- Streamlines workflows with programmable autorun routines to boost productivity and ensure consistent, high-quality results

GIF Continuum K3 System with Stela

- Extends *Counted*EELS and EFTEM below 80 kV
- Optimal for energy-filtered diffraction, MicroED, and 4D STEM
- Captures weak and intense reflections with the highest dynamic range
- Utilizes DECTRIS hybrid-pixel technology

Cipher System for Lithium Analysis

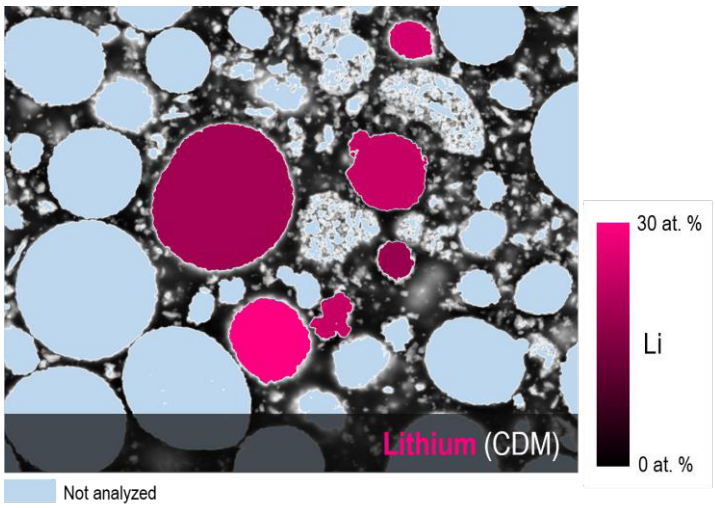

The first and only system that reveals, quantitatively, the distribution of lithium in conventional scanning electron microscopes.

- Exposes the distribution of lithium at the microscale in a wide variety of materials
- Determines the charge state of oxide particles used as cathodes in lithium-ion batteries
- Delivers quantitative analysis of lithium with a greater than ten-fold improvement in the minimum detection limit (sample dependent)

gatan.com | edax.com

GATAN / EDAX

ICPMAT 1-4 December 2025 Chiang Mai, Thailand BRONZE SPONSOR

Microscale evaluation of the lithium content in lithium-ion battery cathode materials in the scanning electron microscope

J. Lee, S. Mu, and D.J. Stowe
Gatan Inc., Pleasanton, CA USA

Abstract

The mean Li content of a metal oxide cathode material used in the construction of lithium-ion batteries was determined experimentally by the Cipher® system to an accuracy of ~1 at. %

A composition-by-difference method using X-ray energy dispersive X-ray spectroscopy (EDS) and quantified backscatter electron (qBSE) imaging in the scanning electron microscope is used to map lithium distribution in the scanning electron microscope (SEM). The mean Li content was determined to be 23.8 at.%.

Introduction

Lithium (Li) ion-based electrochemical cells have a high capacity for energy storage which, combined with their low mass, make them ideal for transport applications.

A lack of microscale analytical techniques with the capability of mapping Li prevents critical degradation mechanisms from being understood (e.g., Li plating, dendrite growth, and solid electrolyte interphase formation) or battery charge cycles from being optimized.

Elemental analysis at the micro- and nano-scales typically uses EDS. However, **EDS remains unfeasible** in commercially important materials for elements of low atomic number (Z < 4), **including Li** [1, 2], because [1, 2]:

- **Characteristic x-rays may not be produced**—bonding state dependent
- X-rays that are generated are (re-) **absorbed strongly**
- **Specialized "Li EDS detectors"** have a limit of detection of ~20 wt. %; equivalent to about half the atoms in a typical sample

However, the composition-by-difference method [3, 4] used in the **Cipher system is not limited by such restrictions.**

Materials & Methods

High-grade **NMC 811** particles of nominal composition $LiNi_{0.8}Mn_{0.1}Co_{0.1}O_2$ were analyzed.

A sample of the NMC 811 was prepared by embedding the powder in epoxy before **a cross-section was prepared by broad-beam argon milling using a PECS™ II system (Gatan, Inc.).**

Calibration of the intensity scale of BSE images was performed using high purity standards of known composition.

The conversion of BSE images from arbitrary units to **mean atomic number** was performed according to the modified electron approach [5] with a screening factor of 0.7.

Results

The **non-Li elements were captured by EDS,** and atomic percent maps were generated for Ni, Mn, Co, and O:

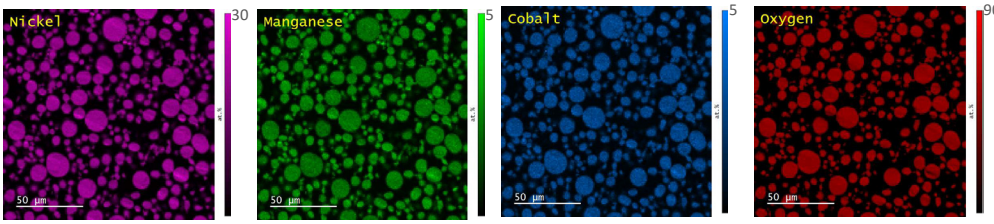

- Quantitative EDS analysis revealed little-to-no inter- or intra-particle variation in elemental composition
- The Ni:Mn:Co ratio was determined experimentally to be **8.07:1.00:1.01**, consistent with the nominal 8:1:1 ratio
- No other elements were found to be present above the minimum detection level

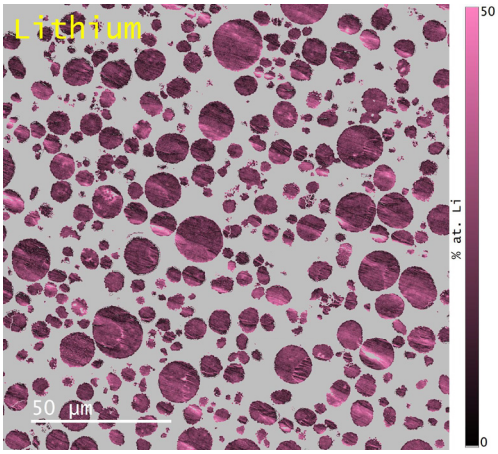

- **More than 100 NMC 811 particles** were analyzed using the **Cipher system**:

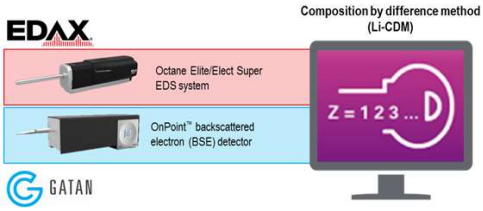

- **Mean lithium determined experimentally** to be **23.8 ± 3.9 at. %**
- Compares very favorably with nominal lithium content 25.0 ± 1.75 at. %

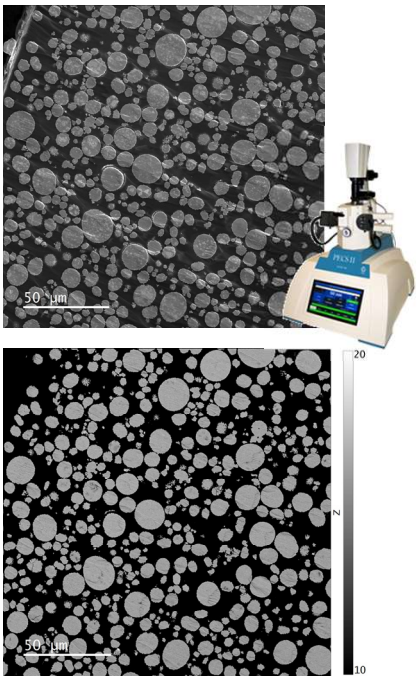

Conclusion

This result demonstrates **quantifiable microscale resolution Li detection in** this prospective **cathode material.**

This is a significant step forward in the analysis of battery materials as, **for the first time, the charge state of a cathode material may be determined in a conventional SEM**.

This result paves the way towards being able to study lithium migration at the microscale during the charge-discharge cycle in battery cells, promising to deliver new insights into structural and compositional evolution over a cell's lifetime.

References

[1] P. Hovington et al., Scanning 38 (2016) 571.
[2] R. Gauvin and N. Brodusch, Microsc. Microanal. 28 (Suppl 1), 2022.
[3] J. A. Österreicher et al., Scripta Materialia 194 (2021) 113664.
[4] J. Lee et al., Microscopy and Microanalysis (2022) 113.
[5] J. J. Donovan et al., Microscopy and Microanalysis 9 (2003) 202.

Contact Information
Jonathan Lee, PhD, Gatan, Inc
Email: Jonathan.Lee@ametek.com

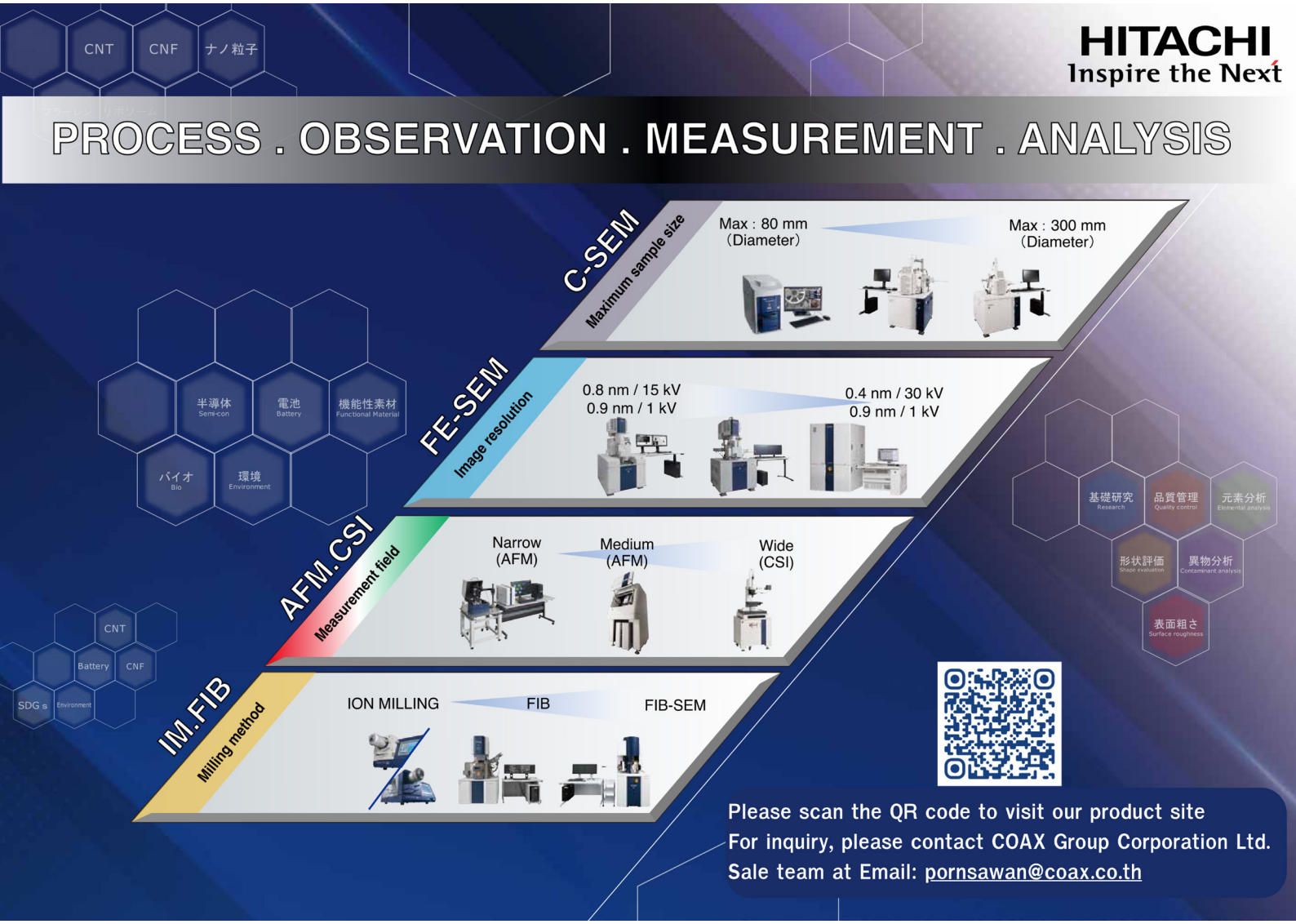
CNT
CNF
ナノ粒子
HITACHI
Inspire the Next
PROCESS . OBSERVATION . MEASUREMENT . ANALYSIS
C-SEM
Maximum sample size
Max : 80 mm
(Diameter)
Max : 300 mm
(Diameter)
FE-SEM
Image resolution
0.8 nm / 15 kV
0.9 nm / 1 kV
0.4 nm / 30 kV
0.9 nm / 1 kV
AFM.CSI
Measurement field
Narrow
(AFM)
Medium
(AFM)
Wide
(CSI)
IM.FIB
Milling method
ION MILLING
FIB
FIB-SEM
半導体
Semi-con
電池
Battery
機能性素材
Functional Material
バイオ
Bio
環境
Environment
基礎研究
Research
品質管理
Quality control
元素分析
Elemental analysis
形状評価
Shape evaluation
異物分析
Contaminant analysis
表面粗さ
Surface roughness
CNT
Battery
CNF
SDG s
Environment
Please scan the QR code to visit our product site
For inquiry, please contact COAX Group Corporation Ltd.
Sale team at Email: pornsawan@coax.co.th

Integrated SEM and Ion Milling Solutions for Advanced Materials Analysis

Hitachi High-Tech provides a comprehensive suite of surface analysis and imaging instruments designed to meet the demands of modern research and manufacturing. Combining the latest Field Emission Scanning Electron Microscopes (FE-SEM) with state-of-the-art Ion Milling Systems enables precise sample preparation and superior imaging quality.

FE-SEM SU8600 / SU8700 – Data-Driven Innovation

The SU8600 and SU8700 represent Hitachi's latest generation of FE-SEMs, engineered for high-resolution imaging, analytical accuracy, and automated data acquisition. These systems support fast, reliable, and repeatable operation for a wide range of applications including nanotechnology, materials science, and semiconductor research.

Key Highlights:

- Ultra-stable cold-field emission (SU8600) and Schottky source (SU8700) for flexible performance.
- Automatic data acquisition with EM Flow Creator for high-throughput analysis.
- Up to 40,960 × 30,720pixel imaging resolution for ultra-wide field-of-view imaging.
- Enhanced signal detection and simultaneous multi-detector capture for richer analytical data.
- Short working distance EDS capability (SU8700) for improved analytical resolution.

Hitachi Ion Milling Systems – Precision Sample Preparation

The Hitachi Ion Milling series (IM4000II and ArBlade5000) offers advanced solutions for cross-section and flat milling, ideal for preparing specimens for SEM, TEM, and EBSD analysis. These systems deliver precise surface finishing without introducing mechanical artifacts, ensuring accurate structural evaluation.

Key Highlights:

- Dual-mode milling (cross-section and flat milling) for versatile specimen preparation.
- Air protection and cryo-compatible options for sensitive materials.
- High-precision ion beam control with automatic milling sequences.
- Large specimen stage and user-friendly interface for efficient operation.
- Compatible with various sample holders, including tilting and cooling stages

Integrated Workflow for SEM and Ion Milling

Combining Hitachi's Ion Milling systems with FE-SEM instruments enables researchers to achieve optimal imaging results. Accurate sample preparation minimizes charging and surface damage, while high-resolution SEM imaging reveals microstructural details essential for advanced material analysis.

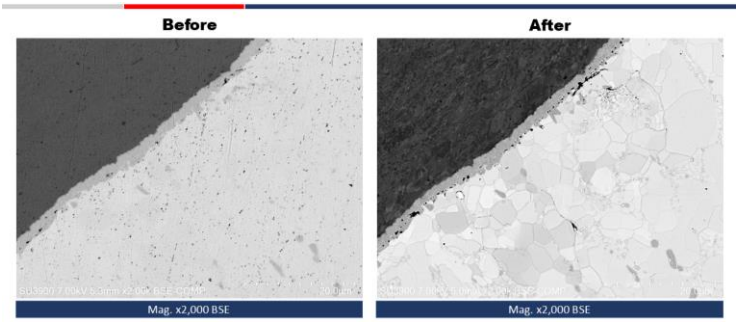

SEM condition : Model SU3900, Accelerating voltage 7 kV, BSE signal
Flat milling condition : Accelerating voltage 3 kV, Time 7 min.

Contact:
Mr. Pornsawan Klayklung
Tel. (668) 6177 5471
Coax Group Corporation Ltd.
https://www.coax.co.th

ICPMAT 1-4 December 2025 Chiang Mai, Thailand

BRONZE SPONSOR

PBP-CMU Electron Linac Laboratory

PCELL

Plasma & Beam Physics Research Facilities

Accelerator Physics & Technology ◇ Advanced Light Sources ◇ Electron Beam Techniques

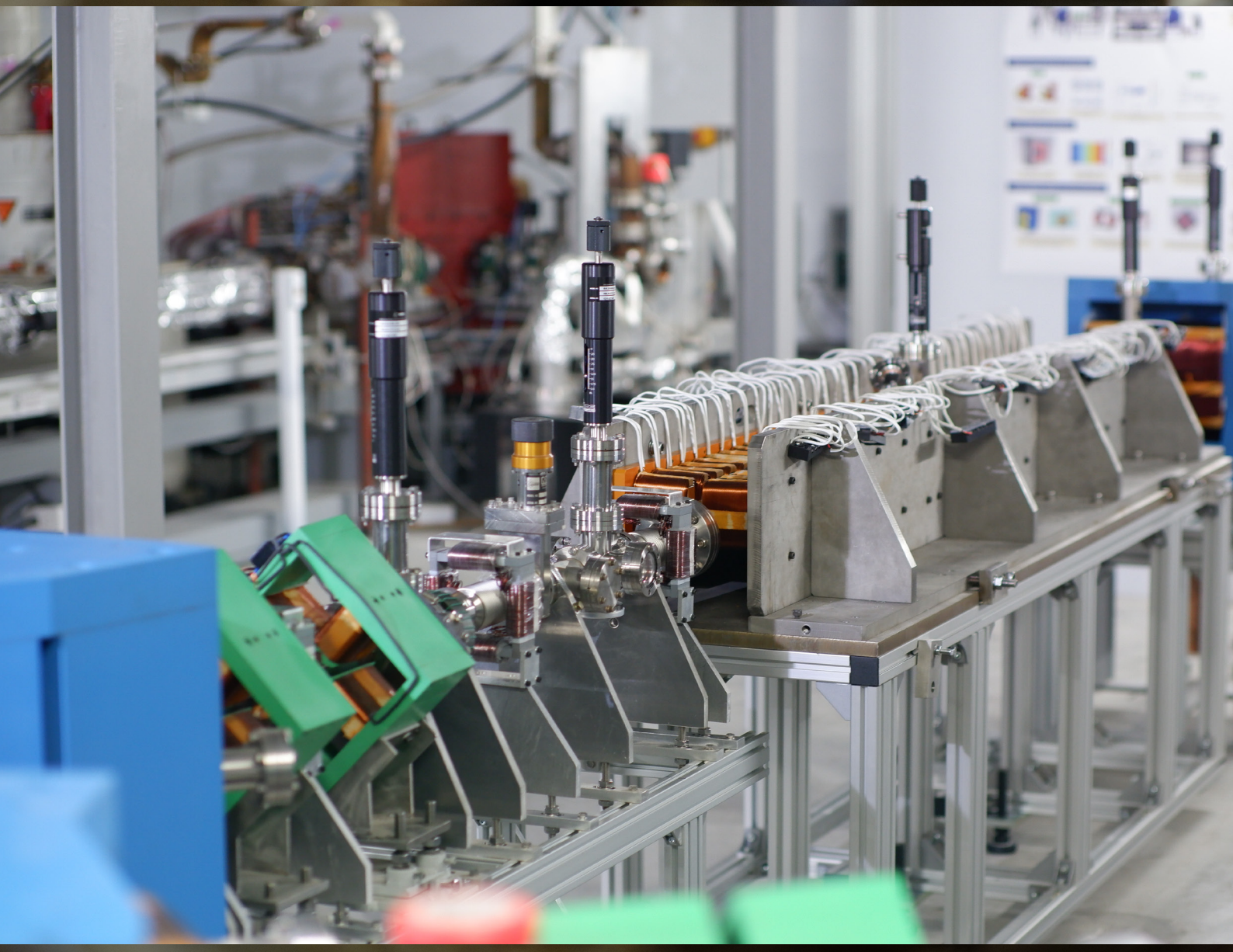

Department of Physics & Materials Science, Faculty of Science, Chiang Mai University

Visit us!

PMU-B

CMU CHIANG MAI UNIVERSITY

PCELL

Particle Accelerators HUB OF TALENTS

Accelerator-based radiation

Station: MIR–THz FELs, TR

Status: Underway

Parameter	MIR FEL	THz FEL	TR
E-beam energy (MeV)	25	10–16	8–22
E-bunch charge (pC)	~60	~50	~60
E-bunch length (fs)	200	200–300	
Wavelength (microns)	9.5–16.6	86–300	120–1000
Rad. pulse length (fs)	300-600	200-300	200-350
Pulse energy (nJ)	120-540	Max. 100	170-250
Peak power (MW)	Max. 1.15	~0.5	0.9–1.5
Repetition rate (Hz)	10		

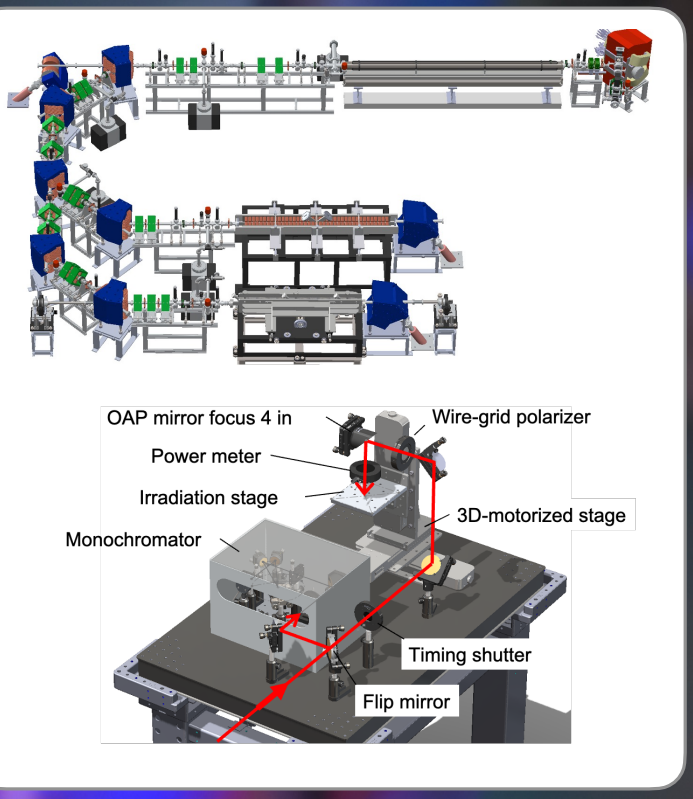

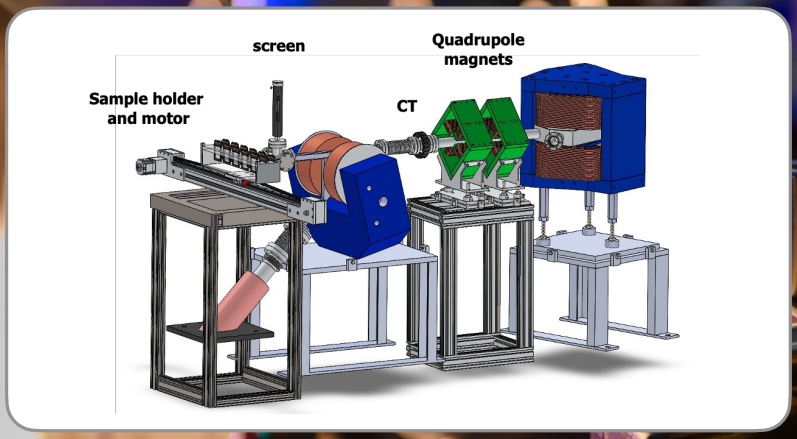

Electron beam irradiation

Station: E-beam irradiation, FLASH

Status: Underway

Parameter	Expected range
Dose rate (Gy/s)	~500–5000
E-bunch charge (pC)	10–100
E-beam energy (MeV)	5–25

FTIR spectrometer

Station: FTIR / astrochemistry

Status: Open for service

Specification	Availability
Model	VERTEX 80v
Spectral range (cm^{-1})	40–4000
Resolution (cm^{-1})	Better than 0.2
Sample form	Solid/liquid/gas/plasma

Short-pulse laser

Station: THz-TDS / non-linear optics

Status: Open for service*

*Contact for details

SOLUTION FOR MATERIAL SCIENCE

NEXOPART

Test Sieve & Shaker

SINCE 1889

Plasma Cleaner

LABCONCO

Controlled Atmosphere Glove Boxes

BEC THAI

KRÜSS

Flame Photometer

Density Meter

velp

Elemental Analyzer

thermo scientific

Raman Spectrometer & Microscope

FTIR Spectrometer & Microscope

UV-Visible Spectrophotometer

TOA DKK

Automatic Titrator

JEOL

Transmission Electron Microscope (TEM)

Scanning Electron Microscope (SEM)

X-ray Fluorescence Spectrometer (XRF)

VACUUBRAND.

Vacuum Pump

heidolph

AN ATS COMPANY

Rotary Evaporator

Magnetic Stirrer

Overhead Stirrer

OXFORD INSTRUMENTS

Atomic Force Microscope (AFM)

memmert

Climate Chamber & Hot Air Oven

DWK LIFE SCIENCES

Laboratory Glassware

USBECK

Laboratory Metalware

Nabertherm

MORE THAN HEAT

Furnace

euromex

microscopes holland

Light Microscope & Stereo Microscope

BRAND

Liquid Handling

99/9 Moo 2, Maha Sawat,
Phutthamonthon,
Nakhon Pathom. 73170. Thailand.
T. +66 3424 5299
F. +66 3424 5250
E. sales@becthai.com

simplify science with complete innovative solutions

BRONZE SPONSOR ICPMAT 2025 1-4 December Chiang Mai, Thailand

ICPM AT

1-4 December 2025

Chiang Mai, Thailand

SPONSORS

Platinum

PMU-B

Gold

Attanam Damayanti Pandita
Chiang Mai University Since 1964
Faculty of Science

MR CENTER
Faculty of Science Chiang Mai University

Bara Scientific
Solution of Success

KEYENCE

SHIMADZU
Excellence in Science

Silver

its

RENISHAW
apply innovation™

Bronze

SCG

PELL

GATAN
AMETEK

crest

MEGA MATT CO.,LTD.

COAX

BEC THAI

HISTOCENTER
Beyond Instruments

Leica
MICROSYSTEMS

KINETICS

JEOL
Solutions for Innovation

LAB CONNECTION
Technology for You